



University  
of Glasgow

Collings, Alexander J. (2022) *Developing leukaemic biomarkers to enable personalised CNS-directed therapy*. PhD thesis.

<https://theses.gla.ac.uk/83152/>

Copyright and moral rights for this work are retained by the author

A copy can be downloaded for personal non-commercial research or study,  
without prior permission or charge

This work cannot be reproduced or quoted extensively from without first  
obtaining permission in writing from the author

The content must not be changed in any way or sold commercially in any  
format or medium without the formal permission of the author

When referring to this work, full bibliographic details including the author,  
title, awarding institution and date of the thesis must be given

Enlighten: Theses

<https://theses.gla.ac.uk/>  
[research-enlighten@glasgow.ac.uk](mailto:research-enlighten@glasgow.ac.uk)

# **Developing Leukaemic Biomarkers to Enable Personalised CNS-Directed Therapy**

**Alexander J. Collings**

BSc (Hons), MSc

Submitted in fulfilment of the requirements for the degree of  
Doctor of Philosophy



University  
of Glasgow

Institute of Cancer Sciences,  
College of Medical, Veterinary and Life Sciences,  
University of Glasgow

April 2022

## Abstract

Acute lymphoblastic leukaemia (ALL) is a cancer of the blood and the most common childhood cancer in the world today. This leukaemia is known to infiltrate the central nervous system (CNS), a sanctuary site where blasts can flourish and cause relapse. There are currently no ways to accurately predict CNS relapse, so all children receive substantial amounts of CNS-directed chemotherapy which can cause short and long-term neurotoxicity.

CNS leukaemia is currently classified by CSF cytology and cell count however, evidence shows that leukaemic blasts adhere to the walls of the leptomeninges which may reduce the ability of FCM and CSF cytology to accurately determine leukaemic burden in the CNS. In order to tailor CNS therapy to a child's individual risk of relapse, better biomarkers, capable of measuring total leukemic burden at this site are needed. This project aimed to develop sensitive biomarkers for the presence of CNS leukaemia and its response to therapy by targeting cell-independent markers in samples of cerebrospinal fluid (CSF). Biomarkers of interest include CSF metabolites, soluble proteins and cell-free DNA (cfDNA).

Semi-untargeted metabolic profiling was performed using Liquid Chromatography Mass Spectrometry (LC-MS) on a large, comprehensive cohort of diagnostic CSF samples and normal control CSF to validate a panel of metabolites that showed promise in detecting a leukaemic metabolic signature. This analysis highlighted Creatine, N4-acetylcytidine, Phenylalanine and Symmetric dimethylarginine as the most promising diagnostic biomarkers. Multivariate biomarker models were created and demonstrated a higher sensitivity and specificity in detecting a leukaemic signature when the biomarkers were used in combination. Phenylalanine also

demonstrated promise as a potential prognostic biomarker, presenting with elevated levels in patients who went onto to relapse in the CNS.

Luminex multiplex-immunoassays were run on a subset of diagnostic CSF samples and matched control CSF for screening and identification of soluble protein/chemokine markers capable of distinguishing CNS leukaemia. Of interest, CD27, presented with elevated levels in patient diagnostic CSF compared to the control CSF.

Several different commercial cfDNA extraction kits and technologies were tested to determine the most suitable kit for extracting cfDNA from low volumes of patient CSF. Two highly sensitive platforms, droplet digital PCR (ddPCR) and next-generation sequencing (NGS) were used to identify leukaemic cfDNA by targeting the KRAS G12D mutation and immunoglobulin heavy chain (IGH) gene rearrangements. This analysis proved that leukaemic cfDNA could be detected in the low samples of patient CSF using both platforms, providing evidence that cfDNA can be used as a highly specific biomarker for CNS leukaemia.

In conclusion, this study identified promising diagnostic, prognostic and predictive biomarkers in the CSF of CNS-ALL patients, each with their advantages and disadvantages, capable of detecting CNS leukaemia taking another step towards personalising CNS-directed therapy with the aim of reducing therapy for those at low risk of CNS recurrence and intensifying treatment for those at high risk.



## Acknowledgements

Firstly, I wish to express my gratitude to the patients and parents who consented to take part in the research presented in this thesis and to the Children's Cancer and Leukaemia Group (CCLG) and the Little Princess Trust for their generous funding of this study.

I would like to thank my brilliant supervisors Professor Christina Halsey and Dr Fiona Thomson for their unfaltering support and guidance during this project. A PhD student couldn't ask for better supervision. I would also like to give a special thank you to Dr Chantevy Pou for all of her invaluable help and mentorship.

I would also like to thank Dr David Sumpton of the Beatson Institute for his help and guidance with the metabolomics work, Sandra Chudleigh of the UK MRD laboratory for kindly allowing me to visit the MRD laboratory, and all my colleagues in the Halsey Laboratory and the Translational Pharmacology Laboratory in the Wolfson Wohl Cancer Research Centre for all their help and friendship over the years.

Finally, I would like to thank my family and Kirstin for their ongoing support and encouragement over the years for which I am very grateful.

## Author's Declaration

I declare that where explicit reference is made to the contribution of others that this thesis is the result of my own work and has not been submitted for any other degree at the University of Glasgow or any other institution.

Signature: .....

Printed name: Alexander J. Collings

# Table of Contents:

<b>Chapter 1: Introduction .....</b>	<b>17</b>
1.1 Background .....	17
1.2 Leukaemogenesis & Prognostic Factors .....	19
1.2.1 Classical prognostic factors .....	20
1.3 Biology of CNS-ALL .....	22
1.3.1 The leptomeninges and cerebrospinal fluid (CSF) .....	22
1.3.2 Mechanisms of CNS infiltration.....	25
1.4 Clinical aspects of CNS-ALL.....	31
1.4.1 CNS-ALL diagnosis .....	31
1.4.2 Relapse .....	34
1.5 Treatment .....	34
1.5.1 Systemic treatment.....	34
1.5.2 Clinical trials in the UK.....	36
1.5.3 CNS-Treatment.....	38
1.6 Minimal Residual Disease (MRD).....	39
1.6.1 Flow Cytometry.....	40
1.6.2 Polymerase chain reaction (PCR) of gene fusions .....	41
1.6.3 PCR of Immunoglobulin (Ig) & T-cell receptor (TCR) gene rearrangements .....	41
1.6.4 Limitations of current MRD analysis techniques .....	51
1.7 Biomarkers.....	52
1.7.1 Background .....	52
1.7.2 Current potential biomarkers for CNS-ALL.....	55
1.8 Summary .....	64
1.8.1 Hypothesis .....	66
1.8.2 Aims.....	66
<b>Chapter 2: Materials &amp; Methods .....</b>	<b>67</b>
2 Materials and supplies.....	67
2.1.1 List of Suppliers, materials and supplies .....	67
2.1.2 List of hardware.....	70
2.1.3 List of software .....	71
2.2 Human Tissue .....	72
2.2.1 Ethics approval.....	72
2.2.2 CSF biobank .....	72
2.2.3 Plasma samples and pooled plasma .....	72
2.3 Techniques: Chapter 1 – Metabolomics .....	73

2.3.1	Materials & supplies .....	73
2.3.2	Metabolite extraction from CSF.....	73
2.3.3	Semi-untargeted mass spectrometry .....	74
2.3.4	Targeted LC_MS .....	74
2.4	Techniques: Chapter 2 - Multiplex immunoassay – Luminex .....	76
2.4.1	Workflow.....	76
2.5	Techniques: Chapter 3 – Cell-free DNA .....	78
2.5.1	Cell culture.....	78
2.5.2	Nucleic Acid Isolation and Extraction .....	80
2.5.3	Preparation of cfDNA surrogate spike-in molecule .....	86
2.5.4	Nucleic Acid Quantification and size (bp) analysis .....	91
2.5.5	Droplet Digital PCR.....	94
2.5.6	Next-Generation Sequencing (NGS) .....	100
2.5.7	TruePrime cfDNA amplification.....	109
2.6	Data analysis.....	111
	<b>Chapter 3: Metabolic biomarkers for CNS-ALL .....</b>	<b>112</b>
3	Introduction and aims.....	112
3.1	Candidate diagnostic biomarkers.....	117
3.1.1	Untargeted reanalysis to find new candidate biomarkers of interest ..	117
3.1.2	Summary .....	125
3.2	Targeted analysis of candidate diagnostic biomarkers – Pilot Cohort .....	127
3.2.1	Univariate analysis of candidate biomarker performance against non-inflammatory and inflammatory control CSF .....	127
3.2.2	Univariate analysis of candidate biomarker performance against combined control CSF .....	140
3.2.3	Summary .....	147
3.2.4	Multivariate analysis of candidate biomarkers – Creation of a model.....	149
3.2.5	Summary .....	157
3.3	Candidate biomarker performance evaluation: Cohort 2.....	160
3.3.1	Background .....	160
3.3.2	CNS Dx vs non-inflammatory & inflammatory CSF controls.....	162
3.3.3	Biomarker performance evaluation.....	172
3.3.3.1	Univariate ROC analysis of leukaemic CSF vs Control CSF .....	172
3.3.3.2	Analysis of CNS1 CNS2 and CNS3 patient sample groups within the CNS Dx patient sample cohort. ....	176
3.3.3.3	CNS1 vs CNS3.....	179
3.3.3.4	Univariate analysis CNS Dx vs CSF CTL .....	183
3.3.4	Multivariate Analysis of candidate biomarkers.....	190
3.4	Measuring true abundance of candidate biomarkers.....	199

3.4.1	Quantification of Creatine and Xanthine levels .....	199
3.4.2	Application of a multi-biomarker model to true abundance levels of candidate biomarkers .....	204
3.5	Prognostic biomarkers .....	209
3.6	Summary and conclusions .....	214
<b>Chapter 4: Discovery of soluble biomarkers of Central-Nervous System Acute lymphoblastic leukaemia.....</b>		<b>223</b>
4	Introduction and aims .....	223
4.1	Primary analysis of potential soluble biomarker candidates .....	226
4.2	Secondary analysis of soluble biomarker candidates .....	231
4.2.1	CD27 .....	231
4.2.2	L-selectin & Osteopontin .....	240
4.2.3	Summary and conclusions .....	246
<b>Chapter 5: Circulating-tumour DNA as a biomarker of central-nervous system acute lymphoblastic leukaemia .....</b>		<b>250</b>
5	Introduction and aims .....	250
5.1	Comparing commercial cfDNA extraction kits .....	254
5.1.1	Quantification by Qubit fluorometry .....	254
5.1.2	Quantification by droplet-digital PCR .....	259
5.1.3	Testing of kit QA sensitivity: Spike-in & recovery .....	266
5.1.4	Patient sample CSF cfDNA .....	277
5.2	Detecting ctDNA from Samples of CSF .....	287
5.2.1	Detection of KRAS G12D using ddPCR .....	287
5.2.2	Detection of IGH rearrangements using NGS .....	295
5.2.2.1	<i>in vitro</i> testing of NGS protocol .....	297
5.2.3	Patient cfDNA .....	300
5.2.3.1	Diagnostic, Day 8 and Day 29 CSF samples .....	300
5.2.3.2	Relapse Samples .....	305
5.2.4	TruePrime amplification .....	312
5.3	Summary and discussion .....	318
<b>Chapter 6: Final Conclusions, discussion and future Directions .....</b>		<b>325</b>
5.4	Summary and discussion of the main findings .....	326
5.5	Final conclusions and future directions .....	338
<b>Chapter 7: References .....</b>		<b>341</b>

# List of Figures

Figure 1-1: Improvements in the overall survival (OS) with the evolution of treatment of paediatric patients with ALL over time .....	18
Figure 1-2: Genetic subtype frequencies in paediatric ALL .....	20
Figure 1-3: Anatomy of the Meninges. ....	23
Figure 1-4: Cerebrospinal fluid secretion and flow around the CNS .....	24
Figure 1-5: The meninges and potential routes of CNS infiltration .....	27
Figure 1-6: Schematic representation of clonal distribution in bone marrow (BM) and CNS in matched diagnostic and relapse samples .....	29
Figure 1-7: Patterns of Clonal distributions by either free blast trafficking between the BM and the CNS (Pattern 1) or clonal evolution occurring in the BM or the CNS (Pattern 2) .....	30
Figure 1-8: Basic schematic diagrams of Ig/TCR rearrangement steps and loci on BCR/TCR phenotypes .....	47
Figure 1-9: 12/23 Spacer sequences and rearrangement mechanisms .....	48
Figure 1-10: Deletional joining mechanism .....	49
Figure 1-11: Inversional joining mechanism .....	50
Figure 1-12: Biomarker development pipeline .....	54
Figure 2-1: Luminex multiplex immunoassay workflow .....	77
Figure 2-2: PGL3 Plasmid map featuring hTERT-Luc plasmid fragment .....	87
Figure 2-3: Droplet digital PCR workflow schematic .....	94
Figure 2-4: Targeted NGS workflow adapted .....	101
Figure 2-5: NGS dual adapter approach schematic .....	102
Figure 3-1: Volcano plot of untargeted metabolomic data. ....	121
Figure 3-2: Violin plots of Inosine and Orotidine CNS Dx patient samples vs matched and unmatched CSF controls .....	122
Figure 3-3: Inosine & Orotidine ROC Curves and optimal cut-off points between CNS Dx and matched and unmatched CSF controls .....	123
Figure 3-4: Violin plots of candidate biomarkers depicting CNS Dx patient group vs non-inflammatory control CSF and inflammatory control CSF .....	131
Figure 3-5: Candidate biomarker ROC Curves and optimal cut-off points between CNS Dx and NI CTL/ I CTL CSF .....	136
Figure 3-6: Candidate biomarker ROC Curves and optimal cut-off points between CNS Dx and NI CTL/ I CTL CSF .....	137
Figure 3-7: Candidate biomarker ROC Curves and optimal cut-off points between CNS Dx and NI CTL/ I CTL CSF .....	138
Figure 3-8: Candidate biomarker ROC Curves and optimal cut-off points between CNS Dx and NI CTL/ I CTL CSF .....	139
Figure 3-9: Boxplots: Noninflammatory and Inflammatory Control CSF comparison of means .....	142
Figure 3-10: Violin plots of candidate biomarkers depicting CNS Dx patient group v control CSF. ....	143
Figure 3-11: Candidate biomarker ROC Curves and optimal cut-off points between CNS Dx and CTL CSF .....	145
Figure 3-12: Candidate biomarker ROC Curves and optimal cut-off points between CNS Dx and CTL CSF .....	146
Figure 3-13: Multivariate ROC analysis .....	151
Figure 3-14: Candidate biomarker ranking as determine by frequency of being selected in the model creation process and average importance from the 100 cross-validations. ....	153

Figure 3-15: Multivariate ROC curve analysis manual model testing by removal of redundant features .....	155
Figure 3-16: Cross-validation Class Prediction confusion matrix. ....	156
Figure 3-17: Permutation testing on 6-variable model .....	159
Figure 3-18: Violin plots of CNS Dx vs Inflammatory and Non-inflammatory control CSF groups .....	164
Figure 3-19: Candidate biomarker ROC Curves and optimal cut-off points between CNS Dx and non-inflammatory and inflammatory controls. ....	168
Figure 3-20: Candidate biomarker ROC Curves and optimal cut-off points between CNS Dx and non-inflammatory and inflammatory controls .....	169
Figure 3-21: Candidate biomarker ROC Curves and optimal cut-off points between CNS Dx and non-inflammatory and inflammatory controls. ....	170
Figure 3-22: Candidate biomarker ROC Curves and optimal cut-off points between CNS Dx and non-inflammatory and inflammatory controls v9. ....	171
Figure 3-23: Boxplots: Noninflammatory and Inflammatory Control CSF comparison of means .....	175
Figure 3-24: Violin plots of Candidate biomarker levels: Control CSF vs CNS1, CNS2 and CNS3 patient groups .....	178
Figure 3-25: Comparison between the means of CNS1 vs CNS3 patients .....	181
Figure 3-26: Comparison between the means of CNS1 vs CNS3 patients. ....	182
Figure 3-27: Violin plots of candidate biomarkers depicting CNS Dx patient group v control CSF .....	186
Figure 3-28: Candidate biomarker ROC Curves and optimal cut-off points between CNS Dx and CTL CSF .....	187
Figure 3-29: Candidate biomarker ROC Curves and optimal cut-off points between CNS Dx and CTL CSF .....	188
Figure 3-30: Multivariate ROC analysis .....	192
Figure 3-31: ROC curve of highest performing 7-variable model and Candidate biomarker ranking. ....	194
Figure 3-32: Cross-validation class prediction probabilities .....	195
Figure 3-33: Permutation test Histogram of permuted data .....	198
Figure 3-34: Violin plots of Creatine and Xanthine CNS Dx patient samples vs matched and unmatched CSF controls .....	201
Figure 3-35: Individual ROC curves for Creatine and Xanthine .....	202
Figure 3-36: ROC curve optimal cut-off determination .....	203
Figure 3-37: Multivariate ROC analysis .....	206
Figure 3-38: Cross-validation Class Prediction confusion matrix. ....	207
Figure 3-39: Comparison between the means of CNS Dx vs CNS DxR patients ....	211
Figure 3-40: Comparison between the means of CNS Dx vs CNS DxR patients. ....	212
Figure 3-41: Allopurinol metabolism .....	221
Figure 4-1: Violin plots of several log10 transformed analyte concentrations from dx vs matched late control sample data .....	229
Figure 4-2: Receiver Operator Curve (ROC) analysis of diagnostic sample (Dx) vs matched late control sample (Late). ....	230
Figure 4-3: CD27 - Violin plots of CD27 levels in control CSF vs CNS1, CNS2 & CNS3 patient sample groups. ....	234
Figure 4-4: CD27 – Violin plot of log10 transformed CD27 levels in control CSF vs CNS Dx patient sample group.....	236
Figure 4-5: ROC analysis CSF vs CNS Dx .....	237
Figure 4-6: Violin plot of log10 transformed CD27 levels in CNS DX samples vs CNS DxR samples .....	239

Figure 4-7: L-selectin – Violin plots of log10 transformed L-selectin levels of control CSF vs CNS1, CNS2 and CNS3 patient samples .	242
Figure 4-8: L-selectin – Violin plots of log10 transformed L-selectin levels of control CSF vs CNS Dx patient samples	243
Figure 4-9: Osteopontin – Violin plots of log10 transformed Osteopontin levels of various analyses	244
Figure 5-1: Box plots of absolute cfDNA extracted quantified by Qubit	255
Figure 5-2: Extraction efficiency of cfDNA kits compared to kit QA.	258
Figure 5-3: Digital PCR Rain-plots : confirmation of detection of hTERT <sub>172</sub> .	260
Figure 5-4: Box plots of absolute quantity of hTERT <sub>172</sub> extracted quantified by ddPCR	261
Figure 5-5: Efficiency of hTERT <sub>172</sub> extraction in all kits compared to kit QA.	263
Figure 5-6: Violin plots of cfDNA extraction volume testing in 2 mL, 1mL and 0.5 mL of plasma surrogate matrix.	267
Figure 5-7: cfDNA Spike-in & recovery experiment from 0.5 mL pooled plasma surrogate matrix	268
Figure 5-8: Bioanalyzer electropherograms	269
Figure 5-9: cfDNA Spike-in & recovery experiment from 0.5 mL and 0.2 mL CSF pooled matrix	272
Figure 5-10: Bioanalyzer electropherograms.	273
Figure 5-11: Pooled control CSF variability.	276
Figure 5-12: Absolute cfDNA quantity from ~100 µL diagnostic CSF samples	279
Figure 5-13: Total levels of extracted cfDNA from patient samples.	280
Figure 5-14: Total cfDNA levels of Relapse patient samples	281
Figure 5-15: Electropherograms of control CSF: cfDNA fragment size analysis	283
Figure 5-16: Electropherograms of patient and matched control CSF.	285
Figure 5-17-1: 1: ddPCR rain plot interpretation	290
Figure 5-17: Fluorescence Amplitude plots of allelic frequencies.	291
Figure 5-18: Frequency Amplitude plots 5 ng spiked into control CSF.	292
Figure 5-19: KRAS G12D/ WT KRAS assay results from 13 patient samples cfDNA extracted with QIAamp circulating nucleic acids kit.	293
Figure 5-20: Bubble plots: VDJ clonotypes from ALL cell-line gDNA and cfDNA detected by NGS	298
Figure 5-21: Bubble plot representing diagnostic patient cfDNA sequencing results from 7 DX samples	303
Figure 5-22: P2 clone prevalence in Dx, D8 and D29 CSF samples	303
Figure 5-23: Bubble plot representing relapse patient cfDNA sequencing results from 4 RL samples	306
Figure 5-24: Line graph: TruePrime cfDNA amplification of RL1, and three CNS3 patient cfDNA samples	313
Figure 5-25: Electropherograms of 1st stage PCR QC check	314
Figure 5-26: Bubble plots of TruePrime amplified cfDNA.	317
Figure 5-27: REH cell line contamination	322



# List of Tables

Table 1-1: CNS-ALL classification .....	32
Table 1-2: Biomarker definitions .....	54
Table 1-3: Experimental metabolomic approaches .....	57
Table 2-1: List of materials and supplies .....	69
Table 2-2: List of Hardware .....	70
Table 2-3: List of software .....	71
Table 2-4: Commercial cfDNA extraction kits tested for evaluation of extraction performance .....	81
Table 2-5: LE220-Plus Focused Ultrasonicator settings .....	85
Table 2-6: PCR reaction master mix components and volume .....	88
Table 2-7: hTERT-Luc plasmid fragment Forward and Reverse primer sequences. ....	88
Table 2-8: Thermocycler conditions .....	89
Table 2-9: PCR reaction master mix components and volume .....	95
Table 2-10: hTERT-Luc plasmid fragment Forward and Reverse primer sequences. ....	95
Table 2-11: Thermocycler conditions .....	96
Table 2-12: PCR reaction master mix components and volume .....	97
Table 2-13: Thermocycler conditions .....	98
Table 2-14: PCR reaction master mix components and volume .....	100
Table 2-15: Thermocycler conditions .....	100
Table 2-16: IGH complete rearrangements forward and reverse 1 <sup>st</sup> stage primers. Forward Primers span the VH1-VH7 gene segment. Reverse consensus primer targeting the J gene segment.....	103
Table 2-17: IGH incomplete rearrangements forward and reverse 1 <sup>st</sup> stage primers. ....	104
Table 2-18: 2nd Stage adapter primer sequences .....	106
Table 2-19: Unique indexes in 2 <sup>nd</sup> stage PCR primers.....	107
Table 2-20: 2 <sup>nd</sup> Stage PCR Mastermix composition .....	108
Table 2-21: 2 <sup>nd</sup> Stage PCR thermocycling conditions .....	108
Table 3-1: Untargeted metabolomic analysis filtering workflow.. ....	118
Table 3-2: Classification designations for AUC .....	120
Table 3-3: Candidate biomarkers: Statistical analysis of the difference between CNS Dx and matched/unmatched CSF controls. ....	124
Table 3-4: ROC curve analysis summary: CNS Dx vs matched/unmatched control .....	125
Table 3-5: Candidate biomarkers selected for further evaluation .....	126
Table 3-6: Control CSF cohorts .....	128
Table 3-7: Patient clinical details for samples in the pilot experiment. ....	129
Table 3-8: Candidate biomarkers: Statistical analysis of the difference between CNS Dx and matched/unmatched CSF controls .....	132
Table 3-9: ROC curve analysis summary: CNS Dx vs NI CTL/ I CTL .....	134
Table 3-10: ROC curve analysis summary: CNS Dx vs CSF CTL .....	144
Table 3-11: Patient demographic .....	161
Table 3-12: Control CSF cohorts .....	161
Table 3-13: Candidate biomarkers: Statistical analysis of the difference between CNS Dx and non-inflammatory and inflammatory CSF controls .....	165
Table 3-14: ROC curve analysis summary: CNS Dx vs NI CTL/ I CTL. ....	167

Table 3-15: Statistical analysis of the difference between non-inflammatory and inflammatory CSF controls .....	174
Table 3-16: Statistical analysis of the difference between candidate biomarker levels in CNS1 and CNS3 patient samples. ....	180
Table 3-17: Statistical analysis of the difference between candidate biomarker levels in the CNS Dx patient group against the Control CSF group. ....	185
Table 3-18: Summary of ROC analysis .....	189
Table 3-19: Candidate biomarker statistical analysis and ROC curve summary.....	202
Table 3-20: Statistical analysis of the difference between candidate biomarker levels in the CNS Dx patient group against the Control CSF group. ....	213
Table 4-1: Diagnostic patient sample information. ....	227
Table 4-2: Analyte concentrations in range of standard curve and descriptive statistics .....	228
Table 4-3: CSF sample types for secondary analysis of candidate biomarkers .....	232
Table 4-4: Receiver Operator Curve (ROC) analysis of non-inflammatory control CSF & inflammatory control CSF vs CNS Dx patient sample groups for L-selectin & Osteopontin .....	245
Table 5-1: Descriptive statistics for each tested kit – Control vs Spiked. ....	257
Table 5-2: Statistical analysis of the differences between the means of kit QA vs all other kits. ....	259
Table 5-3: Descriptive statistics for each tested kit – Control vs Spiked. ....	262
Table 5-4: Statistical analysis of the differences between the means of kit QA vs all other kits .....	264
Table 5-5: hTERT <sub>172</sub> Spike-in recovery using Qubit and confirmation by Bioanalyzer. ....	271
Table 5-6: 0.5 and 0.2 mL CSF spike-in and recovery experiments. ....	274
Table 5-7: cfDNA size fragment analysis from control CSF. ....	284
Table 5-8: cfDNA size fragment analysis from diagnostic (DX) and late (>1 year) samples .....	286
Table 5-9: Expected frequencies and Acceptance criteria for KRASG12D Multiplex I cfDNA RSS – Horizon .....	289
Table 5-10: ddPCR results from 0.2 mL CSF extracted cfDNA. Values given in copies for FAM (mutant) and HEX (WT) .....	292
Table 5-11: NGS metrics. Type = complete or incomplete IGH rearrangements.....	299
Table 5-12: Cohort of CNS3, CNS2 and CNS2 patient samples tested for IGH gene rearrangements .....	301
Table 5-13: Quantified cfDNA from diagnostic CSF samples. cfDNA quantified by Qubit .....	301
Table 5-14: VDJ sequence data of detected clone in diagnostic CSF sample from P2. ....	304
Table 5-15: Relapse sample cfDNA quantification post- extraction .....	305
Table 5-16: Diagnostic bone marrow VDJ clonotypes detected for patients RL1 and RL2. ....	308
Table 5-17: IGH complete rearrangement (VH3) VDJ sequence comparison between bone marrow clone and CSF cfDNA clone. ....	308
Table 5-18: VDJ sequence data of detected clone in diagnostic CSF sample from RL1. ....	309
Table 5-19: VDJ sequence data of detected clone in diagnostic CSF sample from RL CL1 .....	310
Table 5-20: VDJ sequence data of detected clone in diagnostic CSF sample from RL CL2 .....	311
Table 5-21: TruePrime cfDNA amplification of RL1, and three CNS3 patient cfDNA samples. ....	313

Table 5-22: IgBlast analysis of TruePrime amplified cfDNA sequences. ....	316
Table 5-23: Starting concentrations of REH cfDNA in original workflow experiment and TruePrime amplificaiton experiment .....	316

# Abbreviations:

AF	Allelic frequency
AFA	Adaptive focused acoustics
ALL	Acute lymphoblastic leukaemia
AML	Acute myeloid leukaemia
AR	Antigen receptors
ASO	Allele specific oligonucleotides
AUC	Area under the curve
BBB	Blood brain barrier
BCP	B-cell precursor
BCR	B cell receptor
BCSFB	Blood CSF barrier
BDLB	Blood dural lymphatics barrier
BLMB	Blood leptomeningeal barrier
BM	Bone marrow
BR	Broad range
CALLA	Common acute lymphoblastic leukaemia antigen
CCLG	Children's Cancer & Leukaemia Group
CD	Compound discoverer
CDR3	Complementary determining region 3
CI	Confidence intervals
CLL	Chronic lymphocytic leukaemia
CNA	Circulating nucleic acids
CNS	Central nervous system
CNS-ALL	Central nervous system acute lymphoblastic leukaemia
CRUK	Cancer Research UK
CSF	Cerebrospinal fluid
<i>CTC</i>	Circulating tumour cells
CTL	Control
CV	Coefficient of Variation
DI	Delayed intensification
ddPCR	Droplet digital PCR
DNA	Deoxyribose nucleic acid
DX	Diagnosis
EFS	Event free survival
FBS	Fetal bovine serum
FC	Flow cytometry
FCM	Flow cytometric immunophenotyping
HMDB	Human Metabolome Database
HPLC	High-performance liquid chromatography
HS	High sensitivity
HTS	High throughput sequencing
ID	Identification
IG	Immunoglobulin
IGH	Immunoglobulin heavy chain
IQ	intelligence quotient
IV	Intra venous

LAIP	Leukaemia associated immunophenotype
LC-MS	Liquid chromatography mass spectrometry
LOD	Limit of detection
MCCV	Monte-Carlo Cross Validation
MRD	Minimal residual disease
MW	Molecular weight
NGS	Next-generation sequencing
NHEJ	Non-homologous end joining
NI	Non-inflammatory
NIHR	National Biosample Centre
NM	Newmarket Scientific
OOR	Out of range
OPN	Osteopontin
OS	Overall survival
PA	Partial adapter
PB	Peripheral blood
PCA	Principle component analysis
PCR	Polymerase chain reactions
PNQ	Positive non-quantifiable
POS	Positive
PX	Patient
QC	Quality control
RBC	Red blood cell
RF	Random Forests
RI	Remission induction
RL	Relapse
RNA	Ribose nucleic acid
ROC	Receiver Operator Curve
RQ	Relative quantification
RSS	Reference standard set
RSS	Recombination signal sequence
RT	Reverse transcription
SAE	Serious adverse event
SD	Standard deviation
SE	Standard error
SEM	Standard error of mean
L-SLT	L-selectin
TCR	T-cell receptor
TK1	Thymidine Kinase 1
TLP	Traumatic lumbar puncture
TNF	Tumour necrosis factor
TP	TruePrime
UV	Ultra-violet
VDJ	Variable, Diversity, Joining
VEGF	Vascular endothelial growth factor
WBC	white blood cell
WCC	White cell count
WT	Wild type

# Chapter 1: Introduction

## 1.1 Background

Cancers of the blood make up around 7% of total global cancers, and of those, acute lymphoblastic leukaemia (ALL) is the most common childhood cancer. ALL is a rare disease, with around 800 people being diagnosed each year in the UK, most of which are children, teenagers or young adults [1]. This cancer affects white blood cells of the lymphoid lineage, namely B cells and T cells, transforming them into immature, malignant, lymphoid progenitor blasts capable of proliferating aberrantly and avoiding natural cell death mechanisms.

ALL is a systemic disease that originates and accumulates in the bone marrow and is known to infiltrate various extramedullary sites around the body such as the spleen, liver, testes and the central nervous system (CNS) via the blood [2]. This thesis will focus on the development of biomarkers for the detection of central nervous system acute lymphoblastic leukaemia (CNS-ALL) to predict relapse and monitor response to therapy in patients with paediatric ALL.

Over the past sixty years there has been a dramatic increase in the efficacy of ALL treatment and it is now considered one of the best treatment regimens a cancer patient can receive, with overall survival rates today reaching over 90% in most developed countries (**Figure 1-1**) [3]. This can be attributed to the incremental treatment strategies implemented with every clinical trial performed and the development of accurate risk stratification of patients. These trials and further research have allowed extensive identification and characterisation of various ALL subtypes, each with their own unique level of risk and consequent personalised treatment regimen.

Regardless of the remarkable progress achieved in treating ALL, it persists as one of the highest causes of death in children today. Not only this, as treatment dosages have been increased and intensified over the years, coupled with longer duration of treatment regimens (up to 3.5 years) as well as the inclusion of CNS-directed therapy, toxicity has become a major obstacle.

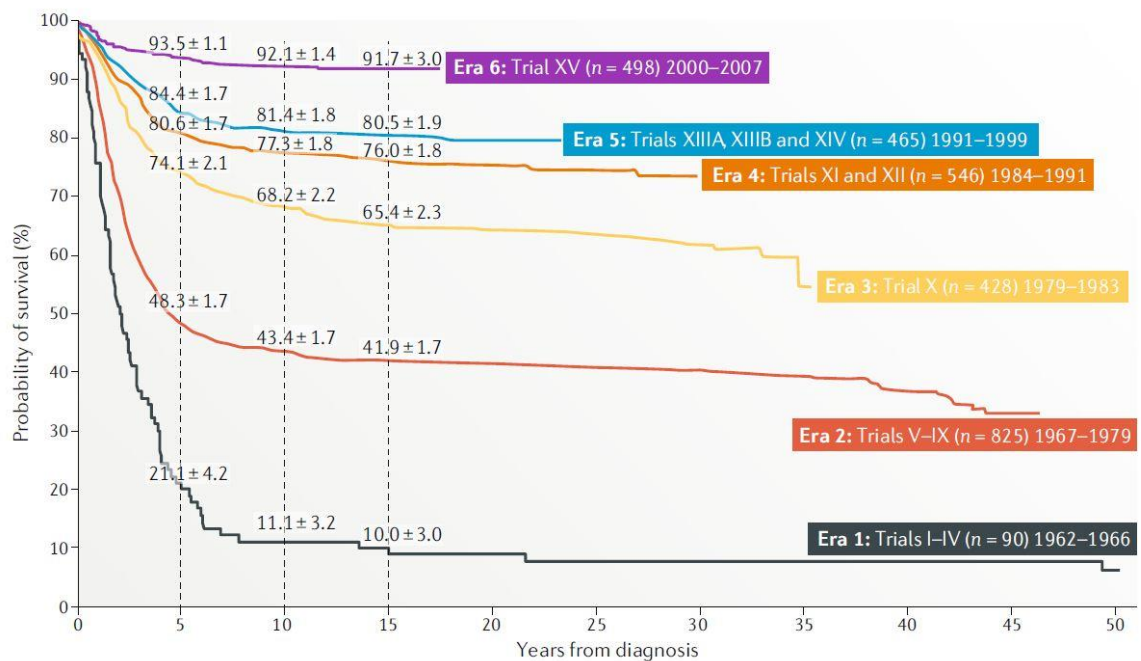


**Figure 1-1: Improvements in the overall survival (OS) with the evolution of treatment of paediatric patients with ALL over time.** OS curves range across 6 eras defined by the introduction of novel treatment strategies for a total of 2,852 children with newly-diagnosed ALL who were enrolled in 15 consecutive Total Therapy studies (I–XV) conducted at St. Jude Clinical Research Hospital from 1962 to 2007 [3].

The high dosage of CNS-directed treatment given to all children with ALL is largely due to the inability to accurately measure leukaemic involvement in the CNS and the high and almost inevitable incidence of relapse if this type of treatment is not administered. These factors make up the face of modern challenges seen in the treatment of paediatric ALL today and has led to an emphasis on achieving

personalised therapy to reinforce the excellent cure rates seen for this disease in children.

## 1.2 Leukaemogenesis & Prognostic Factors

It is currently not known if there is a main cause of leukaemia but there are several risk factors associated with developing an increased risk of ALL that can be divided into genetic and environmental factors. Environmental factors that have been suggested as potential causes for ALL include pre- and post-natal exposure to radiation such as x-rays or high dose therapeutic radiation or chemotherapy. However, evidence for these causes is few and far between. Professor Mel Greaves of the Institute of Cancer Research, UK, offers another possible explanation in the delayed infection hypothesis, with strong evidence suggesting that early infection (in the first year of life) is key to priming the immune system of a child and lower the risk of triggering ALL through an abnormal immune response to common infections later on in childhood [4].

Genetic factors are not hereditary and primarily include cytogenetic variations such as aneuploidy, chromosomal translocations & deletions. Genetic predispositions however, can occur in the form of germline polymorphisms with associated with an increased susceptibility of developing ALL, especially in patients with genetic syndromes. The prevalence of somatic mutations within the different genetic subtypes in ALL varies markedly and patients can possess inherited genetic variants with low or high penetrance (rarer) germline variants such as *ETV6*, *TP53*, *IKZF1* and *PAX5* (**Figure 1-2**) [3].



How quickly the leukaemia is eradicated in response to treatment to the level where it cannot be detected remains the single most powerful prognostic factor in paediatric ALL. The term employed for any approach used to measure and quantify sub-microscopic levels of disease is minimal-residual disease or MRD and will be discussed in detail in section 1.6.

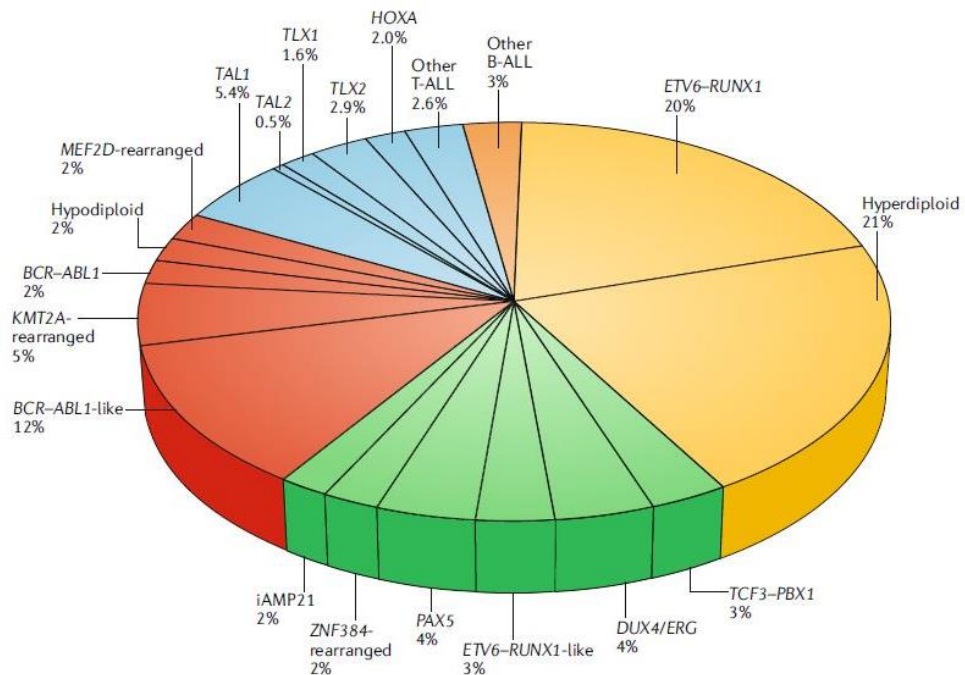


**Figure 1-2: Genetic subtype frequencies in paediatric ALL [3].**

### 1.2.1 Classical prognostic factors

Other than the genetic factors mentioned above, there are several well-established clinical prognostic factors such as age and white blood cell count (WBC) in B-ALL, where older children (>10) and with a WBC >50,000 mm<sup>3</sup> are considered high risk and children <10 years old with a WBC <50,000 mm<sup>3</sup> are considered standard risk [5]. The incidence of ALL peaks between the ages of two and five years old. Cases of infant ALL (<1 year old) comprise about 2-5% of childhood ALL cases and are considered a separate subgroup with poor prognoses as they tend to have a much

higher relapse rate [6, 7]. Age and WBC are unfortunately not a strong prognostic factor for patients with T-ALL. Males tend to have worse outcomes than females and this is thought to be due to the possibility of relapse in the testes and the increased incidence rate of T-ALL in males.

The ability to distinguish immunophenotype (B- or T-cell lineage) is another key prognostic factor in the treatment of ALL. Morphologically it is not possible to clearly distinguish between the two lineages. The expression of lineage specific markers for B-cells, also known as common acute lymphoblastic leukaemia antigen (CALLA), present on leukaemic cells is used for immunophenotyping in ALL and is achieved by multichannel flow cytometry (MFC). This is considered standard protocol in both diagnosis and in MRD monitoring. In B-cell ALL the main cell-surface and cytoplasmic markers used to detect both pre-B cell ALL and pro-B cell ALL are: CD19, CD10, CD22, CD34, CD20, CD24, CD79a and HLA-DR. In T-ALL the following markers are used to identify a T-cell phenotype: CD1a, CD2, CD3, CD4, CD5, CD7 and CD8. These markers are also known as leukaemia associated immunophenotypes (LAIP) because they don't appear in normal lymphocyte precursors [8]. Around 85% of paediatric ALL cases are B-cell-precursor ALL and overall have better outcomes than T-cell ALL cases.

Race and ethnicity remain persistent risk factors in ALL. Hispanic children have the highest risk of developing ALL whereas children of African descent have the lowest. However, children of Black and Hispanic descent tend to have worse prognoses compared to children of White/Asian descent. Epidemiological studies also provide evidence that a child's race or ethnicity also influences treatment efficacy [9, 10].

## 1.3 Biology of CNS-ALL

### 1.3.1 The leptomeninges and cerebrospinal fluid (CSF)

The CNS is composed of the brain and spinal cord which are both protected by the meninges. The meninges are made up of three layers, an outer layer called the dura mater which is the thickest layer lying underneath the skull, and two inner layers called the arachnoid mater and the pia mater which lie on top of the brain tissue. The inner layers are also known as the leptomeninges and the space between them is known as the subarachnoid space, home to cerebral blood vessels, a forest of structural stromal cells and the primary space for CSF circulation throughout the organ (**Figure 1-3**) [11].

CSF is a clear, colourless liquid with an ionic composition mainly comprising of  $\text{Na}^+$ ,  $\text{Cl}^-$  and  $\text{HCO}_3^-$  ions, and various others such as  $\text{K}^+$ ,  $\text{Ca}^{2+}$ ,  $\text{Mg}^{2+}$ ,  $\text{Mn}^{2+}$  and contains micronutrients such as vitamin C, folate thiamine monophosphate, pyridoxal phosphate and trace amounts of macro-molecules such as proteins and immunoglobulins. The majority of macro-molecules such as albumin and some micronutrients which make up the CSF either diffuse through the various blood-brain barriers freely are actively transported from the blood or are actively secreted by the choroid plexus in the brain [12]. The cellular composition of CSF is primarily made up of leukocytes and monocytes in normal “healthy” CSF at a ratio of 2:1 respectively but with a low count of  $<5$  cells /  $\mu\text{L}$  [13].

CSF has several functions in the CNS, primitively, in the protection of the brain tissue, by filling the intermediary space in the leptomeninges and effectively cushioning the brain. It also provides nourishment and removes waste product for the essential metabolic processes that occur in this space through bi-directional flow

of CSF throughout the CNS maintaining a tightly regulated homeostasis [14]. CSF is secreted primarily by the choroid plexus as well as from the ependyma and parenchyma [15]. The flow of CSF has been named the third circulation and after secretion, CSF flows through the lateral ventricles to the third ventricle, through the cerebral aqueduct (aqueduct of sylvius) and into the fourth ventricle where it then fills the subarachnoid space around the brain and spinal cord and finally it is absorbed back into the blood through the arachnoid villi at major veins or potentially through a supporting glymphatic system (**Figure 1-4**).

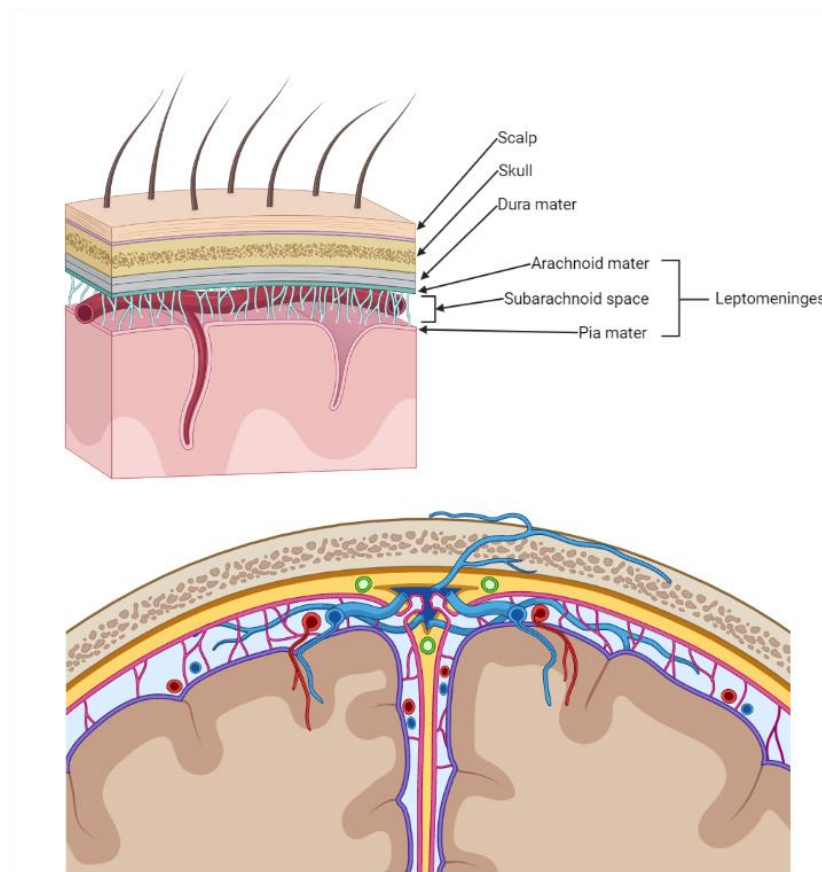


**Figure 1-3: Anatomy of the Meninges.** Image produced on Biorender.

- ① CSF is produced by the choroid plexus in the ventricles.
- ② CSF flows from the third ventricle through the cerebral aqueduct into the fourth ventricle.
- ③ CSF in the fourth ventricle flows into the subarachnoid space by passing through the paired lateral apertures or the single median aperture, and into the central canal of the spinal cord.
- ④ As the CSF flows through the subarachnoid space, it removes waste products and provides buoyancy to support the brain.
- ⑤ Excess CSF flows into the arachnoid villi, then drains into the dural venous sinuses. Pressure allows the CSF to be released into the blood without permitting any venous blood to enter the subarachnoid space. The greater pressure on the CSF in the subarachnoid space ensures that CSF moves into the venous sinuses.

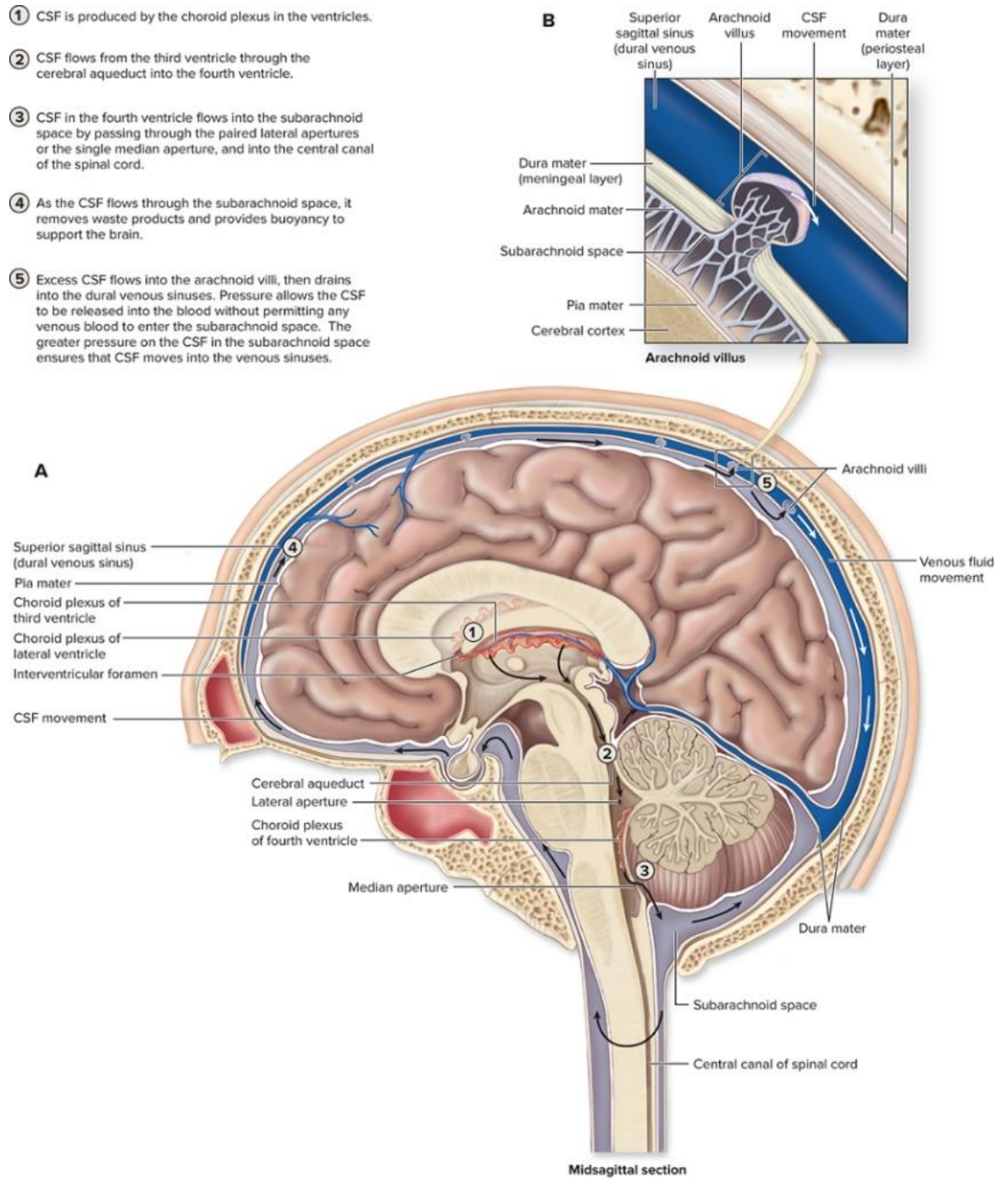


**Figure 1-4: Cerebrospinal fluid secretion and flow around the CNS.** Source: Basso et al., [16]

### 1.3.2 Mechanisms of CNS infiltration

The mechanisms of blast infiltration into the CNS are poorly understood, it appears that following leukaemic origin in the bone marrow and transit into peripheral blood, ALL has a proclivity to metastasize into the CNS. Infiltration has been shown to begin in the walls of the superficial arachnoid veins where it progresses through the leptomeninges, deep arachnoid and, in late-stage disease, into the parenchyma [17]. To date there has been no consensus on the primary avenue blasts take into the CNS. Originally it was thought that CNS infiltration occurred via the blood brain barrier. However, *in vivo* studies have failed to provide solid evidence for this [18].

The other main routes of CNS infiltration which have been most studied are the blood-CSF barrier (BCSFB) located in the choroid plexus and the blood-leptomeningeal barrier (BLMB) found in micro blood vessels on the surface of the pia mater (**Figure 1-5**). Evidence for CNS infiltration through the BCSFB and BLMB can be found in histological analysis of xenograft mice models where infiltration was observed in the arachnoid veins, leptomeninges and surrounding tissues [17, 19]. Post-mortem histopathological data from children with ALL also revealed similar progressive arachnoid infiltration [20]. Another potential route of infiltration is the blood-dural lymphatics barrier (BDLB) located in the dural lymphatic system in the meninges. This system absorbs CSF from the subarachnoid space and is responsible for clearing macromolecules from the CNS [21].

Recent evidence has shed light on a novel mechanism of infiltration through the meningeal vessels and emissary veins connecting the bone marrow and subarachnoid space in the CNS of mice. This novel mechanism is dependent on the expression of  $\alpha 6$  integrin in leukaemic cells and the presence of laminin receptor on the epithelial cells of the vein surface. Most leukaemic blasts are known to express

the laminin receptor  $\alpha 6$  integrin and through a multitude of *in vitro* and *in vivo* experiments. Yao et al., demonstrated that ALL cells infiltrated the CNS through the laminin<sup>+</sup> extracellular matrix of emissary bridging blood vessels [18].

There exists the possibility that blasts may be introduced accidentally during routine clinical procedures involved in the treatment of ALL. Incidence of traumatic lumbar punctures (TLP) occur often where peripheral blood possibly containing blasts, contaminates the CSF [22]. This phenomenon is unproven however, and it is likely that the CNS already contains blasts.

Once the blasts have successfully infiltrated the CNS, evidence shows that they have an inherent tendency to adhere to the meningeal stroma and are typically not found floating in the CSF [37, 39]. An *in vitro* study by Akers et al., provided further evidence of this adherence using co-cultured ALL cell lines (REH and SUPB-15) alongside human meningeal cells, human choroid plexus epithelial cells and human astrocytes where they demonstrated ALL cell migration towards CNS cells by chemotaxis of chemokine CXCL12 (secreted by CNS cells), and subsequent adherence to subarachnoid-derived cells [23]. They also showed that these B-cell leukaemic cell lines expressed adherence junction proteins PECAM1 and VE-cadherin supporting the CNS-entry mechanisms into the CNS through endothelial cells barriers found at sites such as the BCSFB and BLMB. Other molecules such as vascular endothelial growth factor A (VEGFA) has also been shown to be highly expressed in BCP-ALL cells. Muench et al., showed an *in vitro* increase in trans-endothelial migration of ALL cells correlated with high VEGFA expression [24].



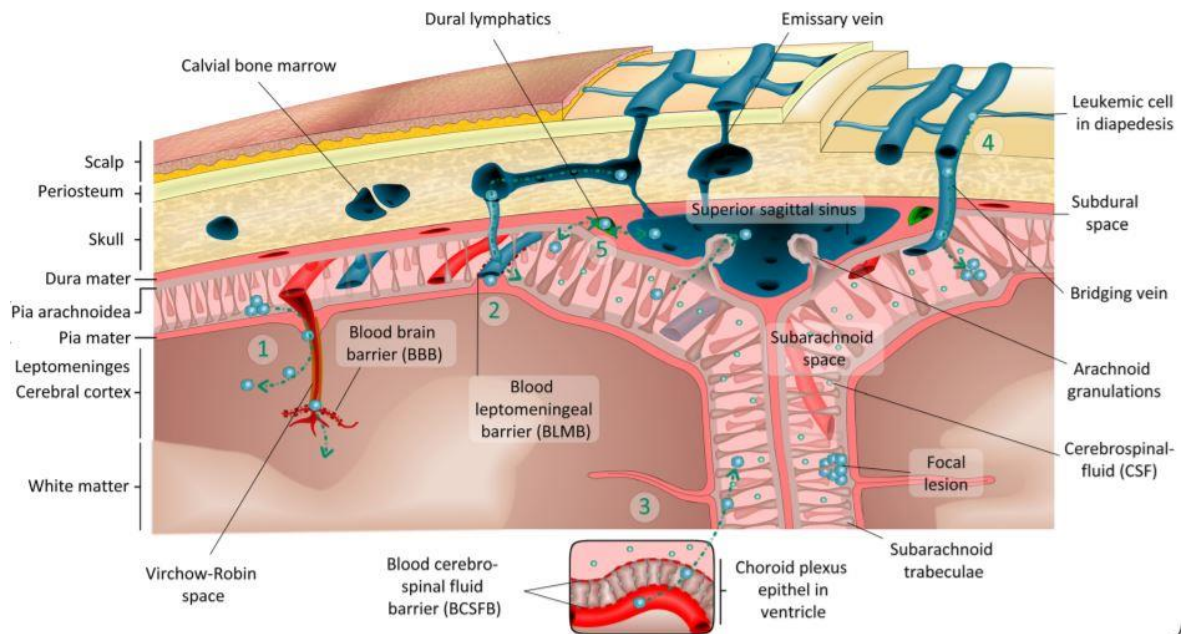


**Figure 1-5: The meninges and potential routes of CNS infiltration.** (1) Infiltration through the BBB; (2) Infiltration through the BLMB; (3) Infiltration through the BCSFB; (4) Infiltration through bridging vessels; (5) Infiltration through the BDLB [25].

What is not yet clear is if the CNS-entry mechanisms for B-cells and T-cells under normal physiological conditions are manipulated in CNS infiltration. T-cell leukaemias are associated with an increase in CNS relapses and both B and T-cells can be found in normal CSF, with higher amounts of T-cells. These T cells have been shown to express high levels of chemokine receptors such as CXCR3 and CCR7. Indeed, malignant T cells have been found to have upregulated CXCR3 and CCR7 and high levels of CCR7 ligand CCL19 in the choroid plexus suggesting a potential entry mechanisms for T-cells [26].

Whether leukaemic blasts have an intrinsic ability to migrate to the CNS is highly debated. One study proposed two potential models where, in model 1, only some leukaemic blasts acquire the ability to traffic to the CNS and, in model 2, all leukaemic blasts can traffic to the CNS regardless of subtype. Using xenograft



mouse models, the authors saw a 79% engraftment of CNS leukaemia supporting model 2, with trafficking to the CNS being a ubiquitous trait of the majority of blast cells, but not all [17]. In another study, Bartram et al., used high throughput sequencing (HTS) of immunoglobulin gene rearrangements to investigate clonal architecture in paired bone marrow and CNS diagnostic and relapse samples in 12 patients with B-cell precursor ALL. The authors hypothesised that leukaemic blasts are capable of trafficking freely between the bone marrow and the CNS. Nine out of eleven relapse patients presented with shared leukaemic subclones between the bone marrow and CNS and a rise and fall in the subclones could be clearly observed suggesting that leukaemic blasts are free to traffic into the CNS and bone marrow (**Figure 1-6**). The rise and fall and consequent dominant presence of a clone(s) in either the bone marrow or the CNS at diagnosis or relapse could be caused by selection pressures such as treatment causing a migratory effect or, alternatively, by clonal evolution occurring in both the CNS and in the bone marrow [27]. Both patterns were seen in this study (**Figure 1-7**).

The authors also analysed paired samples of four patients with apparent isolated CNS relapses. However, using this HTS method the study proved that sub-microscopic levels of the clones were detectable thus strengthening the evidence that leukaemic blast can freely traffic from the bone marrow and CNS and vice versa.

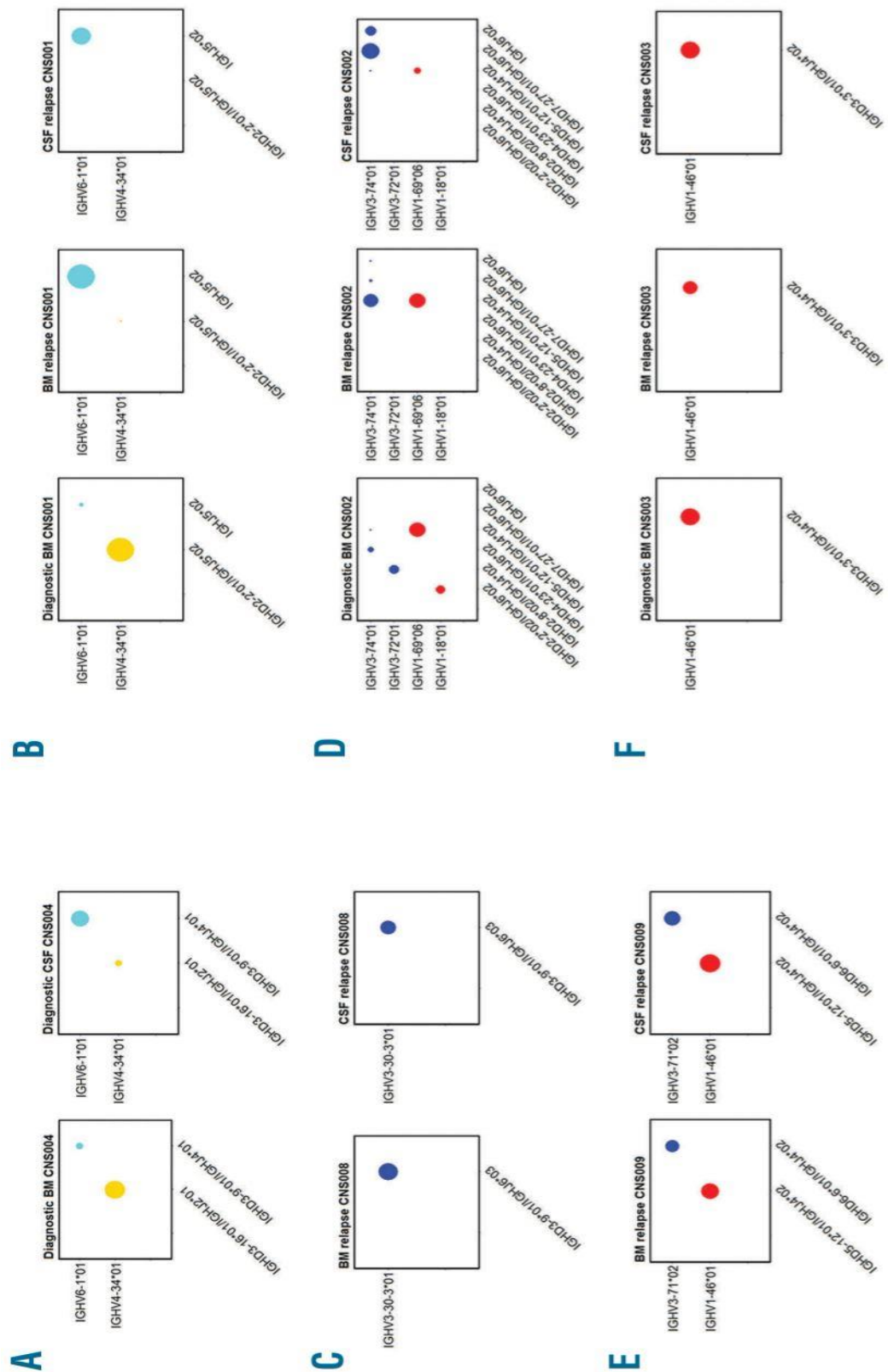


**Figure 1-6: Schematic representation of clonal distribution in bone marrow (BM) and CNS in matched diagnostic and relapse samples.** (A) Shared dominant clones in BM and CSF compartments at diagnosis; (B) Two clones present in diagnostic BM; one dominant, one minor. BM relapse presents with reversed clonal dominance. CSF relapse presents with only one clone and the disappearance of the original major diagnostic BM clone; (C) Shared single dominant clone in BM relapse and CSF relapse; (D) Several clones in Diagnostic BM compartment. BM relapse

and CSF relapse present with two original clones and two new clones which were originally absent in the diagnostic BM compartment; (E) Two shared dominant clones in BM relapse and CSF relapse; (F) Single dominant clone in diagnostic BM compartment present in both BM and CSF relapse [27].

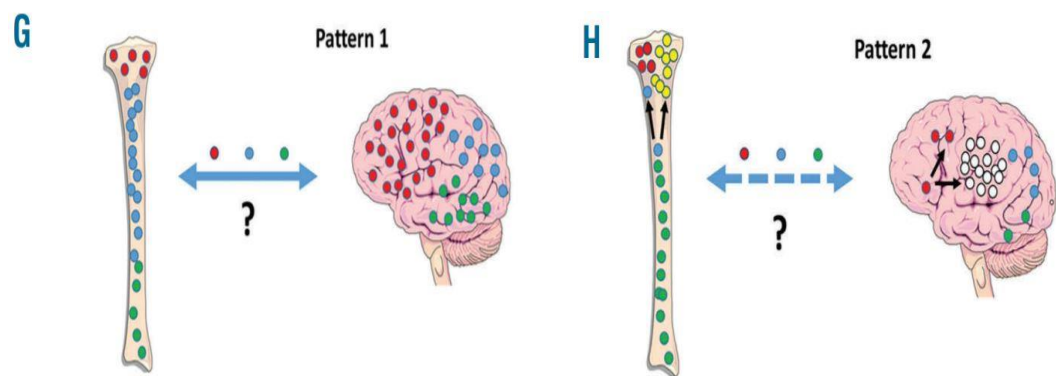


**Figure 1-7: Patterns of Clonal distributions by either free blast trafficking between the BM and the CNS (Pattern 1) or clonal evolution occurring in the BM or the CNS (Pattern 2) [45].**

## 1.4 Clinical aspects of CNS-ALL

### 1.4.1 CNS-ALL diagnosis

Blasts in the CNS generally proliferate at a much slower rate than in the periphery or bone marrow [28]. The ability to detect CNS-ALL most likely occurs from the progressive accumulation of slowly proliferating blasts in the CNS or by continuous infiltration from the periphery by methods of free trafficking discussed above.

Most patients do not present with clinical symptoms of CNS-ALL. CNS-ALL is typically detected and diagnosed by cell count and cytological examination (CM) of the CSF by cytopspin following lumbar puncture. Routine lumbar punctures extract a small volume of CSF (< 1 mL) prior to administering intrathecal chemotherapy [29].

Upon diagnosis, patients are classified as either CNS1, CNS2, CNS3 or TLP+/- (**Table 1-1**) [22, 28]. This diagnostic classification scheme has moderate specificity, although it can correctly classify CNS1 and CNS3 patients relatively well, with clinical outcomes tending to be worse for CNS3 patients than in CNS1 patients; CNS2 patients are often misclassified. A study comparing CSF cytology and flowcytometric immunophenotyping (FCM) (a more sensitive method to detect CNS-ALL) indicated a discordance of between CNS2 patients and flow cytometry negative patients, highlighting a high false-positivity rate when using CSF cytology which could be explained by the poor ability of CSF cytology to differentiate between blasts and reactive T-cells [30]. CSF cytology also has low sensitivity as it currently diagnoses only ~2 - 4% of patients with CNS-ALL. A classification of CNS1 does not necessarily indicate absence of leukaemic infiltration and several studies have shown that the vast majority of CNS relapse cases tend to occur in CNS1 patients and non-high-risk patients [22, 28, 31].

Evidence clearly shows that the risk of CNS-relapse in CNS3 patients is higher although few patients present with CNS3 at the time of diagnosis [32]. This suggests that CNS infiltration occurs much earlier than thought in the progression of the disease. Patients who present with CNS2 and CNS3 are generally put on higher intensity treatment regimens which, in turn, reduces their overall risk of relapse.

<b>Classification</b>	<b>Lymphoblast presence in CSF</b>	<b>WBC count in CSF (cells/uL)</b>	<b>RBC count in CSF (cells/uL)</b>
<b>CNS1</b>	Absent	$\leq 5$	$< 10$
<b>CNS2</b>	Present	$< 5$	$< 10$
<b>CNS3</b>	Present	$\geq 5$	$< 10$
<b>TLP +</b>	Present	$< 5$	$> 10$
<b>TLP -</b>	Absent	$\leq 5$	$> 10$

**Table 1-1: CNS-ALL classification.** WBC - White blood cell; RBC – Red blood cell

TLP occurs in up to 20% of all children and the introduction of peripheral blood into the CSF may compromise CSF analysis. Incidences of TLP with positive blast cytology (TLP+) at diagnosis have also been reported to increase risk of CNS-relapse [31, 33]. Other prognostic factors such as having a T-cell immunophenotype or having high-risk cytogenetics such as *BCR-ABL1* also confer an increased risk of CNS relapse.

A more sensitive method of CNS diagnosis and risk stratification which is commonly used is flowcytometric immunophenotyping (FCM). This technique is common for examination of BM for leukaemic diagnoses and has demonstrated a higher

sensitivity in comparison to conventional FCM examination for detecting CNS-ALL [34, 35]. Its use in identifying leukaemic cells in CSF is effective, although an important limitation is that it most likely does not represent total leukaemic burden in the CNS and rapid death of leukocytes after sampling can occur, however this can be addressed by the use of Transfix stabilisation [34, 36].

Interestingly, recent work by Thastrup et al., 2019, demonstrated that flow cytometry combined with cytopsin analysis of the CSF and other classic prognostic factors provides a strong, independent predictor of relapse in the bone marrow compartment in comparison to cytopsin analysis alone. They revealed that a higher blast level in the CSF correlated with an increased risk of relapse in the bone marrow, however it did not predict CNS-relapse [37]. This study could not identify a low-risk group suitable to reducing treatment. In addition, 25% of CNS1 patients were FCM+ suggesting that these patients would require more therapy above current levels, potentially leading to more toxicity.

Using PCR to amplify and detect genomic DNA isolated from blasts in the CSF is another alternative and potentially highly specific method for detection of sub microscopic CNS-ALL although it is unsensitive as it only detects CNS involvement in a third of patients. The low sensitivity is thought to be caused by clonal evolutions which can occur in the CNS and BM (described in **1.3.2**). Studies have, however, found concordance between cytopsin and PCR+ patients in some cases. Further investigation into whether being PCR+ increases risk of CNS-relapse is needed [38].

The lack of predictive biomarkers for CNS diagnosis/relapse and an incomplete understanding of fundamental CNS-disease mechanisms are the major challenges in improving risk-stratification and treatment of CNS-ALL.

### **1.4.2 Relapse**

The relapse rate for children with ALL is around 10-20% and whether a child will relapse or not is strongly related to the patients' genetic subtype, immunophenotype, and efficiency and duration of remission following frontline therapy. Generally, T-cell leukaemia is more likely to cause relapse than B-cell leukaemia. Evidence has shown that patients who relapse within the first six months following remission, tend to have poor prognoses whereas patients with late relapses have better prognoses.

Before the introduction of intrathecal chemotherapy, the poor penetration of systemic chemotherapy into the CNS led to an increase in CNS relapse rates and high levels of subsequent mortality. The most common sites of relapse in ALL are the CNS, the bone marrow, and the testes in males. The CNS is an important sanctuary site in childhood ALL as it is responsible for >40% of relapses [39]. CNS relapse carries a poor prognosis and even with transplantation the event-free survival is only 45% [40].

## **1.5 Treatment**

### **1.5.1 Systemic treatment**

Until the 1960s ALL was generally a fatal disease and patients were treated with monotherapies resulting in very short remission times. The major breakthroughs in treatment for ALL were: (i) the introduction of combined treatments such as mercaptopurine and methotrexate; (ii) the introduction of structured treatment regimens; (iii) the administration of intrathecal therapy and cranial irradiation to eliminate CNS-ALL; and (iv) the introduction of personalised doses of systemic

methotrexate based on a patient's blood count and mercaptopurine, on the basis of genotype.

Improvements in supportive care therapy over the years also contributed to the improvement of OS. As outcomes improved drastically, these breakthroughs paved the way for the new era of personalised treatment we see today.

Over the years chemotherapy agents such as Daunorubicin (anthracyclines); prednisolone, dexamethasone (corticosteroids); 6-Mercaptopurine (purine analogue) have remained the same in the treatment of ALL. Today, these same drugs are used in combination with a further variety of drugs such as cytarabine, L-asparaginase, etoposide V16, 6-, cyclophosphamide, as well as supportive care therapies such as allopurinol and rasburiscase which are used in the first five days of treatment to prevent tumour lysis syndrome; as well as antibiotics, antifungals, and antivirals. All patients are also treated with intrathecal methotrexate and sometimes this is supported with other agents such as intrathecal cytarabine and hydrocortisone/prednisolone.

Varied versions of the structured treatment regimen first proposed in the 1960s are in use today and the most common structure is composed of four stages: (i) remission induction, (ii) consolidation, (iii) delayed intensification, and (iv) maintenance. In the UK, treatment lasts two years for females and three years for males whereas several other regimens around the world do not give different lengths of treatment [41].

Remission induction (RI) is between four to six weeks long and aims to reduce the high levels of blasts in the body, in particular the bone marrow



and achieve clinical and morphological remission. Patients are treated with dexamethasone/prednisolone, vincristine, daunorubicin, pegaspargase/crisantaspase, intrathecal methotrexate/ cytarabine/hydrocortisone and mercaptopurine. Patients begin intrathecal chemotherapy from Day 1.

Consolidation is between 10-12 weeks long and is tailored to the patients' individual risk to target the residual levels of blasts following remission induction using a variety of combined therapies. It is more intensive than RI and the combination treatments are intended to prevent the development of resistance to chemotherapy.

Delayed Intensification (DI) occurs towards the end of Consolidation and is a shorter combination of the RI and Consolidation.

Maintenance lasts for two to three years depending on gender in some regimens and begins if the leukaemia has remained in remission following the previous stages. The aim of this stage is to target any residual blasts which divide slowly. Most treatment regimens use mercaptopurine, methotrexate (administered weekly), vincristine and either dexamethasone or prednisone.

### **1.5.2 Clinical trials in the UK**

The UKALL trials began in the 1970s and followed on the initial improvements made at St. Jude's (described in **Figure 1-1**). UKALL VIII in the early 1980s introduced continuous, intensive therapy using maximum tolerated dosages, which led to an increase in Event-Free Survival (EFS) by 20%. Trials in the latter half of the 1980s (UKALL X) saw the introduction of two five-day post-remission delayed

intensification treatments at week 5 and week 30 with daunorubicin further increasing EFS to 72%. UKALLXI in the 1990s saw the introduction of a third delayed intensification block of treatment at week 35 as well as the efficacy of continuous high dose intrathecal therapy, namely methotrexate, which would replace the use of cranial irradiation. In the late 1990s, the ALL97/99 trial saw changes in asparaginase dosage practices and a change to a more intensive but less myelosuppressive delayed intensification blocking scheme. It was around this time that patients also began to be treated according to risk-stratification. Patients were placed in treatments arms A, B or C which varied drug usages and doses according to a patient's clinical characteristics. ALL97/99 also saw the use of dexamethasone and prednisolone where patients were randomised to either dexamethasone or prednisolone. The trial resulted in a reduction of both systemic and CNS relapse using dexamethasone alone in a third of patients enrolled on the trial.

Minimal residual disease monitoring and its implementation in risk-stratification was first employed in the UK2003 trial after several large international studies demonstrated it as the single strongest predictor of outcome. This trial showed that patients who were deemed high risk MRD were three times as likely to relapse than low risk MRD patients. This trial however, increased the event-free survival (EFS) of patients to 87.7% and the overall survival to 91.3% in the UK [42].

The aim of UKALL2011 was to build upon and improve the use of MRD to risk-stratify patients and direct treatment by increasing survival rates while maintaining safe and if possible, reduced amounts of chemotherapy. MRD was measured at day 29 and at week 14 using RT-qPCR with a sensitivity down to 0.01%. Patients who took part in the randomised trial were either administered dexamethasone at a low

dose for 28 days or a high dose for 14 days and it was shown that the shorter, more intensive course of treatment was equally as toxic as the longer, less intensive course and no correlation with MRD was found [43, 44]. This trial also saw the introduction of a single DI stage to all patients to try to further reduce toxicity.

The ALLTogether trial is not an exclusive UK trial but is a European collaboration study made up of 14 countries from several study groups including UKALL, NOPHO (Nordic countries + Estonia and Lithuania), DCOG (the Netherlands), COALL (Germany), BSPHO (Belgium), SHOP (Ireland) and SFCE (France). The pilot study began recruitment in 2019 where patients were risk-stratified by a personalised algorithm based on clinical characteristics. The main trial began in 2020 and is ongoing. It involves a more in-depth look at genetic changes throughout treatment and response to therapy.

### **1.5.3 CNS-Treatment**

Today all children with ALL receive a combination of systemic drugs that penetrate the CNS (such as dexamethasone and high dose IV methotrexate as well as harsh and potentially neurotoxic CNS-directed chemotherapy administered intrathecally even if patients present with negative CSF cytology and white cell count to reduce the incidence of CNS-relapse.

Intrathecal administration is crucial as it bypasses the blood-brain barrier (BBB), and the therapy is injected directly into the CSF increasing exposure of the drugs in the CNS [45]. The main drug used to treat CNS-ALL is methotrexate, administered in high doses directly into the CNS. This CNS-directed treatment has resulted in both short and long-term neurotoxicity and detrimental effects on the brains of developing children and can present as serious adverse events (SAEs) including stroke-like

syndrome (SLS), seizures, and posterior reversible encephalopathy syndrome [46, 47].

Results from the MRC UKALL XI trial demonstrated a decline in patient IQ scores three to five years after diagnosis/treatment compared to healthy controls [48]. Patients were enrolled onto treatment regimens of 1) intrathecal methotrexate vs high-dose systemic methotrexate and 2) high-dose systemic methotrexate/intrathecal methotrexate vs short course intrathecal methotrexate/cranial irradiation. Both treatment arms resulted in low IQ scores. At the time cranial irradiation was a highly successful method of treatment but it resulted in an increase of radiation-induced complications and high incidences of secondary malignancies [49]. It wasn't until the introduction of triple intrathecal treatment with methotrexate, hydrocortisone and cytarabine that it was removed as a treatment option for patients in most of the world. However, it is still used in some countries at lower doses and usual only in high-risk patients or those with a high tumour burden in the CNS.

## **1.6 Minimal Residual Disease (MRD)**

Following induction treatment many children with ALL will have residual blasts in their bone marrow and in the CNS as seen in the 10-20% of patients who relapse [50]. The number of remaining blasts can be so low that they can evade traditional detection methods and patients are typically asymptomatic. If left untreated, these residual cells can multiply and lead to relapse. MRD can be defined as any approach used to measure and quantify undetected, sub-microscopic levels of disease in order to measure depth of response to induction therapy and consequently determine the intensity of the follow-on therapy.

MRD is a well-established prognostic tool in ALL and MRD monitoring is considered an extremely accurate method for measuring relapse risk compared to conventional risk factors and patients who are positive for MRD demonstrate an increased risk of relapse. An important factor in the clinical management of childhood ALL patients is tailoring treatment according to the patient's individual risk category. Studies have shown that the absence of MRD in the bone marrow yields a good prognosis and that the level of MRD is proportional to the patient's risk of relapse. In patients who achieve remission, those with residual disease have an increased risk of relapse. It has also been shown to be the most powerful prognostic factor, independent of other clinical risk factors.

There are three main methods of detecting MRD that can reach sensitivity levels of 1 in  $10^3$ - $10^5$ : (i) flow cytometry of immunophenotypic markers; (ii) detection of gene fusions by PCR; (iii) immunoglobulin and T-cell receptor gene rearrangements by PCR.

### **1.6.1 Flow Cytometry**

As mentioned in section 1.2.1, there are several LAIP cellular markers that are differentially expressed in B and T cells, which can be used to identify and track blasts using flow cytometry. It is important to be able to profile the leukaemic phenotype at diagnosis against reference bone marrow samples and fortunately, this technique can be applied to >90% of all cases with a sensitivity of 1 in  $10^{-3}$  -  $10^{-4}$  cells [51]. However, this technique has its limitations as it requires cell samples to be as fresh as possible when being sent to MRD referral laboratories. This may be overcome by using transfix which allows sample stability for up to 72 hours. It also requires a high level of data interpretation due to the complexity in assigning correct ALL phenotypes. False positives arising from the presence of normal lymphoid cells

co-expressing common ALL phenotypes are also another factor for consideration and highlight the need for data interpretation specialists.

### **1.6.2 Polymerase chain reaction (PCR) of gene fusions**

This technique can be used for MRD analysis to target the >40% of patients who harbour aberrant chromosomal translocations. The *ETV6-RUNX1* translocation is the most commonly found chromosomal translocation in 25-30% of patients. Typically, the starting material to target these fusion transcripts is RNA as the translocation breakpoint regions in DNA can be extensive. Evaluation of fusion transcripts is an easy and quick method for diagnostic MRD analysis as the same primers can be used in several patients for the transcripts [52]. The RNA samples can then be quantified using a standard curve comprised of a serial dilution of amplified cell line or plasmid DNA allowing for a sensitivity of  $10^{-5}$ . However, this method is not patient specific, and its accuracy can vary due to the variation in RNA transcript expression within leukaemic cells of the same population as well variation found between different patients.

### **1.6.3 PCR of Immunoglobulin (Ig) & T-cell receptor (TCR) gene rearrangements**

The adaptive immune system in mammals is controlled by B and T lymphocytes and their ability to generate an antigen-specific response to pathogens by the generation of antigen receptors (AR). The highly specific way the body is able to combat antigens lies in gene rearrangements within the immunoglobulin (Ig) and T-cell receptor (TCR) gene loci. PCR amplification of Ig/TCR gene rearrangements is the most common technique used to detect and monitor MRD and can be applied in ~92% of all cases. In most diagnostic protocols MRD is detected using allele specific

oligonucleotide (ASO) primers for RQ-PCR quantification with a sensitivity of  $10^{-5}$  based off the EuroClonality-BIOMED 2 collaborative study performed in 2003 [53].

RQ-PCR is the most widely used tool for monitoring MRD in childhood ALL. Currently, at diagnosis genomic DNA isolated from leukaemic cells in the bone marrow is extracted and Ig/TCR rearrangements in gDNA will be amplified using consensus primers. The PCR product will then undergo clonality assessment using heteroduplex formation or gene scanning. Heteroduplex formation analysis involves denaturing the PCR products at 95°C for five minutes to create single stranded DNA followed by immediate renaturation at 4°C for one hour. This results in the formation of duplex DNA structures which are either heteroduplex when the PCR products are polyclonal, or homoduplex when the PCR products are monoclonal. Polyclonal and monoclonal duplexes run at different migration speeds on a gel where a normal polyclonal sample will appear as a smear whereas lymphoproliferative monoclonal samples will present with a single band. A leukaemic population will typically appear as a monoclonal band and the DNA is subsequently isolated and sequenced using Sanger sequencing to obtain the highly specific junctional region DNA sequence. Patient specific ASO primers are then designed for RQ-PCR against this sequence for subsequent MRD monitoring throughout treatment.

#### **1.6.3.1 Biology of *Ig/TCR* Gene rearrangements**

Malignant cells of a leukaemic population are the offspring of a single transformed cell and therefore a leukaemic cell population which is clonally related and can be classified as monoclonal. Monoclonality in malignant populations is an important hallmark and useful tool which is exploited in MRD monitoring. In lymphoid malignancies, clonality can be tracked by targeting rearrangements of the Ig and TCR genes.

These gene rearrangements are not related to the pathogenesis of ALL but as all leukaemic cells derive from an original malignant, transformed cell, all cells of that population will carry an identical Ig or TCR rearrangement and effectively act as molecular “fingerprints”. The B- lymphocyte Ig repertoire diversity is further amplified when they reach maturity through somatic hypermutation events upon antigen recognition. As leukaemia is a disease of immature lymphoid blasts, this will not be discussed further. Once recombined, these genes form the highly variable region on antibody heavy and light chains (**Figure 1-8C**).

The Ig and TCR gene loci are composed of several variable (V), diversity (D) and joining (J) segments that recombine in a stepwise manner during early lymphoid differentiation to produce highly diverse junctional regions. The Ig cluster of genes include: immunoglobulin heavy chain (IGH), immunoglobulin kappa (IGK) and immunoglobulin lambda (IGL) whereas the TCR cluster of genes include: T-cell receptor alpha (TCR $\alpha$ ), T-cell receptor beta (TCR $\beta$ ), T-cell receptor delta (TCR $\delta$ ), T-cell receptor gamma (TCR $\gamma$ ). Gene rearrangements in IGH, TCR $\beta$  and TCR $\delta$  genes occur stepwise with D to J rearrangement first, followed by V to DJ rearrangement (**Figure 1-8A**). In IGK, IGL, TCR $\alpha$  and TCR $\gamma$  genes there is a sole V to J rearrangement (**Figure 1-8B**).

Throughout these recombination events, nucleotides are also randomly inserted and deleted, massively increasing the diversity of these junctional regions. The junctional region is known as the Complementarity-Determining Region 3 (CDR3) and is highly variable [54]. Following rearrangement of the gene segments, a single, highly specific exon is created marking the clonality of that cell. These gene rearrangements can therefore be used as clonality markers capable of being detected and tracked from diagnosis throughout treatment.



At the coding flanks of V, D, and J segments, there are sequences of conserved bases arranged as heptamers and nonamers with either 12 or 23 base pair spacers located within them. The heptamer/ nonamer sequences contain conserved bases at conserved positions within them and are referred to as recombination sequence signals (RSS) (**Figure 1-9A**). The conserved CAC trio is conserved 99% of the time and the AA doublet is conserved 91% and 97% respectively [55]. The other bases can vary but the most successful recombination's do not stray far from the consensus sequence. RSS are the only DNA segments required to allow VDJ recombination to occur.

The enzymes responsible for binding to the RSS and initiating recombination are the recombination activating genes 1 and 2 (RAG1 & RAG2). RAG enzyme RAG1 is made up of 1040 amino acids and alone can catalyse the rearrangement reaction. It has a core region where it binds to the RSS nonamer sequence and contains the catalytic amino acids necessary for the cleavage reaction. RAG2 is made up of 527 amino acids and generally serves as a cofactor for RAG1 [56].

The RAG1/RAG2 complex binds to the nonamer sequence coding segment with either a 12 or 23 bp spacer. It then bends the DNA around the strand containing the corresponding partner 12 or 23 bp spacer and coding segment. Only this combination of 12 and 23 bp spacer will allow for RAG1/RAG2 recombination to occur. This 12/23 spacer pairing rule therefore only allows the random rearrangement to occur between appropriate V, D or J segments during this process. The orientation of the coding flanks is also a factor in the proceeding rearrangement as it will direct recombination through either deletional, inversional or hybrid joining (**Figure 1-9B**). Deletional joining is the most common type of rearrangement mechanism and occurs 2x more frequently than inversional joining

and it relies on the two corresponding RSS signals having opposing orientations. This rearrangement results in the creation of precise RSS signal joints which are excised as circular by products and imprecise coding joints where random insertion of N-nucleotides and non-random insertion of P-nucleotides occurs between the coding segments. Inversional joining occurs much less frequently and occurs between coding segments with RSS in the same orientation. Hybrid joining is an improper type of recombination and does not result in coding diversity.

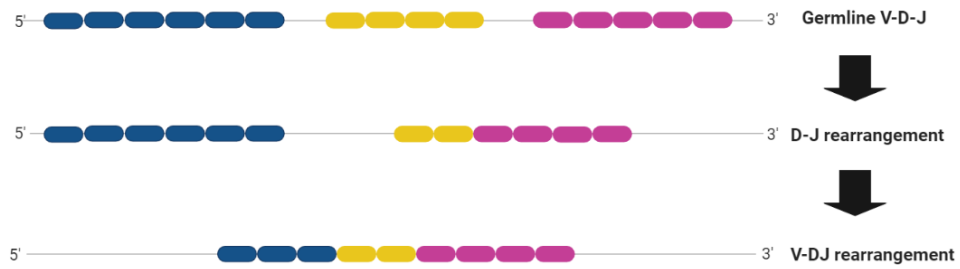
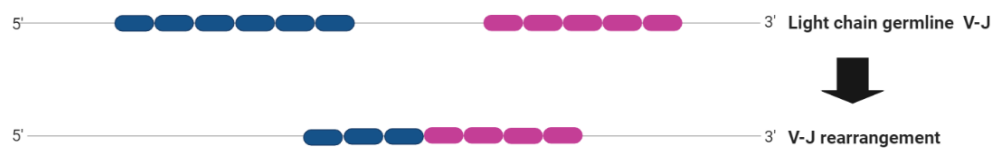
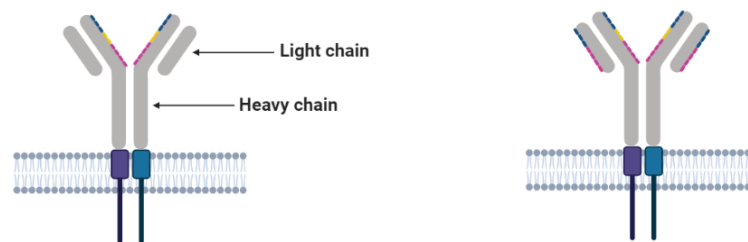
Deletional joining involves the formation of a coding joint and an excised signal joint and the signal joints tend to be around 200 bp apart. The recombinases RAG1/RAG2 bind to the 12RSS or 23RSS of the V, D or J coding segment and form an RSS complex along with DNA bending factors HMG1A/HMG1B. Upon binding, one RSS strand is nicked at the junction between the heptamer and the adjacent coding flank within the RSS complex and this results in the folding of the DNA to bring the downstream or upstream corresponding RSS into proximity and be captured within the RSS complex. Next, the RSS complex nicks the remaining RSS resulting in single-strand breaks with exposed -OH groups. The RSS complex now catalyses the cleavage transesterification reaction to yield clean double-strand breaks following with the formation of a covalently sealed DNA hairpin structure.

The RSS complex resolves the RSS signal joints into circular excision circles. The coding hairpin structures are stabilised, aligned and kept in proximity by recruitment of another protein complex: DNA-PK holoenzyme (composed of Ku70/Ku80, DNA-PKcs, ATM and Artemis) to the RSS complex. DNA-PKcs promotes the hairpin opening activity of Artemis [57]. The hairpins are now opened either symmetrically or asymmetrically. A symmetric hairpin break will result in the random addition of nucleotides to the 5' end by terminal deoxynucleotidyl transferase (TdT) whereas

an asymmetrical hairpin break leads to a palindromic overhang of bases. These bases are now filled in by DNA polymerase or can be randomly excised by exonucleases and the two coding genes are finally ligated by the non-homologous end joining (NHEJ) pathway (**Figure 1-10**).

The inversional joining mechanism is not too dissimilar from deletional joining in principle, it does however involve a more complex loop formation that brings the two RSS signals/ coding joints together. The signal joints to be joined tend to be separated by 3000bp. The signal joint is not excised but is incorporated into the sequence in an inverted orientation and therefore this mechanism involves the formation of two joints [58] (**Figure 1-11**). This type of rearrangement is less common but is seen in half of all V $\kappa$  to J $\kappa$  rearrangement. The fact that the signal joints are separated by 3000 bp may provide an explanation as to why these types of rearrangements occur less frequently [58].

Another possibility is the formation of a hybrid joint, where a coding segment is joined to a signal sequence. The mechanism is thought to be similar to deletional joining and occur frequently but appear to act as an intermediate stage between rearrangement steps [59]. It is unclear the true purpose of hybrid joints, but they are known not to contribute to diversity themselves and do not appear to play a role in oncogenesis.

**(A) IGH, TCR $\beta$  and TCR $\delta$  Gene rearrangement - Heavy chain****(B) IGK, IGL and TCR $\alpha$  Gene rearrangement - Light chain****(C) Loci of rearrangements on membrane bound BCR or TCR phenotype**

**Figure 1-8: Basic schematic diagrams of Ig/TCR rearrangement steps and loci on BCR/TCR phenotypes.** (A) IGH, TCR $\beta$  and TCR $\delta$  proceed with a three-step rearrangement; (B) IGK, IGL and TCR $\alpha$  genes proceed with a two-step rearrangement; Gene segment colours: Blue = V; Yellow = D; Purple = J. (C) Location of heavy chain and light chain loci on the BCR/TCR. Image produced on Biorender.

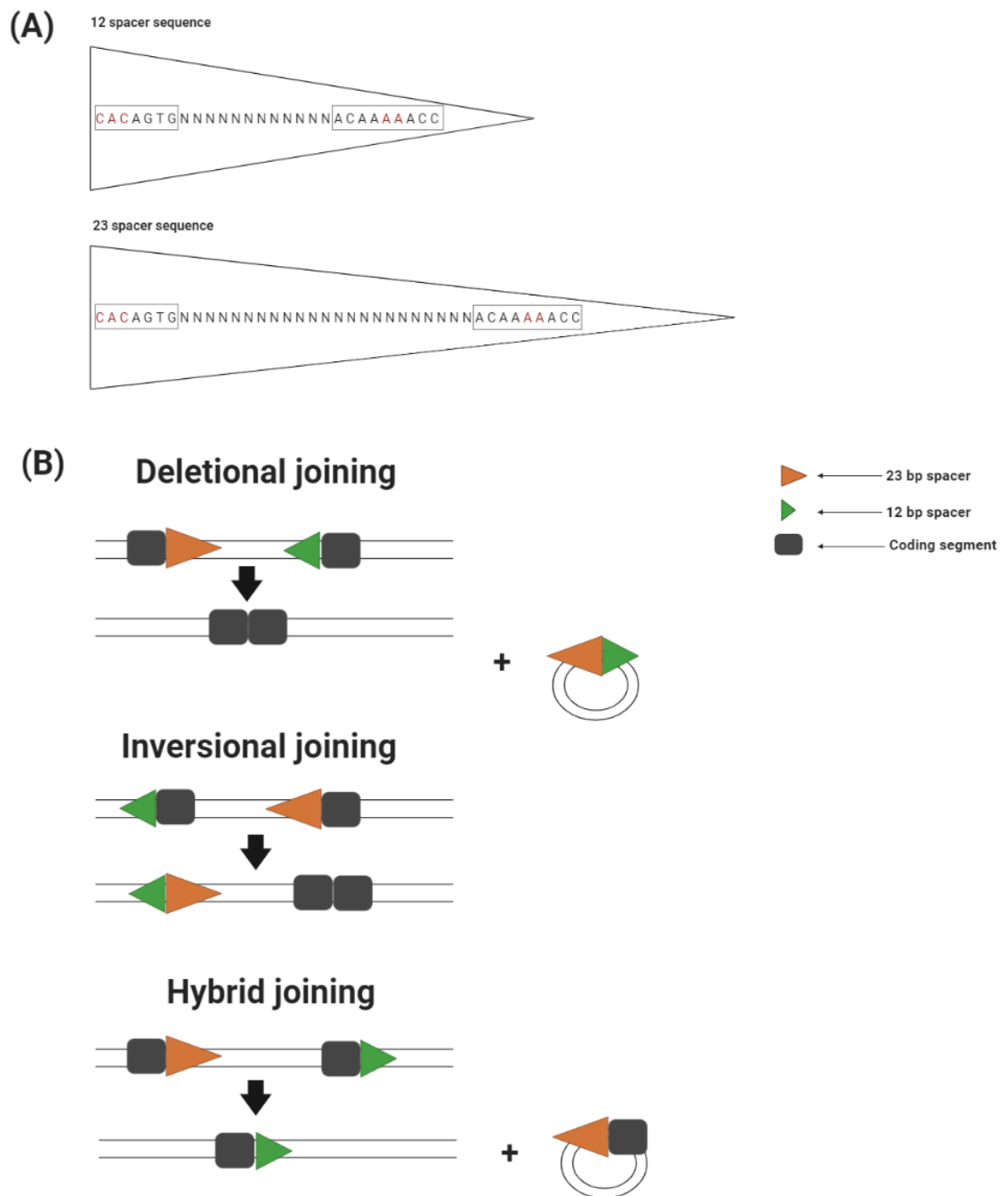


**Figure 1-9: 12/23 Spacer sequences and rearrangement mechanisms.** (A) Composition of 12/23 spacer sequence (ss). Bases in red are the most conserved (CAC – 99%; AA – 91% in 12 ss & 97% in 23ss) (B) Basic schematic diagram of the rearrangement mechanisms.

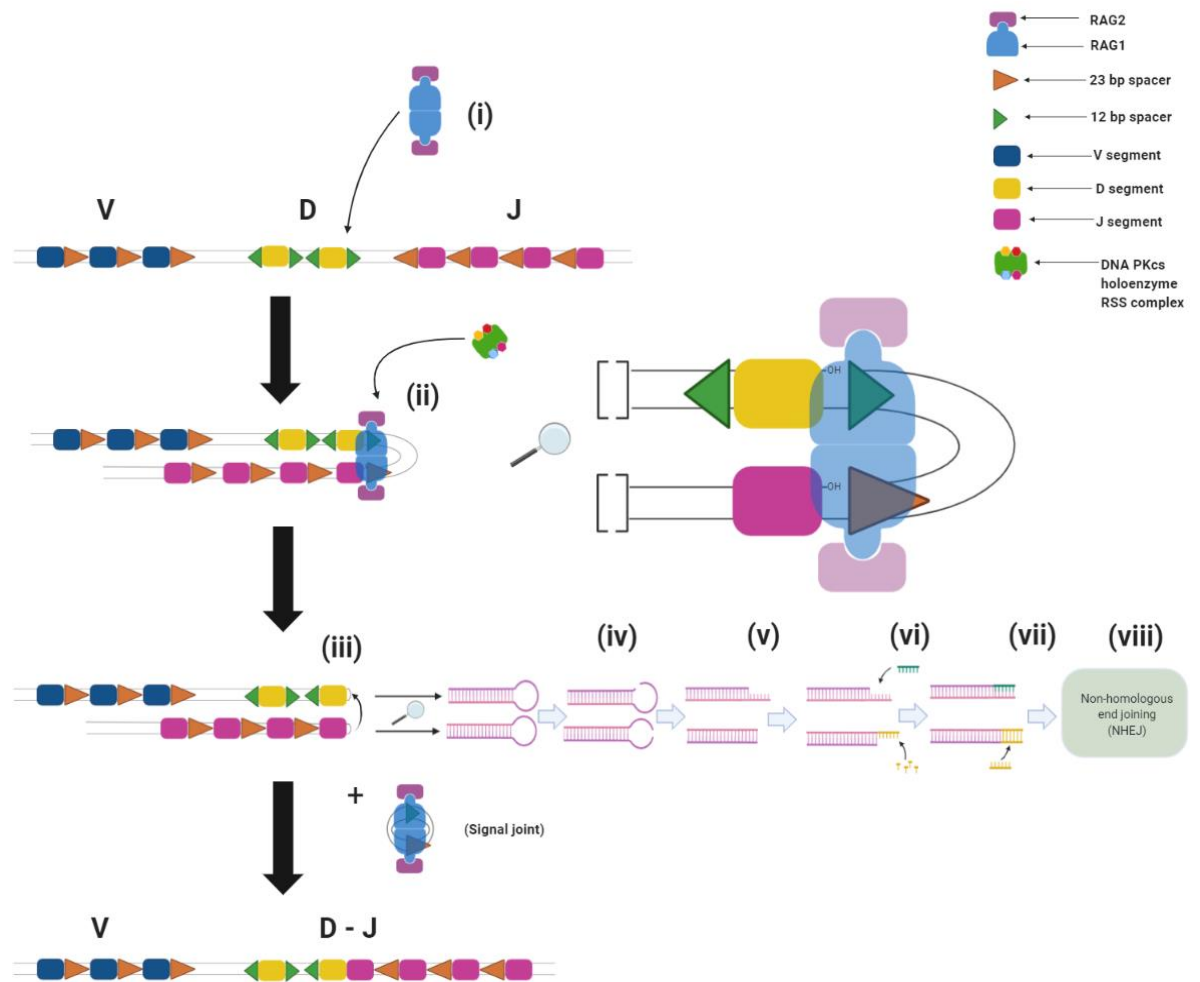


**Figure 1-10: Deletional joining mechanism.** (i) RAG1/2 recognition of RSS; (ii) Binding of DNA PKcs holoenzyme RSS complex to RAG1/2 and formation of recombination complex by DNA bending and secondary recognition and capture of partner RSS. Single-strand DNA cleavage and exposure of -OH groups; (iii) Formation of hairpin and (iv) Random cleavage of hairpin formation and endonuclease generation of P nucleotides and random addition/deletion of N nucleotides to exposed ends; (v-vii) repair and ligation of coding and signal sequences by NHEJ and dissociation of RAG 1/2 and signal joint complex (viii). The DNA holoenzyme complex remains bound after step viii but is not shown for clarity. Image produced on Biorender.

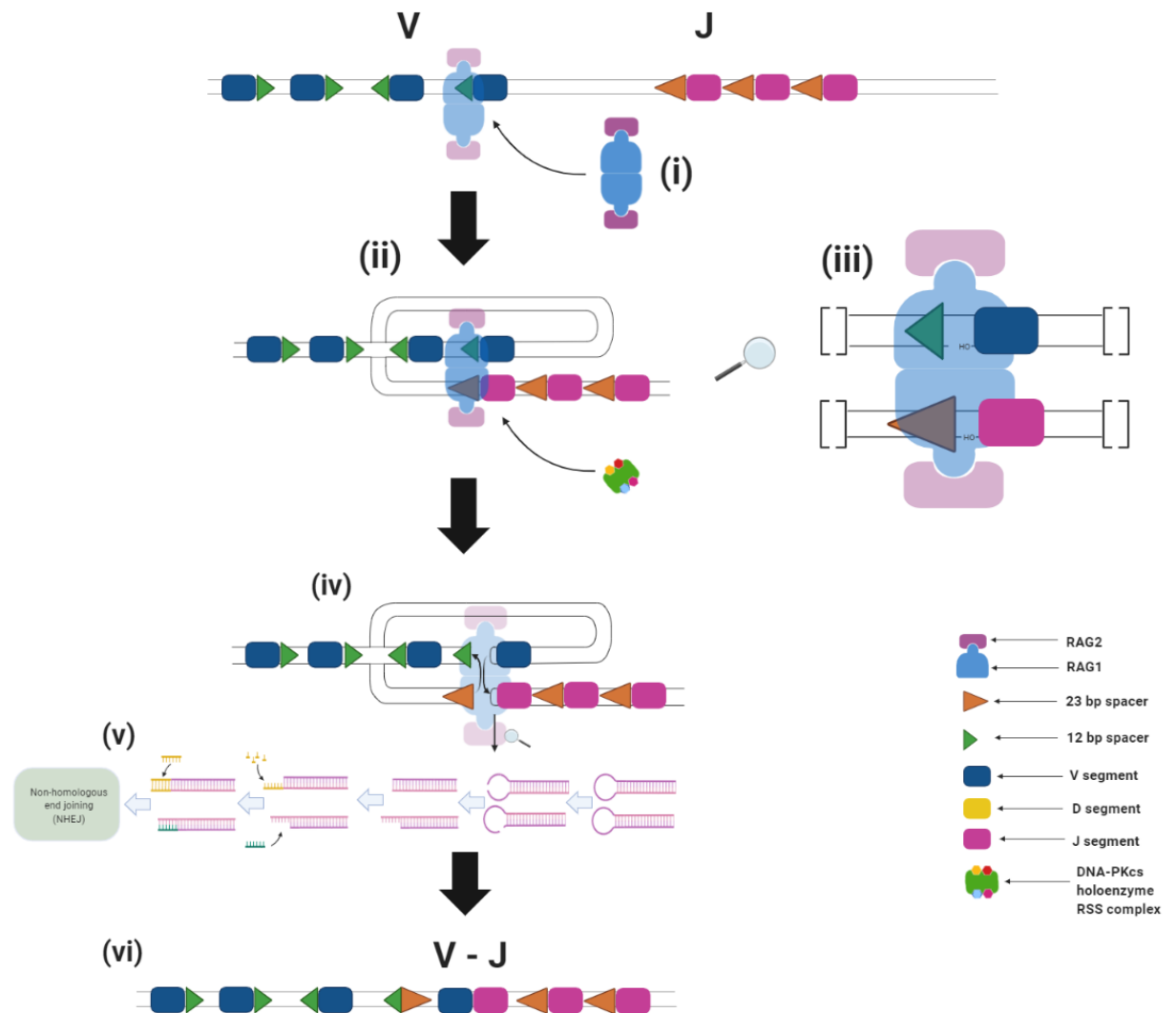


**Figure 1-11: Inversional joining mechanism.** (i) RAG1/2 recognition of RSS; (ii) Formation of recombination complex by DNA bending and secondary recognition and capture of partner RSS. (iii) Single-strand DNA cleavage and exposure of -OH groups; (iv) Formation of hairpin and double strand DNA break by RAG1/2. Inversion and formation of two joints, a coding joint and a signal joint. (v) Random cleavage of hairpin formation by endonuclease generating P nucleotides and random addition or deletion of N nucleotides to exposed ends; (v) repair and ligation of coding and signal sequences by NHEJ and (vi) dissociation of the RAG1/2 complex. Image produced on Biorender.

#### **1.6.4 Limitations of current MRD analysis techniques**

Flow cytometric profiling and real-time quantitative polymerase chain reaction (RQ-PCR) of leukaemic immunophenotypes are routinely used to monitor MRD. However, there can be significant discordance when comparing results. These are most likely due to factors such as clonal PCR-marker quality, non-specific background DNA amplification, oligoclonality and clonal evolution [60]. These methods of monitoring MRD do not consider the small number of cells that may avoid detection. Current flow cytometry methods struggle to reach the desired sensitivity needed for MRD [61].

A limitation of RQ-PCR is that it requires a reference standard curve containing diluted target Ig rearrangements. Sensitivity can also be affected by the presence of inhibitors within the PCR reaction mixture. Robustness is also strained in samples that lie at the maximum quantifiable range. These samples are often classified as positive nonquantifiable (PNQ) but are not considered to be clinically useful [62]. The workflow for RQ-PCR is expensive, complex and labour intensive and in the UK the first MRD test results are given at day 29, which ultimately inform the intensiveness of the remainder of the therapy. Unfortunately, this method is not applicable to ~2% of patients due to either inadequate samples, undetectable MRD targets, insensitive MRD targets caused by a lack of diversity in IG/TCR rearrangements in blasts and difficulties in interpretation when closely related markers appear in Ig or TCR loci.

Despite these limitations treatment strategies for Childhood ALL have been shown to have an excellent track record in delivering personalised risk-adapted therapy for systemic leukaemia [63]. Monitoring treatment response using PCR or flow cytometry (FCM) based BM minimal residual disease (MRD) measurements allows



safe reduction of treatment for low-risk patients and improves outcome by intensification of treatment in high-risk patients [28, 64-67].

Current MRD monitoring is, however, solely performed on bone marrow and has not yet been applied to monitor response to treatment and predict relapse at extramedullary sites such as the CNS and testes. Its use in analysis of peripheral blood has been studied and appears to be inadequate to monitor B-cell leukaemias as MRD levels have been reported to be 1-3 logs lower than in matched bone marrow biopsies [61]. The application of MRD to the CNS is very clinically important for the future of CNS-ALL treatment although it requires more sensitive technologies and workflows.

## **1.7 Biomarkers**

### **1.7.1 Background**

Biological markers or biomarkers can be defined as objective measurable alterations in bodily fluids/tissue and/or biological characteristics that can provide insight into healthy physiology, disease pathogenesis or response to therapy [68]. Common examples of biomarkers include the detection of blood glucose levels for monitoring diabetes or the presence of mutations in known genes such as TP53 to predict poor outcome in leukaemia. The key parameters of a good biomarker are sensitivity, specificity, applicability, reproducibility and cost effectiveness and they are invaluable tools in diagnostics, risk-stratification and in prediction of relapse and therapeutic outcomes. Biomarkers can be defined into several different subtypes according to their various applications (**Table 1-2**).

In biomarker discovery there are two approaches that, when combined, can be used to optimally identify clinically relevant biomarkers. The first being an experimental approach using high-throughput methods capable of detecting differences between patient (disease) and control (non-disease) cohorts through one or several potential biomarkers. The second being a knowledge-based approach relying on understanding fundamental disease biology to identify potential targets of interest.

Once candidate biomarkers have been identified, their adoption into a clinical setting requires rigorous testing to ensure the biomarker test meets the appropriate analytical requirements in terms of precision, accuracy, sensitivity and specificity. Precision can be defined as obtaining reproducible results from repeated sample measurements whereas accuracy can be defined as the ability of a test to correctly identify patients with a specific disease [69]. Appropriate sensitivity and specificity of a biomarker are also essential analytical metrics required for the adoption of a biomarker in a clinical setting. Sensitivity can be defined as the ability to detect disease in patients who are truly positive for that disease, while specificity can be defined as the ability of a tests to correctly identify a non-diseased population as truly negative [70].

Equally important in biomarker discovery and development are the pre-analytical variables which can play a key factor in the measurement of a biomarker. Pre-analytical variables include factors such as sample source, sample collection, sample transport and storage, sample volume, sample preparation and sample extraction. The testing, measurement and reporting of these factors are essential to be able to progress through the biomarker discovery pipeline (**Figure 1-12**).

Type of Biomarker	Definition
Diagnostic	Biomarkers for detecting the presence of a disease in patients. These types of biomarkers are also typically used to classify different sub-types of the same disease.
Monitoring	Biomarkers which are serially assessed to inform of the status of a condition in response to a medical intervention i.e., therapy.
Response	Biomarkers which change in level in response to a medical intervention i.e., therapy. These types of biomarkers are commonly used in drug development.
Prognostic	Biomarkers typically used to inform of a patient's likelihood of experiencing a clinical eventuality such as relapse, or disease progression.
Predictive	Biomarkers which can either be detected or show a change in level that informs of a patient's likelihood of experience an either a beneficial or detrimental reaction to a medical intervention i.e., therapy.

**Table 1-2: Biomarker definitions.** [71]

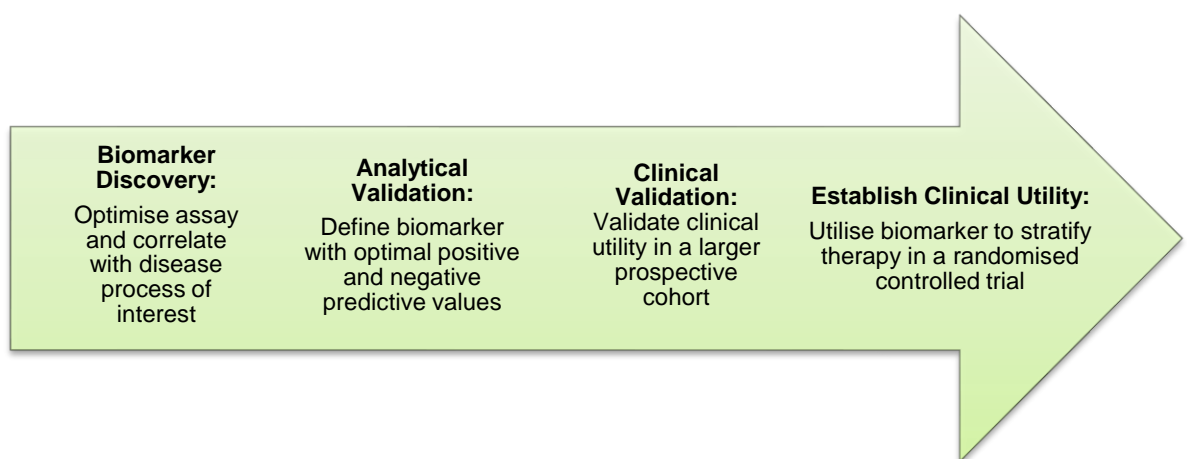


**Figure 1-12: Biomarker development pipeline**

### **1.7.2 Current potential biomarkers for CNS-ALL**

Currently biomarkers that measure leukaemic disease burden are lacking. Research to date has focused on more sensitive detection of free-floating leukaemic cells in the CSF using flow cytometry or PCR based methods. Use of flow cytometry (FCM) increases detection rates from 3% using traditional CSF cytology to 15-30% but FCM positive patients at diagnosis have not yet been shown to have an increased risk of CNS relapse [34]. Pelleting cells from CSF and extracting DNA for PCR also increases detection rates at diagnosis but again, all patients become PCR negative rapidly during induction and it has not been shown to predict CNS relapse. Both these techniques are too insensitive to track response to treatment -- an essential pre-requisite for CSF MRD monitoring.

The search for sensitive biomarkers in the CSF for CNS-ALL has been driven by the advent of multi-omics approaches allowing the detection of various types of different potential biomarkers including metabolomics, proteomics, transcriptomics and genomics. The biomarker areas of interest will be discussed below.

#### **1.7.2.1 Metabolic biomarkers**

Metabolic biomarkers are an area of great interest in biomarker discovery due to the significant differences between tumour cell and normal cell metabolism. Tumour cells require the ability to adapt to their microenvironment to survive and sustain high proliferation rates and they achieve this by altering their metabolism [72]. Alterations in metabolism can potentially reveal quantifiable levels of metabolites that can be isolated from extracellular mediums such as CSF.

Within leukaemia, and ALL in particular, the identification of asparagine-dependence as an intrinsic tool involved in lymphoblast replication has been successfully exploited in treatment regimens. L-asparaginase is now administered as a standard treatment for ALL. It functions by deaminating asparagine and glutamine and consequently causing apoptosis of ALL cells [73]. Information obtained from metabolic profiling is potentially of great value as metabolites are the furthest downstream product and, therefore, are directly representative of the cellular phenotype. However, this presents a variety of complex confounding factors which must be addressed, such as the origin of the metabolite of interest. Tiziani et al., (2013) investigated the metabolomes of both peripheral blood (PB) and BM samples from children with ALL. PB contains a vast number of metabolic products from several organs whereas the BM of an ALL patient at diagnosis is most likely dominated by metabolites derived from the leukaemic blasts. They found significant variation in the levels of certain metabolites between the different microenvironments [74].

Metabolomics is a high-throughput platform for identification of novel metabolites and has proven to be a very powerful tool although, there is a lack of standardised methods related to pre-analysis sample handling and processing. Drug interaction and lifestyle changes (i.e. treatment, exercise, meals, fasting) also play a major role in the levels of certain metabolites and must be considered in order to identify an appropriate metabolite immune to these types of influences [75]. The effect of secondary diseases or comorbidities within patients with cancer may confound the levels of metabolites detected and should also be considered. One study measured metabolite levels from five different gastric diseases as controls compared to gastric cancer and failed to note a difference between them [76].

Metabolic experiments can be conducted by two general different methods: untargeted and targeted approaches (**Table 1-3**). An untargeted approach aims to identify as many metabolites as possible within a pre-specified range of mass values whereas a targeted approach aims to determine the exact concentrations of a panel of metabolites [77]. Both of these methods have their place in biomarker discovery and development.

Untargeted	Targeted
Hypothesis generating	Hypothesis driven
Global comprehensive analysis	Subset analysis
MS/MS correlated to databases, libraries	MS/MS correlated to reference standards
Qualitative identification	Identification already known
Relative quantification	Absolute quantification

**Table 1-3: Experimental metabolomic approaches**

### 1.7.2.2 Soluble biomarkers – Proteins & cytokines

There have been very few cases of successful soluble biomarkers for CNS leukaemia. Recent research has identified differences in the protein expression profile of leukaemic cells in the CNS compared to their site of origin in the bone marrow [64]. This provides the opportunity to search for a specific panel of various potential soluble biomarkers including proteins, adhesion molecules, and cytokines secreted by leukaemic cells.

This study will focus on the following panel of soluble biomarkers which have been shown to have promise as biomarkers capable of detecting and identifying

leukaemic burden within the CNS: Osteopontin, CD27, sL-selectin, VEGF, sIL2-R $\alpha$ , TK1, MMP9, CXCL10 and CCL21.

Osteopontin (OPN) is a secreted phosphorylated glycoprotein protein that mediates a wide range of biological functions and is found to be secreted in various bodily fluids. It is known to be primarily expressed in the bone marrow. The levels of OPN in the CSF showed promise in being a leukaemic signature in a study by Incesoy-Ozdermir et al., (2013) where patients with a high blast count in the CSF were compared with CNS1 patients and presented with a higher level of OPN. Interestingly, this study indicated that levels of OPN increased around the time of relapse [78].

Soluble CD27 is a 32 kD form of the CD27 transmembrane homodimer, a member of the tumour-necrosis-factor (TNF) superfamily. It typically presents in peripheral blood T-cells and a sub-population of B-cells and has been detected in several bodily fluids. One study tested the levels of CD27 in the CSF of patients with CNS leukaemia and found them to be elevated compared to CSF controls from patients who had CSF taken as part of a myelography examination but had a normal CSF profile [79].

L-selectin is a cell-surface adhesion molecule which functions in mediating adherence of lymphocytes to endothelial cells. It is secreted from the cell surface (sL-selectin) and is known to be detected in various bodily fluids. In a study comparing patient ALL CSF samples against CSF controls taken from patients with neurological disorders but were cleared of any malignancy, levels of sL-selectin were found to be elevated patient group who were classified as having sL-selectin positive leukaemia (determined by levels of sL-selectin in plasma) [80].

Vascular endothelial growth factor (VEGF) is an important cytokine responsible for regulating angiogenesis, skeletal growth, and reproductive functions. However, it is reported as a mediator of invasion and tumour survival in several cancers [81]. It belongs to a family of growth factors including placental growth factor (PLGF), VEGF-B, VEGF-C, and VEGF-D which mediate various mechanisms of vascular growth and differentiation [81]. Childhood ALL xenograft cells are reported to directly secrete VEGF and various other leukaemic cells are known to express high levels of VEGF-A and VEGF-C as well as their complementary receptors on the cell surface [81, 82]. One study detected high levels of VEGF-A in the CSF of children with CNS-ALL which is believed to be caused by the upregulation of hypoxic genes (including VEGF-A) in order to adapt to the nutritionally deficient microenvironment [83]. Tang et al., (2013) ran a study on VEGF-A and VEGF-C levels in paired samples of serum and CSF. They found that levels of VEGF-A in CSF were elevated in CNS-leukaemia compared to controls and importantly to patients with leukaemia but without CNS involvement. They also demonstrated a strong correlation between WCC and levels of VEGF-A in the CNS of leukaemic patients supporting the use of VEGF as a potential biomarker for CNS-relapse in paediatric ALL [84].

Interleukin-2 receptor alpha chain (IL2-R $\alpha$ ) is a transmembrane protein which is expressed in both B cells and T cells and is known to be released in soluble form (sIL2-R $\alpha$ ). It has been shown to be elevated in the plasma of patients with ALL [85]. In a study comparing levels of sIL2-R $\alpha$  in paired samples of CSF and serum samples from patients with ALL, levels of sIL2-R $\alpha$  were elevated in the CSF of patients who were positive for CSF cytology compared to patients who were negative for CSF cytology. The levels of sIL2-R $\alpha$  between CSF and the serum samples were found to not have a correlation suggesting specificity of this analytes in the CNS compartment [86].



Thymidine kinase 1 (TK1) is a DNA salvage pathway enzyme and has a key role in DNA synthesis and cell division. It is reported to be elevated in several types of cancers [87, 88]. It has been shown to be elevated in samples of serum from patients with ALL and AML compared to patients without cancer and one study found elevated levels in patients with acute leukaemia which decreased upon administration of CNS-directed therapy [89, 90].

Matrix metalloproteinase 9 (MMP9) is a type IV collagenase belonging to the zinc-metalloproteinase family which mediates the degradation of the extracellular matrix. It has been implicated as a potential biomarker for different cancers with regards to invasion, metastasis and angiogenesis [91]. In leukaemia, it has been shown to be secreted by leukaemic cells and implicated as a disruptor of tight-junction proteins in the BBB [92].

Previous work in the Halsey laboratory identified several chemokine receptors on the cell surfaces of ALL blasts and their counterpart chemokine ligands were explored for use as biomarkers of disseminated ALL in the central nervous system. Of the chemokines tested, CCL21 and CXCL10 showed promise in discriminating CNS-ALL from CSF controls.

The limitations of these studies primarily lie in the lack of follow-up studies testing these findings and the lack of independent validation cohorts. Often these studies also contained small numbers of patient samples which were tested.

### 1.7.2.3 Cell-free DNA / circulating tumour DNA

Cell-free DNA (cfDNA) was first discovered in blood plasma in 1948 by French scientists Mandel and Metais [93]. Twelve years later, the first evidence that a portion of circulating cfDNA contained circulating tumour-derived DNA (ctDNA) appeared, and thus began the idea of ctDNA as an accessible source of genetic material capable of revealing genomic architecture. cfDNA is an extracellular, double-stranded type of DNA, periodically released into the circulation of a multitude of biological matrices such as plasma, serum, CSF, urine, saliva and even in tears and thus provides a potential attractive biomarker as it typically requires a non-invasive procedure and effectively acts as a liquid biopsy.

cfDNA is understood to originate either from cell-death pathways such as apoptosis and necrosis or active secretory pathways (actively secreted in vesicles i.e., exosomes or in complexes with RNA or protein i.e. viroplasm) that occur in healthy and malignant cells alike. However, the exact mechanism remains unclear [94].

The release of ctDNA therefore results in its dilution with cfDNA released from non-malignant cells by the same mechanisms within these different bodily fluids [94].

Structurally, cfDNA are short, double-stranded fragments around 150-180bp, with the most common fragment size at 166bp relating to the DNA being wrapped around a nucleosome and a 20bp linker [95, 96]. ctDNA is typically shorter (134-144bp) than cfDNA as it does not usually contain the linker molecule. However larger fragments of ctDNA are also reported to be found in cancer patients [97]. There is evidence that larger fragments exist and appear to follow a ladder-like pattern in multiples of ~166 bp, similar to an apoptotic DNA fragmentation ladder pattern. Larger fragments up to 10 kb are also believed to originate from necrotic cell death [98].

The fragmented nature of cfDNA also calls into question whether cfDNA is representative of the whole tumour genome. Using whole-genome sequencing, Ma et al., (2017), reported that cfDNA analysis covered ~ 90% of the tumour genomes in late stage gastric and lung cancers supporting the use of targeting cfDNA for the identification of tumour-specific genes for diagnostic and prognostic purposes. The authors also demonstrated that ctDNA coverage did not display bias towards the type of sample used when using matched blood, ctDNA from plasma, ctDNA from the liquid portion of body fluid effusion samples, or tumour samples and, instead in their principle component analysis (PCA) all sample types clustered according to each individual patient [99].

In healthy people, cfDNA detected in blood is reported to be of hematopoietic cell origin (lymphoid or myeloid). cfDNA levels in blood are generally low due to circulating DNase I and II enzymes and clearance by a variety of organs. Its rapid turnover time and clearance from blood is reported to range from as little as 30 minutes to a couple of hours although, the reasons why this is the case are poorly understood. In various reported cancers, cfDNA levels are consistently higher than healthy controls. Despite the clear difference in cfDNA levels, its concentration in cancers can vary greatly and generally seems to be below 100 ng/mL.

Another promising area involving short non-coding nucleic acids in the form of miRNAs (the miR-181 family of miRNAs specifically) has been reported to show increased sensitivity in detecting CNS-leukaemia compared to current CSF cytology. This study looked at the expression these miRNAs in patients classified as CNS-positive and CNS-negative by CSF cytology at diagnosis and found that CNS-positive patients had high levels of miR-181a-5p compared to CNS-negative patients. Interestingly, levels of this miRNA in CNS-positive patients at day 15 of

treatment correlated strongly with the CNS-negative suggesting a response to therapy [100].

## 1.8 Summary

To summarise, the CNS is an important sanctuary site for childhood ALL, being involved in >40% of relapses. Of equal concern, isolated CNS relapse carries a poor prognosis and even with transplantation the event-free survival is only 45% [39, 40]. Given the modern challenges faced in the treatment of paediatric ALL highlighted above, there appears to be three overarching observations in which biomarker discovery and development can improve the outlook of children with acute lymphoblastic leukaemia.

### **1) There is a major need to improve risk-stratification and detoxify CNS-directed therapy.**

All children receive intensive CNS-directed chemotherapy upfront administered via 10-26 invasive lumbar punctures, which can cause significant neurotoxicity and harmful side-effects. Current methods of identifying those at risk are unreliable [28, 48, 101].

### **2) Current diagnostic tests for CNS-ALL are unreliable, insensitive and unable to predict CNS-relapse.**

CNS-ALL is diagnosed by CSF cytology giving a classification of either CNS1, CNS2 or CNS3 in order of suspected leukaemic burden (**Table 1**). However, only about 3% of patients are CNS3 at diagnosis, although without therapy 50-75% of children will suffer CNS relapse with the majority occurring in CNS1 children [20, 22, 31].

Data from post-mortem studies, animal models and clinical observations prior to the administration of CNS-directed therapy suggest that the majority of children have subclinical levels of CNS infiltration at the time of original diagnosis. There is strong evidence that CNS leukaemic cells are generally adherent to the leptomeninges rather than free-floating in the CSF and this could be a possible explanation for the insensitivity of CSF cytology in detecting meningeal disease [17, 19]. This suggests that most patients who are currently classified as CNS1 are likely to have ALL in the CNS at the time of diagnosis.

**3) A method capable of identifying and tracking CNS disease to predict relapse, equivalent to bone marrow MRD is needed.**

In order to personalise CNS-directed treatment it is necessary to be able to quantify the total leukaemic disease burden in the CNS (i.e., both the adherent and free-floating leukaemic cells) and ideally track its response to initial therapy.

- - -

A technique that detects soluble biomarkers released from cells *in situ* is therefore attractive and more likely to accurately measure the overall CNS tumour burden at diagnosis and in response to therapy when compared to techniques that rely on the small proportion of cells free-floating in CSF which rapidly fall to below detection limits with therapy, as seen with CSF cytology.

This study will investigate the use of three techniques for the discovery and development of diagnostic biomarkers and prognostic biomarkers: metabolomics, detection of soluble protein/cytokine biomarkers, and isolation of cell-free DNA.

### **1.8.1 Hypothesis**

The use of sensitive biomarkers for the quantification of total leukaemic burden in samples of cerebrospinal fluid (CSF) from children with CNS-ALL may provide the means to detect CNS leukaemia, monitor response to therapy and predict CNS-relapse with the ultimate aim of escalating or de-escalating treatment based on an extracellular minimal residual disease (MRD) status.

### **1.8.2 Aims**

- 1 – To validate novel metabolic biomarkers in CSF capable of detecting and tracking CNS leukaemia and test the hypothesis that this biomarker is able to track the response of CNS leukaemia to treatment.
- 2 – To discover novel soluble biomarkers in CSF, as alternatives to metabolomic-based methods, using the same criteria as aim 1.
- 3 – To develop a robust and sensitive method for detection of leukaemic cell-free DNA in CSF, using the same criteria as aim 1.
- 4 – To use data gathered from aims 1-3 to identify the optimal biomarker(s) to take forward for further validation and clinical testing.

# Chapter 2: Materials & Methods

## 2 Materials and supplies

### 2.1.1 List of Suppliers, materials and supplies

Supplier	Location	Catalogue number	Material
Agilent Technologies	Santa Clara, California, USA	5067-4626	Agilent High Sensitivity DNA Kit Syringe Chip Priming Station
Beckman Coulter Life Sciences	Brea, California, USA	A63880	Agencourt AMPure XP magnetic beads
Biorad	Hercules, California, USA	1864034 1863024 1863004 12001925 1814040	QX200 ddPCR EvaGreen Supermix ddPCR Supermix for Probes (No dUTP) ddPCR Droplet Reader Oil ddPCR 96-Well Plates DG8 Cartridge PCR Plate Heat Seal, foil, pierceable
Corning Inc.	New York, USA		All plastic products unless otherwise mentioned
Covaris	Woburn, Massachusetts, USA	520221	truXTRAC cfDNA Kit – Magnetic Bead Purification
DSMZ	Leibniz, Germany	ACC 546 ACC 22 ACC 389	SEM – immortalized childhood ALL cells REH – Immortalised childhood ALL cells SUPB15 – Immortalised childhood ALL cells
Eppendorf	Hamburg, Germany		Microcentrifuge tubes
New England Biolabs	Massachusetts, USA	M0544S	NEBNext Q5 Ultra II q5 Master Mix
Nonacus	Birmingham, UK	C3016SK	Cell3 Xtract: cell-free DNA Extraction Kit
Qiagen	Hilden, Germany	55114 55204 28104 79654 203601	QIAamp circulating nucleic acids kit QIAamp MinElute ccfDNA Mini Kit QIAquick PCR purification kit QIAshredder HotStarTaq Plus DNA polymerase



		28704	QIAquick Gel Extraction Kit
R&D Systems	Minneapolis, USA	LXSAHM-04	Human magnetic Luminex Assay
Sigma – Aldrich	Missouri, USA		NGSO Bronze primers
			Easy oligos
			DNA custom Oligos
		T2569-1L	Trizma hydrochloride solution
		P1379-1L	Tween 20
		89510-250G	Poly(ethylene) glycol (PEG)
		S6546-1L	Sodium chloride solution
		C1016	2-Propanol (Isopropanol)
			Ethanol
		10270106	Fetal Bovine Serum
Starlab	Milton Keynes, UK		Pipette tips
Bioo Scientific	Austin, Texas, USA	3825-01	NextPrep-Mag cfDNA Isolation Kit
Thermo Fisher Scientific	Waltham, Massachusetts, USA	4311806	Amplitaq Gold DNA polymerase with Gold Buffer & MgCl <sub>2</sub>
		18427013	dNTP Mix (10 mM)
		10223471	DNA AWAY Surface Decontaminant
			Qubit RNA BR Assay Kit
		Q10210	Qubit dsDNA HS Assay Kit
		Q32851	Qubit dsDNA BR Assay Kit
		Q32850	TaqMan Advanced miRNA Assay
		A25576	TaqMan Advanced miRNA cDNA Synthesis Kit
		A28007	TaqMan Fast Advanced Master Mix
		4444556	TAE Buffer
		70011044	PBS (10X)
		14200059	RPMI (1640)
		21875158	Penicillin/ Streptomycin
		15140122	L-Glutamine
		25030032	IMDM GlutaMAX
		31980048	High-capacity RNA-to-cDNA kit
		4397406	MicroAMP Fast Optical 96-Well Reaction
		4346907	Plate, 0.1 mL

		10509821	Syringe Filter 0.2µm filter
		12027	DynaMag -96 Side Skirted Magnet
4basebio	Heidelberg, Germany	330025	TruePrime Necrotic Cell-free ctDNA Amplification Kit
		340020	TruePrime Apoptotic cell-free DNA amplification kit
		S33102	SYBR Safe DNA gel stain
		15250061	Trypan Blue Solution, 0.4%
		R0611	DNA Gel Loading Dye (6X)
Promega	Madison, Wisconsin, USA	R0104S	HindIII
		R0146S	XhoI
			PGL3 plasmid

**Table 2-1: List of materials and supplies**

## 2.1.2 List of hardware

Supplier	Location	Catalogue number	Instrument
Qiagen	Hilden, Germany	19413	QIAvac 24 Plus Vacuum Manifold
		19419	QIAvac Connecting System
		19530	Vacuum Regulator
		84020	Vacuum Pump
		19408	VacValves
		19541	QIAvac Luer Adapter Set
BioRad	Hercules, California, USA	1864001	QX200 Droplet Digital PCR System
		1864002	QX200 Droplet generator
		1864003	QX200 Droplet Reader
		1814000	PX1 PCR Plate sealer
		1851197	C1000 Touch Thermal cycler
		171000201	Bio-Plex 200 multiplex plate reader
Thermo Fisher Scientific	Waltham, Massachusetts, USA	IQLAAEGAAPFALGMBDK	Orbitrap Q-Exactive (LC-MS) - pHILIC_Qexplus
		Q33216	Qubit 3.0 Fluorometer
Agilent	Santa Clara, California, USA	G2939BA	2100 Bioanalyzer
Promega	Madison, Wisconsin, USA	AS4500	Maxwell 16 Instrument
Covaris	Woburn, Massachusetts, USA	500569	LE220-plus Focused Ultrasonicator
Mettler Toledo	Colombus, Ohio, USA	30087635	XP105 Delta Range Balance
Illumina	San Diego, California, USA	SY-410-1003	MiSeq instrument

**Table 2-2: List of Hardware**

### 2.1.3 List of software

Supplier	Location	Software	Version
Thermo Fisher Scientific	MA, USA	Compound discoverer	3.1.0.305
		TraceFinder	4.1
Agilent	Santa Clara, California, USA	2100 Expert	B.02.10.SI764
CRiStAL, Bonsai bioinformatics lab	Lille, France	Vidjil	beta
Glasgow Polyomics, University of Glasgow	Glasgow, Scotland, UK	Galaxy	Heighliner
GraphPad	San Diego, California, USA	Prism	8
BioRad	Watford, UK	QuantaSoft	1.7
Metaboanalyst	Canada	Metaboanalyst	5.0

**Table 2-3: List of software**

## **2.2 Human Tissue**

### **2.2.1 Ethics approval**

All human research conducted in this study was in accordance with the ethical standards of the Helsinki declaration and was approved by the West of Scotland Research Ethics Committee (WoSREC 09/S0703/77).

### **2.2.2 CSF biobank**

CSF samples from the Halsey Biobank, Glasgow were processed as follows by Dr Saeeda Bhatti and Dr Yasar Yousafzai: CSF was taken from children during lumbar punctures performed as part of routine clinical care at the Royal Hospital for Children, Glasgow and centrifuged at 4°C, 1000 x *g* for 10 minutes and the supernatant was carefully aliquoted into fresh microcentrifuge tubes. All samples were frozen at -80°C and thawed on ice before use. Freeze/thaw cycles were avoided where possible. CSF samples were also obtained from the Blood Cancer UK Childhood Leukaemia CellBank at the NIHR National Biosample Centre (UK Biocentre) who were kind enough to send us 228 patient diagnostic CSF samples. Control CSF samples were obtained from the WoS Neuroimmunology BioBank. 16/WS/0152; IRAS project ID 210043.

### **2.2.3 Plasma samples and pooled plasma**

Human plasma was supplied by the Blood Transfusion Service (Glasgow, UK) and the donation of blood was approved by a Research Ethics Committee. Plasma samples were obtained from 6 healthy donors and 5 mL of plasma from each donor pooled together to make a stock solution of plasma.

## **2.3 Techniques: Chapter 1 – Metabolomics**

### **2.3.1 Materials & supplies**

All supplies for liquid-chromatography-mass spectrometry (LC-MS) were kindly provided by the metabolomics unit in the Beatson Institute for Cancer Research, Glasgow. These supplies included HPLC-grade Acetyl Nitrate and methanol; Xanthine, & Creatine purified standards; glass vials and glass-tapered tube extenders.

### **2.3.2 Metabolite extraction from CSF**

CSF samples were removed from -80°C and thawed on ice. Once thawed and at ~4°C, 10 µL of CSF was diluted 1:20 with extraction solvent (50% methanol/30% acetonitrile/20% deionised water) and mixed thoroughly by vortexing for 30 seconds. The samples were then centrifuged at 16,000 x *g* for 10 minutes at 4°C and half of the supernatants were transferred to glass vials with tapered inserts (for volumes <150 µL). These vials were stored at -80°C until analysis.

Before every extraction, 5 µL was taken from every CSF sample and pooled together separately in a 2 mL centrifuge tube to create a pooled quality control (QC) sample for normalization and for creation of a standard curve. Three procedural blanks were created using 200 µL of the extraction solvent (50% methanol/30% acetonitrile/20% deionised water) in an Eppendorf tube which was processed via the extraction protocol in the same manner as every sample. Three solvent blanks were used by transferring 200 µL of the extraction solvent (50% methanol/ 30% acetonitrile/20% deionised water) directly into a glass vial for analysis.

### **2.3.3 Semi-untargeted mass spectrometry**

An Orbitrap Q-Exactive pHLIC\_Qexplus instrument (Thermo Fisher Scientific) was used for liquid chromatography-mass spectrometry (LC-MS). This study took a semi-untargeted LC-MS approach in that the samples were run in an untargeted mode for global detection of metabolites with a targeted analysis of metabolites of interest. The samples were run with a chromatography time of 25 minutes switching between both positive and negative polarisations to produce both positive and negative ions. Retention times were aligned, all gaps were filled across all samples, and elemental compositions for all compounds were predicted for all compounds using Compound Discoverer software v3.1.0.305. Chemical background signal was subtracted using the blank control samples. All samples were batch-normalised based on the QC sample described above.

Peaks were automatically identified initially by the software using comparisons with mzCloud (with ddMS2 data) and ChemSpider (with formula or exact mass of compounds) databases. Identified compounds were mapped to known biological pathways using the KEGG database. Peaks were also matched with compound identity metrics from a database of internal standards provided by the Metabolomics Unit, Beatson Institute (CRUK). Finally, peaks identities were compared to online database The Human Metabolome Database (HMDB) [102].

### **2.3.4 Targeted LC\_MS**

Targeted mass spectrometry was run using the same methods as above with the addition of standards curves for Xanthine and Creatine. Data was analysed using TraceFinder 4.1 software (Thermo Fisher Scientific) where peak identification was performed using known retention times provided by the internal standards.

#### **2.3.4.1 Creation of standard curves for metabolite quantification**

A nine-point standard curve was created for the metabolites xanthine, creatine and inosine using pooled CSF. To determine the range of values which the standard curve would encompass, values were taken from the Human Metabolome Database (<https://hmdb.ca/>). Concentrations of “normal” levels and “abnormal” levels (disease) of Xanthine, Creatine and Inosine in CSF were averaged and used as the midpoint for the standard curve. Points either side of this midpoint progressed 2-fold (four points above and below the midpoint) to determine the range of the standard curve.

An un-spiked sample of pooled CSF served as the blank. Xanthine was diluted in 1M NaOH and creatine was diluted in deionised H<sub>2</sub>O to create 100 mM stock solutions from which the standard curve points were created by serial dilution. 15 µL of pooled CSF was initially diluted to 1:17 with extraction solvent and then further diluted to the final dilution of 1:20 by spiking 15 µL of each xanthine and creatine at the desired concentration. The samples were then centrifuged at 16,000 x *g* for 10 minutes at 4°C and half of the supernatants were transferred to glass vials with tapered inserts (for volumes <150 µL) and stored at -80°C until analysis.



## **2.4 Techniques: Chapter 2 - Multiplex immunoassay – Luminex**

### **2.4.1 Workflow**

Multiplex immunoassays can be used to detect and quantify several chosen markers simultaneously on a 96-well plate using the sample principle as a sandwich ELISA assay. Luminex assays were performed for the detection of several proteins/chemokines & cytokines in samples of CSF. All samples, standards and reagents were equilibrated to room temperature for at least 30 minutes before use. Standards for each marker of interest were reconstituted using Calibrator Diluent RD6-52 according to manufacturer's instructions and 100  $\mu$ L of each standard were mixed into a fresh Eppendorf tube to a final volume of 1 mL. This standard cocktail mix served as the high standard for every marker of interest and was used to create a 6-point dilution series consisting of 3-fold dilutions per point. Calibrator RD6-52 served as the blank sample. Samples were diluted 1:2 using Calibrator Diluent RD6-53 and 50  $\mu$ L was added to the wells. All samples, blanks and standards were run in duplicate.

Marker specific antibodies are precoated onto magnetic microparticle beads which contain unique fluorophores capable of distinguishing each microparticle bead region being targeted. The microparticle bead solution and the biotinylated antibody cocktail were diluted using RD2-1 solution. These microparticle beads were added to samples, blanks and standards in the 96-well plates and left to incubate for 2 hours at room temperature on a horizontal orbital microplate shaker set at 800 rpm. The beads were subsequently washed using Wash Buffer provided and a magnetic plate attachment to remove any unbound proteins in the sample and 50  $\mu$ L of biotinylated antibody cocktail acting as the secondary antibody specific to the

analyte of interest was added. The plate was then covered with a foil plate sealer and incubated for 1 hour at room temperature on an orbital shaker set to 800 rpm.

A second wash was then performed and streptavidin-phycoerythrin (Streptavidin-PE) was added to each well for binding with the biotinylated antibody and the plate was then covered with a foil plate sealer, incubated for 30 minutes at room temperature on an orbital shaker set to 800 rpm. One more wash was performed and the microparticles were resuspended with 100  $\mu$ L of Wash Buffer, incubated for 2 minutes on the shaker at 800 rpm before being read and analysed on a Bio-Plex 100 multiplex plate reader (Bio-Rad). Fluorescence was measured in each well and the fluorescence values in the standard wells were used to create a standard curve for each marker of interest. Fluorescence values from each sample were quantified using the standard curve to give a measure for each marker of interest per sample.

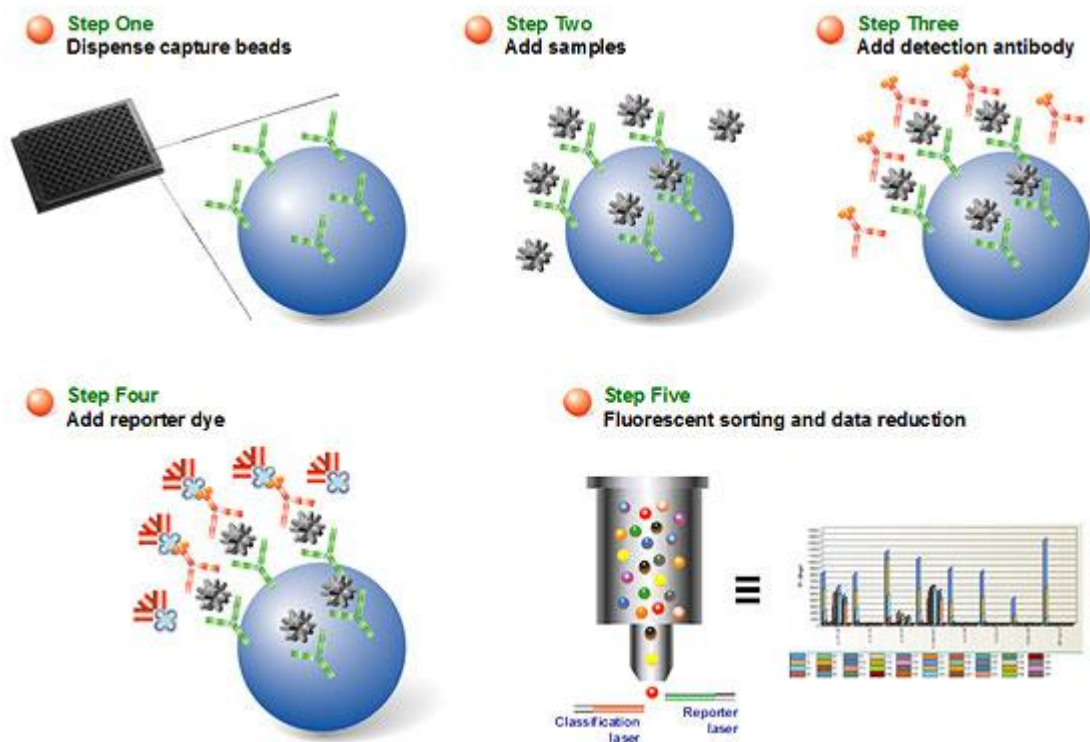


**Figure 2-1: Luminex multiplex immunoassay workflow** [<https://www.bio-rad.com/en-uk/applications-technologies/bio-plex-multiplex-immunoassays?ID=LUSM0ZMNI>]

## **2.5 Techniques: Chapter 3 – Cell-free DNA**

### **2.5.1 Cell culture**

#### **2.5.1.1 Cell Lines**

Cell lines: SEM, REH and SUPB15 were previously purchased from DSMZ (German collection of Microorganisms and Cell Cultures). All cell lines were stored in liquid nitrogen (-196°C) until use. Cell lines were authenticated at the Beatson Institute of Cancer Research, Glasgow before use. Human cell lines were authenticated using Promega GenePrint 10 Kit, a short tandem repeat multiplex assay that amplifies 9 tetranucleotide repeat loci and the Amelogenin gender determining marker in a single PCR amplification. The kit uses a five dye (PET, LIZ, 6-FAM, VIC and NED) fluorescent system for automated fragment analysis. Samples were run on a 3130xl DNA analyser and data was compared with ATCC (LGC standards) and DSMZ databases.

#### **2.5.1.2 Cell culture procedures**

All cell culture procedures were performed in a tissue culture laminar flow hood which was sterilised using 70% ethanol before and after use. All materials used were sterile and sprayed and wiped with 70% ethanol before being used.

#### **2.5.1.3 Thawing / freezing cells**

Cell lines were put on ice following removal from liquid nitrogen and subsequently thawed in a 37°C water bath. The cells were then transferred to a fresh 50 mL centrifuge tube and 5 mL prewarmed complete culture media was added dropwise to the cells to help dissociation of DMSO. The cells were then centrifuged at 300 x *g* for 5 minutes, the supernatant was then aspirated carefully, and the cells were

resuspended in 20 mL pre-warmed complete cell culture media. The cells were then transferred to 25 cm<sup>2</sup> cell culture flasks for cell passage.

Stocks of cells were frozen according to DSMZ recommendations in DMSO. Cells were spun down at 300 x *g* for 10 minutes, the supernatant was discarded, and the cell pellet was resuspended in 70% media, 20% FBS and 10% DMSO in cryostorage tubes. Cells were frozen to -80°C overnight then transferred to liquid nitrogen the following day.

#### **2.5.1.4 Cell passage**

All cell lines were incubated at 37°C; 5% CO<sub>2</sub>. Cells were passaged according to suppliers' recommendations in complete cell culture media. All cell lines were tested for mycoplasma soon after being passaged for the first time by the service provided at the Wolfson Wohl Cancer Research Centre. To passage the cells, the cells were transferred to a 20 mL centrifuge tube and spun at 300 x *g* for 5 minutes, the supernatant was discarded, and the cells were resuspended in 10 mL complete media for cell counting. The cells were then seeded according to suppliers' recommendations in 20 mL of fresh complete media in a new 25 cm<sup>2</sup> tissue culture flask and incubated as mentioned above.

#### **2.5.1.5 Cell Counting**

Cell counts were performed using an Improved Neubauer haemocytometer. Cells were first spun down at 300 x *g* for 5 minutes; the supernatant was discarded, and the cell pellet was resuspended in 10 mL of complete media. 50 µL of the 10 mL cell suspension was diluted 1:2 using 0.4% trypan blue dye and incubated at room temperature for 2 minutes. 10 µL of the cells-trypan blue solution was then

transferred onto the counting chamber beneath a glass coverslip. The haemocytometer was then placed under an inverted light microscope and cells were counted in the four  $10^{-4}$  corner squares. Viable cells were distinguished from non-viable cells using the trypan blue exclusion method. Cell numbers were multiplied by  $10^4$  and then by the dilution factor (2) to give the number of cells/mL (in 10 mL). Percentage of viable cells was calculated by dividing the number of viable cells by the number of total cells and multiplied by 100. Cells were passaged only when viability was > 90%.

## **2.5.2 Nucleic Acid Isolation and Extraction**

### **2.5.2.1 *In vitro* cfDNA isolation from cell culture media**

Cell-free DNA was isolated from cell culture flasks which had reached at ~80-90% confluence by transferring the cell culture media with cells to a 20 mL centrifuge tube and centrifuging at  $300 \times g$  for 5 minutes to pellet the cells. The supernatant was then aspirated and transferred to a clean petri dish. The liquid was then re-aspirated using a 20 mL syringe and passed through a  $0.2 \mu\text{m}$  filter into a fresh 20 mL centrifuge tube to remove cells and macro-debris from the cell culture media. The filtered cell culture media was then subjected to cfDNA purification with the Qiagen, QIAamp Circulating nucleic acids kit.

## 2.5.2.2 Cell-free DNA extraction kit comparisons

### 2.5.2.2.1 Commercial cfDNA extraction kits tested for evaluation of extraction performance.

Extraction Kit	Kit ID	Manufacturer	Technology	Sample type	Volume capacity	Additional requirements	Automation
QIAamp Circulating Nucleic Acids Kit	QA	QIAGEN	Silica-based membrane	Plasma, serum, urine	Up to 5mL	QIAvac 24 Plus vacuum manifold	No*
QIAamp MinElute ccfDNA kit	QB	QIAGEN	Magnetic bead / silica-based membrane hybrid	Plasma, serum	1-4 mL	Strong magnetic stand	No**
Cell3 Xtract	NN	Nonacus	Column-based	Plasma, serum, CSF, saliva, amniotic fluid	1-10 mL	None	No
Nextprep-Mag cfDNA isolation kit	NM	Newmarket Scientific	Magnetic bead based	Plasma	1-3 mL	Strong magnetic stand	Yes
Maxwell RSC ccfDNA Plasma kit	COV	Promega Ltd.	Magnetic bead based	Plasma, serum, other bodily fluids	1 mL	Maxwell RSC Instrument	Yes
truXTRAC cfDNA kit	MX	Covaris	Magnetic bead based and Adaptive Focused Acoustics (AFA) based DNA extraction	Plasma, other bodily fluids	1 mL	Adaptive Focused Acoustic ultrasonicator and strong magnetic stand	Yes
*Can be automated using QIAcube Connect; **Can be partially automated using QIAcube Connect							

**Table 2-4: Commercial cfDNA extraction kits tested for evaluation of extraction performance**

#### **2.5.2.2.2 QIAamp circulating nucleic acids (QA)**

For all extractions involving plasma, 1 mL of pooled plasma was used. For all extractions using CSF, volumes between 100 µL and 1 mL were used. For all extractions using cell culture supernatant, volumes between 5 mL down to 1 mL were used.

The QIAamp Circulating Nucleic Acids Kit involves four major steps: lysis, binding, wash steps and elution to successfully extract and purify cfDNA. The samples are first lysed under denaturing conditions with the presence of Proteinase K, Buffer ACL and placed in a 60°C water bath for 30 minutes. Binding buffer (Buffer ACB) was then added to the samples and incubated on ice for 5 minutes before applying the samples to the spin columns. Vacuum pressure created by the vacuum manifold (-800 to -900 mbar) then drew the sample through the silica membrane in the spin column to capture cfDNA on the membrane as the lysate passes through the column. Following this, the columns were subjected to three wash steps using Buffer AW1, Buffer AW2 and Ethanol (96-100%). The membrane was dried for 10 minutes at 56°C and then 50 µL of pre-warmed Buffer AVE was added to the centre of the membrane and left to incubate for a further 10 minutes before elution by centrifugation at 20,000 x g for 1 minute. The supernatant was transferred to a fresh 1.5 mL elution tube and stored at -20°C.

#### **2.5.2.2.3 QIAamp MinElute ccfDNA Mini Kit (QB)**

The QIAamp MinElute ccfDNA Mini kit uses both magnetic bead and spin column principles for purification of circulating DNA. Samples of pooled plasma (1mL) were mixed with Bead Binding Buffer, Magnetic Bead Suspension and Proteinase K to dissociate cfDNA from any bound complexes. Once the cfDNA was bound to the

magnetic beads, the beads were pelleted on a magnetic plate and the supernatant was discarded. The DNA was then eluted using Elution Buffer and the magnetic beads were pelleted using the magnetic plate before the supernatant was transferred to a fresh tube. Buffer ACB was then added to the sample and mixed to facilitate binding of the cfDNA to the silica membrane of the spin column. The sample was applied to the spin column and spun in a centrifuge to capture the cfDNA on the silica membrane. The membrane was then washed using Buffer ACW2 and left to air-dry to remove any residual ethanol. 50  $\mu$ L of Ultra-clean water was carefully added to the centre of the spin-column and then spun in a centrifuge to elute the purified cfDNA. The supernatant was transferred to a fresh 1.5 mL elution tube and stored at -20°C.

#### **2.5.2.2.4 NextPrep-Mag cfDNA Isolation Kit (NM)**

The NextPrep-Mag cfDNA Isolation Kit (Bioo Scientific) relies solely on the magnetic bead principle for cfDNA purification. Samples of pooled plasma (1mL) were mixed with a Binding Solution, Magnetic beads and Proteinase K and incubated for 15 minutes at 55°C. The samples were then applied to a magnetic plate and the magnetic beads were pelleted before the supernatant was aspirated and discarded. The beads were then washed twice using Wash 1 solution and further washed once with Wash 2 solution. 50  $\mu$ L of elution buffer was then added to the beads, the sample was resuspended by vortexing and incubated for 5 minutes at 55°C. The sample was reapplied to the magnetic plate to pellet the beads and the supernatant was transferred to a fresh 1.5 mL elution tube and stored at -20°C.



#### **2.5.2.2.5 Cell3 Xtract: cell-free DNA Extraction Kit (NN)**

The Cell3 Xtract cell-free DNA Extraction Kit (Nonacus) relies solely on centrifugation steps for isolation of cfDNA. Samples of pooled plasma (1mL) were mixed with 5X Digestion Buffer and Proteinase K and incubated at 55°C for 30 minutes. Two volumes of DNA Binding Buffer were added, mixed by vortexing, carefully transferred to a spin column, then centrifuged at 1000 x *g* for 1 minute. The collection tube and flow-through was discarded and the spin column was placed in a fresh collection tube. The spin column was washed with 400 µL of Wash Buffer and centrifuged at full speed for 1 minute to remove the wash buffer. The spin column was then placed into a 1.5 mL elution tube and 50 µL Elution Buffer was added to the centre of the membrane and the spin columns were incubated at room temperature for 3 minutes. The spin columns were centrifuged at maximum speed for 1 minute into a clean elution tube and stored at -20°C.

#### **2.5.2.2.6 Maxwell RSC ccfDNA Plasma Kit (MX)**

The Maxwell RSC ccfDNA Plasma Kit (Promega) can be used in a fully automated manner with the use of a Maxwell RSC 48 instrument. It relies on the magnetic bead principle for purifying cfDNA. RSC ccfDNA Plasma Cartridges were placed on the deck tray with the largest well facing away from the elution tubes and the seal was carefully removed. Samples of pooled plasma (1mL) were added to the largest well and a plunger was added into the last well. A fresh 1.5 mL elution tube was placed in the elution tube well on the deck tray and 60 µL of Elution Buffer was added to the elution tube (for a final solution of 50 µL after sample processing). The Maxwell RSC 48 instrument was then initiated and the cfDNA extraction was performed.

### 2.5.2.2.7 truXTRAC cfDNA Kit (COV)

The truXTRAC cfDNA Kit (Covaris) utilizes the magnetic bead principle for extraction of cfDNA with the added step of adaptive focused acoustics (AFA) technology to ultrasonicate samples. This step dissociates cfDNA in a sample from any proteins, histones, protein-DNA complexes, and apoptotic machinery. A Buffer M1/ Proteinase K master mix and a Magnetic Bead Suspension/ Isopropanol master mix were created according to the supplier's recommendations

Samples of pooled plasma (1mL) were added to milliTUBEs. Buffer M1/ Proteinase K master mix was added to the tubes and the samples were mixed by inverting the tubes 10 times. The milliTUBES were then incubated at room temperature for 15 minutes. The milliTUBES were then placed into the 1 mL milliTUBE rack and ultrasonicated in a LE220-plus Focused ultrasonicator with the following settings:

Settings	
Water level	0
Chiller set point	18°C
Duty Factor	20%
Peak Incidence Power	350 Watts
Cycles per burst	200
Treatment time	60 seconds
Instrument Temperature	20°C

**Table2-5: LE220-Plus Focused Ultrasonicator settings**

Following the ultrasonication step, the samples were transferred to 5 mL Eppendorf tubes and vortexed for 10 seconds. The Magnetic Bead Suspension/Isopropanol Mix was vortexed for 10 seconds before 1.6 mL of the mix was added to the samples. The samples were then vortexed for 10 seconds and the placed on a

magnetic rack and incubated for 5 minutes. The supernatant was discarded and 1 mL of Buffer WB2 was added to the 5 mL Eppendorf tube. The tube was vortexed for 10 seconds until the beads were re-suspended before being placed back on the magnetic rack for a further 5 minutes. The supernatant was discarded and 1 mL of 80% ethanol was added to the tube and incubated for 30 seconds before the ethanol was removed and discarded. Both wash steps were repeated once more before air-drying the beads for 15 minutes on the magnetic rack. The tubes were removed from the magnetic rack and the beads were resuspended with 50  $\mu$ L Elution Buffer BR by pipetting up and down at least 20 times to ensure proper resuspension. The tubes were placed on the magnetic rack once more and incubated for 1 minute before the eluate was transferred to a clean Elution Tube and stored at -20°C.

### **2.5.3 Preparation of cfDNA surrogate spike-in molecule**

#### **2.5.3.1 hTERT-Luc plasmid fragment spike-in molecule**

A linearized hTERT-Luc plasmid fragment from a PGL3 plasmid (Promega) was used in this part of the study (approximately 172 bp) as a surrogate cfDNA spike-in molecule. The plasmid fragment was created from a double digest reaction containing *HindIII* and *XhoI* restriction enzymes and was incubated in a thermocycler for 90 minutes at 37°C. The double digest product was then subjected to agarose gel electrophoresis, excision and purification (see section 1.5.3). Purified samples of the plasmid fragment were stored at 4°C for short-term use or 20°C for long term storage.

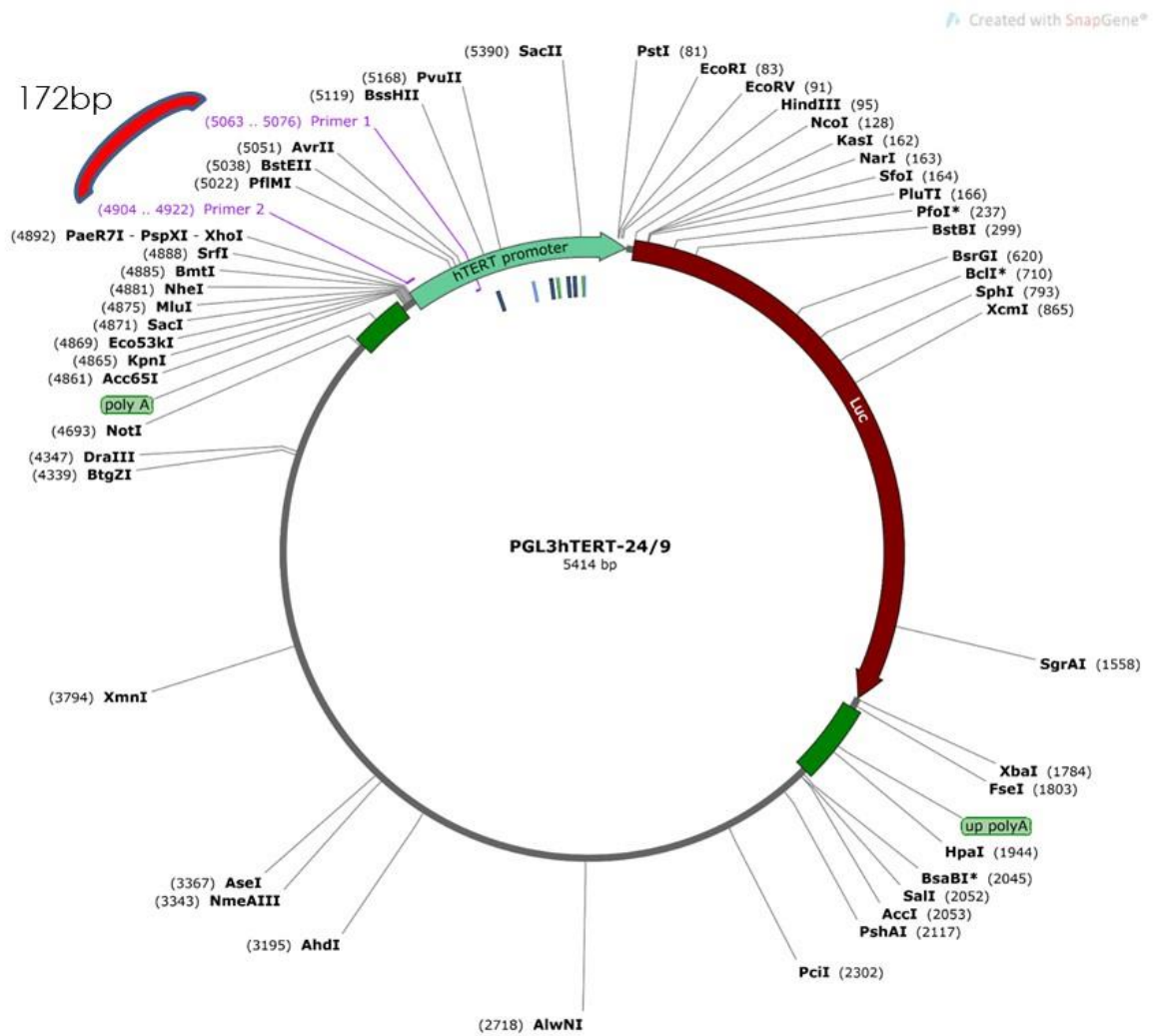


Figure 2-2: PGL3 Plasmid map featuring hTERT-Luc plasmid fragment

### 2.5.3.2 Polymerase Chain Reaction (PCR) of hTERT-Luc Plasmid Fragment – cfDNA surrogate spike-in

To amplify the hTERT-Luc plasmid fragment the following PCR reaction was created. A 10% excess in reagents was used as to ensure enough reaction per sample:

<b>Master mix</b>	<b>Per Well (<math>\mu</math>L)</b>
10x Buffer	2.5
dNTPs (200uM)	0.5
Q solution	5.0
Forward Primer	0.5
Reverse Primer	0.5
HotStartaq	0.2
H <sub>2</sub> O	14.8
DNA template (25 ng/ $\mu$ L)	1.0
Total Volume	25.0

**Table 2-6: PCR reaction master mix components and volume**

<b>PCR Primers hTERT-Luc plasmid fragment</b>	<b>DNA sequence</b>
Forward	CATTCGTGGTGCCCGGAGC
Reverse	GCCCCAGCGGAGAGAGGTCTG
Bilsland A. et al. 2007 (DOI: 10.1158/0008-5472.CAN-06-3000 Published February 2007)	

**Table2-7: hTERT-Luc plasmid fragment Forward and Reverse primer sequences.**

The reaction mixes were then subject to the following thermocycler conditions:

Step	Temperature	Time	Cycles
1	95°C	15 minutes	1
2	95°C	30 seconds	32
	58°C	45 seconds	
	72°C	30 seconds	
3	72°C	5 minutes	1
4	4°C	hold	

**Table 2-8: Thermocycler conditions**

### **2.5.3.3 Electrophoresis, Gel Excision, DNA Purification of PCR product and DNA quantification**

#### **2.5.3.3.1 Agarose gel preparation**

An agarose gel for electrophoresis was prepared by transferring 1g of agarose to an Erlenmeyer flask and 100 mL of 1X TAE buffer was added. The flask was microwaved at full power every 15 seconds for a total of 2 minutes, swirling the solution between heating and was left to cool for 10-15 minutes.

During cooling, the electrophoresis plate was taped on both sides and an appropriate well comb was placed on the holder. Once the agarose solution had cooled, 10 µL of SYBRSafe DNA gel stain (Thermo Fisher Scientific) was added to the Erlenmeyer flask and mixed well by swirling vigorously. The agarose solution was then poured into the electrophoresis plate and left to cool and solidify.

During cooling, 10 µL of 6X gel loading dye (Thermo Fisher Scientific) was added to 50 µL of the PCR product, mixed thoroughly by pipetting and kept on ice until use. Once the gel had solidified, the comb was carefully removed, placed into the

electrophoresis which was filled with 1X TAE Buffer. The wells were then loaded with a 100 bp ladder and the DNA/ Gel Loading dye (6X) mix and electrophoresis was run at 150 V for 60 minutes. The resulting gel was then verified and visualised for the successful PCR reaction using and SnapGene viewer software.

To isolate the desired fragment of DNA from the gel, the gel was exposed to UV light and the gel band was excised using a clean, sharp scalpel. The gel was weighed using a XP105 Delta Range Balance (Mettler Toledo) ready for DNA purification using the QIAquick Gel Extraction Kit.

#### **2.5.3.3.2 QIAquick Gel Extraction Kit**

Three volumes of QG Buffer were added to the 1 gel volume and was incubated at 50°C for 10 minutes in a Techne Dri-Block DB-2A heating block. The sample was vortexed every 2 minutes to facilitate the dissolving of the gel. The samples were treated with Isopropanol and then added to a QIAquick spin column. The spin column was centrifuged at 13000 rpm for 1 minute and the flow-through was discarded. The spin column was placed in a fresh 1.5 mL elution tube and 50 µL of Buffer EB was added to the centre of the membrane. The spin column was centrifuged at 13,000 rpm for 1 minute to elute the DNA. The DNA was quantified using the Qubit dsDNA BR Assay Kit. The DNA was stored at 4°C for short-term use or 20°C for long-term storage.

#### **2.5.3.3.3 DNA clean-up - QIAGEN QIAquick PCR Purification Kit**

This kit was used to purify PCR products from residual reagents from the PCR process and relies on spin-column technology which has selective binding

properties through the use of a silica membrane. Once nucleic acids are bound to the silica membrane, a series of wash steps are performed to remove any residual reagents prior to elution.

PCR products were mixed with Buffer PB in a 5:1 volume and vortexed to create a homogenous solution. The samples for purification were then added to a QIAquick spin column to bind the DNA to the silica membrane and the spin column was centrifuged at 17,900 x *g* for 1 minute. The flow-through was discarded and the spin column was placed in a fresh collection tube. The spin column was then washed with Buffer PE and centrifuged again as above. The flow-through was discarded and the spin column was placed in the same collection tube and spun again as above to remove any residual wash buffer. The spin column was placed in a clean 1.5 mL elution tube and 50 µL of Buffer EB was added to the centre of the silica membrane. The spin column was then centrifuged at 17,900 x *g* for 1 minute to elute the DNA. Purified DNA was stored at -20°C

## **2.5.4 Nucleic Acid Quantification and size (bp) analysis**

### **2.5.4.1 DNA quantification by Qubit**

DNA was quantified using a Qubit Fluorometer and the Qubit dsDNA HS Assay Kit or the Qubit dsDNA BR Assay Kit. All DNA samples were equilibrated to room temperature before the assay was run. A 1X working solution was prepared using Qubit dsDNA HS/BR reagent and Qubit dsDNA HS/BR Buffer by diluting the reagent 1:200 with a 200 µL final volume per sample. Samples were diluted (5 µL:195 µL) and standards #1 and #2 were diluted (10 µL:190 µL) with 1X working solution, vortexed for 5 seconds and incubated at room temperature for 2 minutes before being read on a Qubit 2.0 fluorometer. Standards #1 and #2 were run first by placing



the Qubit tube into the sample chamber, closing the lid and reading the standard. Samples were read in the same manner and DNA was quantified in ng/  $\mu$ L units.

#### **2.5.4.2 DNA quantification and quality assessment by Bioanalyzer**

DNA samples were quantified and analysed for size in (bp) using Agilent's High Sensitivity DNA Assay Kit and an Agilent 2100 Bioanalyzer instrument. All reagent and samples were allowed to reach room temperature for 30 minutes before the assay was run.

The High Sensitivity DNA dye concentrate was vortexed for 10 seconds and spun down in a microcentrifuge before 15  $\mu$ L was added to the High Sensitivity DNA gel matrix vial. The mixed vial was then vortexed for 10 seconds and the gel-dye mix was transferred to the top of the spin filter. The spin filter was centrifuged for 10 minutes at 2240 x *g* at room temperature. The filter was then discarded, and the tube was wrapped in tin foil to protect the gel-dye mix from light. The dye concentrates and gel-dye mix was stored at 4°C in the dark when not in use.

A new High Sensitivity DNA chip was placed on the Chip Priming Station and 9  $\mu$ L was added to the well marked G. The chip was pressurised using the syringe which was set to 1 mL and pressed down until it was held by the clip and held for 60 seconds exactly. After the 60 seconds the clip was released, and the plunger was slowly returned to the 1 mL mark. 9  $\mu$ L of the gel-dye mix was added to the remaining wells marked G and then 5  $\mu$ L of High Sensitivity DNA marker was added to the ladder well and into the 11 sample wells. 1  $\mu$ L of High Sensitivity DNA ladder was added to the ladder well. 1  $\mu$ L of sample was added to each of the sample wells,

where there was an unused well, 1  $\mu\text{L}$  of the High Sensitivity DNA marker was added to the well. The DNA Chip was placed horizontally on the IKA vortex mixer and vortexed for 60 seconds at 2400 rpm. A cleaning chip with 350  $\mu\text{L}$   $\text{dH}_2\text{O}$  was loaded onto the bioanalyzer and the lid was shut for 10 seconds and opened and left open for 10 seconds to dry. The DNA Chip was then loaded into the bioanalyzer. Data was analysed using the Agilent 2100 Expert software.

### 2.5.5 Droplet Digital PCR

Droplet digital polymerase chain reaction (ddPCR) platforms comprise the next generation of nucleic acid quantification overcoming the limitations seen in qPCR. In principle samples are diluted and divided into several thousand miniscule partitions, typically using either emulsifying oil droplets or micro-wells within a microfluidic chip so that each individual partition contains either no copies of the template molecules, or one copy per partition.

All wells with a target copy will then be simultaneously amplified within their partition and the emitted fluorescence is subsequently detected at the end of the PCR. Poisson statistics are used to account for variation across the random distribution of template copies across the partitions and analyses based off the Poisson algorithm used allows for calculation of the total number of total positive partitions against the negative partitions to deliver an absolute quantification of the original starting template material.



**Figure 2-3: Droplet digital PCR workflow schematic**

All droplet digital PCR (ddPCR) assays were performed using QX200 Droplet Digital PCR system (Bio-Rad, Hercules, USA).

### 2.5.5.1 EvaGreen ddPCR preparation

EvaGreen chemistry contains a dsDNA dye which binds to double-stranded DNA during amplification cycles in a PCR reaction, akin to SYBR Green assays for qPCR. This dye is incorporated into the ddPCR Supermix used for the following experiments. All reagents and DNA samples were thawed to room temperature, vortexed gently and briefly centrifuged before use. DdPCR assays were performed using BioRad's QX200 Droplet Digital PCR system and an EvaGreen assay (BioRad Laboratories LTD, Watford, UK). All samples were prepared to a volume of 22  $\mu$ L with 11  $\mu$ L of ddPCR Supermix for EvaGreen (2X), 0.5  $\mu$ L of each primer, 5  $\mu$ L of the cfDNA template and 5  $\mu$ L of nuclease-free water. The PCR reaction mix was prepared as follows:

Reagent	Volume ( $\mu$ L)
2X QX200 ddPCR EvaGreen SuperMix (1X)	11
Forward Primer (100-250 nM)	0.5
Reverse Primer (100-250 nM)	0.5
cfDNA template (Up to 100 ng)	5
Nuclease-free water	5
Total Volume	22

**Table 2-9: PCR reaction master mix components and volume**

ddPCR Primers hTERT-Luc plasmid fragment	DNA sequence
Forward	CATTCGTGGTGCCCGGAGC
Reverse	GCCCCAGCGGAGAGAGGTCTG
Bilsland A. et al. 2007 (DOI: 10.1158/0008-5472.CAN-06-3000 Published February 2007)	

**Table 2-10: hTERT-Luc plasmid fragment Forward and Reverse primer sequences.**

Once made up, the PCR reaction solutions were mixed thoroughly by vortexing and then 20  $\mu$ L of the PCR mix were loaded into the middle sample wells of the DG8 Cartridge. QX200 Droplet Generation Oil for EvaGreen (70  $\mu$ L) was then added into the oil wells and the cartridge was covered with a rubber gasket before being loaded into the QZ200 Droplet Generator.

Following the droplet generation process, 40  $\mu$ L of droplets were then transferred to a 96-well plate. The plate was sealed using the PX1 PCR Plate Sealer and then loaded into the BioRad C10000 Touch Thermal Cycler for thermocycling at the following settings:

Step	Temperature °C	Time	No. of cycles
Enzyme activation	95	5 min	1
Denaturation	95	30 sec	40
Annealing/ extension	60	1 min	
Signal	4	5 min	1
Stabilization	90	5 min	
Hold	4	hold	1
Ramp rate 2°C/sec; Heated lid set to 105°C; Sample volume 40 $\mu$ L			

**Table 2-11: Thermocycler conditions**

Following thermocycling, the sealed plate was loaded into the QX200 Droplet Reader for analysis.

## 2.5.5.2 Probe-based ddPCR

### 2.5.5.2.1 Patient purified CSF cfDNA

Similar to qPCR, primers can be used in conjunction with dual-labelled probes in ddPCR to measure fluorescence of specific amplified templates. All reagents and DNA samples were thawed to room temperature, vortexed gently and briefly centrifuged before use. DdPCR assays were performed using BioRad's QX200 Droplet Digital PCR system and a Probe assay with FAM and Hex labelled probes (BioRad Laboratories LTD).

All samples were prepared to a volume of 22  $\mu\text{L}$  with 10  $\mu\text{L}$  of ddPCR Supermix for probes (2X), 1  $\mu\text{L}$  of each primer, 7  $\mu\text{L}$  (maximum volume) of cfDNA template (patient & control) and 2  $\mu\text{L}$  of nuclease-free water. The PCR reaction mix was prepared as follows:

Reagent	Volume ( $\mu\text{L}$ )
2X ddPCR Supermix for Probes [1X]	10
20 x Target primers/probes (FAM or Cy5) [900 nM/250 nM]	1
20 x Target primers/probes (HEX/VIC or Cy5.5) [900 nM/250 nM]	1
DNA template ( Up to 330 ng)	7
Nuclease-free water	2
Total volume	<b>22</b>

**Table 2-12: PCR reaction master mix components and volume**

Once made up, the PCR reaction solutions were mixed thoroughly by vortexing and then 20  $\mu\text{L}$  of the PCR mix were loaded into the middle sample wells of the DG8 Cartridge. QX200 Droplet Generation Oil for EvaGreen (70  $\mu\text{L}$ ) was then added into the oil wells and the cartridge was covered with a rubber gasket before being loaded into the QZ200 Droplet Generator.

Following the droplet generation process, 40  $\mu\text{L}$  of droplets were then transferred to a 96-well plate. The plate was sealed using the PX1 PCR Plate Sealer and then loaded into the BioRad C10000 Touch Thermal Cycler for thermocycling at the following settings:

Step	Temperature $^{\circ}\text{C}$	Time	No. of cycles
Enzyme activation	95	10 min	1
Denaturation	94	30 sec	40
Annealing/ extension	60	1 min	
Enzyme deactivation	98	10	1
Hold	4	hold	1
Ramp rate $2^{\circ}\text{C}/\text{sec}$ ; Heated lid set to $105^{\circ}\text{C}$ ; Sample volume 40 $\mu\text{L}$			

**Table 2-13: Thermocycler conditions**

### **2.5.5.2.2 Mutation detection assay - KRAS G12D**

To determine the lower limit of detection (LOD) of the RSS DNA assay [40 ng/ $\mu$ L] (each vial with a known KRAS allelic frequencies of 100% WT, 6.3%, 1.3% and 0.13%) the contents of each vial was diluted in Buffer AVE and made up to 50 ng, 10 ng, 5 ng and 1 ng and was added to a 20  $\mu$ L PCR reaction mix. Negative controls used water instead of DNA.

All reagents and DNA samples were thawed to room temperature, vortexed gently and briefly centrifuged before use. DdPCR assays were performed using BioRad's QX200 Droplet Digital PCR system and a Probe assay with FAM and Hex labelled probes (BioRad Laboratories LTD, Watford, UK). All samples were prepared to a volume of 22  $\mu$ L with 10  $\mu$ L of ddPCR Supermix for probes (2X), 1  $\mu$ L of each primer, variable quantity of template and nuclease-free water.

Once made up, the PCR reaction solutions were mixed thoroughly by vortexing and then 20  $\mu$ L of the PCR mix were loaded into the middle sample wells of the DG8 Cartridge. QX200 Droplet Generation Oil for EvaGreen (70  $\mu$ L) was then added into the oil wells and the cartridge was covered with a rubber gasket before being loaded into the QX200 Droplet Generator. Following the droplet generation process, 40  $\mu$ L of droplets were then transferred to a 96-well plate. The plate was sealed using the PX1 PCR Plate Sealer and then loaded into the BioRad C10000 Touch Thermal Cycler for thermocycling at the following settings:



Reagent	Volume (μL)
2X ddPCR Supermix for Probes [1X]	10
20 x Target primers/probes (FAM or Cy5) [900 nM/250 nM]	1
20 x Target primers/probes (HEX/VIC or Cy5.5) [900 nM/250 nM]	1
DNA template ( Up to 330 ng)	Variable
Nuclease-free water	Variable
Total volume	22

**Table 2-14: PCR reaction master mix components and volume**

Step	Temperature °C	Time	No. of cycles
Enzyme activation	95	10 min	1
Denaturation	94	30 sec	40
Annealing/ extension	60	1 min	
Enzyme deactivation	98	10	1
Hold	4	hold	1
Ramp rate 2°C/sec; Heated lid set to 105°C; Sample volume 40 μL			

**Table2-15: Thermocycler conditions**

### 2.5.6 Next-Generation Sequencing (NGS)

Next-generation sequencing is the successor technology to Sanger sequencing and is also known as massively parallel, high-throughput sequencing. There are now several different platforms available for NGS but in this thesis, a targeted Illumina (San Diego, California, USA) sequencing approach was used. The Illumina NGS workflow involves four major steps: library preparation, cluster generation, sequencing and data analysis. All samples were sequenced on a MiSeq instrument with V2 2x150-cycle flow cells 4 million reads, paired-end reading mode with a

reading depth of 100,000 - 350,000. This project targeted Ig gene rearrangements , specifically IGH VDJ gene rearrangements exhibited by leukaemic B-cells.

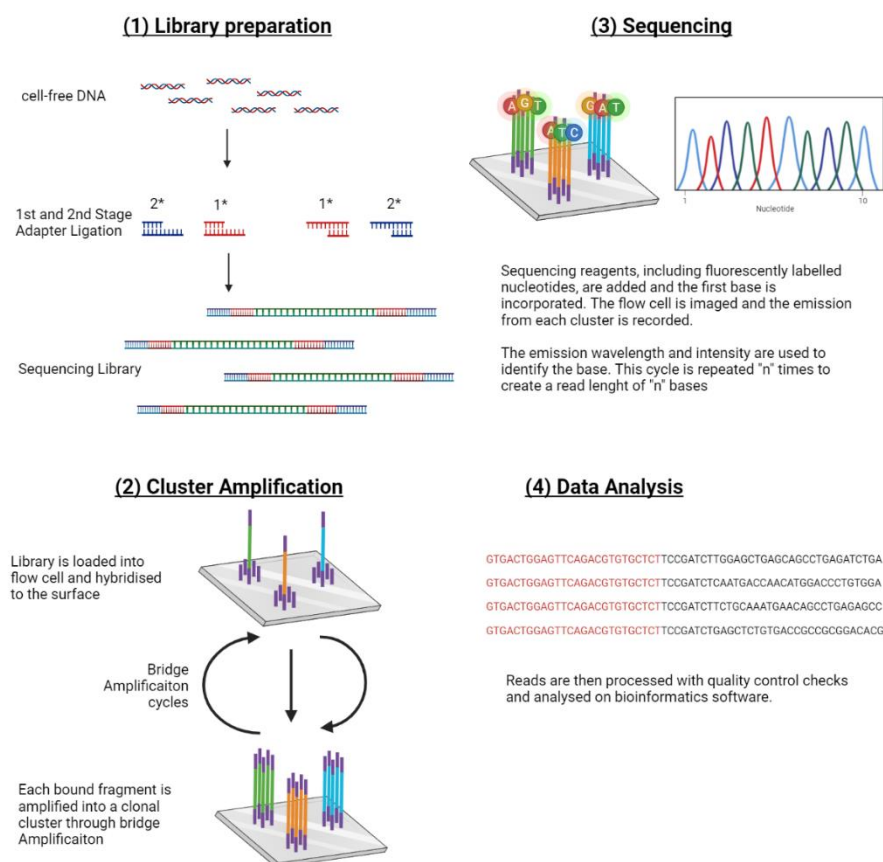


**Figure 2-4: Targeted NGS workflow.** Adapted from: [www.illumina.com/technology/next-generation-sequencing.html](http://www.illumina.com/technology/next-generation-sequencing.html). Created on Biorender.

## 2.5.6.1 Library preparation

### 2.5.6.1.1 1<sup>st</sup> Stage PCR adapter ligation

Targeted NGS libraries were prepared using a multiplex, two-stage PCR reaction. Prior to the NGS workflow, samples of purified cfDNA or genomic DNA were quantified and either 19 µL of purified cfDNA was added when the DNA quantity was low or 100 ng per reaction where possible (when using genomic DNA).

The first stage PCR reaction was composed of reagents Amplitaq Gold DNA polymerase with Gold Buffer &  $MgCl_2$  and a set of modified “inside” primers containing the first stage MiSeq partial adaptor (PA) sequences on the 5’ ends of the forward primer and the 3’ end of the consensus reverse primers.

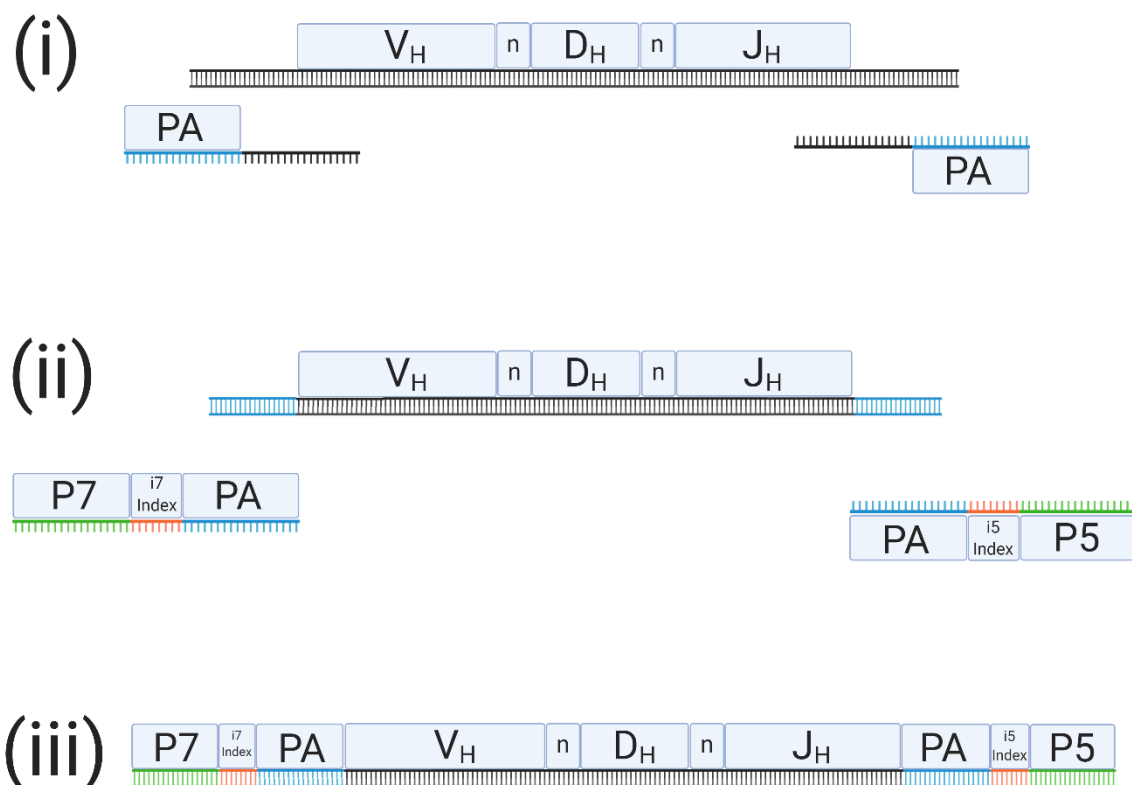


**Figure 2-5: NGS dual adapter approach schematic**

IGH	Complete rearrangements - Sequence 5' – 3'
<b>Forward</b>	
V <sub>H</sub> 1	GTGACTGGAGTTCAGACGTGTGCTCTTCCGATCTTGGAGCTGAGCAGCCTGAGATCTGA
V <sub>H</sub> 2	GTGACTGGAGTTCAGACGTGTGCTCTTCCGATCTCAATGACCAACATGGACCCTGTGGA
V <sub>H</sub> 3	GTGACTGGAGTTCAGACGTGTGCTCTTCCGATCTTCTGCAAATGAACAGCCTGAGAGCC
V <sub>H</sub> 4	GTGACTGGAGTTCAGACGTGTGCTCTTCCGATCTGAGCTCTGTGACCGCCGCGGACACG
V <sub>H</sub> 5	GTGACTGGAGTTCAGACGTGTGCTCTTCCGATCTCAGCACCGCCTACCTGCAGTGGAGC
V <sub>H</sub> 6	GTGACTGGAGTTCAGACGTGTGCTCTTCCGATCTGTTCTCCCTGCAGCTGAACTCTGTG
V <sub>H</sub> 7	GTGACTGGAGTTCAGACGTGTGCTCTTCCGATCTCAGCACGGCATATCTGCAGATCAG
<b>Reverse</b>	
J <sub>H</sub> Cons	ACACTCTTCCCTACACGACGCTCTTCCGATCTCTTACCTGAGGAGACGGTGACC

**Table 2-16: IGH complete rearrangements forward and reverse 1<sup>st</sup> stage primers.** Forward Primers span the V<sub>H</sub>1-V<sub>H</sub>7 gene segment. Reverse consensus primer targeting the J gene segment

IGH	Incomplete rearrangements - Sequence 5' – 3'
<b>Forward</b>	
D <sub>H</sub> 1	GTGACTGGAGTTCAGACGTGTGCTCTTCCGATCTGGCGGAATGTGTGCAGGC
D <sub>H</sub> 2	GTGACTGGAGTTCAGACGTGTGCTCTTCCGATCTGCACTGGGCTCAGAGTCCTCT
D <sub>H</sub> 3	GTGACTGGAGTTCAGACGTGTGCTCTTCCGATCTGTGGCCCTGGGAATATAAAA
D <sub>H</sub> 4	GTGACTGGAGTTCAGACGTGTGCTCTTCCGATCTAGATCCCCAGGACGCAGCA
D <sub>H</sub> 5	GTGACTGGAGTTCAGACGTGTGCTCTTCCGATCTCAGGGGGACACTGTGCATGT
D <sub>H</sub> 6	GTGACTGGAGTTCAGACGTGTGCTCTTCCGATCTTGACCCCAGCAAGGGAAGG
D <sub>H</sub> 7	GTGACTGGAGTTCAGACGTGTGCTCTTCCGATCTCACAGGCCCCCTACCAGC
<b>Reverse</b>	
<b>J<sub>H</sub>Cons</b>	ACACTCTTCCCTACACGACGCTCTTCCGATCTCTTACCTGAGGAGACGGTGACC

**Table 2-17: IGH incomplete rearrangements forward and reverse 1<sup>st</sup> stage primers.** Forward Primers span the DH1-DH7 gene segment. Reverse consensus primer targeting the J gene segment.

The products of the first stage PCR reaction were then purified using the AMPure XP bead purification method.

### 2.5.6.2 AMPure XP beads – Library purification

An AMPure XP bead purification method was used to purify PCR products for the two-stage PCR reaction. Each reagent for the clean-up procedure was made up fresh. The Elution Buffer was made up by mixing 1M Trizoma HCl ((Sigma-Aldrich, USA), Tween 20 (Sigma-Aldrich, USA) and dH<sub>2</sub>O and vortexing to ensure a homogenous solution. The Binding Buffer was made up by dissolving 2g of PEG (Sigma-Aldrich, USA) with 5 mL of NaCl (Sigma-Aldrich, USA) and then topped up

to 10 mL with dH<sub>2</sub>O and vortexed thoroughly to ensure a homogenous solution. All solutions were poured into individual disposable reservoirs.

The AMPure XP beads were allowed to equilibrate to room temperature for 30 minutes before use. The PCR products were mixed with 25 µL of Elution buffer and 50 µL of AMPure XP beads in PCR tube strips and incubated at room temperature for 5 minutes. The PCR tubes were then placed on a magnetic rack and left for 2 minutes before the supernatant was aspirated and discarded. The beads were then washed with 80% ethanol twice before being air dried for 5 minutes. The beads were then resuspended in elution buffer, mixed with binding buffer and incubated for 5 minutes at room temperature. The beads were then pelleted on the magnetic rack and left for 2 minutes before the supernatant was aspirated and discarded. The beads were then washed twice with 80% ethanol before being left to air-dry for 5 minutes. The beads were removed from the magnet and were resuspended with 50 µL of elution buffer. The beads were once again pelleted on the magnet for 2 minutes before the eluate was removed and transferred into a fresh 1.5 mL elution tube. Purified DNA was stored at -20°C.

#### **2.5.6.2.1 2<sup>nd</sup> Stage PCR adapter ligation**

The eluted, purified 1<sup>st</sup> stage PCR product was then quantified using the Qubit dsDNA HS Assay and analysed for size and quality using the Bioanalyzer 2100 instrument as described in section 1.5.4. The purified products were then used as template DNA for the second stage PCR reaction which used NEBNext Q5 Ultra II q5 Master Mix (New England Biolabs, Ipswich, MA, USA) and a set of secondary “outside” primers containing secondary matching adaptor sequences, sample-specific barcode sequences and flow cell ligation adapter sequences.

Stage 2 Primers	Sequence 5' – 3'
i7_01	CAAGCAGAAGACGGCATACGAGATCTAGCTAGTGACTGGAGTTCAGACGTGTGCTCTTCCGATC*T
i7_03	CAAGCAGAAGACGGCATACGAGATAGGTTGGCGTGACTGGAGTTCAGACGTGTGCTCTTCCGATC*T
i7_04	CAAGCAGAAGACGGCATACGAGATGACCAACGGTGACTGGAGTTCAGACGTGTGCTCTTCCGATC*T
i7_05	CAAGCAGAAGACGGCATACGAGATGCGGAGTTGTGACTGGAGTTCAGACGTGTGCTCTTCCGATC*T
i7_06	CAAGCAGAAGACGGCATACGAGATGTGCCATAGTGACTGGAGTTCAGACGTGTGCTCTTCCGATC*T
i7_07	CAAGCAGAAGACGGCATACGAGATTAAATGTCCGTGACTGGAGTTCAGACGTGTGCTCTTCCGATC*T
i7_08	CAAGCAGAAGACGGCATACGAGATCGAAGGACGTGACTGGAGTTCAGACGTGTGCTCTTCCGATC*T
i7_10	CAAGCAGAAGACGGCATACGAGATAGAACATTGTGACTGGAGTTCAGACGTGTGCTCTTCCGATC*T
i7_11	CAAGCAGAAGACGGCATACGAGATTGTCACTCGTGACTGGAGTTCAGACGTGTGCTCTTCCGATC*T
i7_12	CAAGCAGAAGACGGCATACGAGATCACCGCTTGACTGGAGTTCAGACGTGTGCTCTTCCGATC*T
i5_01	AATGATACGGCGACCACCGAGATCTACACCACTTGAGACACTCTTTCCCTACACGACGCTCTTCCGATC*T
i5_02	AATGATACGGCGACCACCGAGATCTACACGTTACCGAACACTCTTTCCCTACACGACGCTCTTCCGATC*T
i5_03	AATGATACGGCGACCACCGAGATCTACACTGACGACTACACTCTTTCCCTACACGACGCTCTTCCGATC*T
i5_04	AATGATACGGCGACCACCGAGATCTACACACGGATTACACTCTTTCCCTACACGACGCTCTTCCGATC*T
i5_05	AATGATACGGCGACCACCGAGATCTACACCATAGGAACACTCTTTCCCTACACGACGCTCTTCCGATC*T
i5_06	AATGATACGGCGACCACCGAGATCTACACTGGAAGGCACACTCTTTCCCTACACGACGCTCTTCCGATC*T
i5_07	AATGATACGGCGACCACCGAGATCTACACGCATCATGACACTCTTTCCCTACACGACGCTCTTCCGATC*T
i5_08	AATGATACGGCGACCACCGAGATCTACACAGCGGTGAACACTCTTTCCCTACACGACGCTCTTCCGATC*T
i5_10	AATGATACGGCGACCACCGAGATCTACACCATGCATAACACTCTTTCCCTACACGACGCTCTTCCGATC*T
i5_13	AATGATACGGCGACCACCGAGATCTACACTCCAGGTAACACTCTTTCCCTACACGACGCTCTTCCGATC*T

Table 2-18: 2nd Stage adapter primer sequences

Index combination	Index	Index in oligo	Index Read Sequence
1	i5_01	CACTTGAG	CACTTGAG
	i7_01	TCTAGCTA	TAGCTAGA
2	i5_02	GTTACCGA	GTTACCGA
	i7_03	AGGTTGGC	GCCAACCT
3	i5_03	TGACGACT	TGACGACT
	i7_04	GACCAACG	CGTTGGTC
4	i5_04	ACGGATTC	ACGGATTC
	i7_05	GCGGAGTT	AACTCCGC
5	i5_05	CCATAGGA	CCATAGGA
	i7_06	GTGCCATA	TATGGCAC
6	i5_06	TGGAAGGC	TGGAAGGC
	i7_07	TAATGTCC	GGACATTA
7	i5_07	GCATCATG	GCATCATG
	i7_08	CGAAGGAC	GTCCTTCG
8	i5_08	AGCGGTGA	AGCGGTGA
	i7_10	AGAACATT	AATGTTCT
9	i5_10	CATGCATA	CATGCATA
	i7_11	TGTCAGTC	GACTGACA
10	i5_13	TCCAGGTA	TCCAGGTA
	i7_12	CACCGCTT	AAGCGGTG

**Table 2-19: Unique indexes in 2<sup>nd</sup> stage PCR primers**



<b>Mastermix</b>	<b>Per Well (μL)</b>
10x PCR buffer	2.50
dNTPs (200uM)	0.50
Primer Pool (10pmol/primer)	0.40
MgCl <sub>2</sub> (2mM)	2.00
Taq polymerase (2U)	0.20
Water	Variable
DNA	variable
Volume added to wells	<b>5.6</b>
Total Volume	<b>25.0</b>

**Table 2-20: 2<sup>nd</sup> Stage PCR Mastermix composition**

<b>Cycle step</b>	<b>Temperature °C</b>	<b>Hold</b>	<b>No. of Cycles</b>
Pre-activation	95	7 mins	1
Denaturation	95	30 secs	30
Annealing	60	45 secs	
Extension	72	45 secs	
Final Extension	72	10 mins	1
Final hold	4	∞	-

**Table 2-21: 2<sup>nd</sup> Stage PCR thermocycling conditions**

### 2.5.6.2.2 DNA pooling

Prepared libraries were pooled according to their length (bp) based on metrics obtained from the Qubit dsDNA HS assay and the Bioanalyzer HS DNA assay. Libraries were created from samples being pooled to 1-4 nM to create an equimolar final pool of all the loci. These pools were submitted to Glasgow Polyomics for KAPA RQ-PCR quantification and sequencing on a MiSeq instrument (Illumina).

## 2.5.7 TruePrime cfDNA amplification

### 2.5.7.1 TruePrime Apoptotic cfDNA Amplification Kit

The TruePrime Apoptotic cell-free DNA amplification kit relies on a novel method of multiple displacement amplification with the use of *TthPrimPol* DNA primase and Phi29 DNA polymerase to amplify cfDNA from liquid biopsy samples. It targets short fragments of cfDNA (up to 170 bp) which are believed to originate from apoptotic mechanisms. The short cfDNA fragments were first treated with an end-repair and dA-tailing reaction which produced 3'-dA overhangs on both DNA strands in preparation for the subsequent ligation of hairpin adaptors to these overhangs. DNA primase *TthPrimPol* then recognises, binds, and produces primers on the hairpin adaptors and matching sequences are extended by Phi29 DNA polymerase. The strands are subsequently displaced by Phi29 allowing *TthPrimPol* to produce new primers on the newly created hairpin adaptors. This process continues exponentially, in a rolling circle, isothermal amplification method resulting in a vast increase in cfDNA starting material.

Following cfDNA isolation using QIAamp Circulating Nucleic Acids Kit (see section 2.5.2.2.2), 25  $\mu$ L of purified cfDNA was made up to 50  $\mu$ L with nuclease-free H<sub>2</sub>O. For the End-repair + dA-tailing reaction, the cfDNA samples were mixed with End-

repair enzyme mix and End-repair reaction buffer, mixed by pipetting the solution 10 times, then incubated in a thermocycler for 30 minutes at 20°C; 30 minutes at 65°C and held at 4°C with the lid set to a constant to 75°C.

The Adaptor Ligation mix was created by mixing Ligation mix, Enhancer Buffer, Adaptor Solution, and the End-repair + dA-tailing product and was then mixed by pipetting the solution 10 times. The Adaptor Ligation mix was then incubated in a thermocycler for 15 minutes with the lid heating turned off. The adaptor ligated cfDNA was then purified using the AMPure XP Bead clean-up method using a bead ratio of X (as described in section 2.5.6.2). Following the clean-up procedure, the TruePrime amplification mix was created by mixing nuclease-free H<sub>2</sub>O; Reaction Buffer; dNTPs; Enzyme 1 and Enzyme 2 to 15 µL of the clean adaptor ligation mix. The amplification reaction solution was then mixed by pipetting the solution 10 times and incubated in a thermocycler at 30°C for 6 hours; 65°C for 10 minutes to inactivate the reaction; and cooled to 4°C. The samples were then quantified using the Qubit dsDNA BR Assay kit (section **2.5.4.1**).

## 2.6 Data analysis

All statistical analysis was performed on GraphPad Prism v9 unless stated otherwise.

All tables were created using Microsoft® Excel® for Microsoft 365 MSO (Version 2203 Build 16.0.15028.20152) 32-bit and figures were assembled or created using Microsoft® PowerPoint® for Microsoft 365 MSO (Version 2203 Build 16.0.15028.20152) 32-bit or BioRender (BioRender.com)

ROC curve analysis and multivariate biomarker modelling was performed using Metaboanalyst web platform v5.0 (<https://www.metaboanalyst.ca/>) [103].

Digital PCR data was analysed using QuantaSoft Software version 1.7.4.0917. Data representation and statistics were performed using GraphPad Prism version 9 for Windows, GraphPad Software, San Diego, California USA, ([www.graphpad.com](http://www.graphpad.com))

Raw NGS files were pre-processed on a Galaxy server provided by Glasgow Polyomics (<https://www.polyomics.gla.ac.uk/>). Bioinformatic analysis was performed on web application Vidjil (<https://app.vidjil.org/>) [104]

VDJ sequences were compared to IgBlast and IMGT/Vquest databases for analysis of VDJ gene rearrangements: (<https://www.ncbi.nlm.nih.gov/igblast/index.cgi>) (<https://www.imgt.org/>)

## Chapter 3: Metabolic biomarkers for CNS-ALL

### 3 Introduction and aims

Profiling the metabolome of cancers is a growing field in the search for clinically informative biomarkers. Metabolic reprogramming is a known hallmark of cancer, where malignant cells are known to adapt to their microenvironments to survive and replicate through metabolic changes, particularly when microenvironments are harsh i.e., nutrient deficient or hypoxic. The leptomeninges is bathed in nutrient deficient CSF and typically this space has low levels of cells. Leukaemic blasts adapt to this harsh environment through metabolic alterations and consequently might alter the metabolic profile of CSF in the process. To explore the metabolome of the leukaemic CNS space, a technique called liquid chromatography mass spectrometry (LC-MS) was used in this study. LC-MS is a powerful tool which can be used to discriminate between various small, polar metabolites and quantify relative abundance or absolute abundance if a standard curve of target analytes is used.

Metabolomics can be used to identify hundreds to thousands of metabolites simultaneously in a single experiment. This has important implications in the field of biomarker discovery and development as it is commonplace to use several biomarkers in combination for various clinical diagnoses and prognoses. The use of the right combination of multiple biomarkers in parallel can significantly increase the specificity and sensitivity of a diagnosis and aid in personalising medicine for patients with aggressive disease.

In a metabolic biomarker discovery and development pipeline, the process can be generally divided into three stages, 1) Selection of clinically appropriate candidate

biomarkers, 2) Evaluation of candidate biomarker performance, 3) Creation of a multivariate biomarker model. Previous work in the Halsey laboratory identified potential candidate biomarkers in the CSF of children with ALL which showed promise in detecting a potential leukaemic metabolic signature in the CSF of diagnostic patient samples. Patient CSF samples were compared against matched control CSF taken from patients a year into treatment where leukaemic burden in the CNS is expected to be minimal to non-existent and unmatched CSF controls taken from children under the age of 12 who were admitted to hospital for neurological conditions but were cleared from any cancer. The use of the matched control is essential to obtain a “normal state” signature of the candidate biomarker in a controlled cohort of patient samples who are matched for the appropriate age group and clinical setting. The use of the unmatched control cohort again gives us strong insight into the “normal state” of the candidate biomarkers from an external source of CSF originating from the same age group.

The experimental approach taken previously in the Halsey laboratory was an untargeted metabolomic analysis which set the analytical foundation for this analysis and begins to address point 1 of the metabolic biomarker discovery and development pipeline (Biomarker selection). The candidate biomarkers put forward in that study included a range of amino acid derivatives, alpha amino acids, nucleosides, and nucleoside analogues.

This study first reanalysed this data in the search for more candidate biomarkers again using an untargeted experimental approach. With a final list of candidate biomarkers, this study then took a targeted approach focussing on points 2 and 3 of the pipeline, evaluating the candidate biomarkers using two cohorts of patient and control CSF samples. The first cohort was composed of childhood leukaemic CSF

samples originating from the Halsey biobank in Glasgow, UK and two groups of CSF controls. This cohort was used as a small-scale pilot study evaluating the behaviour of the candidate biomarkers against the CSF controls. The first control CSF group, akin to the unmatched control group mentioned previously, was composed of CSF samples taken from patients who were admitted to hospital for suspected non-inflammatory neurological conditions and had a lumbar puncture taken which returned normal results with clinical profiles parallel to normal CSF. The second group of control CSF was composed of CSF samples from patients who were admitted to hospital for suspected inflammatory neurological conditions. Both control CSF groups did not have CSF samples which had any malignant diagnoses.

The second cohort was composed of a large, comprehensive cohort of patient samples obtained from a national childhood leukaemia biobank composed of diagnostic samples from patients classified as CNS1, CNS2 or CNS3 by CSF cytology and more control CSF samples composed of non-inflammatory and inflammatory CSF samples. This cohort was used to further evaluate and validate findings from the pilot study through biomarker evaluation analyses (point 2) and to begin to address point 3 of the metabolic biomarker discovery and development pipeline to test the clinical utility of a panel of successful candidate biomarkers as diagnostic biomarkers of CNS-ALL. This cohort also included several diagnostic samples from patients who went onto have either isolated CNS relapse or combined CNS and bone marrow relapse. These samples are an opportunity to investigate whether the chosen candidate biomarkers express different signatures when compared against each other with the aim of elucidating their efficacy as candidate prognostic biomarkers.

The aim of this part of the study was to further test the candidate biomarkers for their clinical utility as diagnostic and prognostic biomarkers for CNS-ALL. The analysis of candidate biomarkers was performed according to the following specific aims:

1. To perform a new untargeted analysis on a previous dataset of diagnostic ALL CSF samples from the Halsey Biobank and matched/ unmatched controls using a more comprehensive and stringent compound identification software programme to interrogate these results further in the search for more candidate diagnostic biomarkers.
2. To perform a targeted metabolic analysis on a new cohort of CSF samples from the Halsey biobank to validate candidate diagnostic biomarkers identified in (1) and to compare metabolomic signatures between diagnostic ALL CSF samples with inflammatory and non-inflammatory control CSF sample groups.
3. To perform targeted metabolic analysis on a large, comprehensive cohort of diagnostic CSF samples from a national biobank using candidate diagnostic biomarkers identified in (1) and compare metabolic signatures to that of inflammatory and non-inflammatory control CSF groups.
4. To perform both univariate and multivariate analyses of diagnostic patient samples against a combined cohort of CSF controls made up of inflammatory and non-inflammatory control CSF for both datasets in aims 2 and 3.



5. To perform targeted metabolic analysis to identify potential prognostic biomarkers using patient diagnostic samples from patients who went onto relapse in the CNS.

### 3.1 Candidate diagnostic biomarkers

#### 3.1.1 Untargeted reanalysis to find new candidate biomarkers of interest

The first step was to re-analyse the chromatogram from the previous dataset created in the Halsey laboratory using Compound Discoverer (Thermo Fisher) software to identify new potential candidate biomarkers for investigation. This experiment included 19 CNS1 patient samples obtained from the Glasgow Biobank from children with ALL diagnosed between 2009 and 2016 and were compared to both matched and unmatched CSF controls mentioned above.

To begin, the reanalysis consisted of another untargeted approach to analyse the data with a higher resolution in Compound Discoverer (Thermo Fisher) to attempt to discover novel candidate biomarkers which may have been missed initially. First, the raw data was filtered by removing basal levels of metabolites and any low-abundance metabolites, reducing the number of analytes from 1142 to 507 indicating the presence of a lot of background noise in the data. The data was then subjected to statistical analysis to search for differences between the means of the leukaemic samples (henceforth labelled and referred to as “CNS Dx”) and both the matched late control CSF samples and unmatched control CSF samples to further filter down the number of relevant candidate biomarkers (**Table 3-1**).

To ensure that any candidate biomarker would be suitable for further analysis, a ratio filtering method was then applied to all metabolites that were identified as having a significant difference between the CNS Dx group and the means of both control CSF groups. This ratio filtering involved filtering for metabolites that were either clearly higher (where the highest value in both control groups was less than

11% higher than the average of the CNS Dx patient group) or clearly lower (where the lowest value in both control groups was greater than 11% higher than the average of the CNS Dx patient group) than both the late control CSF and unmatched control CSF groups to ensure concordant trends (**Equation 1**).

Software	Filter	Number of metabolites	
Compound Discoverer (CD)	Raw	1142	
	Background + Area >10000	507	
GraphPad Prism v9	Unpaired t-tests	POS = 29	Neg= 45
Microsoft Excel	Ratio filtering	POS=18	Neg = 13
Compound discoverer, Online databases	ID matching + HMDB	POS =0	NEG = 2

**Table 3-1: Untargeted metabolomic analysis filtering workflow.** Initial filtering took place in CD software followed by statistical filtering in GraphPad Prism v9. Ratio filtering was performed on Microsoft Excel. Identification of compounds was performed on Compound discoverer and public databases mzCloud and HMDB.

$$\frac{\text{Max (Matched CTL)}}{\text{Mean (Dx)}} \text{ AND } \frac{\text{Max (Unmatched CTL)}}{\text{Mean (Dx)}} < 1.11$$

Or

$$\frac{\text{Min (Matched CTL)}}{\text{Mean (Dx)}} \text{ AND } \frac{\text{Min (Unmatched CTL)}}{\text{Mean (Dx)}} > 0.89$$

**Equation 1: Ratio filtering**

Following this, candidate biomarkers were identified by matching metabolites to an in-house database from the metabolomics department in the Beatson Institute, Glasgow in the Compound Discoverer software and by using mzCloud and HMDB, two publicly available databases. Candidate biomarkers previously identified by the Halsey lab were excluded from this analysis. This filtering process identified two candidate biomarkers for further investigation, both from the negative ionisation mode, Inosine and Orotidine (**Figure 3-2, Table 3-3**). The performance of the biomarkers in terms of statistical significance and fold change can be seen in (**Figure 3-1, Table 3-3**).

ROC curve analysis was then performed to test the performance of the candidate biomarkers. ROC curves are a powerful and statistically valid tool in biomarker assessment to determine the discriminatory ability of an analyte between a patient (disease) group and a control (non-disease group). Typically, comparisons between disease and non-disease groups reveal natural overlaps in their distributions and ROC curves can be leveraged to test the specificity of the proportion of the control (non-disease) group which correctly identify as negative, as well as the sensitivity of the proportion of the patient (disease) group which correctly identify as positive.

A ROC curve analysis will calculate the frequency of true positives, true negatives, false positives, and false negatives and will subsequently plot a curve and yield the following metrics: 1) A quantified area under curve (AUC) value between 0 and 1 summarizing the overall discriminatory ability of the test to differentiate between the patient (disease) and control (non-disease) groups; 2) 95% confidence intervals which describe the range of values in which a sample will lie upon repeating the same experiment with an independent population of the same disease; 3) A p value testing the null hypothesis that the AUC of a measurement equals 0.5. In which case

a p value less than an alpha of 0.05 will indicate that the feature (analyte) can discriminate between the patient (disease) and control (non-disease) with a high degree of certainty.

The result of a ROC curve analysis can be summarised with the AUC but must be interpreted with care, considering the 95% confidence intervals, and accompanying non-parametric statistical test summarised by the p value yielded (**Table 3-2**).

AUC	Discriminatory performance
$\leq 0.5 - 0.6$	No discrimination
0.6 to 0.7	Poor
0.7 to 0.8	Acceptable
0.8 to 0.9	Good
0.9 to 1.0	Excellent

**Table 3-2: Classification designations for AUC [103, 105].**

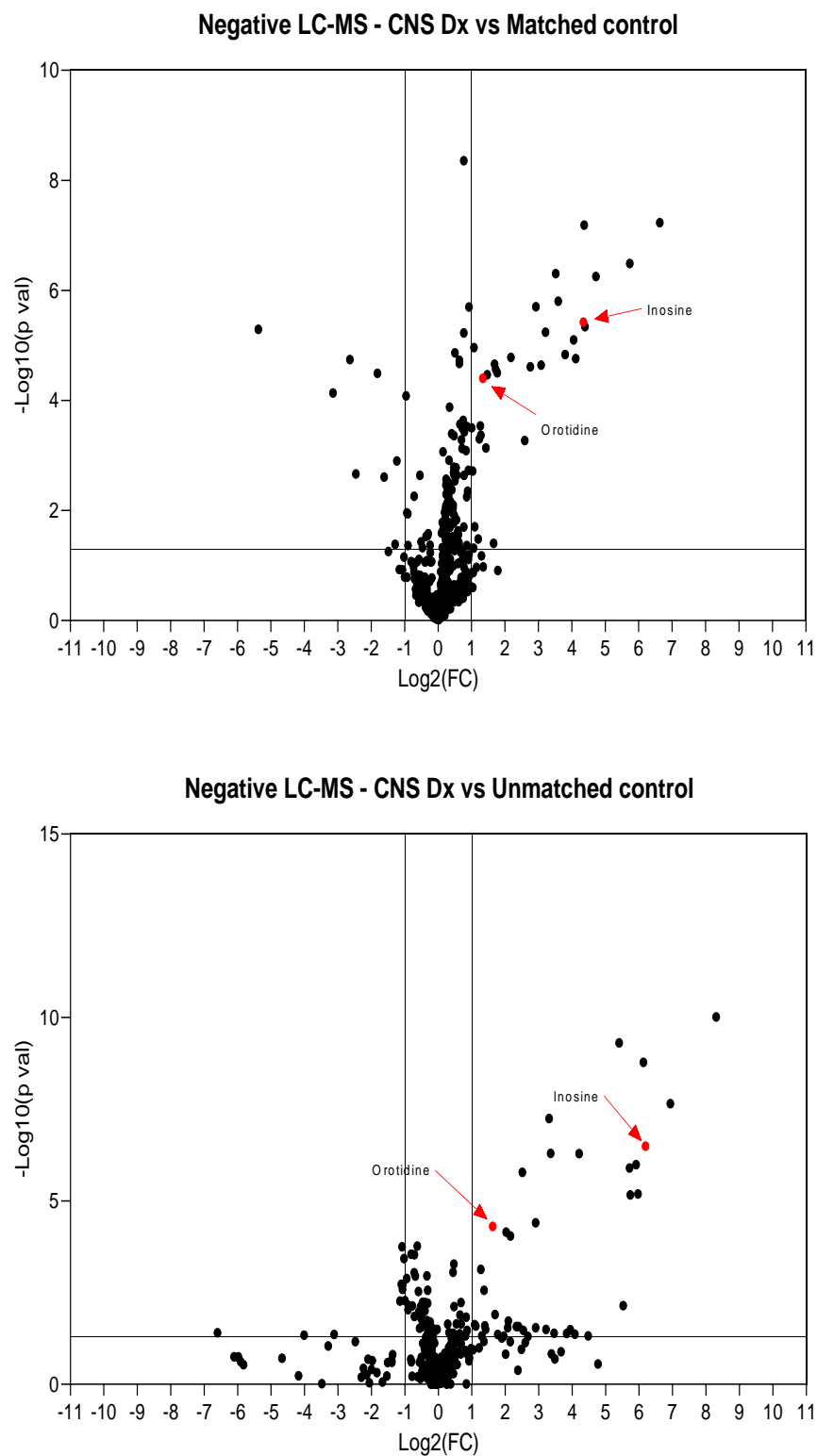


**Figure 3-1: Volcano plot of untargeted metabolomic data.** CNS Dx vs matched CSF control (top) and CNS Dx vs unmatched CSF control (bottom). P values are described to the  $-\log_{10}$  on the y axis and fold change is described as  $\log_2$  on the x axis. Statistically significant increased or decreased metabolites are present in the top left and top right quadrants. Graphs created on GraphPad Prism v9.

In this study, calculated AUCs will be categorised according to (**Table 3-2**). Results from this analysis show concordance between the CNS Dx group vs both matched and unmatched controls with good AUCs for both candidate biomarkers Inosine and Orotidine (0.87 & 0.88 respectively) , similar 95% confidence intervals and p values, both  $<0.001$ , suggesting that both candidate biomarkers show good ability to discriminate between disease and non-disease samples (**Table 3-4, Figure 3-3**).

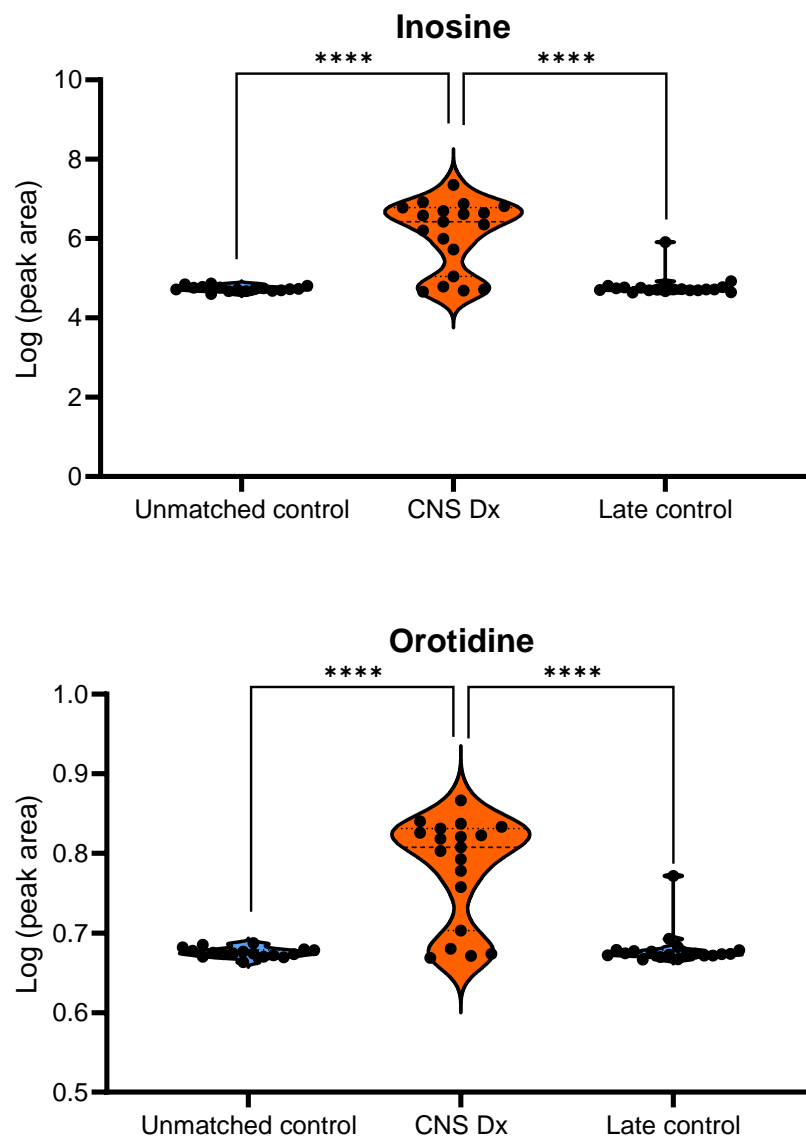


**Figure 3-2: Violin plots of Inosine and Orotidine CNS Dx patient samples vs matched and unmatched CSF controls.** CNS Dx n=19; matched control n=19; unmatched control n=17. Data was log transformed and graphs were created on GraphPad Prism v9.

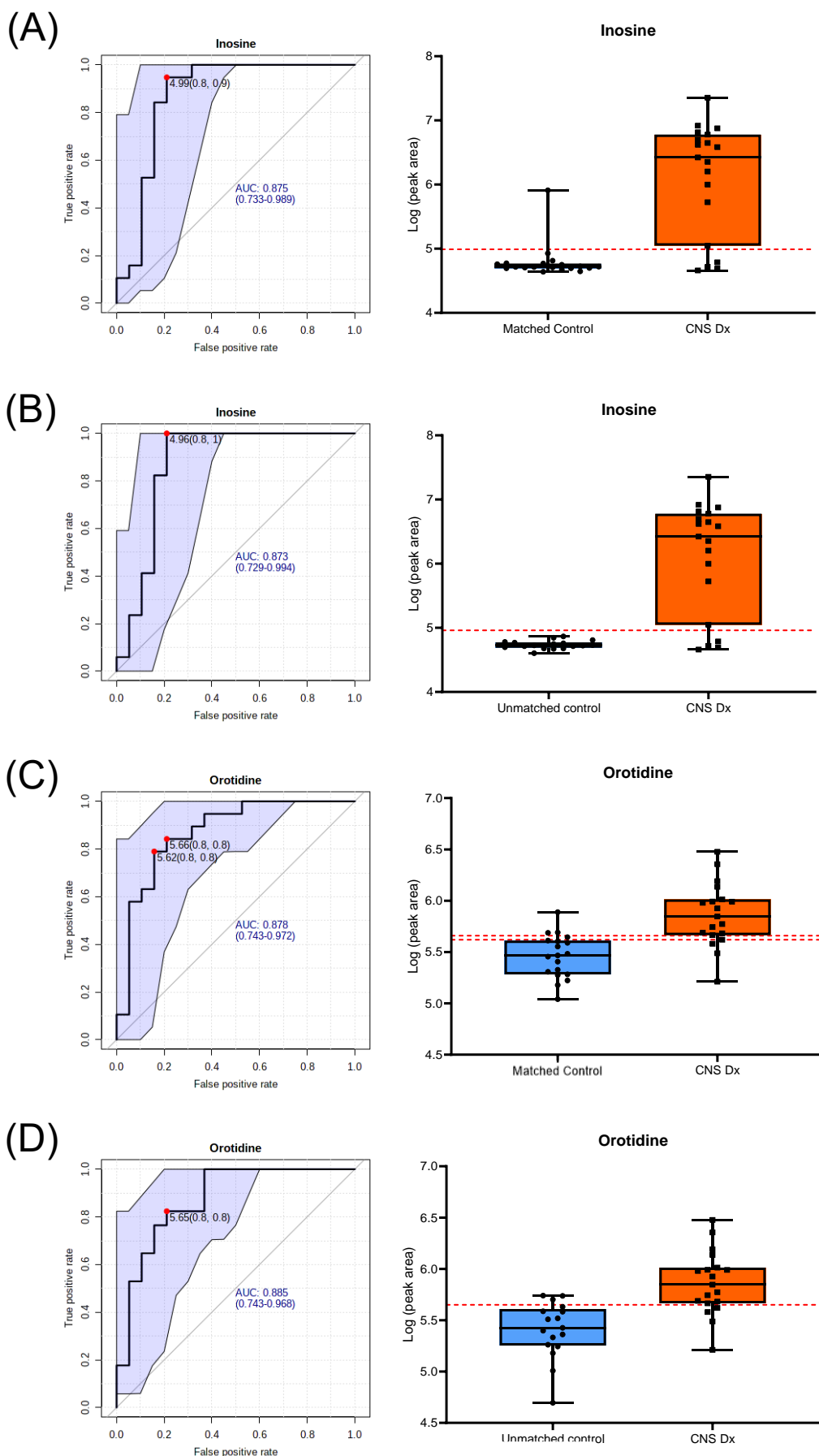


**Figure 3-3: Inosine & Orotidine ROC Curves and optimal cut-off points between CNS Dx and matched and unmatched CSF controls.** Optimal cut-off points (red dotted line) determined as “closest to top left” described by  $d = \sqrt{[1 - \text{Sensitivity}]^2 + [1 - \text{Specificity}]^2}$ . (A) Inosine – CNS Dx vs matched control; (B) Inosine – CNS Dx vs Unmatched control ; (C) Orotidine – CNS Dx vs matched control; (D) Orotidine – CNS Dx vs unmatched control. ROC curves created on Metaboanalyst; Box plots created on GraphPad Prism v9.



Candidate biomarker	Control	CNS Dx	SEM	95% confidence interval	R <sup>2</sup>	Log 2 FC	P value	Adj. p value
Inosine CNS Dx vs matched control	4.792	6.100	0.21	-1.729 to - 0.8882	0.7039	5.4202	0.0000004402	0.0000008805
Inosine CNS Dx vs unmatched control	4.736	6.100	0.22	-1.802 to - 0.9261	0.5410	6.1955	0.0000003217	0.0000006433
Orotidine CNS Dx vs matched control	5.459	5.861	0.086	-0.5586 to - 0.2455	0.6180	1.5191	0.0000388679	0.0000388679
Orotidine CNS Dx vs unmatched control	5.407	5.861	0.098	-0.6529 to - 0.2554	0.3881	1.628	0.0000495428	0.0000495428

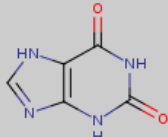
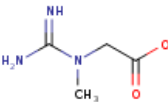
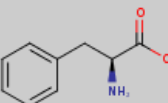
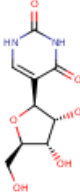
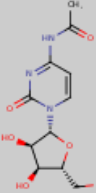
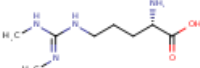
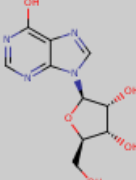
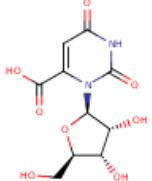
**Table 3-3: Candidate biomarkers: Statistical analysis of the difference between CNS Dx and matched/unmatched CSF controls.** Data was log transformed prior to statistical analysis. Paired t-test – CNS Dx vs matched control; Unpaired t-test CNS Dx vs unmatched control. Multiple comparisons corrected by Holm-Sidak method with  $\alpha=0.05$  and statistic described by adjusted p value. All statistics were performed on GraphPad Prism v9.

ROC	CNS Dx vs matched control				CNS Dx vs Unmatched control			
Metabolite	AUC	95% CI	p value	Optimal cut-off	AUC	95% CI	p value	Optimal cut-off
Inosine	0.86	0.73 to 0.99	4.4063E-7	4.99	0.87	0.73 to 0.99	3.2202E-7	4.96
Orotidine	0.88	0.74 to 0.97	3.8863E-5	5.62, 5.66	0.88	0.74 to 0.98	4.949E-5	5.65

**Table 3-4: ROC curve analysis summary: CNS Dx vs matched/ unmatched control.** AUC = Area under the curve; CI = confidence intervals. P value calculated by non-parametric t-test. Optimal cut-off points determined as “closest to top left” described by  $d = \sqrt{[1 - \text{Sensitivity}]^2 + (1 - \text{Specificity})^2}$ .

### 3.1.2 Summary

Both Inosine and Orotidine show promise in discriminating CNS-ALL from both matched and unmatched control CSF. The data shows elevated levels of the respective analyte in the CNS Dx group compared to both controls and are the result of a stringent filtering process thus, these two candidate biomarkers were taken forward alongside the previously discovered candidate biomarker metabolites, Xanthine, Creatine, Phenylalanine, Pseudouridine, N4-acetylcytidine and Symmetric dimethylarginine (**Table 3-5**).

Candidate Biomarkers	Structure	Formula	Av. MW	HMDB ID & online reference
Xanthine		C <sub>5</sub> H <sub>4</sub> N <sub>4</sub> O <sub>2</sub>	152.1109	HMDB0000292 <a href="https://hmdb.ca/metabolites/HMDB0000292">https://hmdb.ca/metabolites/HMDB0000292</a>
Creatine		C <sub>4</sub> H <sub>9</sub> N <sub>3</sub> O <sub>2</sub>	131.1332	HMDB0000064 <a href="https://hmdb.ca/metabolites/HMDB0000064">https://hmdb.ca/metabolites/HMDB0000064</a>
Phenylalanine		C <sub>9</sub> H <sub>11</sub> N O <sub>2</sub>	165.1891	HMDB0000159 <a href="https://hmdb.ca/metabolites/HMDB0000159">https://hmdb.ca/metabolites/HMDB0000159</a>
Pseudouridine		C <sub>9</sub> H <sub>12</sub> N <sub>2</sub> O <sub>6</sub>	244.2014	HMDB0000767 <a href="https://hmdb.ca/metabolites/HMDB0000767">https://hmdb.ca/metabolites/HMDB0000767</a>
N4-acetylcytidine		C <sub>11</sub> H <sub>15</sub> N <sub>3</sub> O <sub>6</sub>	285.2533	HMDB0005923 <a href="https://hmdb.ca/metabolites/HMDB0005923">https://hmdb.ca/metabolites/HMDB0005923</a>
Symmetric dimethylarginine		C <sub>8</sub> H <sub>18</sub> N <sub>4</sub> O <sub>2</sub>	202.2541	HMDB0003334 <a href="https://hmdb.ca/metabolites/HMDB0003334">https://hmdb.ca/metabolites/HMDB0003334</a>
Inosine		C <sub>10</sub> H <sub>12</sub> N <sub>4</sub> O <sub>5</sub>	268.2261	HMDB0000195 <a href="https://hmdb.ca/metabolites/HMDB0000195">https://hmdb.ca/metabolites/HMDB0000195</a>
Orotidine		C <sub>10</sub> H <sub>12</sub> N <sub>2</sub> O <sub>8</sub>	288.2109	HMDB0000788 <a href="https://hmdb.ca/metabolites/HMDB0000788">https://hmdb.ca/metabolites/HMDB0000788</a>

**Table 3-5: Candidate biomarkers selected for further evaluation.** Source: The human metabolome database (HMDB).

## 3.2 Targeted analysis of candidate diagnostic biomarkers – Pilot Cohort

### 3.2.1 Univariate analysis of candidate biomarker performance against non-inflammatory and inflammatory control CSF

The next step was to test all candidate biomarkers using a targeted metabolomics approach with a small pilot cohort of patient and control CSF samples. This cohort of patient samples derived from the same local biobank in the Halsey laboratory, Glasgow, as the previous experiment. Patient samples were compared against two types of CSF control samples derived from samples taken from adults who were admitted to hospital for either non-inflammatory or inflammatory conditions but were cleared of any cancer (**Table 3-6**). For the following experiments, the non-inflammatory control cohort will act as a surrogate “normal CSF” control for the unmatched CSF control and the matched late control from the previous experiment.

The control samples from the inflammatory CSF cohort were used to test the specificity of the candidate biomarker for leukaemia. It was hypothesized that a specific candidate biomarker for CNS-leukaemia in this setting would concord with both the inflammatory control or non-inflammatory control CSF as being either clearly higher or lower than the patient group. A candidate biomarker’s discordancy in the comparisons between the leukaemic patient sample group and the inflammatory control CSF would thus suggest a non-specific phenotype for CNS-ALL.

In this experiment, ten diagnostic CNS1 patient CSF samples were compared against ten non-inflammatory control CSF samples (also referred to as NI CTL) and ten inflammatory control CSF samples also referred to as I CTL) (**Figure 3-4, Table**

**3-6, 3-7).** Statistical analysis was performed to test for significant differences between the means of the comparators. Of the eight candidate biomarkers tested, Xanthine (CNS Dx vs NI CTL p value <0.0001; CNS Dx vs I CTL p value <0.0001) and Inosine (CNS Dx vs NI CTL p value = 0.012675; CNS Dx vs I CTL p value = 0.012970) showed highly elevated levels compared to both controls and statistical analysis indicated significant differences between the means of the comparisons (**Figure 3-4, Table 3-8**).

CSF control demographic			
Control type	Ages	Sex	Diagnosis
NI control n=10	26- 73	14 F	Migraine, headache, Functional*, motor neuronopathy, delirium, epilepsy
		6 M	
I control n=10	18 - 57	13 F	Neurosarcoidosis, post-infectious movement disorder, RRMS**,
		7 M	

**Table 3-6: Control CSF cohorts – non-inflammatory and inflammatory CSF.** F= Female; M = Male. \* Functional = Body symptoms which appear to be caused by the CNS, but are not, medically unexplained. \*\* RRMS = Relapsing-Remitting Multiple Sclerosis.

Patient ID	Age @ Dx	Sex	CNS status
Patient 1	4.6	F	1
Patient 2	7.9	F	1
Patient 3	1.8	F	1
Patient 4	5.5	F	1
Patient 5	2.9	F	1
Patient 6	3.2	F	1
Patient 7	15.7	F	1
Patient 8	2	M	1
Patient 9	6.2	F	1
Patient 10	3.2	M	1

**Table 3-7: Patient clinical details for samples in the pilot experiment.**

Creatine presented with an inverse trend with decreased levels compared to both controls and statistical analysis indicated a highly significant difference between the means of the comparators (CNS Dx vs NI CTL p val <0.0001; CNS Dx vs I CTL p val <0.0001).

N4-acetylcytidine and Symmetric dimethylarginine also had elevated means in the CNS Dx group compared to both CSF controls and presented with significant differences between the means with p values <0.05.

Phenylalanine and Orotidine showed slightly elevated means in the CNS1 Dx group (8.58 & 5.95 respectively) compared to both CSF controls (NI CTL= 8.52; I CTL= 8.51 & NI CTL =5.78; I CTL = 5.73) and the spread of the data in the violin plots indicates the data trends higher than the means of both controls but statistical analysis did not reveal any significant differences between the means of either comparison (**Figure 3-4, Table 3-8**).

Pseudouridine presented with effectively equal amounts in all comparisons and statistical analysis revealed no significant difference between the means of either comparison (**Figure 4, Table 3-8**).

Next, ROC curve analysis was performed, and results were concordant between the CNS Dx group and both CSF controls for Xanthine, Creatine, N4-acetylcytidine, Symmetric dimethylarginine, and Inosine (**Figure 3-5, 3-6, 3-7 & 3-8; Table 3-9**). Creatine showed the best ability to discriminate between the CNS Dx group and both CSF control groups with very high-performance ROC curve metrics. The AUC for both comparisons suggest that Creatine is an excellent discriminator (AUC 0.98 for both comparisons) and this was accompanied by higher and narrow 95% confidence intervals (0.88 to 1.00 & 0.90 to 1.00 respectively) and p values <0.05 (**Table 9; Figure 5 B1-B2**).

Xanthine showed excellent discriminatory ability with an AUC of 0.93; 0.76 to 1.00 95% CI; p= <0.05) in the CNS Dx vs NI CTL comparison. This was concordant in the CNS Dx vs I CTL comparison with an AUC of 0.90; p val <0.05 however, with wider 95% confidence intervals in this comparison, stretching from 0.67 to 1.00, but both with accompanying p values <0.05 (**Table 9, Figure 5 A1-A2**) .

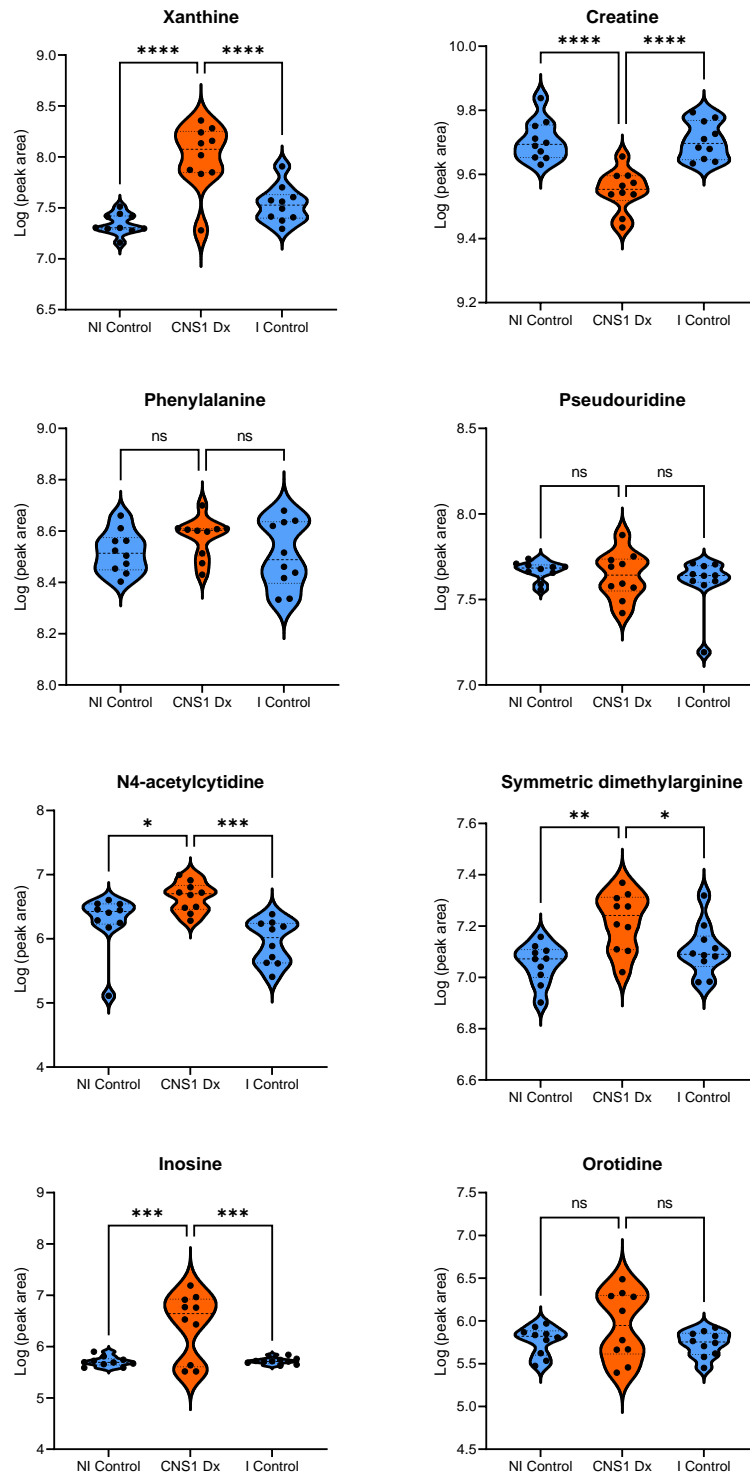


**Figure 3-4: Violin plots of candidate biomarkers depicting CNS Dx patient group vs non-inflammatory control CSF and inflammatory control CSF.** CNS1 Dx: Diagnostic leukaemic patient samples (n=10); NI Control: Non-inflammatory control CSF (n=10); I Control: Inflammatory control CSF (n=10). Statistics performed on GraphPad Prism v. One-way ANOVA; means of Controls compared with mean on CNS Dx group with Dunnett's multiple comparisons test  $\alpha=0.05$ . Data was log transformed and graphs were created on GraphPad Prism v9.



Candidate biomarker	Control Mean	CNS Dx Mean	SE of difference	95% confidence interval	ANOVA R <sup>2</sup>	Log 2 FC	ANOVA P value	Adjusted p Value
Xanthine CNS Dx vs NI CTL	9.706	9.550	0.02784	-0.2209 to -0.09096	0.6077	2.43	0.000003	<0.0001
Xanthine CNS Dx vs I CTL	9.706		0.02784	-0.2208 to -0.09090	0.6077	1.71		<0.0001
Creatine CNS Dx vs NI CTL	7.341	8.002	0.09730	0.4338 to 0.8879	0.6440	-0.52	<0.000001	<0.0001
Creatine CNS Dx vs I CTL	7.533		0.09730	0.2422 to 0.6963	0.6440	-0.52		<0.0001
Phenylalanine CNS Dx vs NI CTL	8.519	8.575	0.04445	-0.04739 to 0.1601	0.08924	0.19	0.283118	0.354887
Phenylalanine CNS Dx vs I CTL	8.507		0.04445	-0.03632 to 0.1711	0.08924	0.19		0.240042
Pseudouridine CNS Dx vs NI CTL	7.667	7.641	0.05426	-0.1527 to 0.1006	0.04975	0.03	0.502127	0.847648
Pseudouridine CNS Dx vs I CTL	7.603		0.05426	-0.08853 to 0.1647	0.04975	0.13		0.708210
N4-acetylcytidine CNS Dx vs NI CTL	6.283	6.650	0.1542	0.007148 to 0.7269	0.4350	1.04	0.000450	0.045257
N4-acetylcytidine CNS Dx vs I CTL	5.947		0.1542	0.3430 to 1.063	0.4350	2.16		0.000200
Symmetric dimethylarginine CNS Dx vs NI CTL	7.055	7.219	0.04357	0.06284 to 0.2662	0.3553	0.57	0.002668	0.001565
Symmetric dimethylarginine CNS Dx vs I CTL	7.107		0.04357	0.01039 to 0.2137	0.3553	0.51		0.029574
Inosine CNS Dx vs NI CTL	5.707	6.422	0.1666	0.3261 to 1.104	0.4735	3.31	0.000173	0.000408
Inosine CNS Dx vs I CTL	5.715		0.1666	0.3183 to 1.096	0.4735	3.30		0.000462
Orotidine CNS Dx vs NI CTL	5.767	5.946	0.1179	-0.09561 to 0.4544	0.1226	1.00	0.171075	0.237723
Orotidine CNS Dx vs I CTL	5.733		0.1179	-0.06218 to 0.4878	0.1226	1.13		0.144175

**Table 3-8: Candidate biomarkers: Statistical analysis of the difference between CNS Dx and matched/unmatched CSF controls.** Data was log transformed prior to statistical analysis. One-way ANOVA; means of Controls compared with mean on CNS Dx group with Dunnett's multiple comparisons test  $\alpha = 0.05$ . Statistics performed on GraphPad Prism v9.

N4-acetylcytidine presented with elevated levels in the CNS Dx group compared to both CSF controls with a significant difference between the means. ROC curve analysis was concordant however the CNS Dx vs NI control comparison saw notably wide 95% confidence intervals (0.55 to 0.97) as is further supported by the closeness of the data seen in (**Figure 3-7 E1**). Other than this, this comparison had a high AUC of 0.81 and a p value <0.05. The CNS Dx vs I control comparison had a very high AUC of 0.99 and the narrowest 95% confidence intervals of 0.96 to 1.00 of all the candidate biomarkers for all comparisons and a p value <0.05 (**Table 3-9, Figure 3-6 E2**).

Symmetric dimethylarginine presented with elevated levels in the CNS Dx group compared with both controls and with concordant AUCs (CNS Dx vs NI CTL:AUC 0.89; 95% CI 0.71 to 1.00; p value <0.01) outperforming the CNS Dx v I control (AUC 0.8; p value <0.05) with notably wide 95% confidence intervals of 0.44 to 0.97, but equally suggesting this candidate biomarker as having excellent ability to discriminate between both comparator groups. This can be seen visually in the data at the overlap in between the I control CSF and the CNS1 Dx group (**Table 3-9, Figure 3-7 F1-F2**).

ROC	CNS1 Dx vs NI CTL				CNS1 Dx vs I CTL			
Metabolite	AUC	95% CI	t-test p value	Optimal Cut-off	AUC	95% CI	t-test p value	Optimal Cut-off
Xanthine	0.93	0.76 to 1.00	6.0772E-6	7.67	0.90	0.67 to 1.00	6.8754E-4	7.77
Creatine	0.98	0.88 to 1.00	3.5525E-5	9.61	0.98	0.90 to 1.00	2.3558E-5	9.62
Phenylalanine	0.70	0.42 to 0.91	0.13246	8.58	0.59	0.32 to 0.83	0.17634	8.56
Pseudouridine	0.52	0.27 to 0.80	0.58067	7.62	0.53	0.20 to 0.80	0.5599	7.67
N4-acetylcytidine	0.81	0.55 to 0.97	0.029762	6.47	0.99	0.96 to 1.00	3.7358E-5	6.27 6.39*
Symmetric Dimethylarginine	0.89	0.71 to 1.00	0.0012347	7.11	0.80	0.55 to 0.97	0.030025	7.17
Inosine	0.71	0.40 to 1.00	0.0024514	6.17	0.70	0.40 to 1.00	0.0025295	6.14
Orotidine	0.60	0.28 to 0.84	0.20535	6.04	0.63	0.36 to 0.88	0.13018	6.02

**Table 3-9: ROC curve analysis summary: CNS Dx vs NI CTL/ I CTL.** AUC = Area under the curve; CI = confidence intervals. P value calculated by non-parametric t-test. Optimal cut-off points determined as “closest to top left” described by  $d=\sqrt{[1-\text{Sensitivity}]^2 + (1 - \text{Specificity})^2}$ . \*Two optimal cut-off points identified by “closest to top left” equation.

The ROC curve results for Inosine classify the candidate biomarker are acceptable in discriminating the CNS1 Dx group from both control CSF groups with very similar ROC curve metrics (CNS1 Dx vs NI CTL AUC 0.71; 0.40 to 1.00 95% CI; p value= 0.0012347) (CNS1 Dx vs I CTL AUC 0.70; 0.40 to 1.00 95% CI; 0.0025295; p value= 0.0025295) (**Table 3-7**) (**Figure 3-8 G1-G2**)

ROC analysis of the remaining three candidate biomarkers, Phenylalanine, Pseudouridine and Orotidine, indicates that these metabolites have no better than

a 50% chance at discriminating between the CNS1 Dx group and the CSF control groups due to their p values  $> 0.05$  regardless of the AUC metric presented. The very wide 95% confidence intervals corroborate this, and the data can be seen to majorly overlap (**Table 3-9, Figure 3-6 C1-C2, D1-D2; Figure 3-8 H1-H2**).

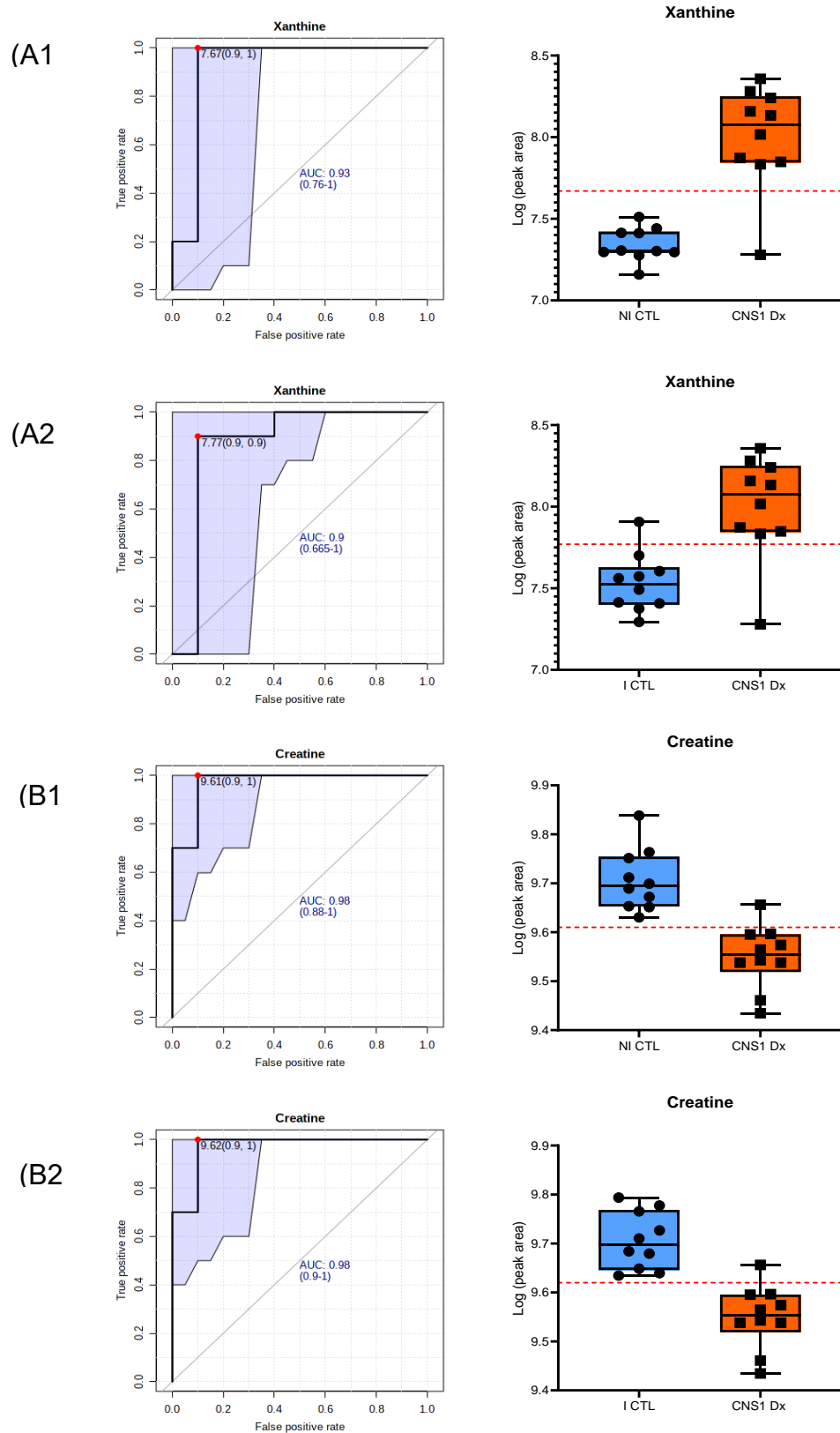


**Figure 3-5: Candidate biomarker ROC Curves and optimal cut-off points between CNS Dx and NI CTL/ I CTL CSF.** Optimal cut-off point (red dotted line) determined as “closest to top left” described by  $d = \sqrt{[1 - \text{Sensitivity}]^2 + [1 - \text{Specificity}]^2}$ . (A1) Xanthine – CNS Dx vs NI CTL; (A2) Xanthine – CNS Dx vs I CTL; (B1) Creatine – CNS Dx vs NI CTL; (B2) Creatine – CNS Dx vs I CTL. ROC curves created on Metaboanalyst; Box plots created on GraphPad Prism v9.

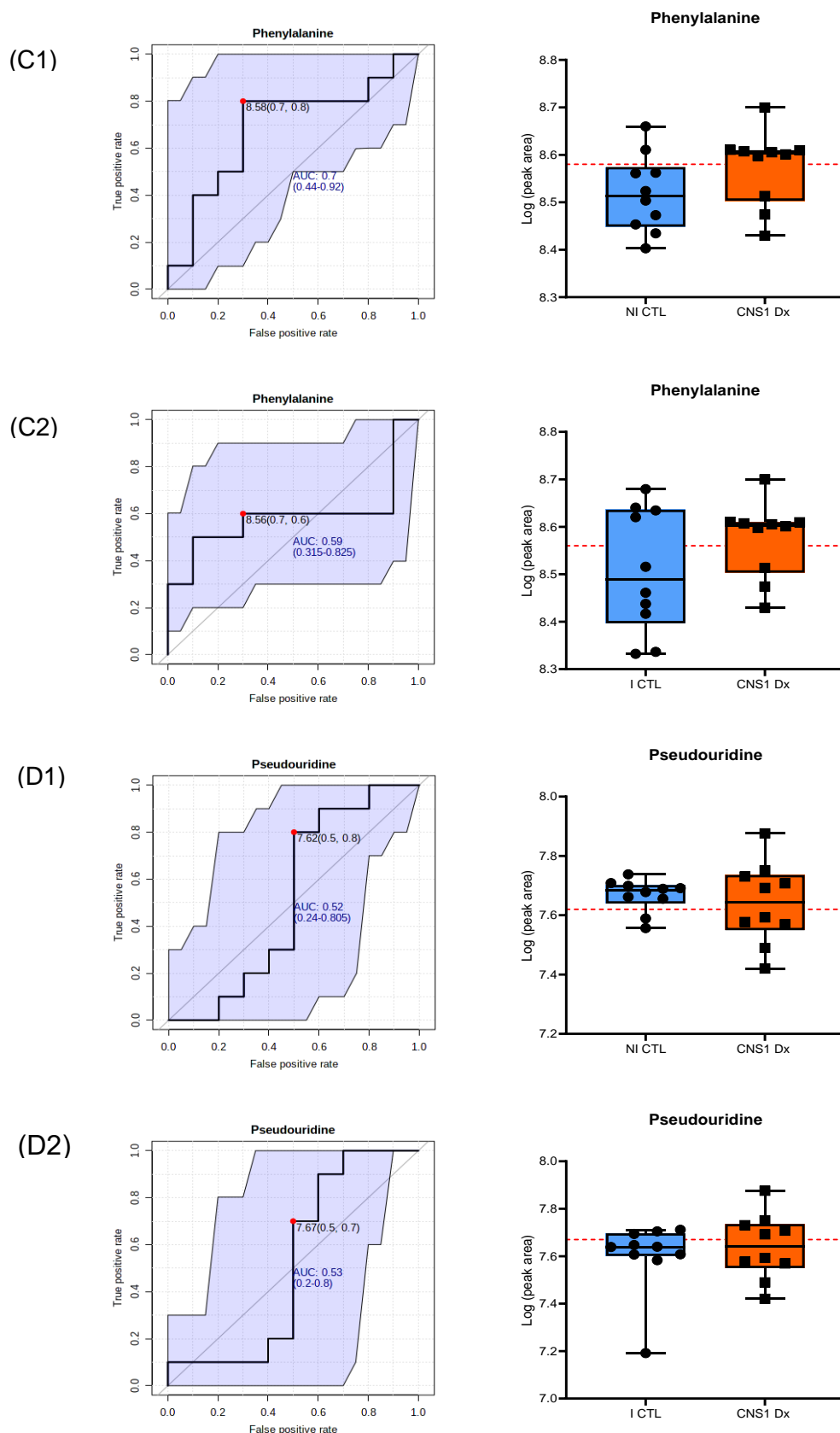


**Figure 3-6: Candidate biomarker ROC Curves and optimal cut-off points between CNS Dx and NI CTL/ I CTL CSF.** Optimal cut-off point (red dotted line) determined as “closest to top left” described by  $d = \sqrt{[1 - \text{Sensitivity}]^2 + (1 - \text{Specificity})^2}$ . (C1) Phenylalanine – CNS Dx vs NI CTL; (C2) Phenylalanine – CNS Dx vs I CTL; (D1) Pseudouridine – CNS Dx vs NI CTL; (D2) Pseudouridine – CNS Dx vs I CTL. ROC curves created on Metaboanalyst; Box plots created on GraphPad Prism v9.

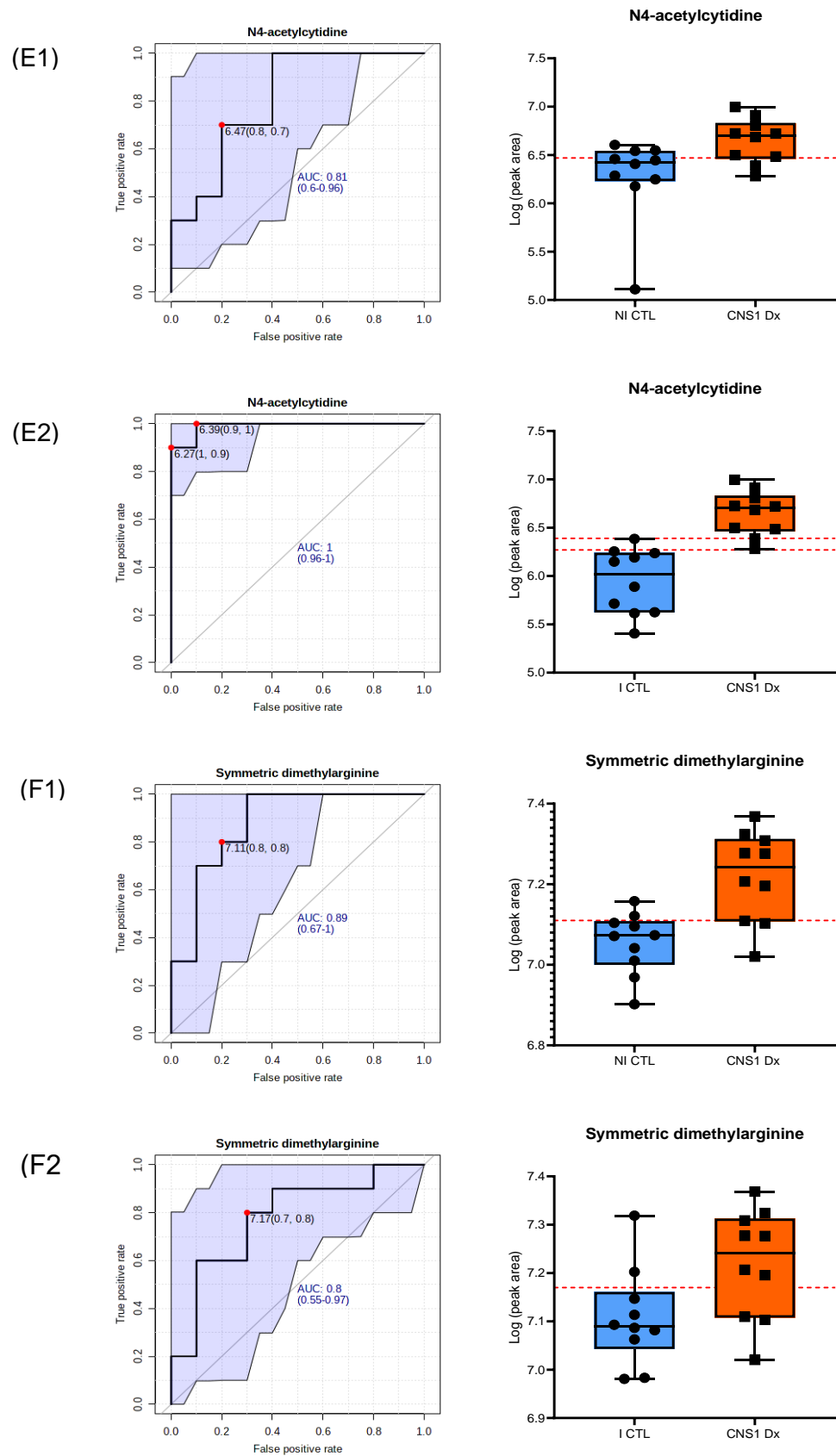


**Figure 3-7: Candidate biomarker ROC Curves and optimal cut-off points between CNS Dx and NI CTL/ I CTL CSF.** Optimal cut-off point (red dotted line) determined as “closest to top left” described by  $d = \sqrt{[1 - \text{Sensitivity}]^2 + [1 - \text{Specificity}]^2}$ . (E1) N4-acetylcytidine – CNS Dx vs NI CTL; (E2) N4-acetylcytidine – CNS Dx vs I CTL; (F1) Symmetric dimethylarginine – CNS Dx vs NI CTL; (F2) Symmetric dimethylarginine – CNS Dx vs I CTL. ROC curves created on Metaboanalyst; Box plots created on GraphPad Prism v9.

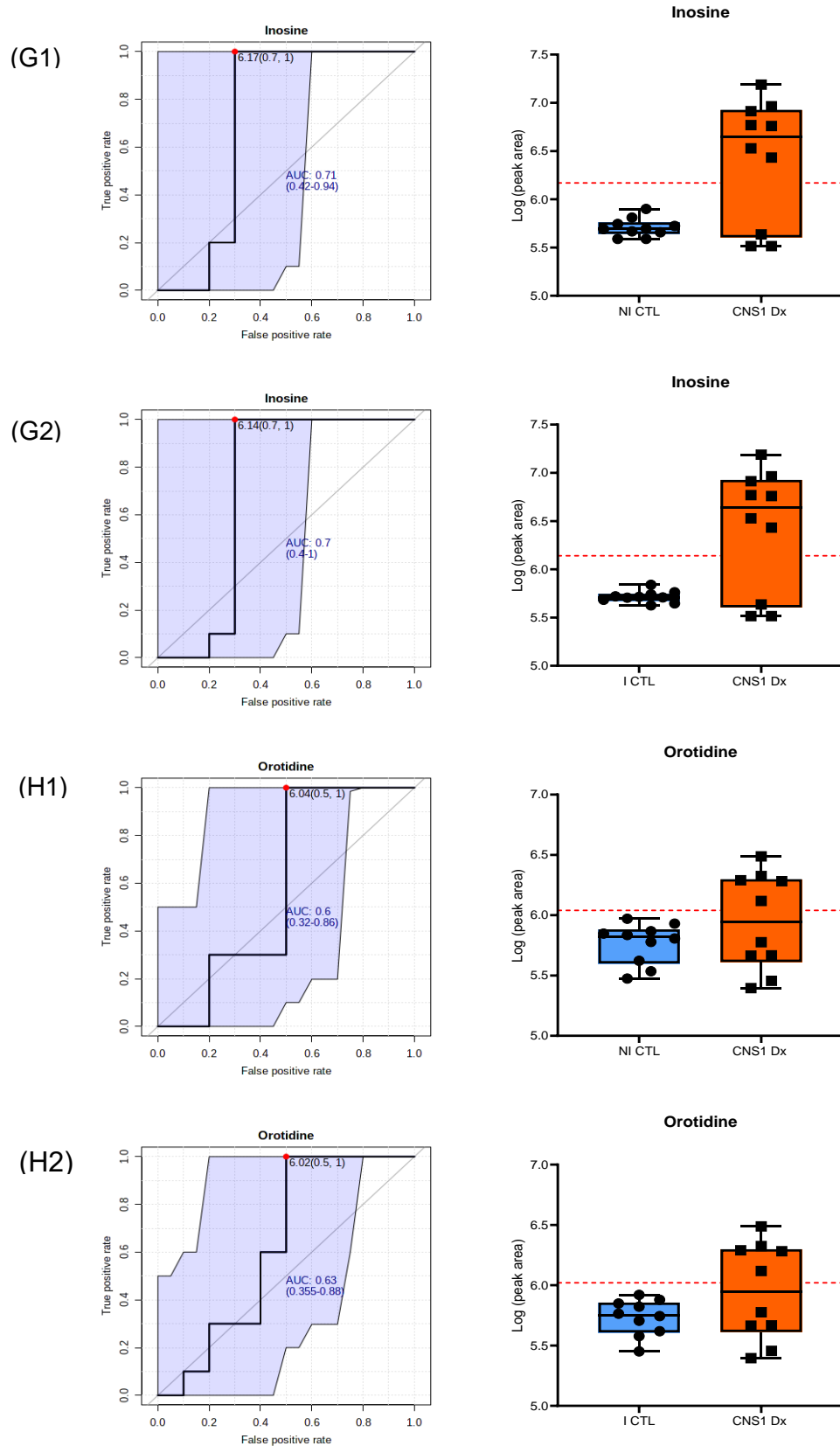


**Figure 3-813: Candidate biomarker ROC Curves and optimal cut-off points between CNS Dx and NI CTL/ I CTL CSF.** Optimal cut-off point (red dotted line) determined as “closest to top left” described by  $d = \sqrt{[1 - \text{Sensitivity}]^2 + [1 - \text{Specificity}]^2}$ . (G1) Inosine – CNS Dx vs NI CTL; (G2) Inosine – CNS Dx vs I CTL; (H1) Orotidine – CNS Dx vs NI CTL; (H2) Orotidine – CNS Dx vs I CTL. ROC curves created on Metaboanalyst; Box plots created on GraphPad Prism v9.



### 3.2.2 Univariate analysis of candidate biomarker performance against combined control CSF

Due to the general level of concordance between the non-inflammatory and inflammatory control CSF against the CNS Dx group as can be observed in **Figure 3-4**, it was then decided to combine the two CSF controls for comparison against the CNS Dx group to increase the power of the tested controls tested. First, the means of both controls were tested against each other to test for any statistically significant differences between them. All metabolites had similar means between the non-inflammatory and inflammatory CSF groups apart from Xanthine which had slightly higher levels in the inflammatory control CSF. Conversely, N4-acetylcytidine presented with slightly lower levels in the inflammatory control CSF but there was no statistically significant difference between the means of any of the candidate biomarkers in the control CSF (**Figure 3-9**).

The CNS Dx group was then compared to the combined CSF control (henceforth referred to as CSF CTL) to look for differences between the means. As before, there was a significant difference between the means in Xanthine  $p = 0.0000005$ ; Creatine  $p = 0.000003$ ; N4-acetylcytidine  $p = 0.003958$ ; Symmetric dimethylarginine  $p = 0.004412$  and Inosine  $p = 0.000158$  (**Figure 3-10**).

ROC curve analysis was then performed between the CNS Dx group and the control CSF group. Creatine performed best with a high AUC of 0.97; 95% CI 0.87 to 1.00;  $p$  value =  $6.5338E-7$ . The optimal cut-off point indicated an overall sensitivity of 100% and specificity of 90% (**Figure 3-11 B**; **Table 3-10**).

Xanthine and N4-acetylcytidine performed next best with AUCs >0.9 and high 95% CIs and p values <0.05. The optimal cut-off point gave Xanthine a sensitivity of 95% and a specificity of 90% while N4-acetylcytidine had a sensitivity of 85% and a specificity of 80%) (**Figure 3-11 A, Table 3-10**).

Symmetric dimethylarginine and Inosine presented with AUCs of 0.86 and 0.71 and more variable 95% CIs ranging from 0.66 to 0.99 and 0.42 to 0.97 respectively and p values <0.05. Sensitivity and Specificity of Symmetric dimethylarginine and Inosine were of 90% and 70%; 100% and 70% respectively (**Figure 3-12 F,G; Table 3-10**).

Phenylalanine, Pseudouridine and Orotidine all had p values > 0.05 and thus were not considered as having the ability to discriminate between the disease and non-disease groups (**Figure 3-11 C, D, Figure 3-12 H; Table 3-10**).

These results were concordant with the previous analysis indicating that the combined CSF controls can be combined for testing against the leukaemic patient sample group effectively.

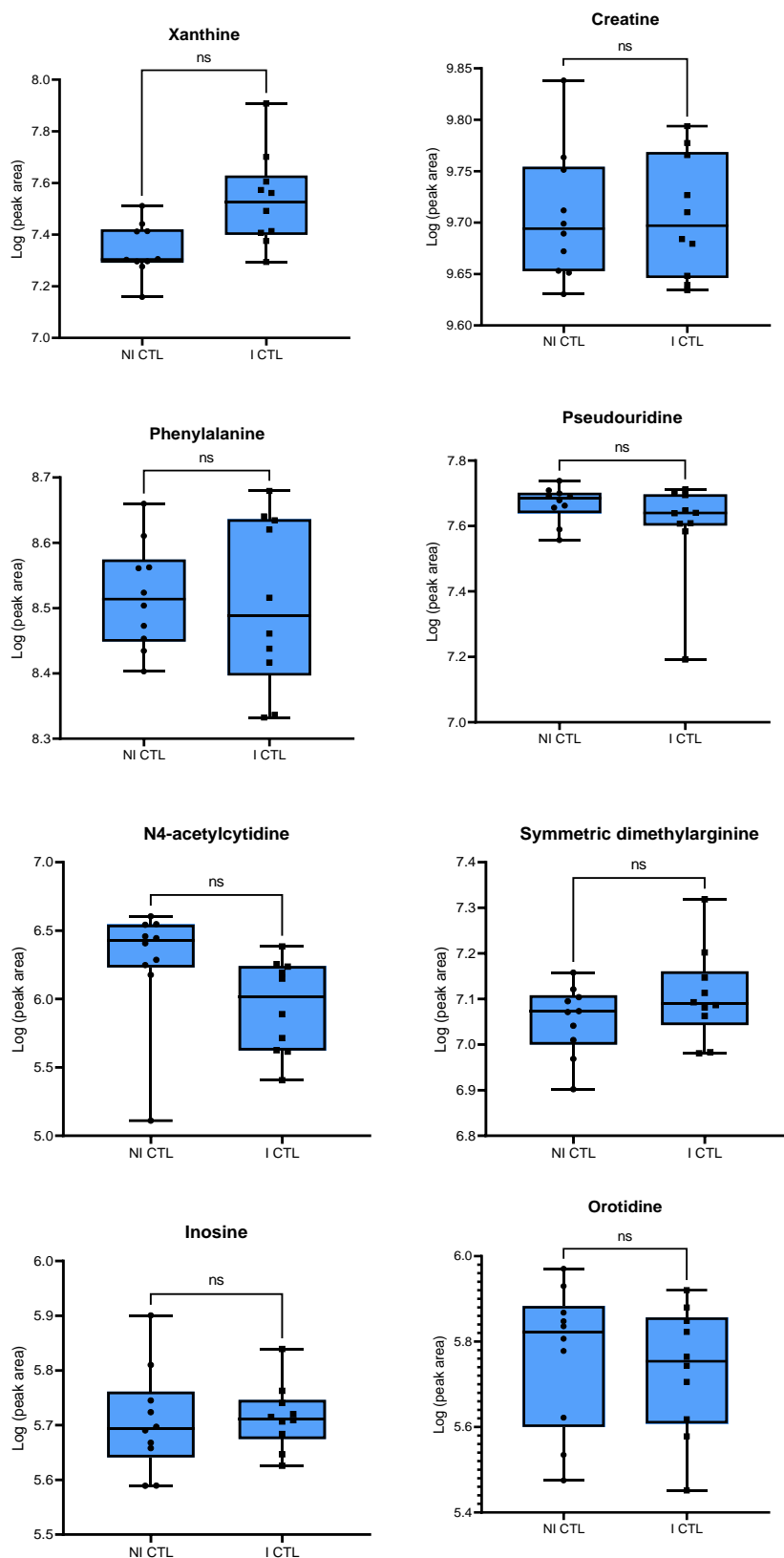


**Figure 3-9: Boxplots: Noninflammatory and Inflammatory Control CSF comparison of means.**

NI control (n=10); I control (n=10). Two-tailed unpaired t-test with an  $\alpha = 0.05$ . Graphs created on GraphPad Prism v9.

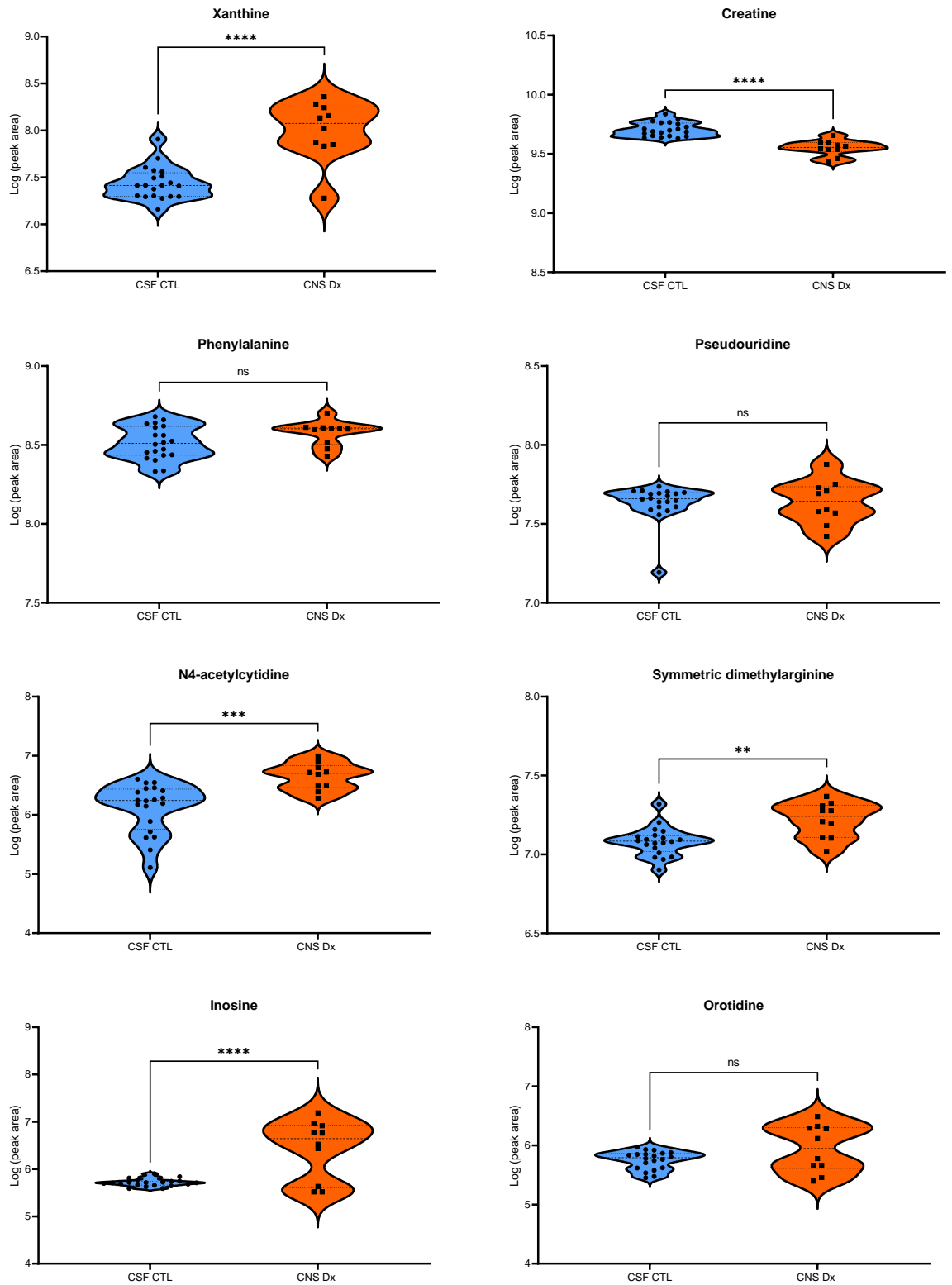


**Figure 3-10: Violin plots of candidate biomarkers depicting CNS Dx patient group v control CSF.** CNS Dx: Diagnostic leukaemic patient samples (n=10); Combined CSF control (n=20); Two-tailed unpaired t-test; Multiple un-paired t-tests corrected using Holm-Sidak method,  $\alpha = 0.05$ . Statistics performed on GraphPad Prism v9.

ROC	CNS Dx vs Control CSF					
Metabolite	AUC	95% CI	t-test P value	Optimal Cut-off	Sensitivity	Specificity
Xanthine	0.905	0.71 to 1.00	6.5338E-7	7.77	95% (0.85-1.00)	90% (0.7-1.00)
Creatine	0.97	0.87 to 1.00	3.7956E-7	9.61	100% (1.00-1.00)	90% (0.7-1.00)
Phenylalanine	0.64	0.43 to 0.84	0.11247	8.58	70% (0.5-0.9)	70% (0.5-0.95)
Pseudouridine	0.51	0.25 to 0.775	0.89959	7.60	80% (0.6-0.95)	50% (0.3-0.8)
N4-acetylcytidine	0.91	0.80 to 0.99	7.9113E-4	6.47	85% (0.7-1.00)	80% (0.55-1.000)
Symmetric Dimethylarginine	0.86	0.66 to 0.97	0.0011049	7.18	90% (0.77-1.00)	70% (0.4-0.95)
Inosine	0.71	0.42 to 0.97	2.637E-5	6.17	100% (1.00-1.00)	70% (0.4-1.00)
Orotidine	0.62	0.33 to 0.87	0.06071	6.04	100% (1.00-1.00)	50% (0.2-0.8)

**Table 3-10: ROC curve analysis summary: CNS Dx vs CSF CTL.** AUC = Area under the curve; CI = confidence intervals. P value calculated by non-parametric t-test. Optimal cut-off points determined as “closest to top left” described by  $d = \sqrt{[1 - \text{Sensitivity}]^2 + (1 - \text{Specificity})^2}$ .

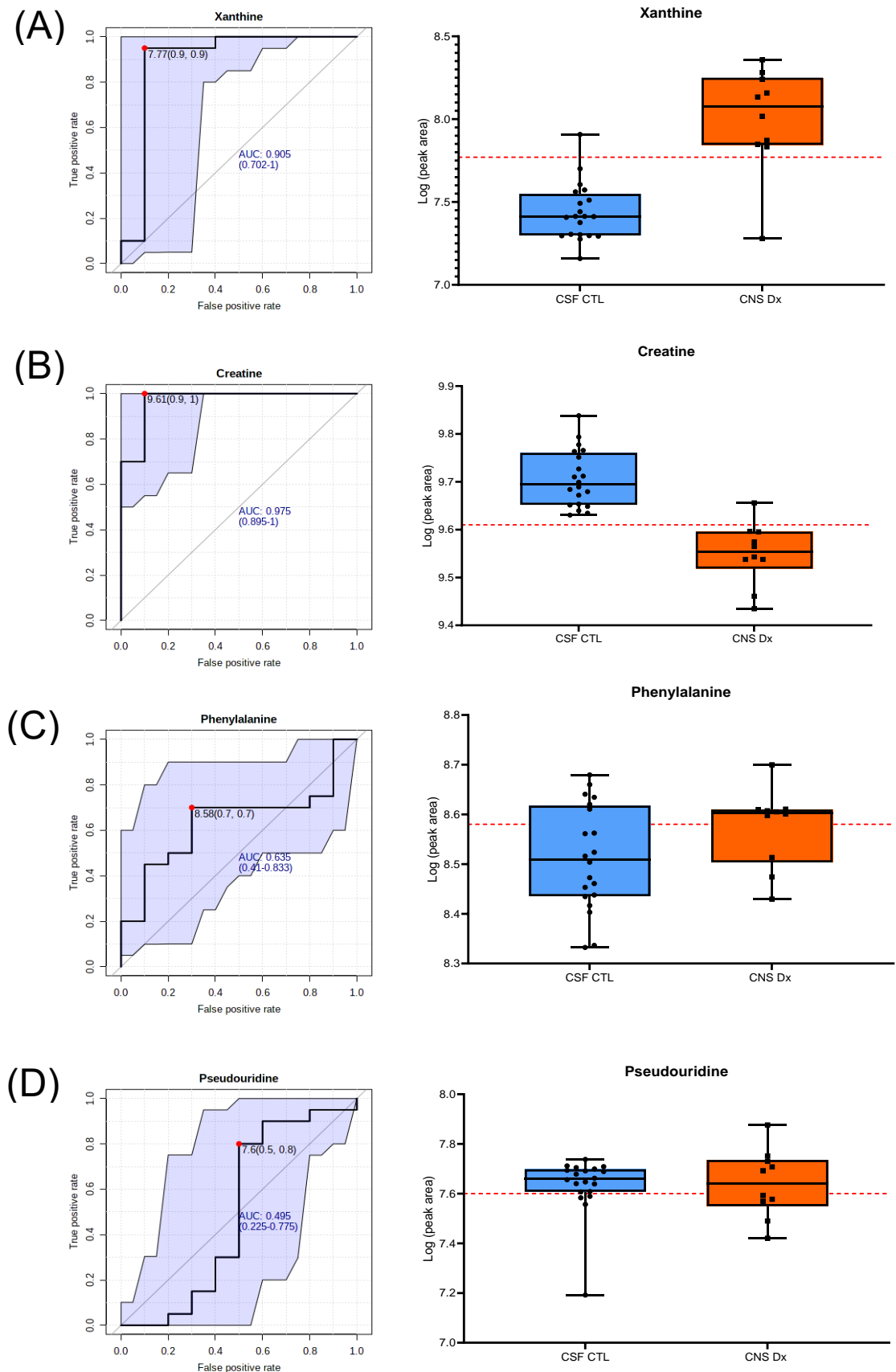


**Figure 3-11: Candidate biomarker ROC Curves and optimal cut-off points between CNS Dx and CTL CSF.** Optimal cut-off point (red dotted line) determined as “closest to top left” described by  $d = \sqrt{[1 - \text{Sensitivity}]^2 + [1 - \text{Specificity}]^2}$ . (A) Xanthine; (B) Creatine (C) Phenylalanine; (D) Pseudouridine. ROC curves created on Metaboanalyst; Box plots created on GraphPad Prism v9.

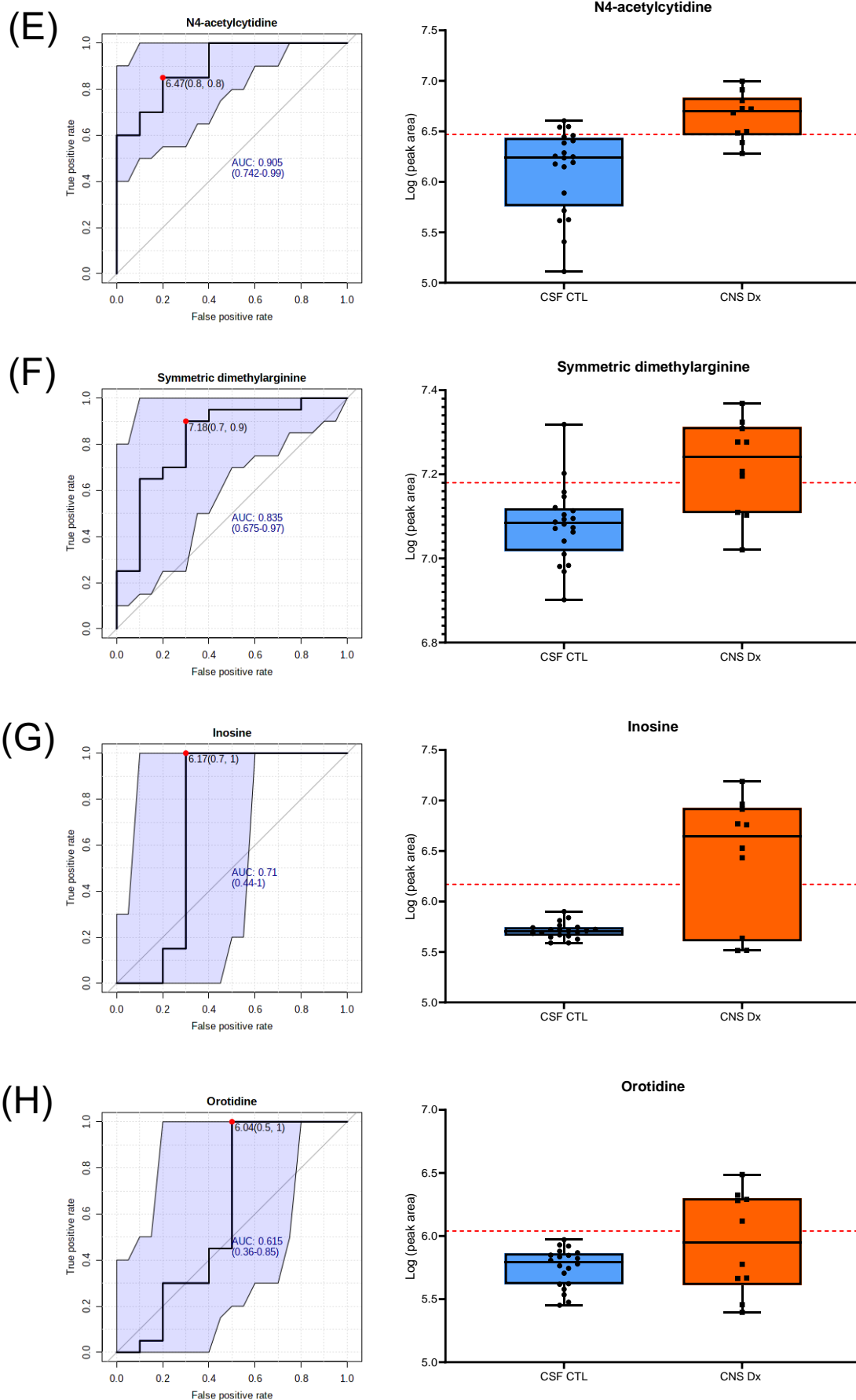


**Figure 3-12: Candidate biomarker ROC Curves and optimal cut-off points between CNS Dx and CTL CSF.** Optimal cut-off points (red dotted line) determined as “closest to top left” described by  $d = \sqrt{[1 - \text{Sensitivity}]^2 + [1 - \text{Specificity}]^2}$ . (E) N4-acetylcytidine; (F) Symmetric dimethylarginine (G) Inosine; (H) orotidine. ROC curves created on Metaboanalyst; Box plots created on GraphPad Prism v9.

### 3.2.3 Summary

This analysis tested the performance of these candidate biomarkers discriminating against both inflammatory and non-inflammatory control CSF and subsequently a combined CSF control group. Xanthine and Creatine performed best, first in terms of the CNS Dx group having concordant, statistically significant differences compared to both CSF controls. Secondly, ROC curve analysis returned supporting concordant evidence to corroborate this in terms of specificity and sensitivity of the respective metabolite when tested against both CSF controls and the combined control.

N4-acetylcytidine, Symmetric dimethylarginine and Inosine also performed reasonably well in distinguishing between the leukaemic and control groups to a lesser degree than Xanthine or Creatine and results from ROC curve analysis corroborate this finding.

Individually, the data indicates that these metabolites are capable of discriminating CNS leukaemia from control CSF suggesting that these candidate biomarkers are potentially capturing metabolic signatures for the presence of leukaemia in the CNS.

The remaining candidate biomarkers Phenylalanine, Pseudouridine and Orotidine did not have any significant differences between the means of the CNS Dx group and both controls or the combined control. ROC curve analysis suggests these metabolites are poor discriminators for CNS leukaemia.

Phenylalanine and Orotidine did present with a trend potentially indicating higher levels of the respective metabolite in the CNS Dx group which would fit with the findings of the original untargeted metabolomics experiment. The variability in this



experiment may perhaps be explained by the low numbers of samples tested in this experiment.

### **3.2.4 Multivariate analysis of candidate biomarkers – Creation of a model**

By measuring thousands of metabolites in parallel, a single metabolomics experiment can allow for the potential discovery of several biomarkers which may, when identified together, lead to a highly clinically informative panel of biomarkers. The next stage of this part of the study was to test the candidate biomarkers as a collective of potentially clinically informative biomarkers. Individually, most of the candidate biomarkers performed well in the univariate analyses used to discriminate between the patient group and the control CSF group. Metabolomic data can be combined with multivariate data analysis techniques to combine the performance of individual metabolites into a single multivariate model. The diagnostic patient CSF samples in this study are essentially a real-time record of the result of thousands of metabolic processes occurring in the CNS at the time of sample extraction.

To begin, a multivariate ROC curve analysis was performed using a supervised machine learning algorithm, the Random forests (RF) algorithm and the candidate biomarkers were ranked by their t-test statistical significance to create several models testing different combinations of the eight candidate biomarkers. RF is deemed an excellent tool for classification which is stable, insensitive to noise, has almost none or no overfitting and can compensate for having uneven sample groups such is the case in this study where the patient group to control group ratio is 1:2.

The multivariate ROC curve was generated by using the Monte-Carlo Cross Validation (MCCV) technique. This involves randomly separating two thirds of the total samples (patients and controls) for evaluating the importance of each candidate biomarker followed by using the most highly ranked features to build

several models for optimal classification (i.e., patient vs control). The multivariate analysis will then plot the ROC curves based on several models using various combinations of the candidate biomarkers created to classify patient samples or controls. The models are then validated on the last third of the samples. This procedure was repeated 100 times and the results were averaged to generate the multivariate ROC curve (**Figure 3-13 A**).

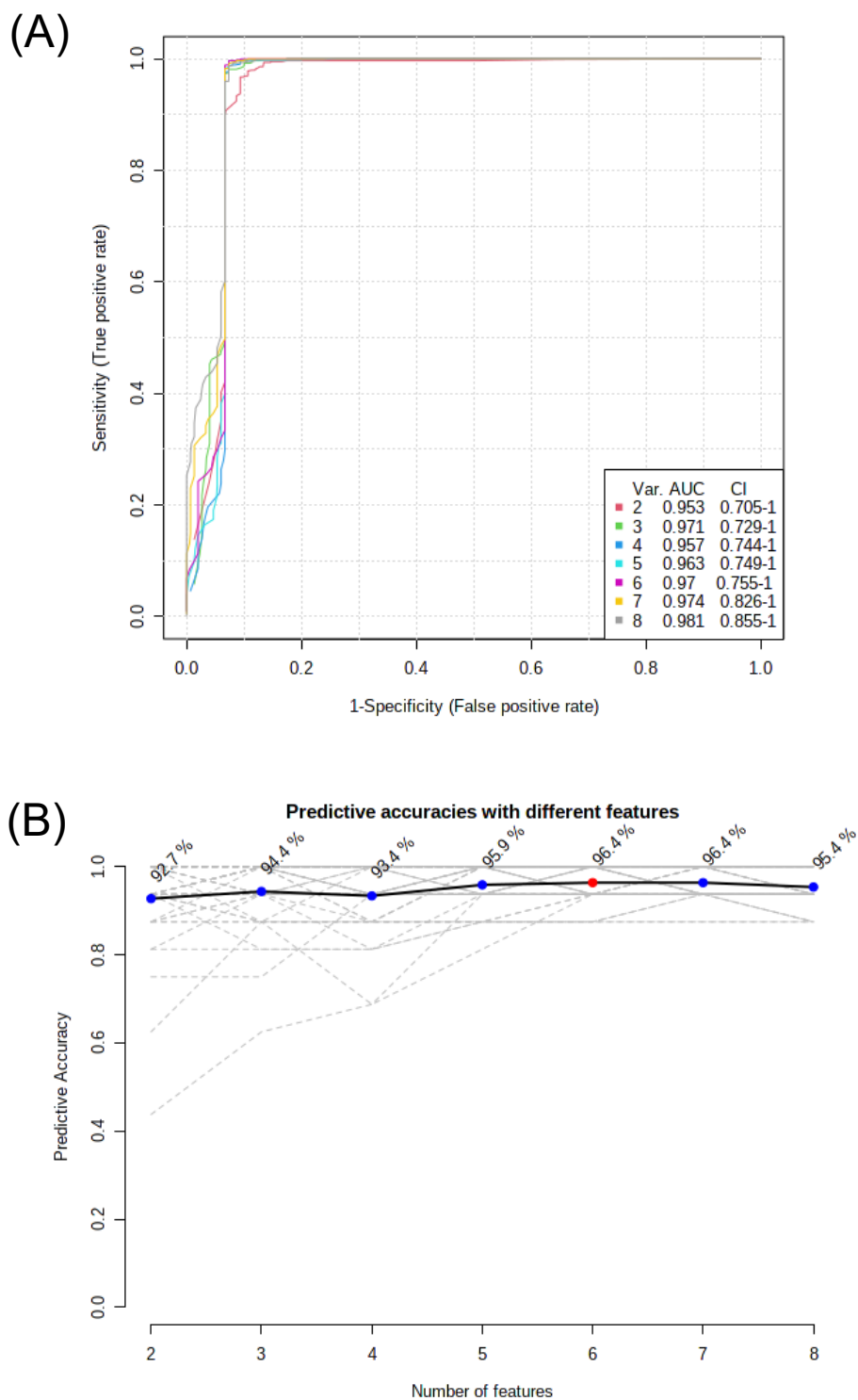


**Figure 3-13: Multivariate ROC analysis.** (A) Multivariate ROC curve with variable model averages plotted with associated AUC values and 95% confidence intervals; AUC = Area under the curve; CI = confidence intervals (B) Predictive accuracies of the best performing created models with different features. ROC curves created on Metaboanalyst. Classification method used: Random Forests, Feature ranking method based on statistical t-test.

Every model plotted on the multivariate ROC curve performed with AUC >0.9 which varied depending on the number of features used in the that model but generally it was observed that increasing the number of features, increased the AUC (**Figure 3-13 A**). The predictive accuracies of each model suggest however that the best performing model, irrespective of the AUC, is composed of a 6-variables (six out of eight candidate biomarkers) with this model giving the highest shared predictive accuracy of 96.4% as a 7-variable model also had a predictive accuracy of 96.4% (**Figure 3-13 B**). This suggests that one variable makes no real contribution to the multivariate model and there are two variables which behave similarly in their contribution to the model.

The candidate biomarkers were then ranked by the frequency of their selection during the model building process and they were also quantitatively ranked by the average importance of their contributions to the model from each of the 100 cross-validation runs in order of most discriminating to least discriminating. Both ranking methods yielded an identical rank order of the candidate biomarkers. The concordant ranking order suggests with a high degree of certainty that the best performing model includes Creatine, Xanthine, N4-acetylcytidine, Inosine and Symmetric dimethylarginine with these candidate biomarkers being selected in every model created (100% frequency) and with the highest average importance score. As expected, Pseudouridine was ranked last in both lists suggesting that this candidate biomarker bears little to no influence on the discriminatory utility of the model. Phenylalanine and Orotidine has the next best selected frequency which appeared even, although when ranked by average importance, Phenylalanine ranked slightly higher than Orotidine (**Figure 3-14**).

Next, different models were tested for their performance manually by first removing Pseudouridine, in line with the previous data which led to an increase in predictive accuracy from 0.95 to 0.952 (**Figure 3-15 A-B**). Phenylalanine and Orotidine were then removed from the model separately resulting in the best performing model being a 7-variable model including Phenylalanine with a predictive accuracy of 0.962 (**Figure 3-15 C-D**). Of note, the removal of variables did lead to a marginal reduction in the AUC and a slight widening of the 95% confidence intervals.

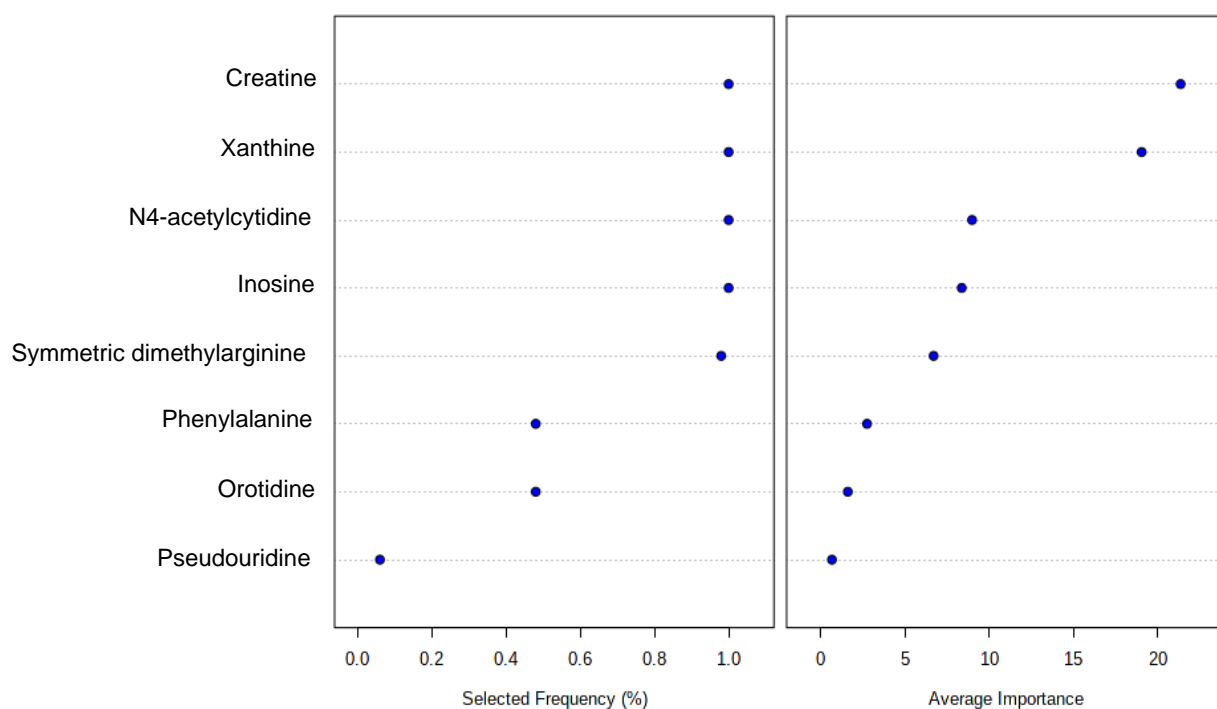


**Figure 3-14: Candidate biomarker ranking as determine by frequency of being selected in the model creation process and average importance from the 100 cross-validations.**

To test the predictive capability of the final 6-variable model from this analysis (Creatine, Xanthine, N4-acetylcytidine, Inosine, Symmetric dimethylarginine and Phenylalanine), average predicted class probabilities were plotted for each CNS Dx and control sample across the 100 performed Monte-Carlo cross-validations to create a confusion matrix. The data shows that out of the 10 CNS Dx samples tested all of them were correctly identified as belonging to the CNS Dx group of samples and 19/20 of the control samples were classified correctly as belonging to the control group giving an overall predictive accuracy of 96.6% (**Figure 3-16**). The one sample which was incorrectly classified was an inflammatory control CSF sample.

Next, a second validation of the model was performed using permutation testing, a re-sampling based statistical test which postulates a null hypothesis that the 6-variable model described here could also have been discovered if every sample was randomly assigned a classification (either CNS Dx or control CSF) in the same quantities with respect to the group sample numbers. The permutation test was run  $n=1000$  times using the 6-variable model and for every permutation, a RF model was built and tested for a statistical difference between the CNS Dx and control CSF

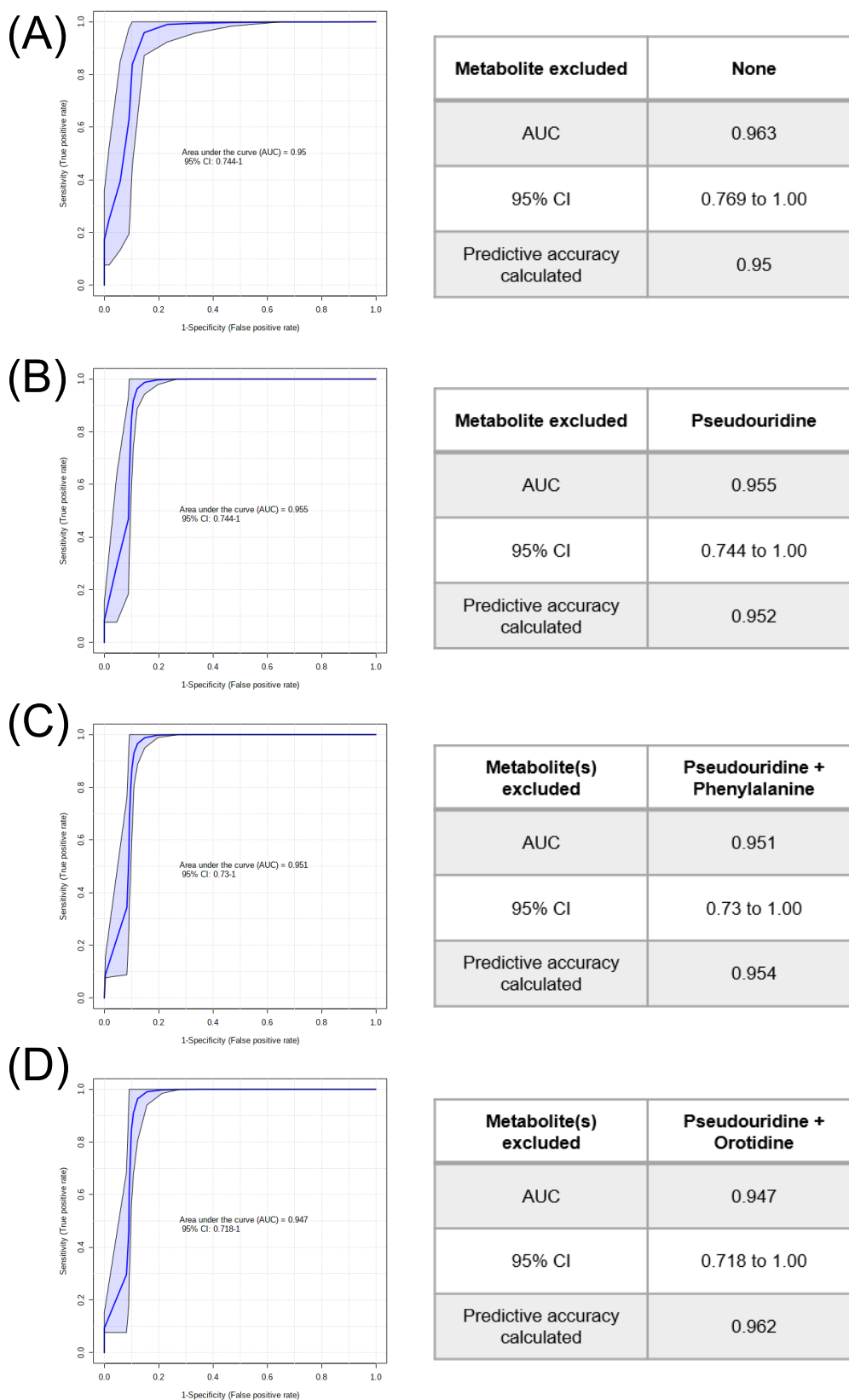
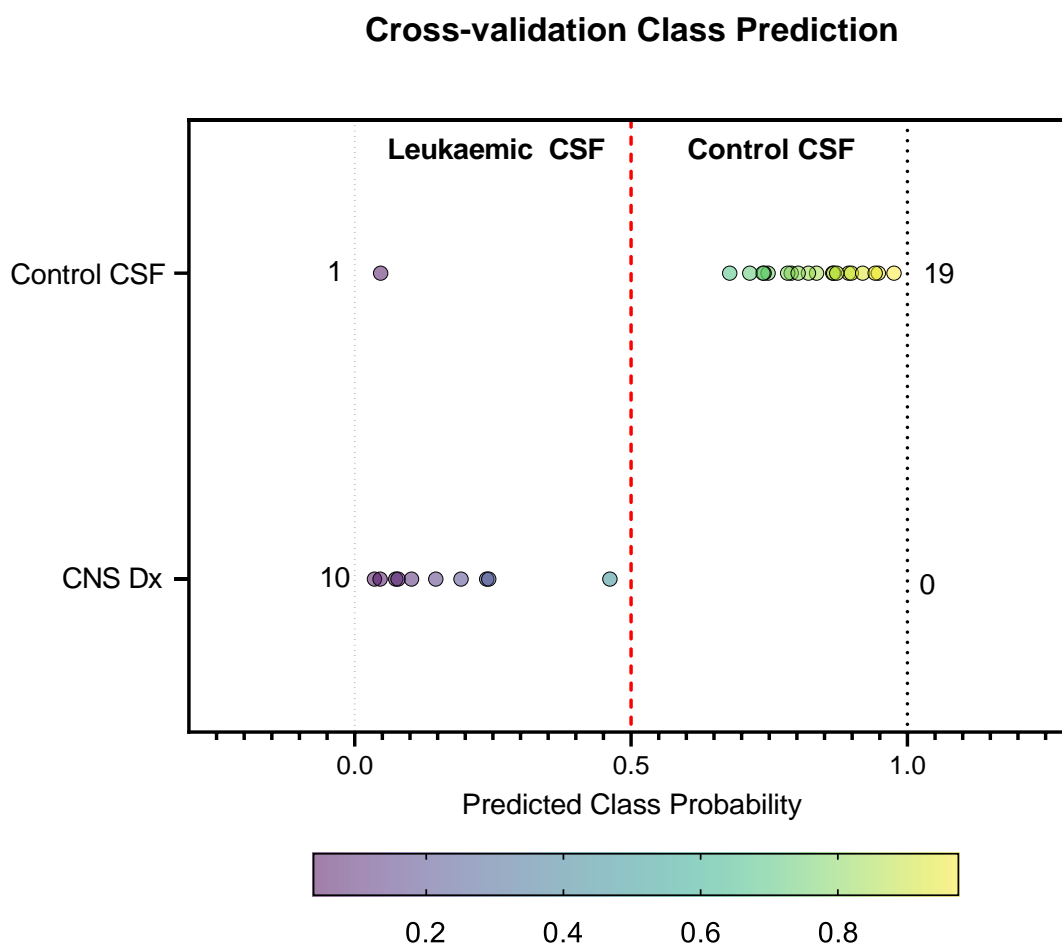


**Figure 3-15: Multivariate ROC curve analysis manual model testing by removal of redundant features.** AUC = Area under the curve; CI = confidence intervals; (A) No metabolites excluded; (B) Pseudouridine excluded; (C) Pseudouridine and phenylalanine excluded; (D) Pseudouridine and Orotidine excluded; ROC curves created on Metaboanalyst.





Confusion Matrix Summary (100 X Cross-Validations)			
	Leukaemic CSF	Control CSF	
Control CSF	1	19	96.6%
CNS Dx	10	0	

**Figure 3-16: Cross-validation Class Prediction confusion matrix.** This graph plots the average predicted class probabilities of each sample from 100 cross-validations. The classification boundary is set to 0.5 and sample probabilities range from 0-1. Probabilities < 0.5 will belong to the leukaemic CSF sample group and probabilities >0.5 will belong to the Control CSF. Each sample is coloured by their probability score. Graph Created on GraphPad Prism v9.

groups resulting in a distribution of the permuted data. The performance score of the original model was then compared to the permuted distribution resulting with a significant p value of  $<0.000006$  which lay outside of the of the distribution indicating a significant separation between the two groups (**Figure 3-17 A**). This suggests that there is a  $<5\%$  chance that a permuted model could perform as well as the original model tested. A permutation test was also run to test the null hypothesis that the AUC of the 6-variable model equals 0.5, meaning the test has no discriminatory ability to distinguish between the disease and non-disease group. This analysis resulted in an empirical p value of 0.002 suggesting that the calculated AUC of the model was not obtained by chance and the model is capable of distinguishing CNS Dx samples from control CSF samples (**Figure 3-17 B**).

### 3.2.5 Summary

In summary, the data shown by this analysis reveals that the use of this panel of candidate biomarkers can provide a highly accurate method of identifying leukaemic CSF in comparison with control CSF composed of both inflammatory and non-inflammatory CSF controls. Together, each candidate biomarker tested in the 6-variable model was able to discriminate leukaemic CSF from control CSF.

The limitations of this analysis must be addressed, principally in the low numbers of leukaemic diagnostic CSF samples tested against the CSF controls meaning that these patient samples tested here only represents a small fraction of the true diseased population. This can have big implications on the subtleties of a candidate biomarkers detection, such as can be seen with Phenylalanine and Orotidine in this analysis, where the data seems to point to slightly elevated levels in the leukaemic group compared to the control group, but statistical analysis indicates no significant difference found. So far, the evidence put forward in this study points to

Pseudouridine being a redundant marker, nonetheless it will continue to be tested with subsequent analysis to provide further evidence of the utility of this candidate biomarker for the detection of CNS-ALL.

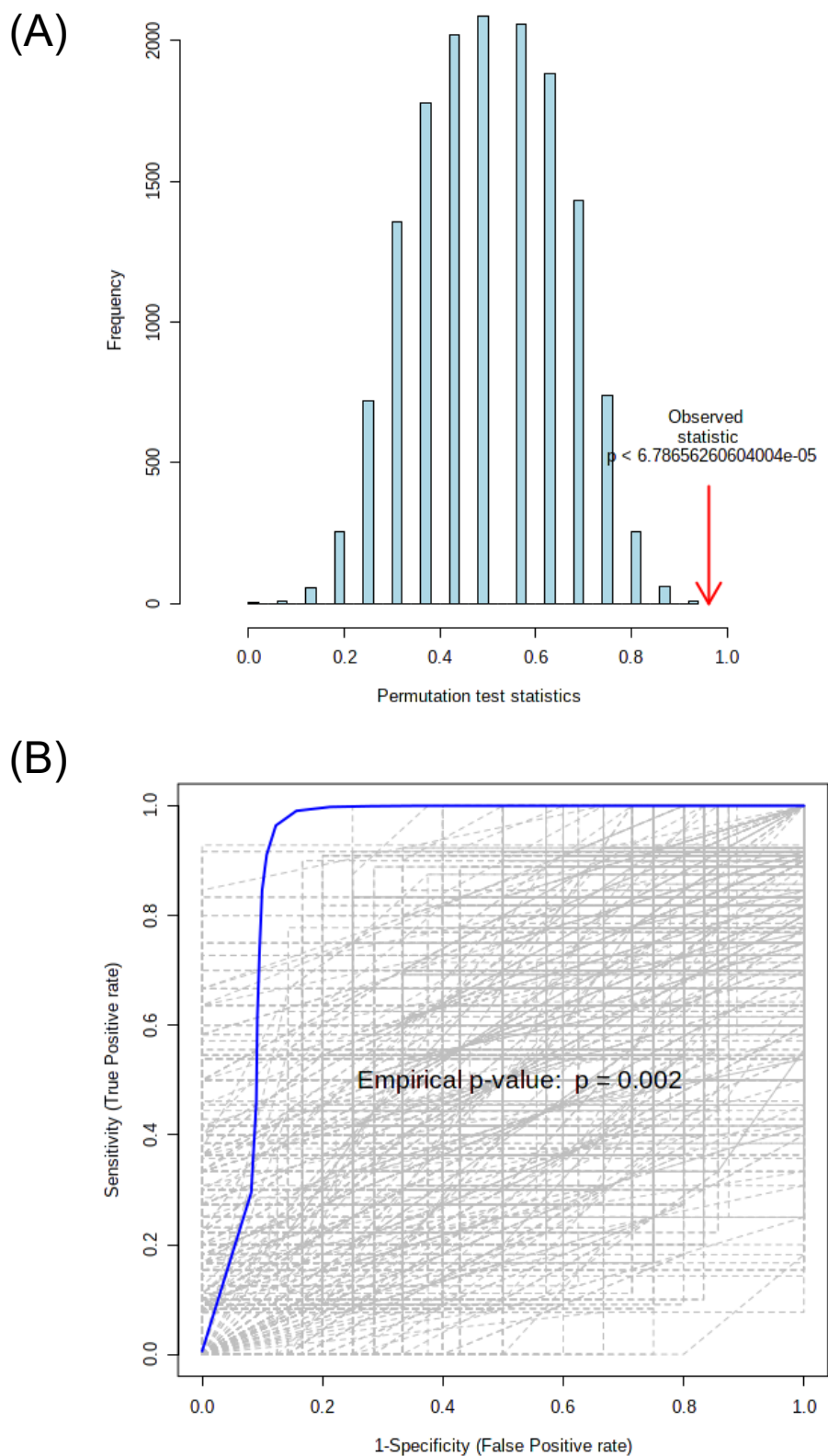


**Figure 3-17: Permutation testing on 6-variable model.** (A) Permuted data statistical test distribution; Performance t-test score of the original model against the permuted data highlighted by the red arrow. (B) Permutation empirical p value calculated from statistical test to disprove the null hypothesis that the AUC equals 0.5. Graphs exported from Metaboanalyst.

### **3.3 Candidate biomarker performance evaluation:**

#### **Cohort 2**

##### **3.3.1 Background**

The next part of this study was to assess and validate previous findings by testing the candidate biomarkers with a larger and more comprehensive cohort of diagnostic patient CSF samples. These samples were obtained from a national biobank and consist of several patients who were classified as CNS1, CNS2 or CNS3 by CSF cytology. First the candidate biomarkers were tested with a large subset of CNS Dx patients (composed of CNS1 CNS2 and CNS3 patients) and non-inflammatory and inflammatory control CSF both separately and combined following in the previous analysis. The larger number of patient samples and controls will give a truer representation of the leukaemic and non-leukaemic population.

Next, the CNS1, CNS2 and CNS3 patients were compared individually to the CSF control group to investigate for any differences in the patient sample groups. CNS3 patients are classified as having more leukaemic burden in the CNS than CNS1 patients and thus it was hypothesized that the candidate biomarkers may be able to identify an elevated metabolic signature in the CNS3 patient group when compared to the CNS1 patient group.

Finally, to confirm the significance of the multivariate model developed in the pilot cohort, the candidate biomarkers were tested as a collective again with the large subset of patient and control samples to further evaluate the performance of the model and validate its predictive performance. A small subset of patient samples from the Halsey biobank which were untested by any of the previous analyses were used to test the model with an unsupervised approach.

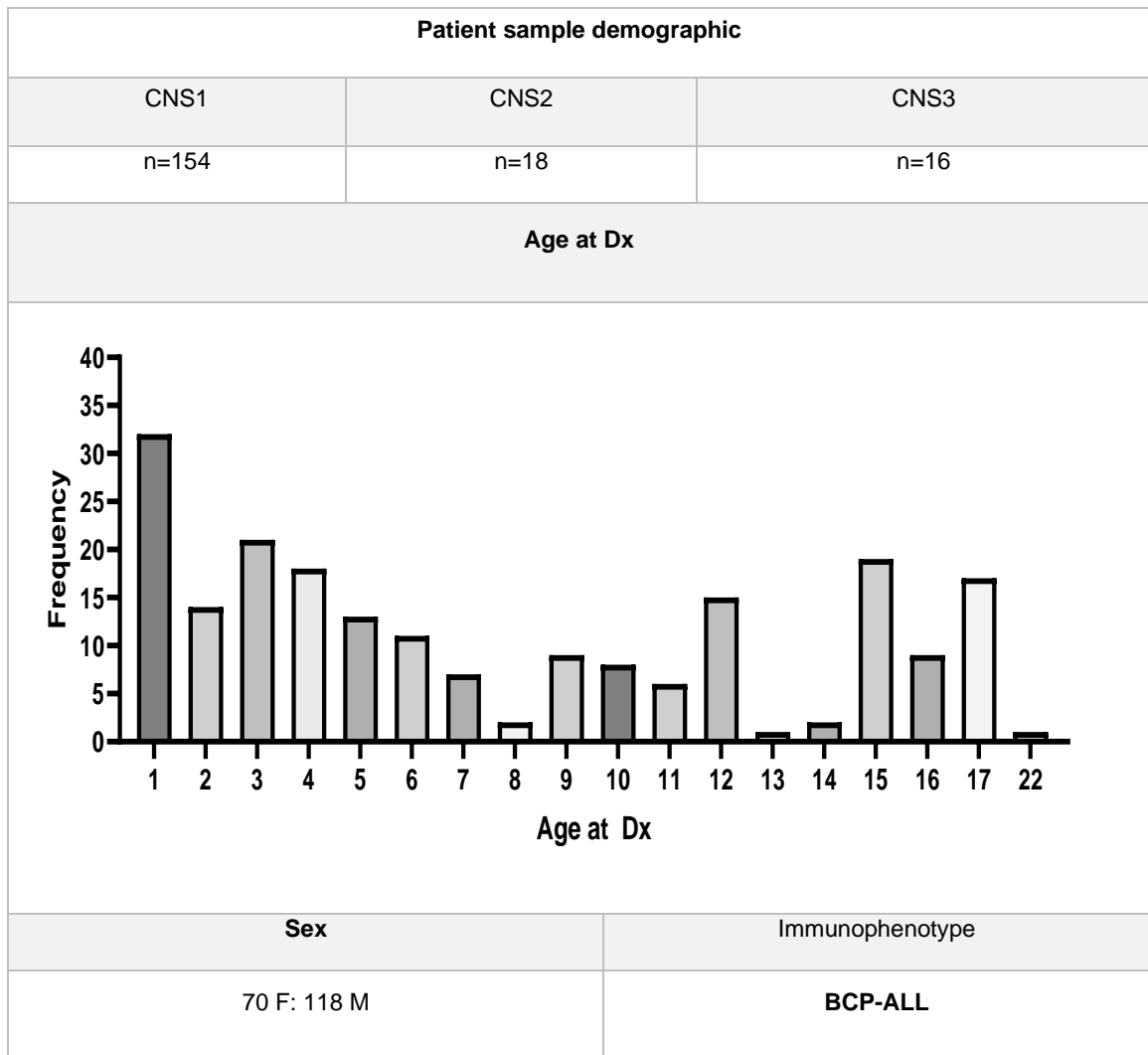


**Table 3-11: patient demographic.** YO= years old. F = Female, M= Male; BCP-ALL = B-cell precursor ALL.

CSF control demographic			
Control type	Ages	Sex	Diagnosis
NI control n=20	26- 77	14 F	Migraine, headache, Functional*, motor neuronopathy, small vessel ischaemia, delirium, epilepsy, small vessel disease
		6 M	
I control n=20	18 - 57	13 F	Neurosarcoidosis, post-infectious movement disorder, RRMS***, GAD encephalitis**, neuroinflammatory disorder, neuroborreliosis
		7 M	

**Table 3-12: Control CSF cohorts – non-inflammatory and inflammatory CSF.** F= Female; M = Male. \* Functional = Body symptoms which appear to be caused by the CNS, but are not, medically unexplained. \*\* GAD encephalitis = Anti-glutamic acid decarboxylase encephalitis

### 3.3.2 CNS Dx vs non-inflammatory & inflammatory CSF controls

In this analysis, all the patient samples were compared as one large leukaemic sample cohort labelled CNS Dx against all CSF controls available from both the non-inflammatory and inflammatory control CSF cohorts to test the behaviour of the candidate biomarkers (**Tables 3-11, 3-12**). The patient sample group contained a mix of CNS1, CNS2 and CNS3 classified patients and the rationale behind grouping and testing all the leukaemic samples together for analysis was to have a large cohort, truly representative of the real leukaemic diseased population.

As with the previous experiment, this analysis followed the same statistical analyses performed on the candidate biomarkers, firstly by looking for differences between the averages of the patient group and both control CSF groups. Upon first inspection, the means of all metabolites were elevated in the patient group compared to both controls apart from creatine which followed its inverse trend of being clearly lower than both controls as seen in the previous experiment, and Pseudouridine which had similar levels in the patient group and the non-inflammatory control, but interestingly was lower in the inflammatory control CSF than both former groups. Statistical analyses indicated highly significant, concordant differences between the patient group and both CSF controls in all candidate biomarkers with the exception of Pseudouridine corroborating the observed trend mentioned in the pilot cohort (**Figure 3-18, Table 3-13**).

A key observation with this analysis is the high number of patients with clearly higher (or lower in the case of Creatine) levels of their respective biomarkers. As the control CSF was taken from an adult population, quantifiable differences which may be due to the age difference between the patient and control groups must be considered. Of all the candidate biomarkers, Creatine is the only metabolite which presents with

lower levels in the patient group compared to both controls and could be subject to age-dependent differences in the levels of this metabolite, but as the data in these experiments mimic very closely the trend seen in the initial experiment comparing leukaemic patient samples to matched and unmatched childhood ALL controls, this concordance strongly suggests that the phenotype presented here is a result of a leukaemic signature in the CSF. The other metabolites are “easier” to hypothesize as being leukaemia-specific due to their elevated levels compared to the controls, which again was observed in the initial experiment with the CSF of children.



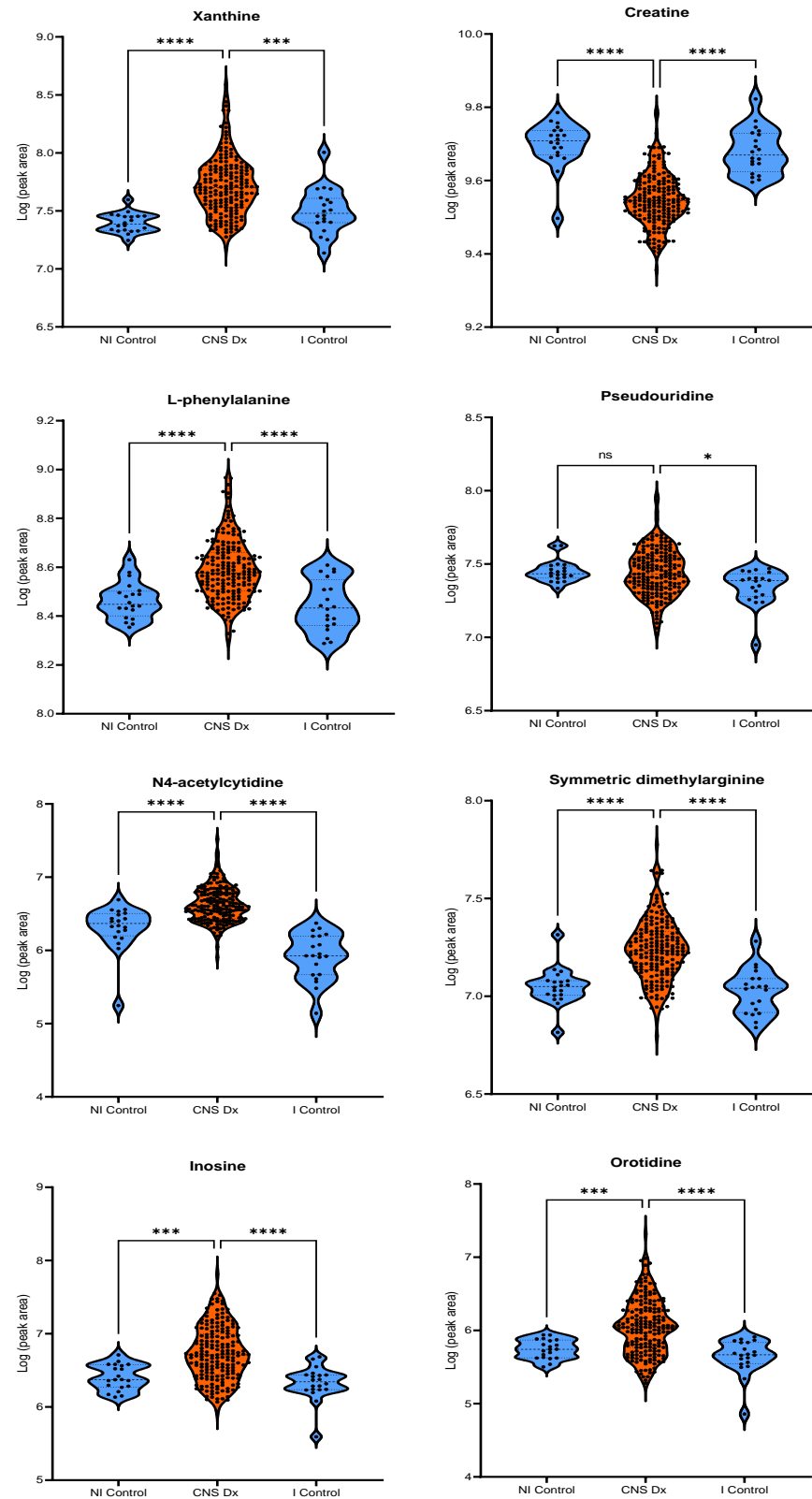


**Figure 3-18: Violin plots of CNS Dx vs Inflammatory and Non-inflammatory control CSF groups.** CNS Dx (n= 188), non-inflammatory control (n=20), Inflammatory control (n=20). Statistics performed on GraphPad Prism v. One-way ANOVA; means of Controls compared with mean on CNS Dx group with Dunnett's multiple comparisons test  $\alpha= 0.05$ . Graphs created on GraphPad Prism v9.

Candidate biomarker	Control Mean	CNS Dx Mean	SE of difference	95% confidence interval	ANOVA R <sup>2</sup>	Log 2 FC	ANOVA P value	Adjusted p Value
Xanthine CNS Dx vs NI CTL	7.397	7.712	0.05618	0.1891 to 0.4420	0.1584	1.31	0.0000000038	<0.0001
Xanthine CNS Dx vs I CTL	7.498		0.05618	0.08760 to 0.3405		0.85		0.000359
Creatine CNS Dx vs NI CTL	9.699	9.548	0.01641	-0.1878 to -0.1139	0.3755	-0.49	<0.000001	<0.0001
Creatine CNS Dx vs I CTL	9.679		0.01641	-0.1679 to -0.09404		-0.43		<0.0001
Phenylalanine CNS Dx vs NI CTL	8.463	8.589	0.02776	0.06408 to 0.1890	0.1648	0.46	<0.000001	<0.0001
Phenylalanine CNS Dx vs I CTL	8.443		0.02776	0.08397 to 0.2089		0.51		<0.0001
Pseudouridine CNS Dx vs NI CTL	7.449	7.444	0.03534	-0.08509 to 0.07395	0.03426	0.06	0.019808	0.984248
Pseudouridine CNS Dx vs I CTL	7.345		0.03534	0.01916 to 0.1782		0.38		0.011328
N4-acetylcytidine CNS Dx vs NI CTL	6.311	6.627	0.05900	0.1830 to 0.4485	0.4212	1.06	<0.000001	<0.0001
N4-acetylcytidine CNS Dx vs I CTL	5.914		0.05900	0.5801 to 0.8456		2.30		<0.0001
Symmetric dimethylarginine CNS Dx vs NI CTL	7.049	7.236	0.03492	0.1083 to 0.2655	0.2096	0.68	<0.000001	<0.0001
Symmetric dimethylarginine CNS Dx vs I CTL	7.024		0.03492	0.1329 to 0.2901		0.75		<0.0001
Inosine CNS Dx vs NI CTL	6.404	6.733	0.08142	0.1461 to 0.5126	0.1439	1.52	<0.000001	0.000144
Inosine CNS Dx vs I CTL	6.326		0.08142	0.2239 to 0.5904		1.73		<0.0001
Orotidine CNS Dx vs NI CTL	5.744	6.049	0.08306	0.1179 to 0.4918	0.1317	1.54	<0.000001	0.000605
Orotidine CNS Dx vs I CTL	5.643		0.08306	0.2182 to 0.5920		1.78		<0.0001

**Table 3-13: Candidate biomarkers: Statistical analysis of the difference between CNS Dx and non-inflammatory and inflammatory CSF controls.** Data was log transformed prior to statistical analysis. One-way ANOVA; means of Controls compared with mean on CNS Dx group with Dunnett's multiple comparisons test  $\alpha = 0.05$ . Statistics performed on GraphPad Prism v9.

As before, the candidate biomarkers were then tested for their specificity and sensitivity with ROC curve analysis between the patient group and the control CSF groups independently. Following the trend in the first experiment, Creatine performed best with an AUC of  $>0.9$  in both comparisons, very narrow 95% confidence intervals ranging between 0.86 to 0.98 and 0.88 to 0.96 in the CNS Dx group vs the non-inflammatory control CSF group and inflammatory control CSF group respectively and extremely low p values  $<0.0001$  (**Table 3-14, Figure 3-19 B1-B2**).

Xanthine, Phenylalanine, N4-acetylcytidine and Symmetric dimethylarginine performed next best in comparison, all with AUCs of  $>0.8$ , with slightly more variable but high performance 95% confidence intervals but with p values of  $<0.0001$  (**Table 3-14, Figure 3-19 A1-A2, Figure 3-20 C1-C2, Figure 3-21 respectively**).

Interestingly, Inosine and Orotidine had “acceptable” AUC’s of  $> 0.7$  with more variable 95% confidence intervals ranging from 0.69 to 0.89 but low p values of  $< 0.001$  indicating more overlap between the control group and the non-inflammatory patient group (**Table 3-14, Figure 3-22 G1, H1**). Their performance compared to the inflammatory control however yielded “excellent” AUCs of  $>0.8$ ; 95% confidence intervals ranging from 0.74 to 0.89 and p values  $< 0.0001$  (**Table 3-14, Figure 3-22 G2, H2**).

Pseudouridine performed least best with a no discrimination classification with an AUC of 0.52 and a large p value  $=0.87682$  suggesting that this metabolite has no utility in discriminating the patient group from the non-inflammatory control group (**Table 3-14, Figure 3-20 D1**). When compared against the inflammatory control CSF group, Pseudouridine showed poor discriminatory ability with an AUC of 0.68,

with a wide 95% confidence interval, but a low p value <0.001 nonetheless, deeming this metabolite as a poor discriminator (**Table 3-14, Figure 3-20 D2**).

ROC	CNS Dx vs NI Control				CNS Dx vs I Control			
Metabolite	AUC	95% CI	t-test P value	Optimal Cut-off	AUC	95% CI	t-test P value	Optimal Cut-off
Xanthine	0.89	0.84 to 0.94	9.696E-8	7.47	0.76	0.65 to 0.85	3.1633E-4	7.61
Creatine	0.93	0.86 to 0.98	8.2181E-17	9.66	0.93	0.88 to 0.96	1.6263E-13	9.61
Phenylalanine	0.82	0.74 to 0.90	1.071E-5	8.5	0.82	0.71 to 0.89	6.5737E-7	8.51
Pseudouridine	0.52	0.44 to 0.52	0.87692	7.42	0.68	0.59 to 0.76	0.0075172	7.41
N4-acetylcytidine	0.82	0.74 to 0.90	1.0863E-7	6.51	0.99	0.97 to 1.00	1.4525E-26	6.3
Symmetric Dimethylarginine	0.86	0.79 to 0.92	3.7899E-7	7.11	0.87	0.80 to 0.93	1.5008E-8	7.09
Inosine	0.78	0.71 to 0.89	1.0982E-4	6.58	0.82	0.75 to 0.89	2.5872E-6	6.46
Orotidine	0.76	0.69 to 0.82	4.2512E-4	5.94	0.81	0.74 to 0.87	4.8928E-6	5.87

**Table 3-14: ROC curve analysis summary: CNS Dx vs NI CTL/ I CTL.** AUC = Area under the curve; CI = confidence intervals. P value calculated by non-parametric t-test. Optimal cut-off points determined as “closest to top left” described by  $d = \sqrt{[1 - \text{Sensitivity}]^2 + (1 - \text{Specificity})^2}$ .

This experiment demonstrates that all the candidate biomarkers except for Pseudouridine can discriminate the patient sample cohort from both inflammatory and non-inflammatory control CSF with the exception of Pseudouridine.

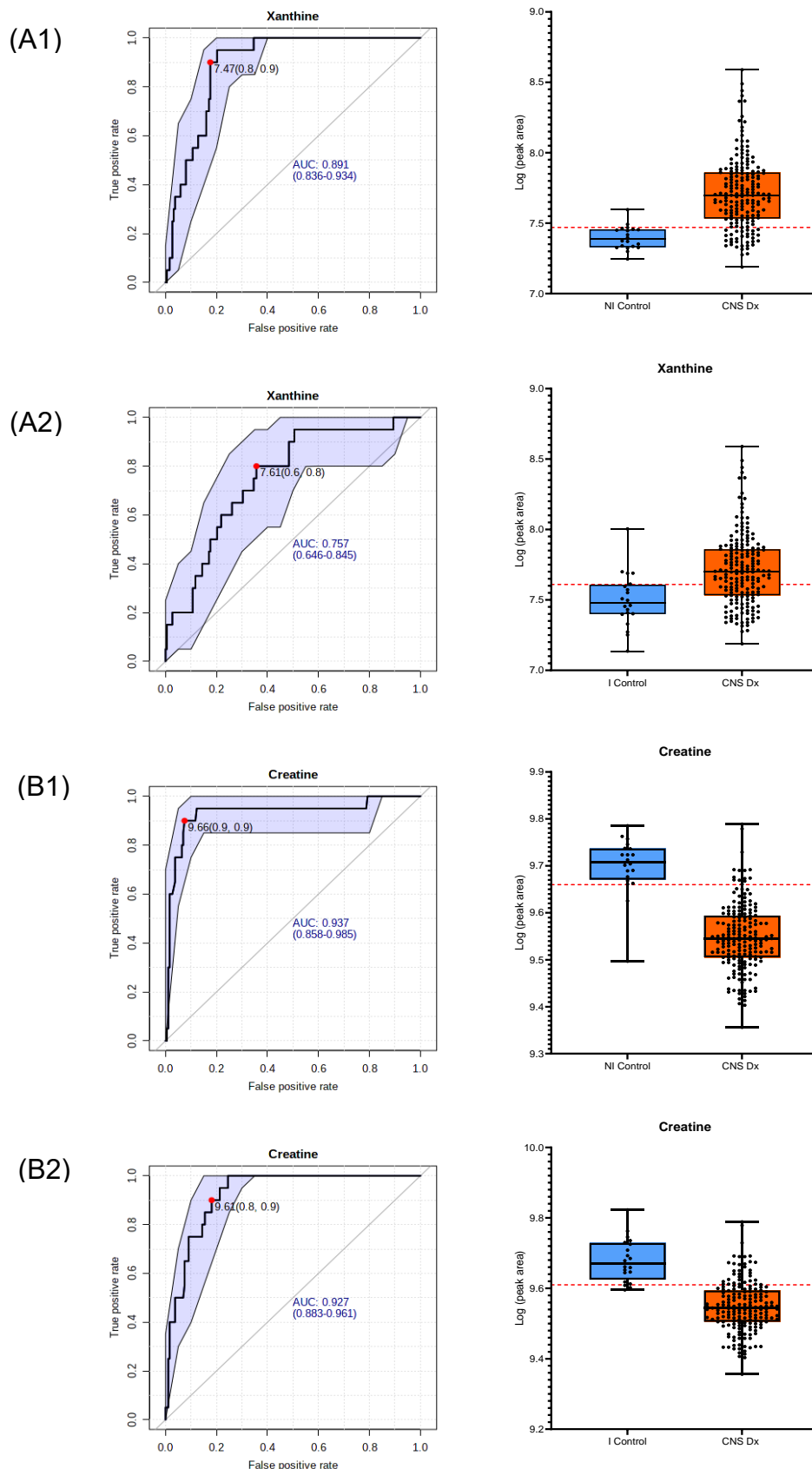


**Figure 3-19: Candidate biomarker ROC Curves and optimal cut-off points between CNS Dx and non-inflammatory and inflammatory controls.** Optimal cut-off points (red dotted line) determined as “closest to top left” described by  $d = \sqrt{[1 - \text{Sensitivity}]^2 + [1 - \text{Specificity}]^2}$ . (A1) Xanthine – CNS Dx vs non-inflammatory control; (A2) Xanthine – CNS Dx vs inflammatory control ; (B1) Creatine – CNS Dx vs non-inflammatory control; (B2) Creatine – CNS Dx vs inflammatory control. ROC curves created on Metaboanalyst; Box plots created on GraphPad Prism v9.

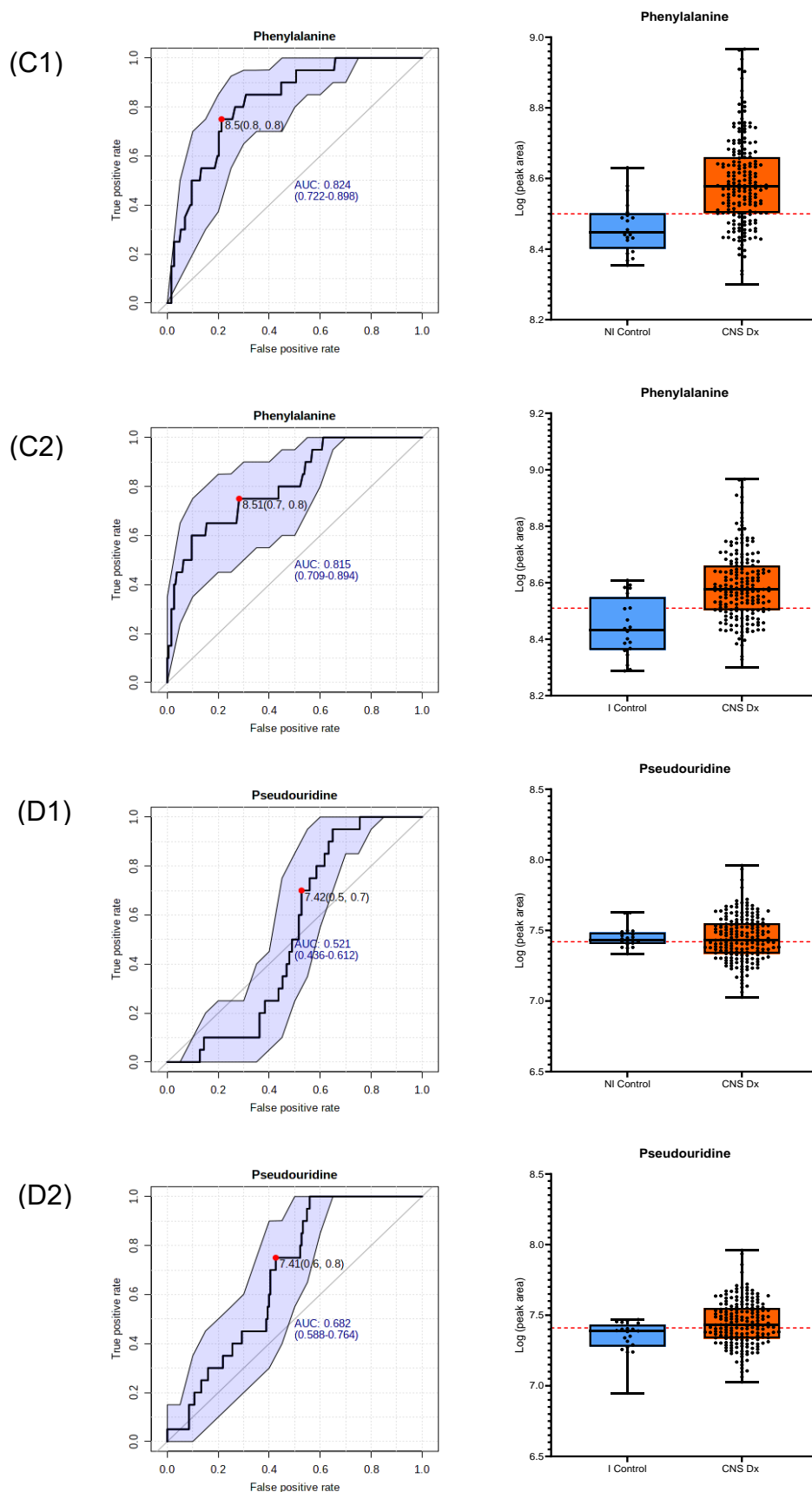
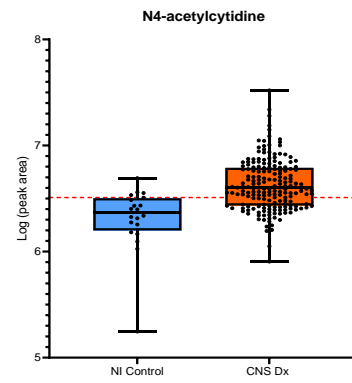
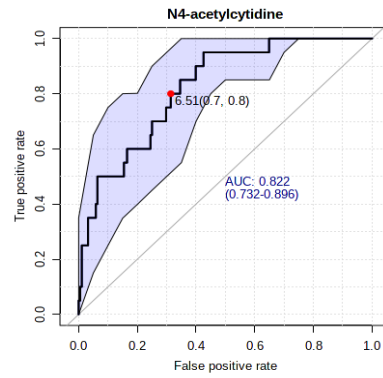
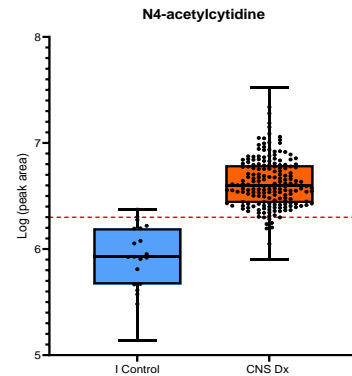
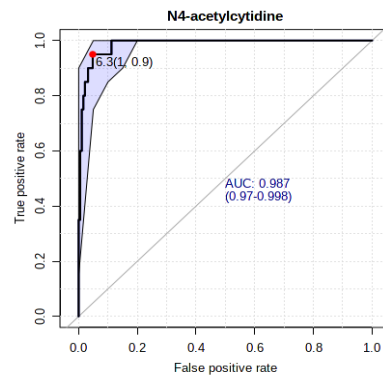


**Figure 3-20: Candidate biomarker ROC Curves and optimal cut-off points between CNS Dx and non-inflammatory and inflammatory controls.** Optimal cut-off points (red dotted line) determined as “closest to top left” described by  $d = \sqrt{[1 - \text{Sensitivity}]^2 + [1 - \text{Specificity}]^2}$ . (C1) Phenylalanine – CNS Dx vs non-inflammatory control; (C2) Phenylalanine – CNS Dx vs inflammatory control ; (D1) Pseudouridine – CNS Dx vs non-inflammatory control; (D2) Pseudouridine – CNS Dx vs inflammatory control. ROC curves created on Metaboanalyst; Box plots created on GraphPad Prism v9.

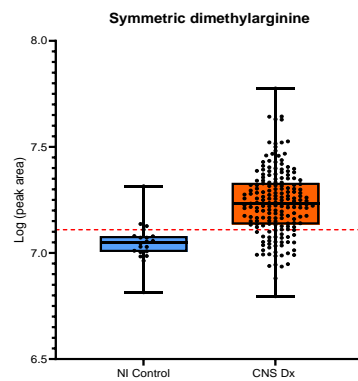
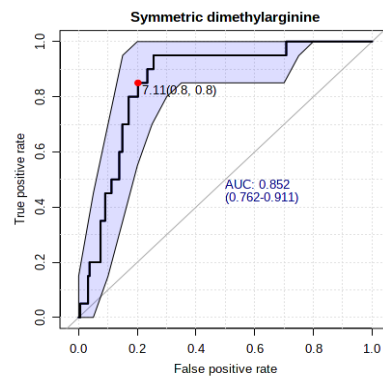
(E1)



(E2)



(F1)



(F2)

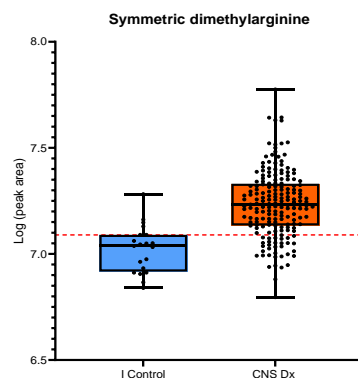
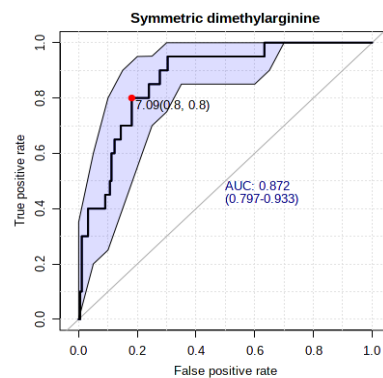


**Figure 3-21: Candidate biomarker ROC Curves and optimal cut-off points between CNS Dx and non-inflammatory and inflammatory controls.** Optimal cut-off points (red dotted line) determined as “closest to top left” described by  $d = \sqrt{[1 - \text{Sensitivity}]^2 + (1 - \text{Specificity})^2}$ . (E1) N4-acetylcytidine – CNS Dx vs non-inflammatory control; (E2) N4-acetylcytidine – CNS Dx vs inflammatory control ; (F1) Symmetric dimethylarginine – CNS Dx vs non-inflammatory control; (F2) Symmetric dimethylarginine – CNS Dx vs inflammatory control. ROC curves created on Metaboanalyst; Box plots created on GraphPad Prism v9.

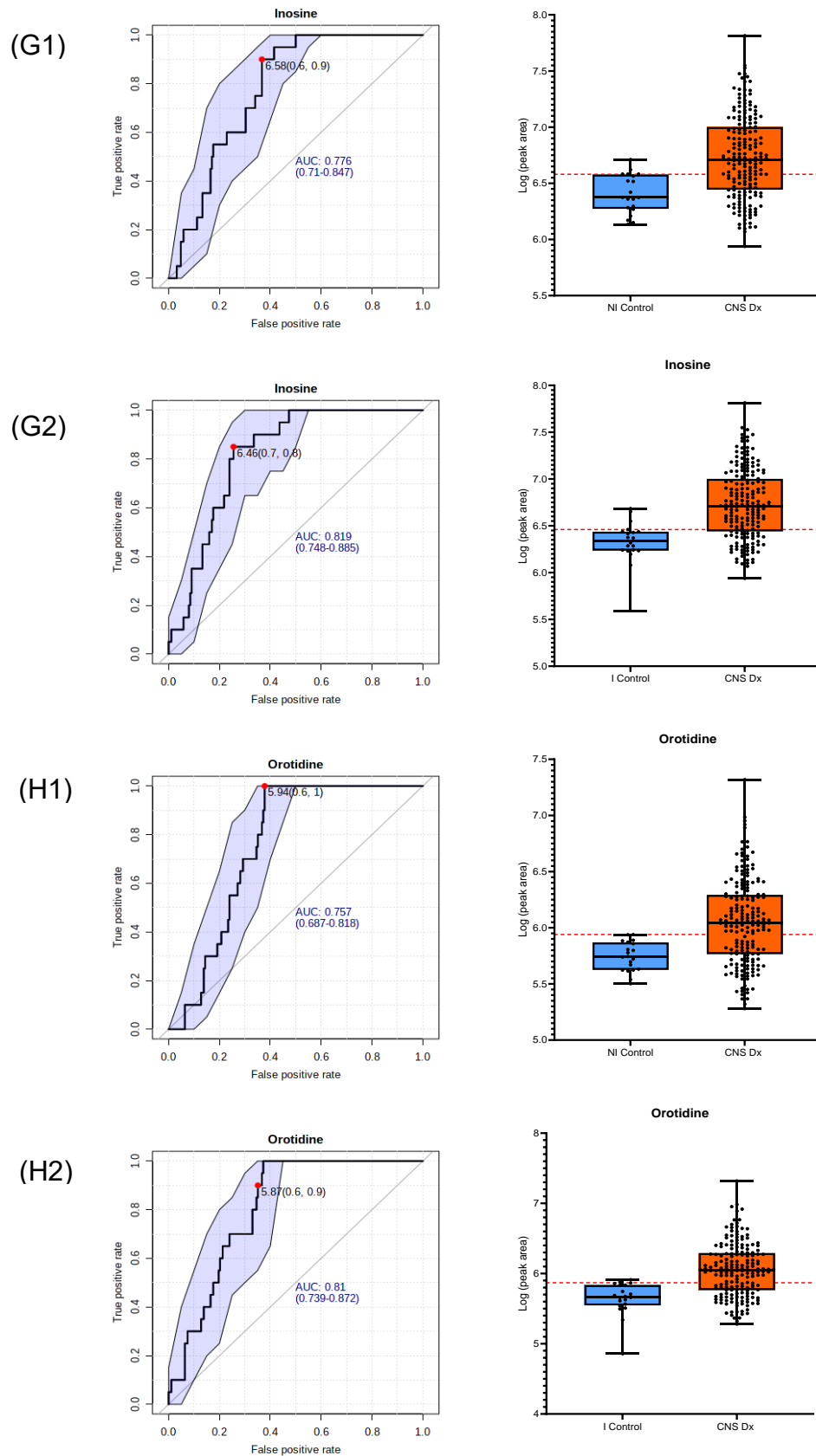


**Figure 3-22: Candidate biomarker ROC Curves and optimal cut-off points between CNS Dx and non-inflammatory and inflammatory controls.** Optimal cut-off points (red dotted line) determined as “closest to top left” described by  $d = \sqrt{[1 - \text{Sensitivity}]^2 + [1 - \text{Specificity}]^2}$ . (G1) Inosine – CNS Dx vs non-inflammatory control; (G2) Inosine – CNS Dx vs inflammatory control ; (H1) Orotidine – CNS Dx vs non-inflammatory control; (H1) Orotidine – CNS Dx vs inflammatory control. ROC curves created on Metaboanalyst; Box plots created on GraphPad Prism v9.



### 3.3.3 Biomarker performance evaluation

#### 3.3.3.1 Univariate ROC analysis of leukaemic CSF vs Control CSF

Having tested the CNS Dx patient group against both CSF controls and finding concordant trends between the patient group and the control CSF groups in all three CNS patient groups (CNS1, CNS2 & CNS3), the next part of the study was to further evaluate the performance of the candidate biomarkers against the combination of the CSF controls. First, the means of the candidate biomarkers was compared in the two groups of CSF controls to search for any statistical differences between the means.

As can be observed in the previous analyses above in N4-acetylcytidine, the leukaemic patient group mean was elevated compared to both controls and both differences were statistically significant. Noticeably, the means of the CSF controls were also different with levels in the inflammatory controls being moderately lower than its counterpart and statistical analysis between the means of revealed a significant difference between the means of these two controls (**Table 3-15, Figure 3-23**).

Pseudouridine presented with a similar trend to N4-acetylcytidine in terms of the differences between the two CSF controls with a decreased mean of the inflammatory control CSF control compared to the non-inflammatory control. Statistical analysis also revealed a significant difference between the two control CSF groups (**Table 3-15, Figure 3-23**).

Creatine, Phenylalanine, Symmetric dimethylarginine, Inosine and Orotidine all had very similar levels in the non-inflammatory and inflammatory CSF groups and statistical analysis indicated no significant difference between the means of the two groups for all metabolites (**Table 3-15, Figure 3-23**).

Xanthine did present with slightly elevated levels in the inflammatory control, but no statistically significant difference was found between the means of the two CSF controls.

For 6/8 metabolites, there appears to be no real evidence that the levels of these metabolites differ between non-inflammatory and inflammatory CNS microenvironments. This potentially suggests that these metabolites may be at their “normal” levels as a constituent of CSF and that their pathways are not obviously affected by the numerous different conditions highlighted in **Table 3-12**.

The phenotype seen in the control CSF groups for N4-acetylcytidine and Pseudouridine is interesting, and it appears that inflammation in the CNS can cause variability in the levels of these metabolites. The CNS of leukaemic patients is considered to be an area of inflammation and, if indeed N4-acetylcytidine and Pseudouridine are biomarkers for CNS-leukaemia, it appears that the phenotype for these metabolites is more closely linked to the levels present in a non-inflammatory CSF environment.

Candidate biomarker	NI CTL mean	I CTL Mean	± SE	95% confidence interval	R <sup>2</sup>	P value	Adj p value
Xanthine	7.397	7.498	0.04689	-0.1965 to -0.006613	0.1098	0.036701	0.200962
Creatine	9.699	9.679	0.01943	-0.01946 to 0.05921	0.02680	0.312758	0.675414
Phenylalanine	8.463	8.443	0.02865	-0.03810 to 0.07789	0.01253	0.491597	0.703358
Pseudouridine	7.449	7.345	0.03152	0.04044 to 0.1681	0.2235	0.002065	0.014363
N4-acetylcytidine	6.311	5.914	0.09797	0.1988 to 0.5954	0.3019	0.000241	0.001925
Symmetric dimethylarginine	7.049	7.024	0.03261	-0.04142 to 0.09062	0.01475	0.455351	0.703358
Inosine	6.404	6.326	0.06432	-0.05235 to 0.2080	0.03712	0.233614	0.655023
Orotidine	5.744	5.643	0.06074	-0.02271 to 0.2232	0.06690	0.107074	0.432355

**Table 3-15: Statistical analysis of the difference between non-inflammatory and inflammatory CSF controls.** Data was log transformed prior to statistical analysis. Statistics performed on GraphPad Prism v9.

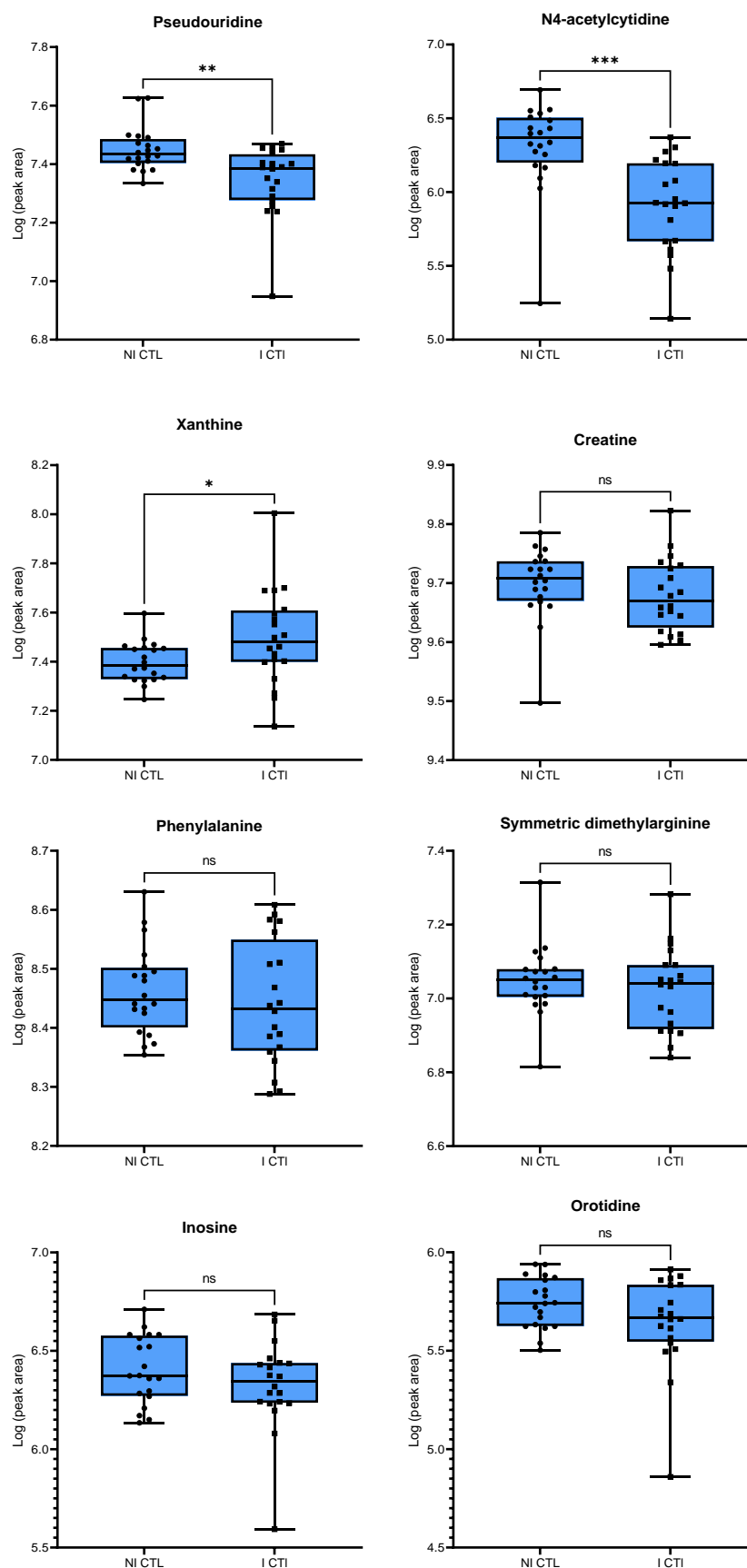


**Figure 3-23: Boxplots: Noninflammatory and Inflammatory Control CSF comparison of means.** NI control (n=20); I control (n=20). Graphs created on GraphPad Prism v9.

### **3.3.3.2 Analysis of CNS1 CNS2 and CNS3 patient sample groups within the CNS Dx patient sample cohort.**

The CNS Dx patient sample cohort was made up of patients who were classified as either CNS1, CNS2 or CNS3 by CSF cytology. The next analysis involved breaking the combined cohort down into their separate classification categories and investigating the behaviour of the candidate biomarkers against the combined CSF control to check for any differences between the three classifications. The core of the CNS Dx cohort was composed of CNS1 patients, and as expected, the CNS1 patient samples behaved identically to the CNS Dx cohort in terms of the trends observed for each candidate biomarker apart from Pseudouridine (**Figure 3-24**).

Pseudouridine had with no real difference in the mean between the CNS1 Dx group and the control CSF group. Statistical analysis revealed no significant difference between these means, however the difference between the CNS1 Dx group.

The CNS2 group also behaved similarly to the CNS Dx group when compared to the CSF control with significant differences found between the CNS Dx group and the control CSF group, apart from Pseudouridine and Inosine, in which the mean appeared elevated, but no statistical difference was found (**Figure 3-24**). Pseudouridine, again performed poorly, with no statistically significant difference found between the means of the patient group and the control group.

CNS3 Dx patients saw a similar trend to the CNS Dx trends with Creatine, Phenylalanine, N4-acetylcytidine, Symmetric dimethylarginine, Inosine and Orotidine performing as seen in the CNS Dx comparison. Interestingly, the levels of Xanthine appeared decreased compared to the CNS1 and CNS2 groups and

statistical analysis revealed no significant difference between the means of the CNS3 group and the CSF control (**Figure 3-24**).

Overall, the candidate biomarkers behaved similarly in their separated classifications when compared to the CNS Dx cohort.

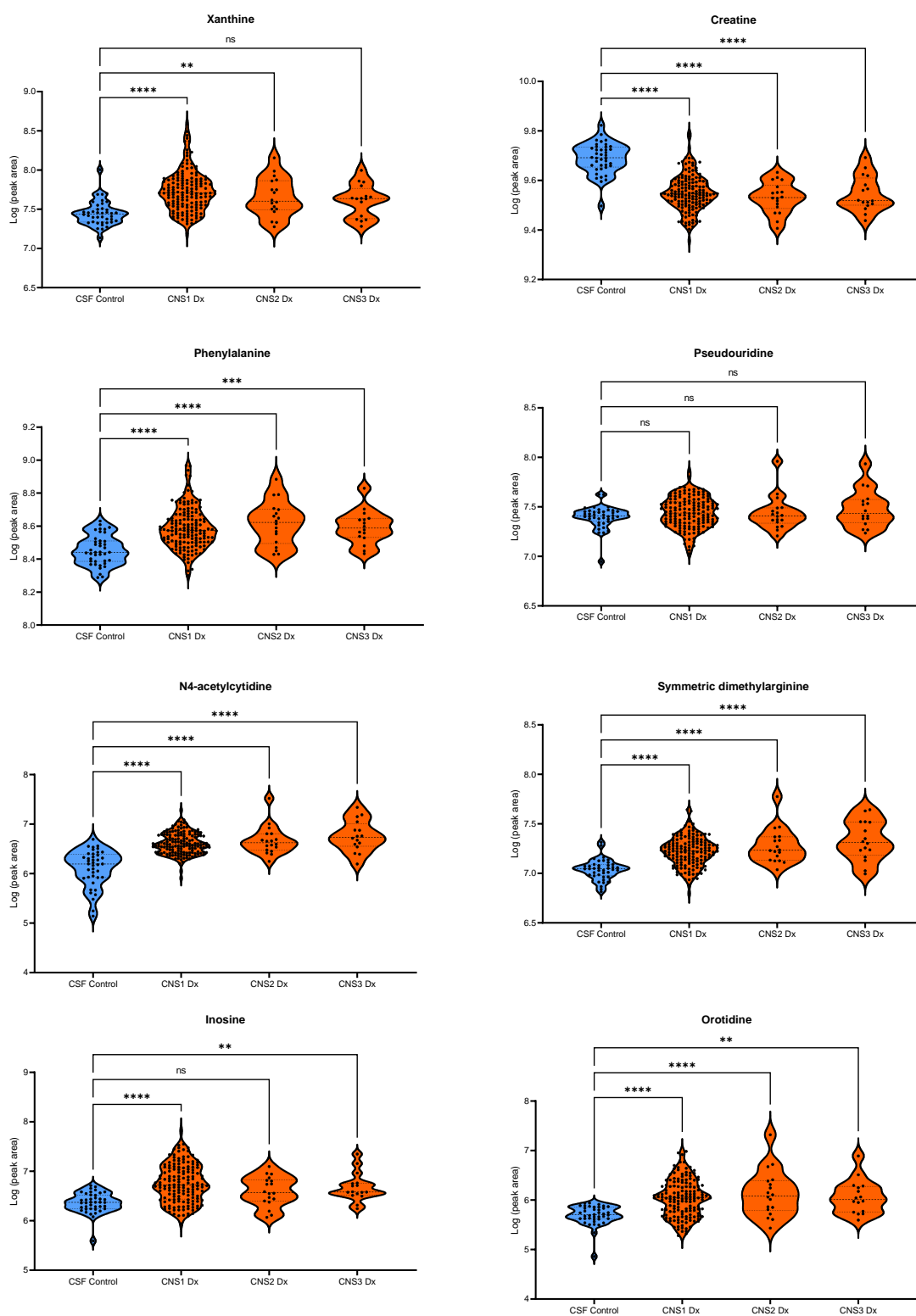


**Figure 3-24: Violin plots of Candidate biomarker levels: Control CSF vs CNS1, CNS2 and CNS3 patient groups.** CSF control (n=40); CNS1 (n=154), CNS2 (n=18); CNS3 (n=16). Data was log transformed and statistics performed on GraphPad Prism v9.

### 3.3.3.3 CNS1 vs CNS3

Next, it was prudent to test the levels of the candidate biomarkers in the CNS1 patient group against the CNS3 patient group as patients who are classified as CNS3 by CSF cytology are considered high risk and it is hypothesized that these children have high leukaemic burdens in the CNS at the time of diagnosis in comparison to CNS1 patients who have no detectable blasts in the CSF and are typically considered lower risk. In this analysis the means of the CNS1 and CNS3 patient sample groups were compared to look for differences in the levels of the candidate biomarkers. It was hypothesized that CNS3 patients would have higher or lower levels (depending on the biomarkers observed biological phenotype) than the CNS1 patients.

Statistical analysis to test for differences between the means of the CNS1 group and the CNS3 group was performed, and the results indicated a significant difference in N4-acetylcytidine and Symmetric dimethylarginine alone with an increasing trend going from CNS1 to CNS2 to CNS3 patients (**Figure 3-26, Table 3-16**). This result potentially suggests that these biomarkers are directly influenced by the level of leukaemic burden in the CNS. Unfortunately, the CNS2 and CNS3 groups do not have as many patient samples as the CNS1 group, and the majority of data points lie between two standard deviations of the mean of the CNS1 group.



Candidate biomarker	CNS1 Mean	CNS3 Mean	± SEM	95% confidence interval	R squared (eta squared)	P value
Xanthine	7.730	7.609	0.05575	0.005194 to 0.2377	0.1909	0.068916
Creatine	9.551	9.547	0.01872	-0.03523 to 0.04329	0.002511	0.832496
Phenylalanine	8.586	8.592	0.02704	-0.06267 to 0.05011	0.002675	0.845348
Pseudouridine	7.441	7.481	0.04907	-0.1437 to 0.06319	0.03785	0.333076
N4-acetylcytidine	6.608	6.758	0.08010	-0.3190 to 0.01969	0.1741	0.013604
Symmetric dimethylarginine	7.221	7.330	0.05149	-0.2173 to 0.0003183	0.2102	0.006955
Inosine	6.755	6.676	0.07743	-0.08211 to 0.2399	0.04702	0.816441
Orotidine	6.038	6.061	0.08928	-0.2094 to 0.1643	0.003333	0.422169

**Table 3-16: Statistical analysis of the difference between candidate biomarker levels in CNS1 and CNS3 patient samples.** Data was log transformed prior to statistical analysis. Two-tailed unpaired t-test;  $\alpha=0.05$ . Statistics performed on GraphPad Prism v9.

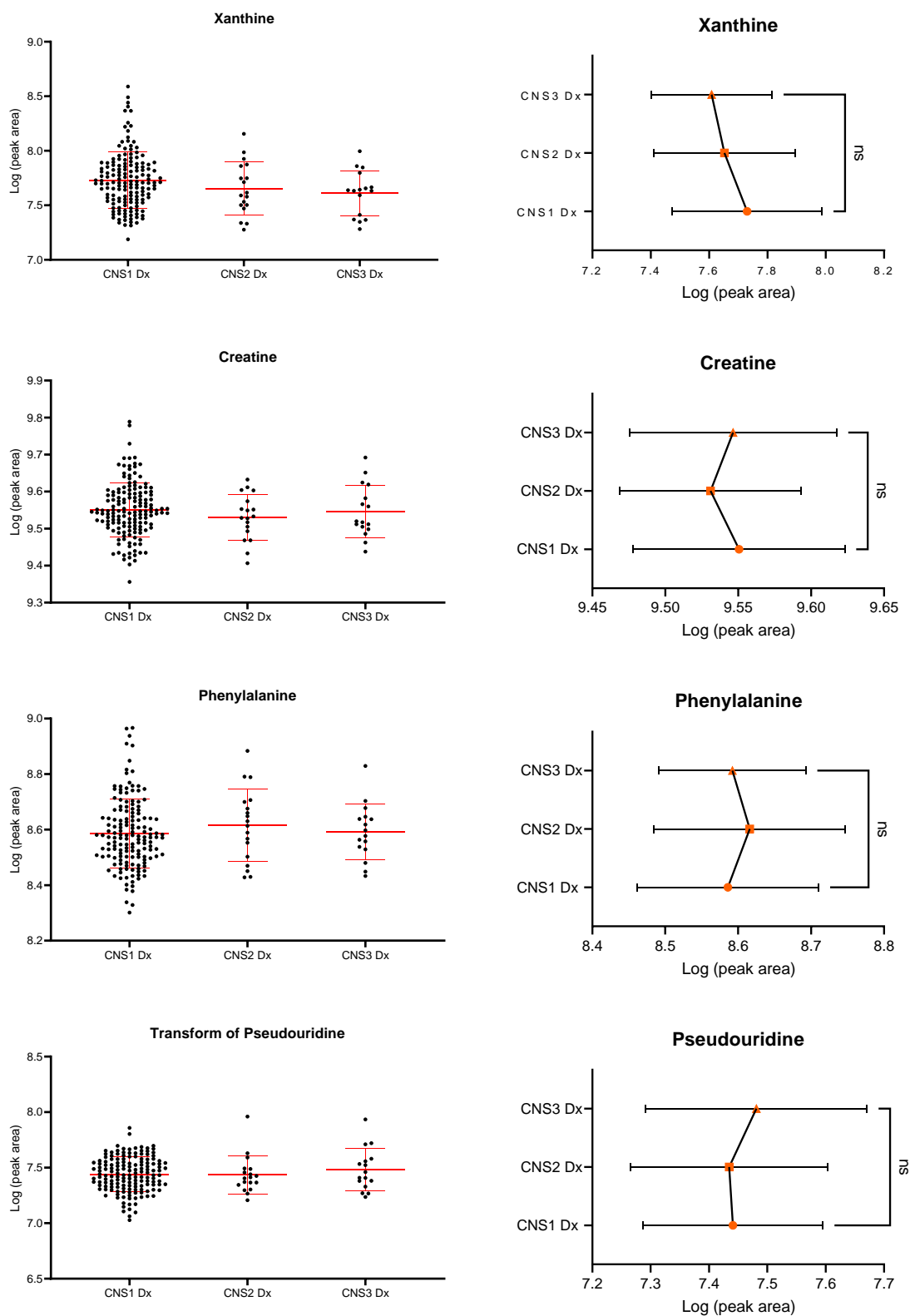


**Figure 3-25: Comparison between the means of CNS1 vs CNS3 patients.** Data was log transformed prior to statistical analysis. Two-tailed unpaired t-test;  $\alpha=0.05$ . Mean and Standard deviation shown on both plots. Scatter and line plots created on GraphPad Prism v9.

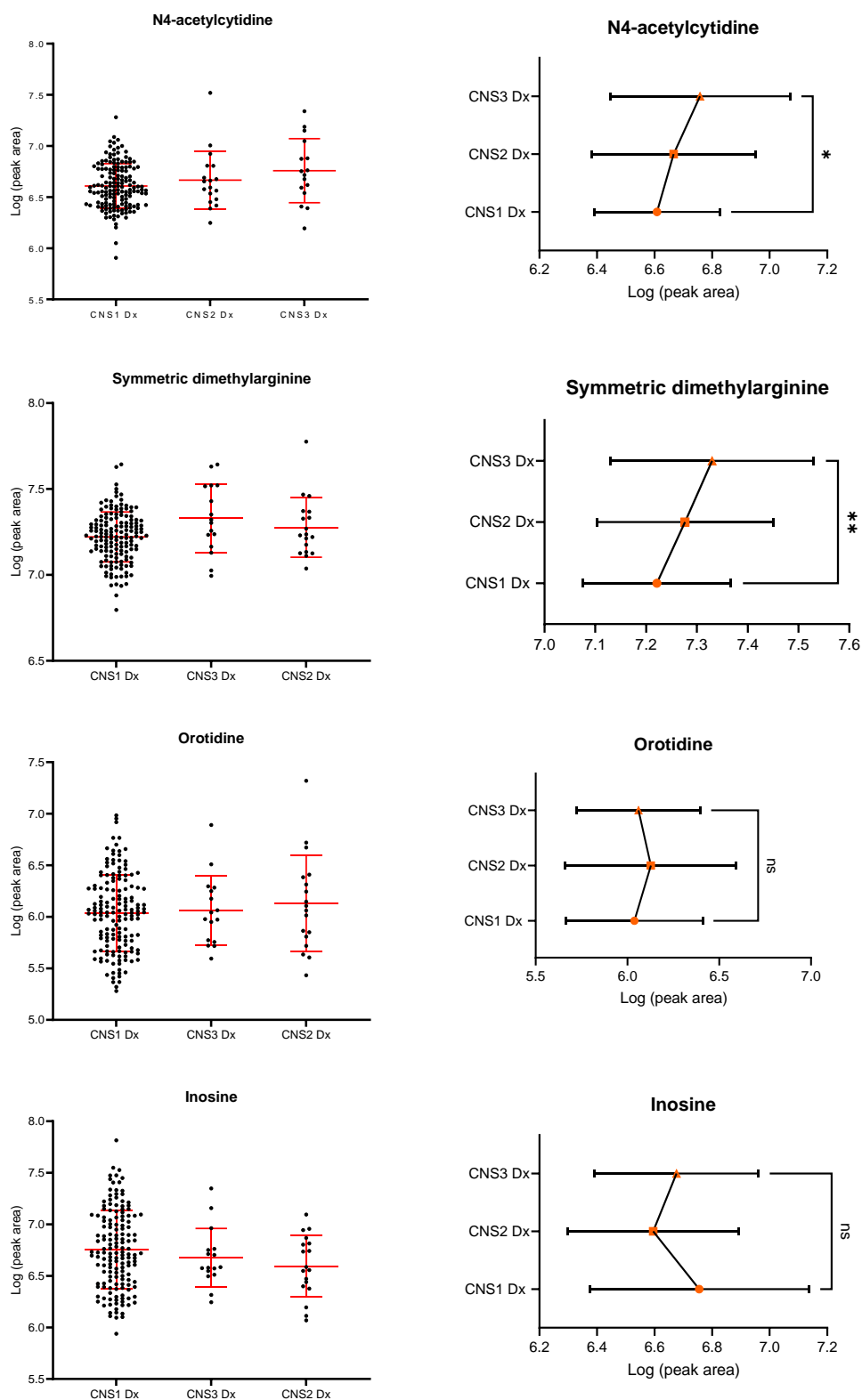


**Figure 3-26: Comparison between the means of CNS1 vs CNS3 patients.** Data was log transformed prior to statistical analysis. Two-tailed unpaired t-test;  $\alpha=0.05$ . Mean and Standard deviation shown on both plots. Scatter and line plots created on GraphPad Prism v9.

### 3.3.3.4 Univariate analysis CNS Dx vs CSF CTL

Due to the lack of difference between the two CSF controls for the majority of the candidate biomarkers and their concordance when compared to the leukaemic patient CSF group, the next step was to re-test the CNS Dx group against the combined data from both control CSF groups as one control CSF cohort.

All metabolites apart from Pseudouridine, showed a stark difference in the means between the patient group and the control group and statistical analysis indicated very low p values of  $<0.0001$  for all candidate biomarkers. The levels of Pseudouridine appeared essentially equivalent between the patient group and the control CSF group with no statistically significant difference found between the means (**Table 3-17**).

A final univariate ROC analysis was then performed on each candidate biomarker to test their specificity and sensitivity compared to the combined CSF control. In line with the previous analysis, Creatine performed best with an AUC of 0.93 with high 95% confidence intervals (0.88 to 0.97) and a p value  $< 0.00001$ . The levels of Creatine were clearly lower in leukaemic patient CSF compared to the control CSF with minor overlapping data points between the two groups (**Table 3-18, Figure 3-29 B**).

Next best, was N4-acetylcytidine which exhibited ROC metrics akin to Creatine with an AUC of 0.91; 95% confidence intervals 0.86 to 0.95 and a p value  $<0.00001$ . The violin plot shows very clustered data around the mean for the leukaemic group and again N4-acetylcytidine was clearly higher than the control CSF group (**Table 3-18, Figure 3-29 E**).

Xanthine, Phenylalanine, Symmetric dimethylarginine showed high levels of discriminatory ability between the leukaemic group and the control CSF group followed by Orotidine, all with acceptable to good 95% confidence intervals and p values  $<0.00001$  (**Table 3-18, Figures 3-28, 3-29**). Again, the means of these metabolites were clearly higher in the leukaemic patient group compared to the control CSF group however a proportion of the data points can be observed to be overlapping in the violin plots (**Figures 3-28, 3-29**).

Pseudouridine performed poorly as a discriminator between patient and control CSF with an AUC of 0.58 and a p value  $>0.05$ . This corroborates its poor performance in previous analyses and experiments (**Figure 3-19**).

This data suggests that all candidate biomarkers apart from Pseudouridine, are capable of distinguishing leukaemic CSF when compared to control CSF composed of a mixture of inflammatory and non-inflammatory metabolomes. The use of both controls combined in this experiment create a variable but concordant control population from which the leukemic group was tested against and succeeded in being sensitive enough and specific enough to generate robust data. While this type of CSF, as it originates from adults, is not the perfect control for this analysis, the trends seen across the three experiments hold providing strong evidence to propose that the levels of these candidate biomarkers in the CSF of matched and unmatched children would lie between the lower and upper bounds of the CSF control used in this analysis.

Candidate biomarker	Control CSF mean	CNS Dx Mean	Log2 Fc	± SEM	95% CI	R <sup>2</sup>	P value	Adj P Value
Xanthine	7.448	7.712	1.058	0.04167	-0.3469 to -0.1827	0.1516	<0.000001	<0.000001
Creatine	9.689	9.548	-0.462	0.01215	0.1170 to 0.1648	0.3733	<0.000001	<0.000001
Phenylalanine	8.453	8.589	0.484	0.02052	-0.1769 to -0.09607	0.1637	<0.000001	<0.000001
Pseudouridine	7.397	7.444	0.211	0.02638	-0.09854 to 0.005428	0.01359	0.078958	0.078958
N4-acetylcytidine	6.112	6.627	1.551	0.04594	-0.6048 to -0.4238	0.3567	<0.000001	<0.000001
Symmetric dimethylarginine	7.037	7.236	0.718	0.02581	-0.2501 to -0.1484	0.2086	<0.000001	<0.000001
Inosine	6.365	6.733	1.6229	0.06021	-0.4869 to -0.2496	0.1420	<0.000001	<0.000001
Orotidine	5.694	6.049	1.662	0.06146	-0.4761 to -0.2339	0.1286	<0.000001	<0.000001

**Table 3-17: Statistical analysis of the difference between candidate biomarker levels in the CNS Dx patient group against the Control CSF group.** Data was log transformed prior to statistical analysis. Two-tailed unpaired t-test;  $\alpha=0.05$ . Statistics performed on GraphPad Prism v9.

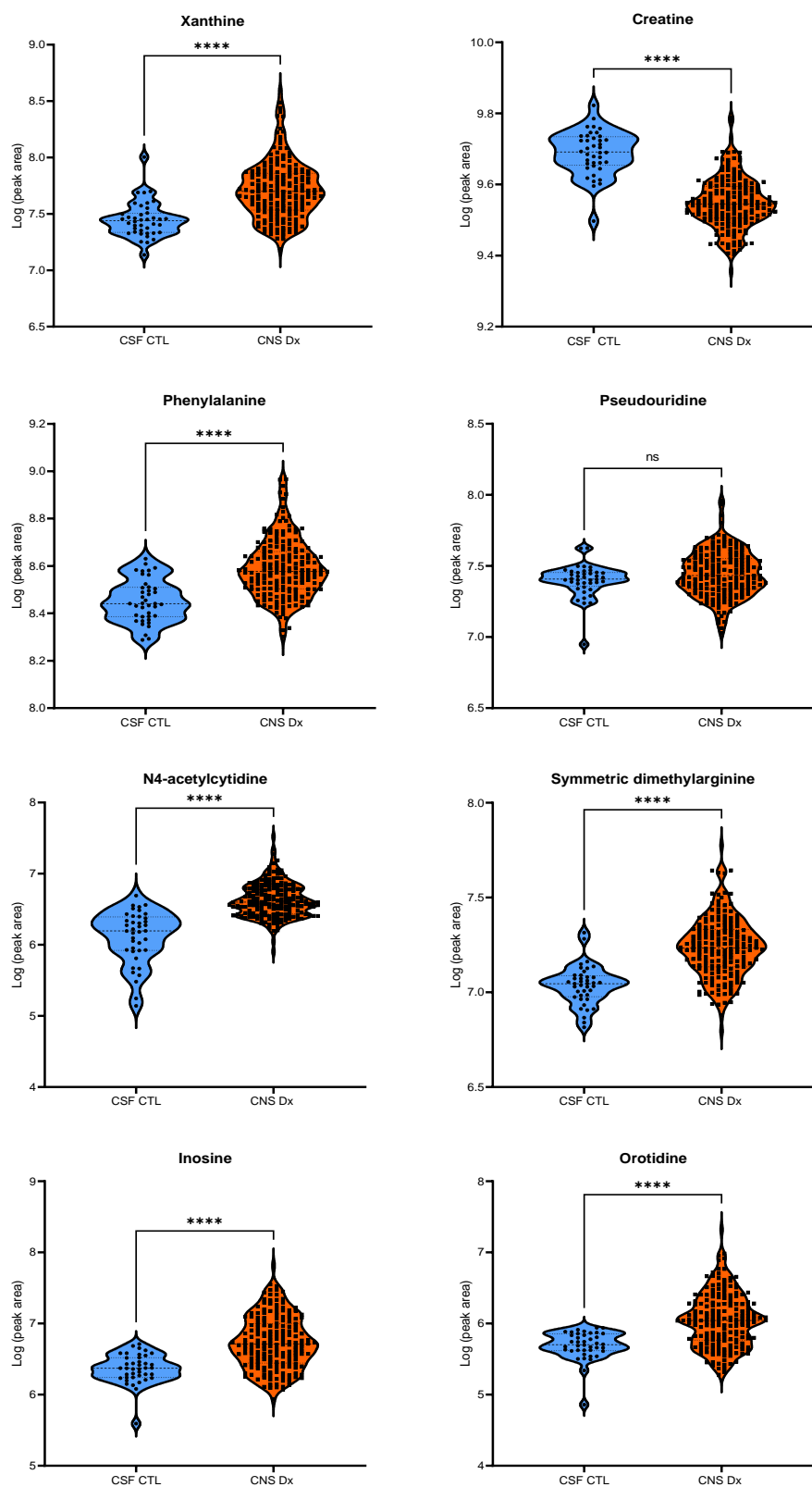


**Figure 3-27: Violin plots of candidate biomarkers depicting CNS Dx patient group v control CSF.** CNS Dx: Diagnostic leukaemic patient samples (n=188); Combined CSF control (n=40); Two-tailed unpaired t-test; Multiple un-paired t-tests corrected using Holm-Sidk method,  $\alpha = 0.05$ . Data was log transformed and statistics performed on GraphPad Prism v9.

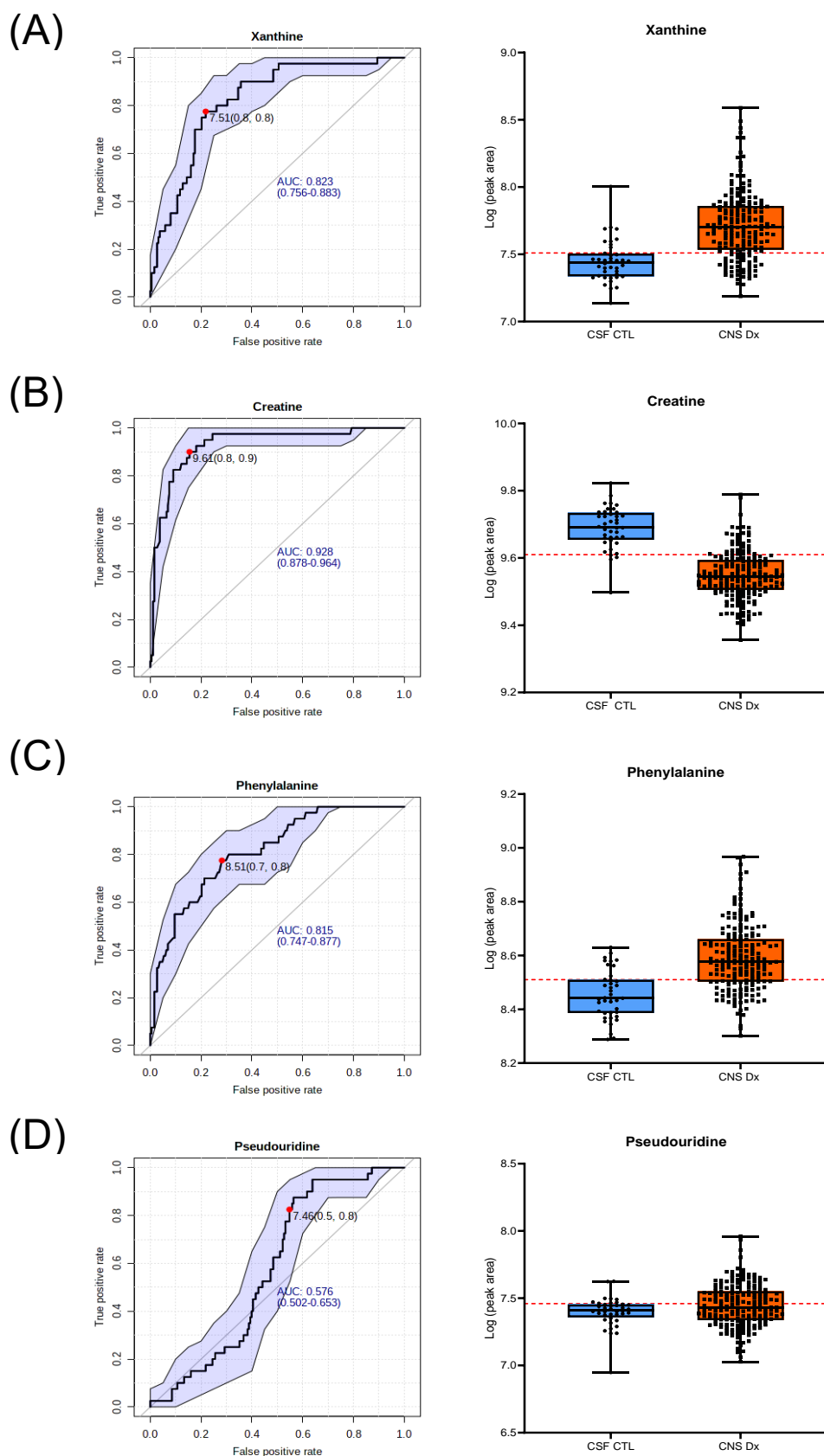


**Figure 3-28: Candidate biomarker ROC Curves and optimal cut-off points between CNS Dx and CTL CSF.** CNS Dx (n=188); control CSF (n=40). Optimal cut-off point (red dotted line) determined as “closest to top left” described by  $d = \sqrt{[1 - \text{Sensitivity}]^2 + [1 - \text{Specificity}]^2}$ . (A) Xanthine; (B) Creatine (C) Phenylalanine; (H2) Pseudouridine. ROC curves created on Metaboanalyst; Box plots created on GraphPad Prism v9.



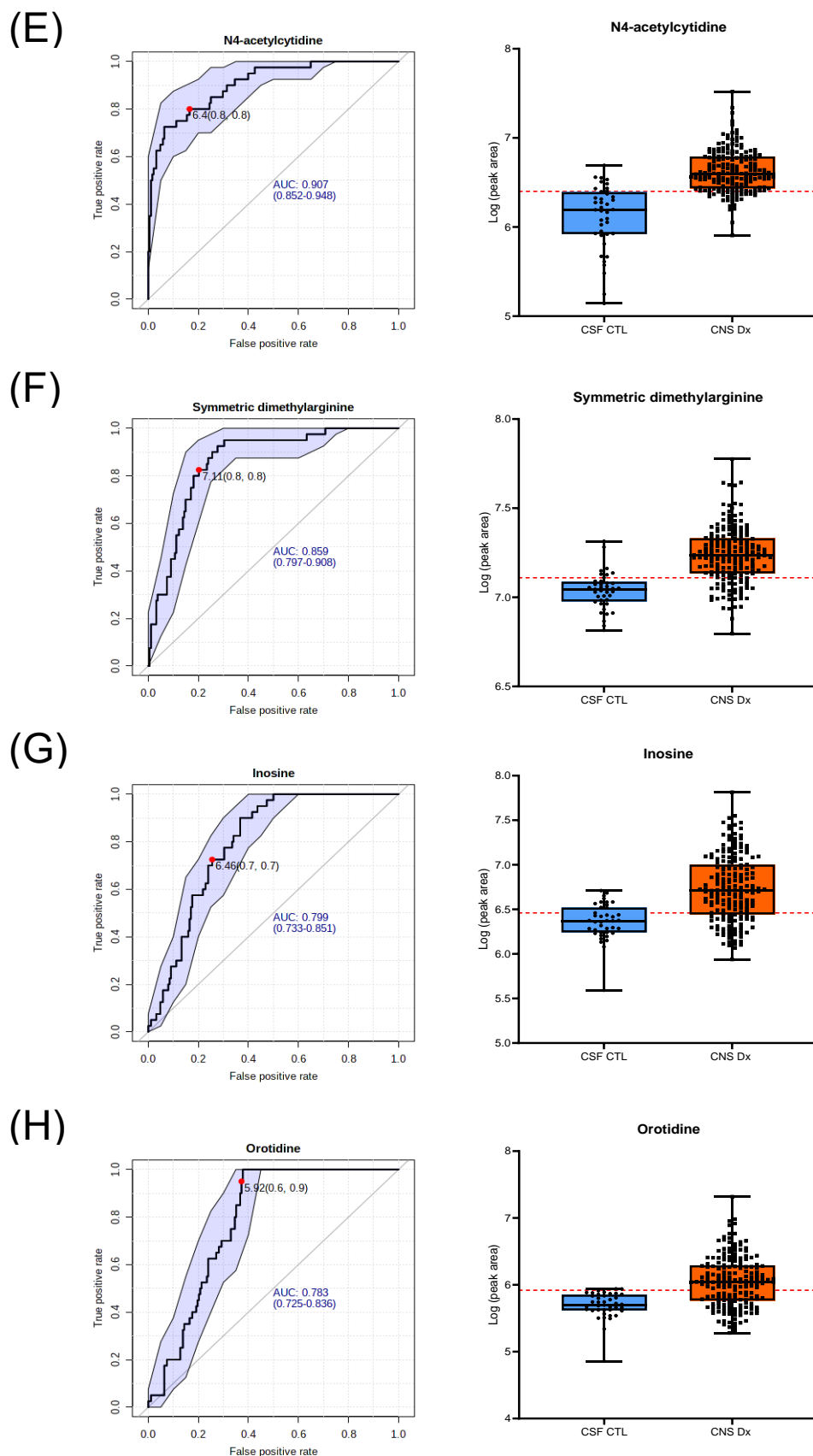


**Figure 3-29: Candidate biomarker ROC Curves and optimal cut-off points between CNS Dx and CTL CSF.** CNS Dx (n=188); control CSF (n=40). Optimal cut-off points (red dotted line) determined as “closest to top left” described by  $d = \sqrt{[1 - \text{Sensitivity}]^2 + (1 - \text{Specificity})^2}$ . (A) N4-acetylcytidine; (B) Symmetric dimethylarginine (C) Inosine; (H2) Orotidine. ROC curves created on Metaboanalyst; Box plots created on GraphPad Prism v9.

ROC	CNS Dx vs Control CSF			
Metabolite	AUC	95% CI	t-test P value	Optimal Cut-off
Xanthine	0.82	0.76 to 0.88	1.1356E-9	7.51
Creatine	0.93	0.88 to 0.97	1.0113E-24	9.61
Phenylalanine	0.82	0.75 to 0.88	2.1569E-10	8.51
Pseudouridine	0.58	0.50 to 0.66	0.078958	7.46
N4-acetylcytidine	0.91	0.86 to 0.95	1.9718E-23	6.40
Symmetric Dimethylarginine	0.87	0.81 to 0.91	3.748E-13	7.11
Inosine	0.80	0.73 to 0.85	4.1864E-9	6.46
Orotidine	0.78	0.72 to 0.84	2.5217E-8	5.92

**Table 3-18: Summary of ROC analysis**

In with the findings of this analysis, the data suggests that Pseudouridine is a poor candidate biomarker for discriminating leukaemic in the CNS and thus will be excluded from further analysis.

### 3.3.4 Multivariate Analysis of candidate biomarkers

The final part of this analysis was to re-implement the multivariate methodologies with our proposed model from the previous analysis on a new large cohort of patient samples. Once again, a multivariate ROC curve analysis was performed using the Random forests (RF) algorithm and the candidate biomarkers were ranked by their t-test statistic calculations to create various models containing different combinations of the seven candidate biomarkers (excluding Pseudouridine). In this study the patient group outweighed the control group in terms of sample numbers with a ratio of 5.7/1 (228 CNS Dx to 40 control).

The multivariate ROC curve was generated by using the Monte-Carlo Cross Validation (MCCV) technique by separating two thirds of the total samples (patients and controls) for evaluating the importance of each candidate biomarker followed by using the most highly ranked features to build several models for optimal classification (i.e. patient vs control). The models were then validated on the last third of the samples. This procedure was repeated 100 times and the results were averaged to generate the multivariate ROC curve (**Figure 3-30 A**).

The multivariate ROC curve shows that the AUC and the 95% confidence intervals increase with the number of variables tested, suggesting that a model with all seven candidate biomarkers performs best in discriminating between the CNS Dx group and the control CSF (**Figure 3-30 A**). The predictive accuracies of the different models can be seen in **Figure 3-30 B** and when the 7-variable model with all seven candidate biomarkers was used, the predictive accuracy was at its highest (93.8%) when compared to models which had lesser numbers of variables. The individual ROC curve of this 7-variable model can be seen in **Figure 3-31 A** depicting a very

high performing ROC curve produced by the combination of these seven candidate biomarkers with an AUC of 0.988, 95% confidence intervals of 0.974 to 0.996.

The candidate biomarkers were then ranked quantitatively by their average importance of their classification contributions from each cross-validation run and then by the frequency of the metabolites selected during the building of the model and the subsequent cross-validation in order of most discriminating at the top down to least discriminating. Both ranking methods yielded an identical rank order of the candidate biomarkers in terms of importance, unsurprisingly starting with Creatine then followed by N4-acetylcytidine, Symmetric dimethylarginine, Xanthine, Phenylalanine, Inosine then Orotidine (**Figure 3-31 B**).

To test the predictive capability of the 7-variable model, average predicted class probabilities were then calculated for each leukaemic sample and control across the 100 performed Monte-Carlo cross-validations and plotted to generate a confusion matrix. The data shows that out of the 188 leukaemic samples tested from the CNS Dx cohort, 179 were correctly classified into the leukaemic patient sample group and from the control CSF group consisting of 40 CSF samples (both non-inflammatory and inflammatory CSF), 39 were correctly identified as belonging to the control CSF group (**Figure 3-32**). Of the misclassified patient samples in this cohort, seven were CNS1 patients and two were CNS3. The misclassified control CSF sample was a non-inflammatory control CSF sample.

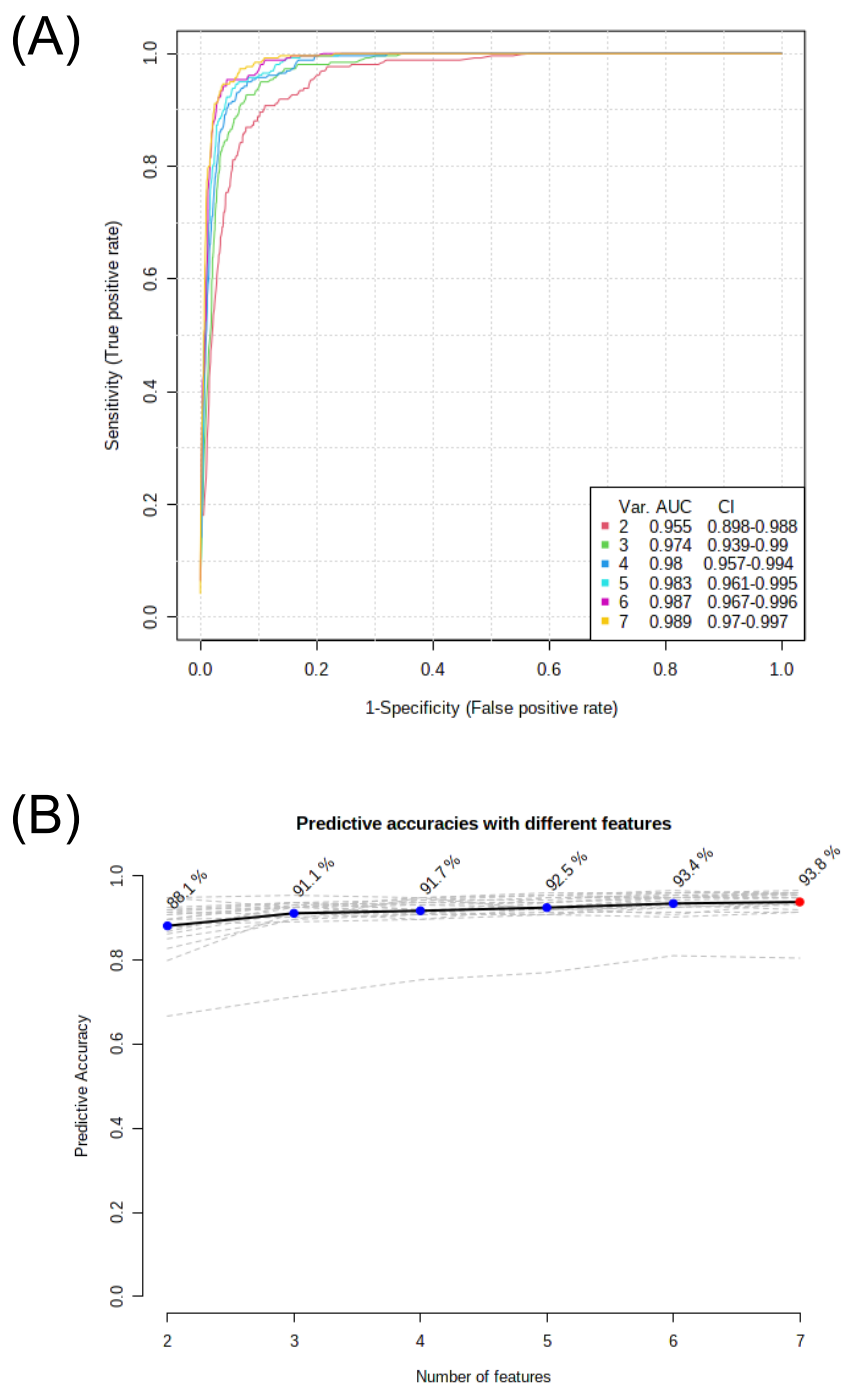


**Figure 3-30: Multivariate ROC analysis.** (A) Multivariate ROC curve with variable model averages plotted with associated AUC values and 95% confidence intervals; AUC = Area under the curve; CI = confidence intervals (B) Predictive accuracies of the best performing created models with different features. ROC curves created on Metaboanalyst. Classification method used: Random Forests, Feature ranking method based on statistical t-test.

This experiment also included 10 samples from the local Halsey biobank (a separate biobank to the samples involved in this analysis) which were purposefully not included in any of the previous candidate biomarker evaluation analyses. These samples were composed of 9 diagnostic CNS1 patient CSF samples and a relapse CNS3 CSF sample from a patient who relapsed in the CNS.

These samples were subsequently analysed using the 7-variable predictive model and their data was input into the algorithm without a class identifier (leukaemic or control CSF). The predictive model was able to correctly classify all new samples into the leukaemic patient sample group (**Figure 3-32**). The overall predictive accuracy was calculated as 95.6%.

Next, a second validation of the model was performed using permutation testing, a re-sampling based statistical test which postulates a null hypothesis that the 7-variable model described here could also have been discovered if every sample was randomly assigned a classification (either leukaemic or control CSF) in the same quantities with respect to the group sample numbers.

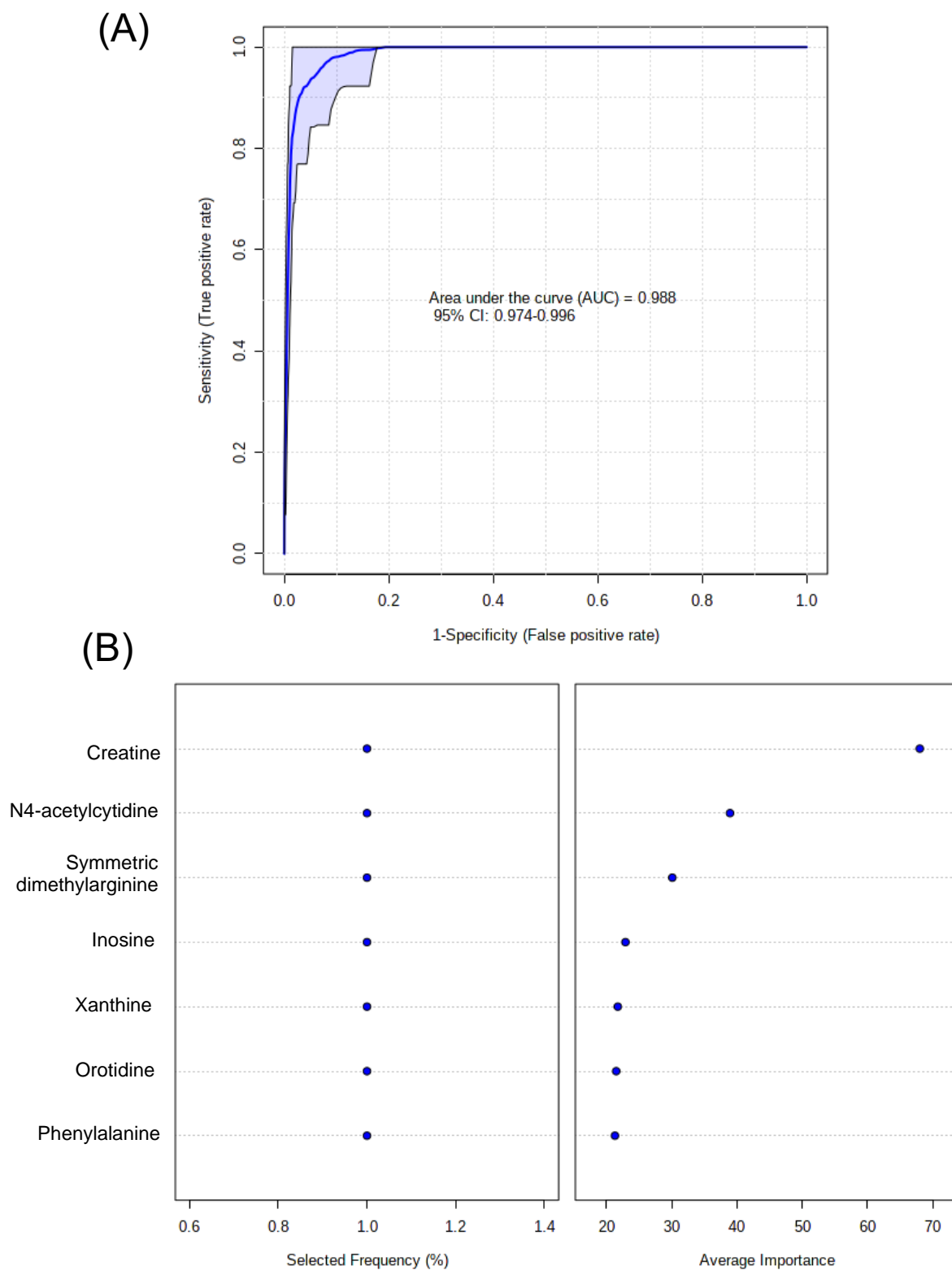
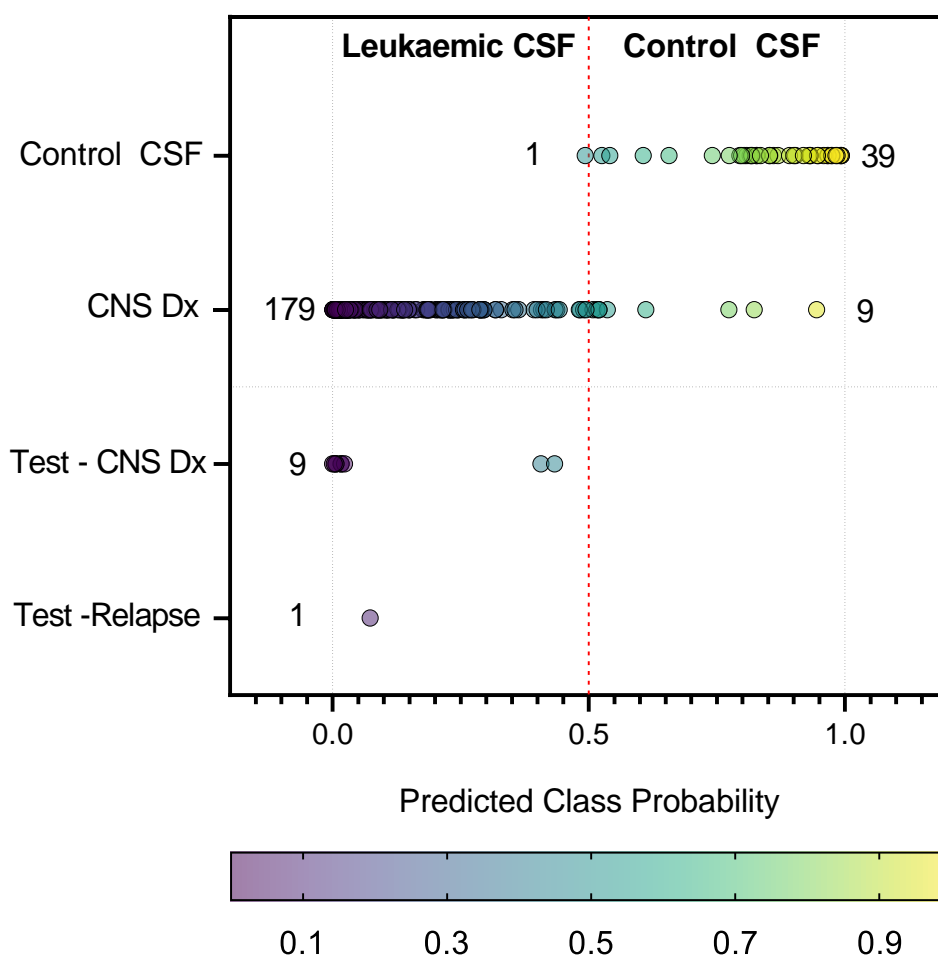


**Figure 3-31: ROC curve of highest performing 7-variable model and Candidate biomarker ranking.** (A) Combined ROC of 7-biomarker model. (B) Feature ranking: determine by frequency of being selected in the model creation process and average importance from the 100 cross-validations.

### Cross-validation Class Prediction



Confusion Matrix Summary (Cross-Validation)			
	Leukaemic CSF	Control CSF	Overall Predicted accuracy of 7-variabel model
Control CSF	1	39	95.6%
CNS Dx	179	9	
Test – CNS Dx	9	0	100%
Test- Relapse	1	0	

**Figure 3-32: Cross-validation class prediction probabilities.** Cross-validation Class Prediction confusion matrix. This graph plots the average predicted class probabilities of each sample from 100 cross-validations. The classification boundary is set to 0.5 and sample probabilities range from 0-1. Probabilities < 0.5 will belong to the leukaemic CSF sample group and probabilities >0.5 will belong to the Control CSF. Each sample is coloured by their probability score. Graph created on GraphPad Prism v9.



The permutation test was run ( $n=1000$ ) times using the 7-variable model and for every permutation, a RF model was built and tested for a statistical difference between the leukaemic and control CSF groups which was then compared to the original performance of the model resulting in a distribution of the permuted data (**Figure 3-33 A**). The performance score of the original model was then compared to the permuted distribution which gave a significant p value of  $<0.000002$  which lay outside of the distribution indicating a significant separation between the two groups (**Figure 3-33 A**). This suggests that there is a  $<5\%$  chance that a permuted model could perform as well as the original model tested.

A permutation test was also run to test the null hypothesis that the AUC of the 7-variable model equals 0.5, meaning the test has no discriminatory ability to distinguish between the disease and non-disease group. This analysis resulted in an empirical p value of 0.002 suggesting that the calculated AUC of the model was not obtained by chance and the model is capable of distinguishing CNS Dx samples from control CSF samples (**Figure 3-33 B**).

In summary, the data shown by this analysis reveals that the use of this 7-variable panel of candidate biomarkers provides a highly accurate method of discriminating leukaemic CSF in comparison with control CSF composed of both inflammatory and non-inflammatory CSF controls. Individually, each candidate biomarker tested in this model was able to discriminate leukaemic CSF from control CSF to different degrees of specificity and sensitivity but when combined, worked synergistically to classify a very high proportion of samples correctly with an overall prediction accuracy of 95.6%

This experiment validated the created model from the pilot experiment and performed as predicted in showing clear separation between the CNS Dx leukaemic CSF and the control CSF.

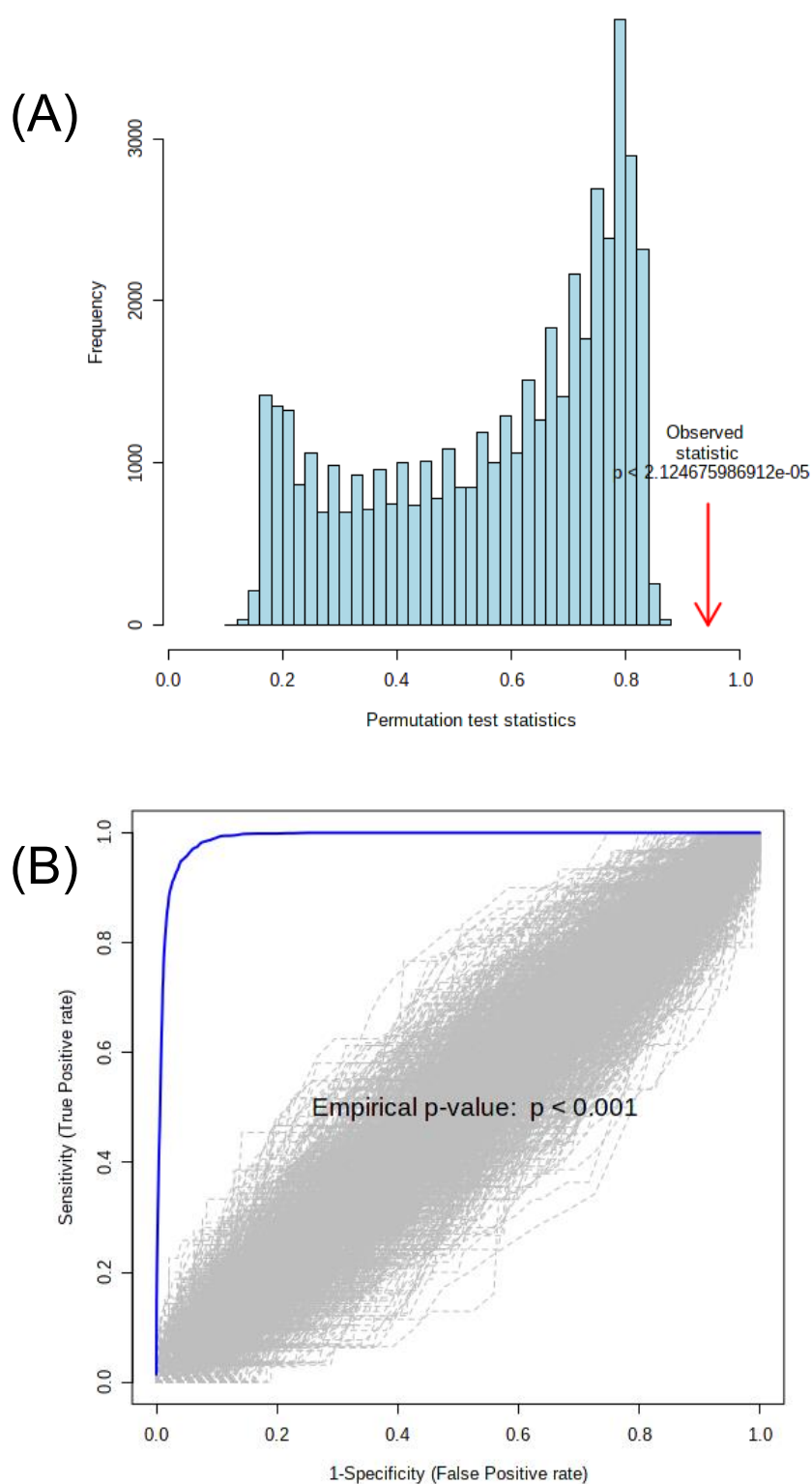


**Figure 3-33: Permutation test Histogram of permuted data.** Permutation testing on 6-variable model. (A) Permuted data statistical test distribution; Performance t-test score of the original model against the permuted data highlighted by the red arrow. (B) Permutation empirical p value calculated from statistical test to disprove the null hypothesis that the AUC equals 0.5. Graphs exported from Metaboanalyst.

### 3.4 Measuring true abundance of candidate biomarkers

#### 3.4.1 Quantification of Creatine and Xanthine levels

To support the findings above, with the material available to the laboratory at the time, the top performing biomarker Creatine, was quantified along with Xanthine using external standards to create a calibration curve using the Standard addition method in TraceFinder software (Thermo Fisher). Unfortunately, all seven candidate biomarkers could not be measured in this study due to material and time limitations caused by the Sars-CoV-2 pandemic.

Following the same methodology as before, first, the differences between the means of the CNS Dx and the control CSF group were analysed. Statistical analysis indicated a statistically significant difference between the means of the two groups for both candidate biomarkers ( $p < 0.000001$  &  $p = 0.0011$ ). The mean Creatine levels of the patient leukaemic group were found to be at  $2.33 \mu\text{M}$  in comparison with elevated levels of Creatine in the control CSF group at  $3.1 \mu\text{M}$  (**Table 3-19, Figure 3-34**).

ROC curve analysis was then performed to leverage an AUC resulting in an excellent AUC of 0.91 with 95% confidence intervals of 0.85 to 0.95 and an accompanying low  $p$  value  $< 0.000001$  for Creatine and an AUC of 0.76, 95% confidence intervals of 0.69 to 0.83 and a  $p$  value of 0.0015 for Xanthine (**Table 3-19, Figure 3-35**).

The optimal cut-off between the two groups was then determined by looking at the performance of the ROC curve where the trade-offs between sensitivity and specificity are at their highest possible within the analysis yielding a cut-off point of

2.63  $\mu\text{M}$ , a level at which sensitivity of this test was at 87.5% and the specificity was 79.3% for Creatine. For Xanthine, the optimal cut-off point was 188.5 nM resulting in a sensitivity of 70% and a specificity of 75.5% (**Table 3-19, Figure 3-36**).

This result was highly concordant with the previous analysis of Creatine, thus showing strong evidence of the discriminatory ability of this candidate biomarker. Xanthine still performed reasonably well with calculated absolute abundance; however, its performance was lessened compared to its performance in the previous analysis with lower ROC curve metrics: AUC 0.76; 95% confidence intervals 0.69 to 0.83 and a p value < 0.05 (previously AUC 0.82; 95% confidence intervals 0.76 to 0.88; p value= 1.1356E-9) (**Table 3-19**).

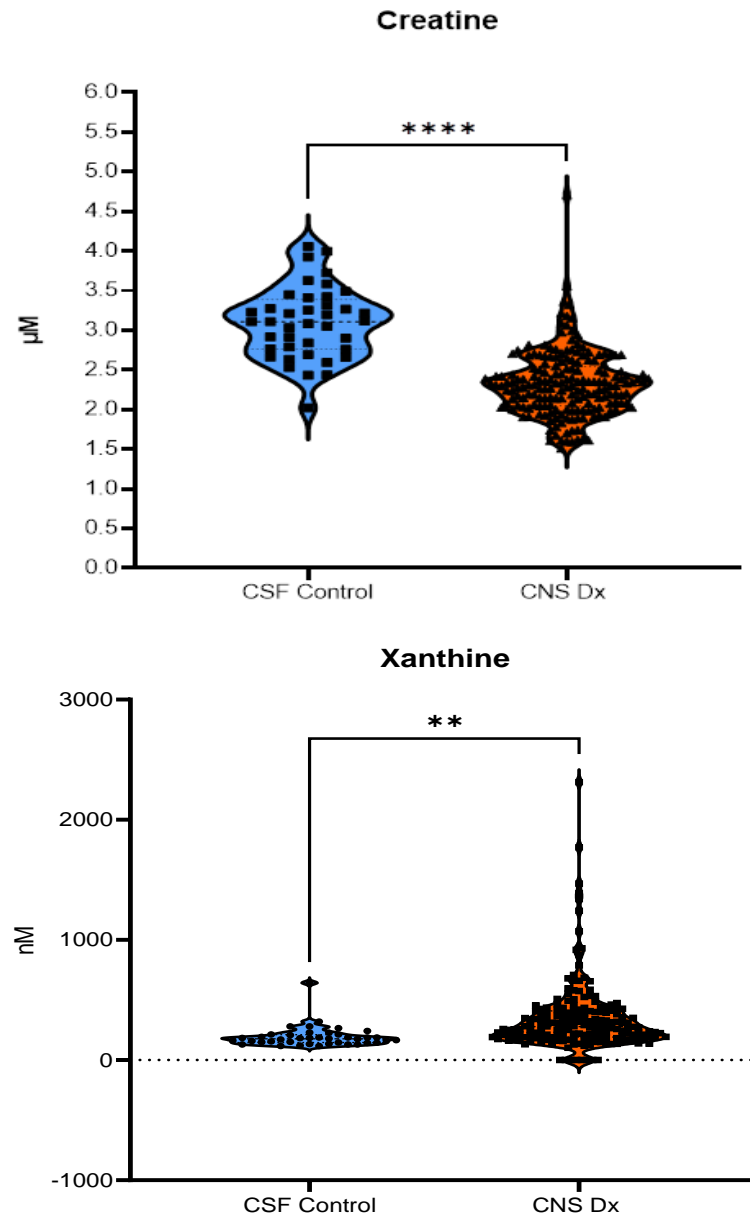


**Figure 3-34: Violin plots of Creatine and Xanthine CNS Dx patient samples vs matched and unmatched CSF controls.** CNS Dx n=188; Control CSF n=40. Data was log transformed and graphs were created on GraphPad Prism v9. Xanthine concentration expressed in nM, Creatine concentration express in  $\mu\text{M}$ .

Candidate biomarker	Control CSF mean	CNS Dx Mean	± SEM	95% CI		Unpaired -test P value
Creatine	3.093 µM	2.325 µM	0.07268	0.6250 to 0.9115		<0.000001
Xanthine	192.4 nM	348.0 nM	47.06	-248.4 to -62.87		0.001100
ROC	AUC	95% CI	p value	Optimal Cut-off	Sensitivity	Specificity
Creatine	0.91	0.85 to 0.95	<0.000001	2.63	87.5%	79.3%
Xanthine	0.76	0.694 to 0.83	0.0014609	188.5	70%	75.5%

**Table 3-19: Candidate biomarker statistical analysis and ROC curve summary:** Statistics performed on GraphPad Prism v9.

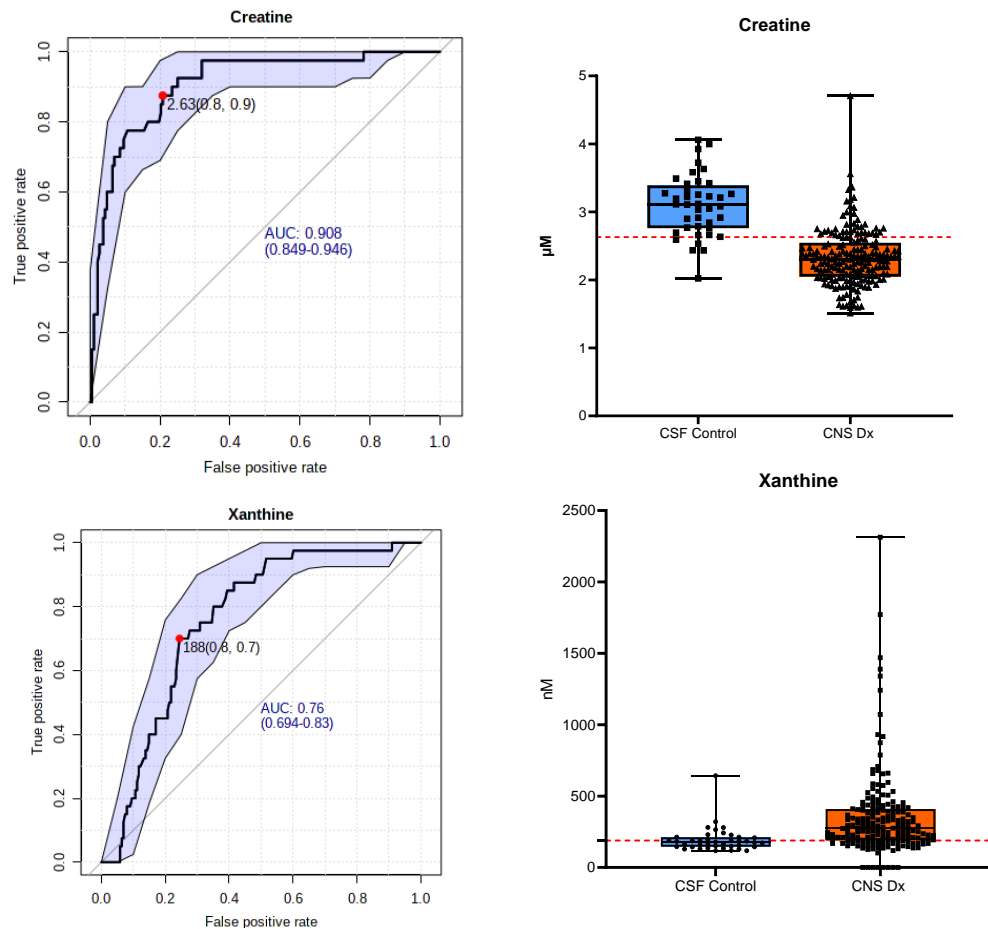


**Figure 3-25: Individual ROC curves for Creatine and Xanthine.** AUC = Area under the curve; CI = confidence intervals. . Optimal cut-off points (red dotted line) determined as “closest to top left” described by  $d = \sqrt{(1 - \text{Sensitivity})^2 + (1 - \text{Specificity})^2}$ .

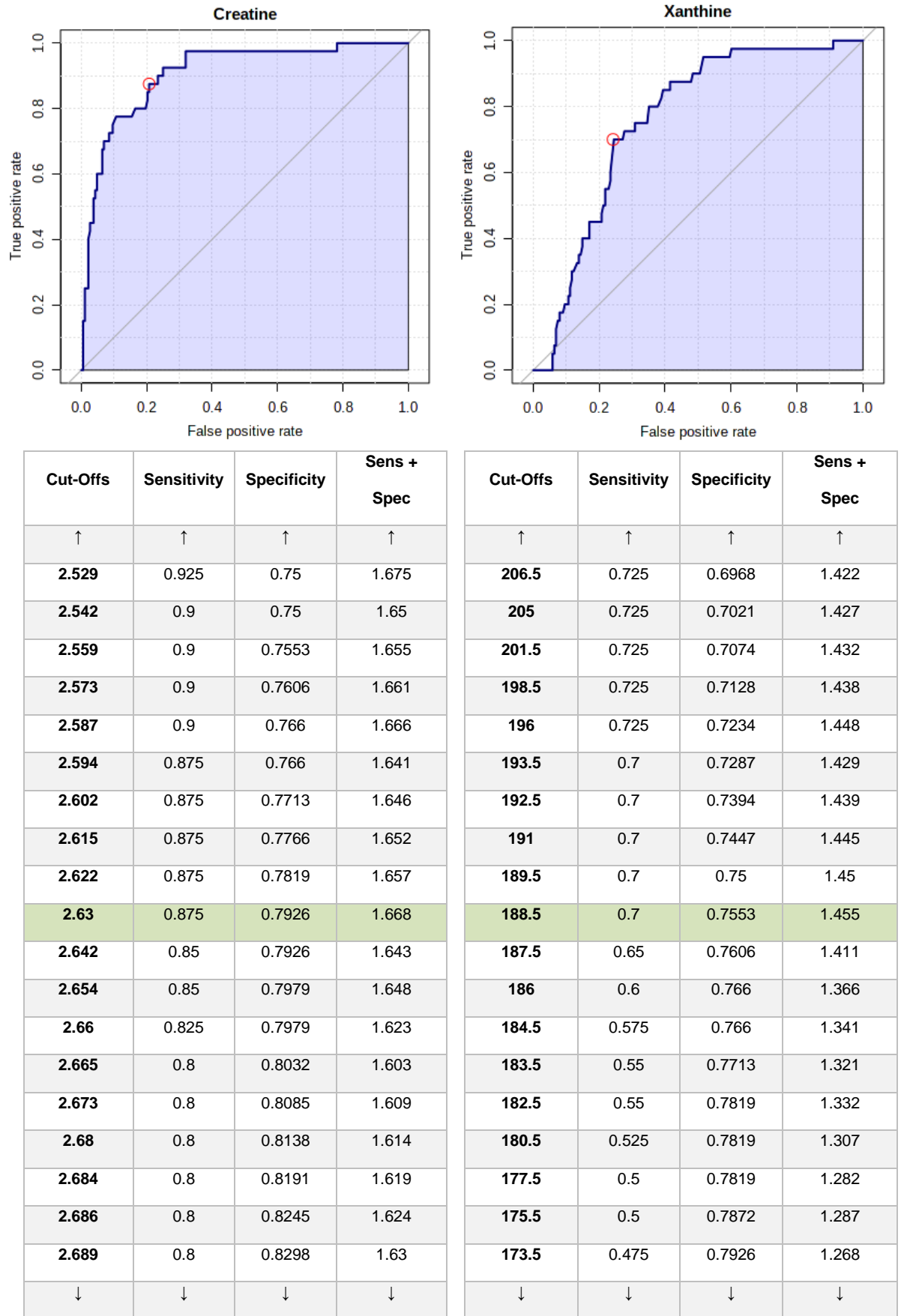


**Figure 3-36: ROC curve optimal cut-off determination:** Optimal cut-off points determined as “closest to top left” described by  $d = \sqrt{[1 - \text{Sensitivity}]^2 + (1 - \text{Specificity})^2}$ . Red circle indicates optimal cut-off point. Arrows indicate data direction towards infinity.



### 3.4.2 Application of a multi-biomarker model to true abundance levels of candidate biomarkers

The next step was to replicate the multi-biomarker model discussed previously with true abundance data. Unfortunately, this could only be replicated with two out of the seven candidate biomarkers so the goal here was to see if we see an increase in performance when using a multi-biomarker model with two of the seven candidate biomarkers compared to their individual performance, in with the findings of the previous analysis.

The multivariate ROC curve plot indicated a decrease in AUC from 0.903 to 0.897 when using two-variable models compared to the precited performance of using a one-variable model (**Figure 3-37 A, C**). The predictive accuracy however increased very slightly from 84% to 84.9% when using 2-variable models compared to just the one-variable models created (**Figure 3-37 B**). The average importance of the metabolites in the creation of the model indicates as expected, that Creatine contributes to the discriminatory ability significantly greater than Xanthine (**Figure 3-37 D**).

To test the predictive capability of the 2-variable model, average predicted class probabilities were then calculated for each leukaemic sample and control across the 100 performed Monte-Carlo cross-validations and plotted to generate a confusion matrix. Confusion matrices were created for the individual one-biomarker models for comparison. The data shows that out of the 188 leukaemic samples tested from the CNS Dx cohort, 160 were correctly classified into the leukaemic patient sample group and from the control CSF group consisting of 40 CSF samples, 35 were correctly identified as belonging to the control CSF group, ultimately giving us an

overall predicted accuracy of 88.5% In comparison, the individual biomarker models which yielded overall predicted accuracy of 83.3 (Creatine) and 63.6% (Xanthine) **(Figure 3-38)**.

Results from the permutation testing for the two-model biomarker model yielded a statistically significant p value of 0.011053 and an empirical p value of <0.001 suggesting robust modelling.

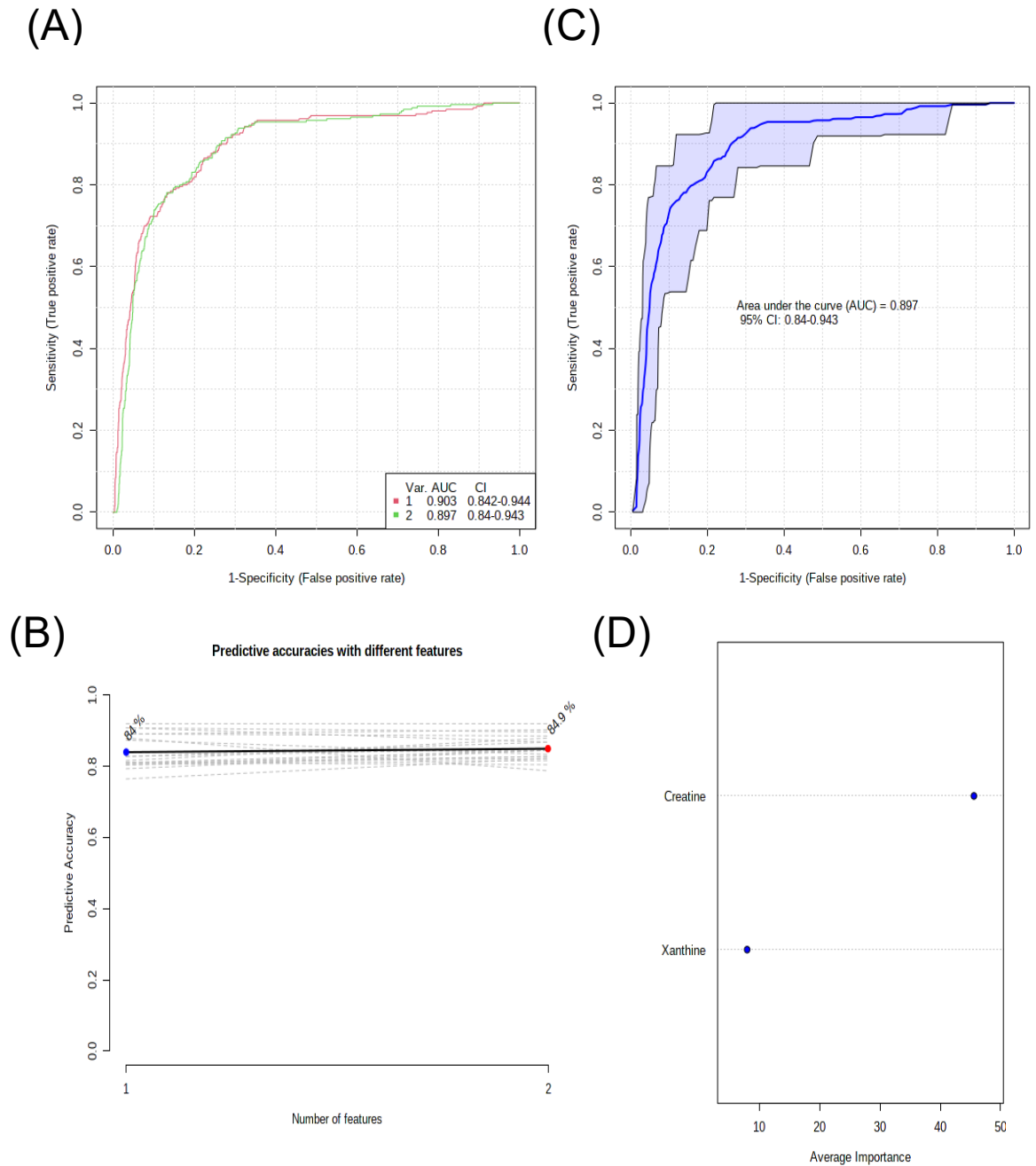
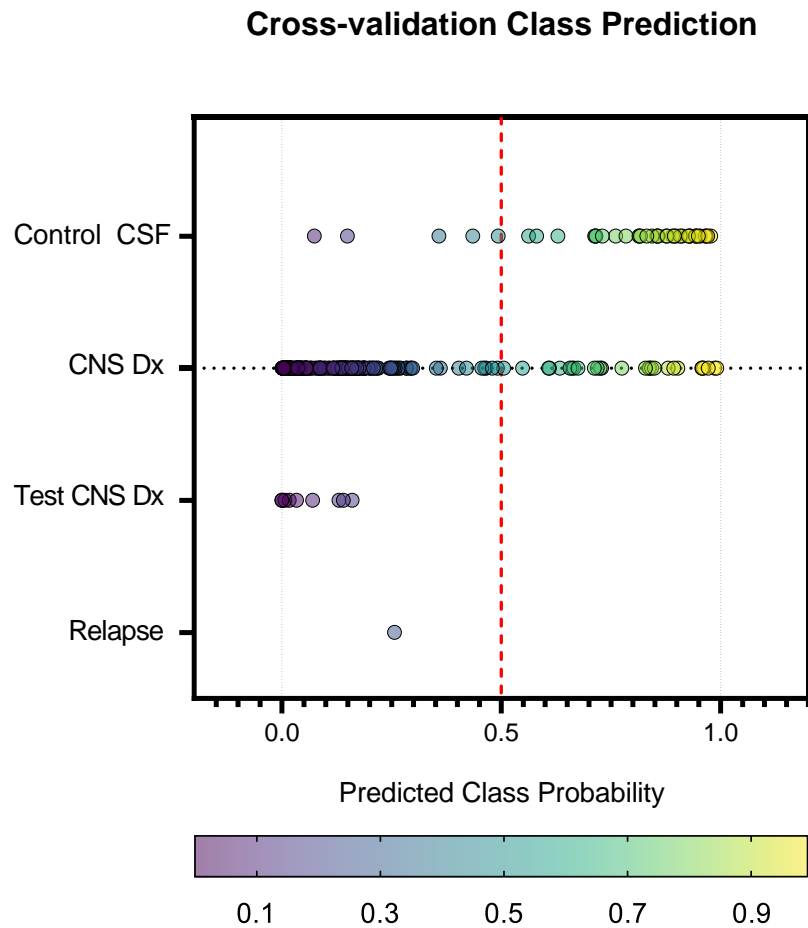


**Figure 3-37: Multivariate ROC analysis.** (A) Multivariate ROC curve with variable model averages plotted with associated AUC values and 95% confidence intervals; AUC = Area under the curve; CI = confidence intervals (B) Predictive accuracies of the best performing created models with different features. (C) Combined ROC plot of 2-variable model. (D) Candidate biomarker ranking as determined by average importance from the 100 cross-validations. ROC curves created on Metaboanalyst.



Confusion Matrix Summary (100 X Cross-Validations)			
Multi-biomarker model	Leukaemic CSF	Control CSF	Overall Predicted accuracy of 2-variable model
Control CSF	5	35	88.5%
CNS Dx	160	28	
Test – CNS Dx	9	0	100%
Test- Relapse	1	0	
Individual biomarker model: Creatine – Data not shown			
Control CSF	7	33	83.3%
CNS Dx	147	41	
Individual biomarker model: Xanthine – Data not shown			
Control CSF	11	29	63.6%
CNS Dx	116	72	

**Figure 3-38: Cross-validation Class Prediction confusion matrix.** This graph plots the average predicted class probabilities of each sample from 100 cross-validations. The classification boundary is set to 0.5 and sample probabilities range from 0-1. Probabilities < 0.5 will belong to the leukaemic CSF sample group and probabilities > 0.5 will belong to the Control CSF. Each sample is coloured by their probability score. Graph Created on GraphPad Prism v9.

This data generated from true abundance of the candidate biomarkers Creatine and Xanthine strongly supports the findings of the previous analysis by demonstrating that a multi-biomarker model performs better than an individual biomarker in correctly identifying leukaemic samples from control CSF samples. While it would have been ideal to have been able to measure true abundance of all seven candidate biomarkers, the data shown here follows the trends described previously.

### 3.5 Prognostic biomarkers

The final part of this study involved the testing of the candidate biomarkers for their prognostic capabilities as biomarkers capable of predicting CNS relapse. Several of the diagnostic samples from the patient cohort were chosen for this study as they were patients who went on to have either an isolated relapse in the CNS or a combined relapse in the CNS and bone marrow (henceforth referred to as CNS DxR samples). It was hypothesized that these patients may have distinct metabolomic phenotypes compared to patients who did not go on to relapse and that these could be identified using the biomarkers identified in this study.

The mean of the CNS Dx group was compared to the mean of the CNS DxR samples and upon first inspection only Phenylalanine, N4-acetylcytidine and Symmetric dimethylarginine appeared to have elevated means in the CNS DxR group compared to the CNS Dx group. The means were then tested for statistically significant differences and only Phenylalanine presented with a significant difference between the means with a p value  $<0.05$  (**Table 3-20, Figure 3-39**).

The CNS DxR did not have as many patient samples as the CNS Dx group, and most data points for Phenylalanine lie between two standard deviations of the mean of the CNS Dx group indicating that these patient samples may make up part of the true population rather than being elevated. However, the CNS DxR samples were matched with 2-5 CNS Dx controls for age, sex, CNS status, and risk. This significant difference seen between the groups for Phenylalanine potentially suggest that elevation of this candidate biomarker may indicate an increased risk of relapse in the CNS. It is unlikely however that it can act on its own as a prognostic biomarker,

but it may provide some clinical utility as part of a combined score using appropriate clinical and other CSF variables.

The other candidate biomarkers in this analysis did not seem to confer any prognostic utility.

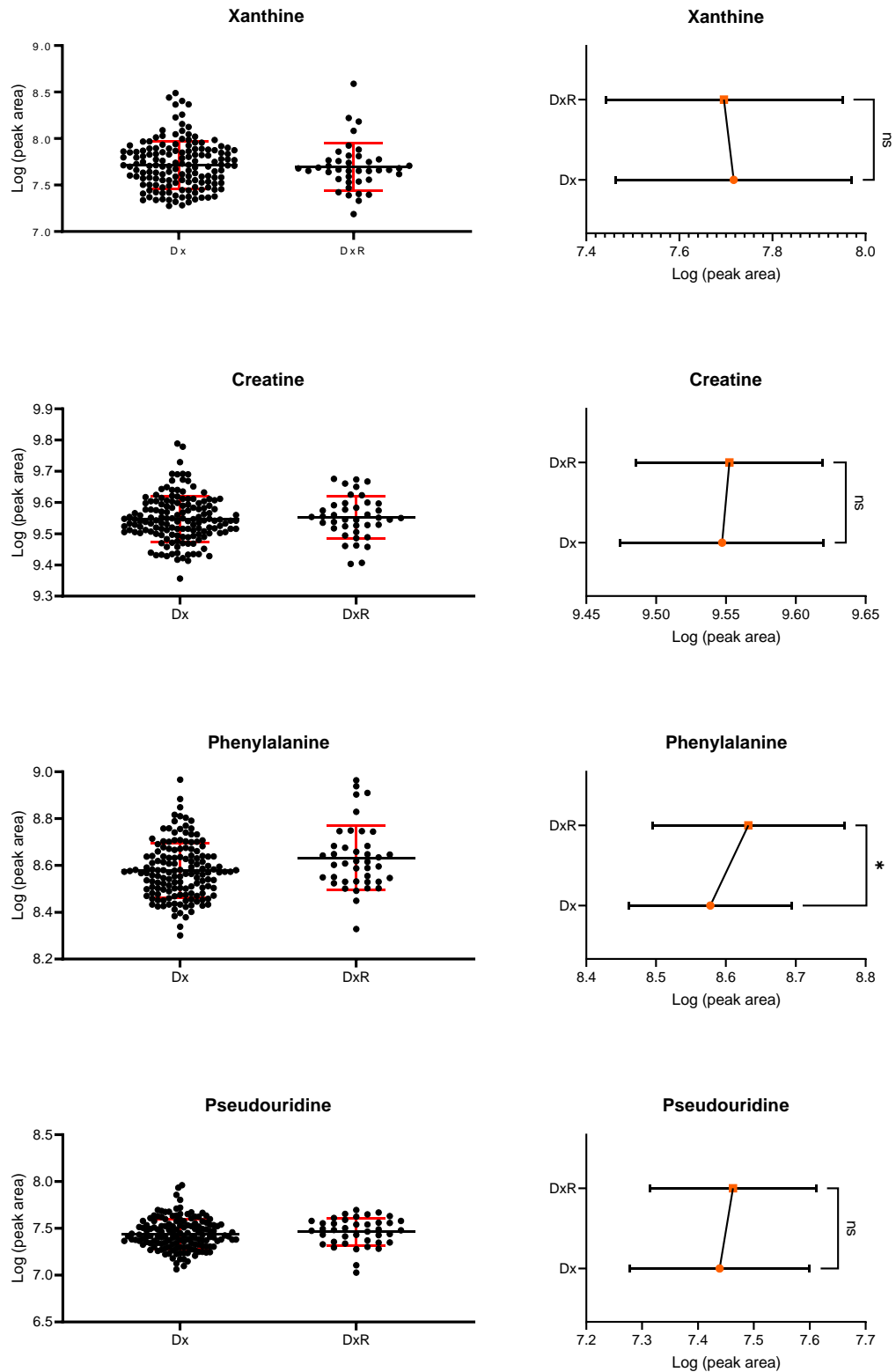


**Figure 3-39: Comparison between the means of CNS Dx vs CNS DxR patients.** Data was log transformed prior to statistical analysis. Two-tailed unpaired t-test;  $\alpha=0.05$ . Mean and Standard deviation shown on both plots. Scatter and line plots created on GraphPad Prism v9. CNS Dx (n=148) CNS DxR (n= 40).



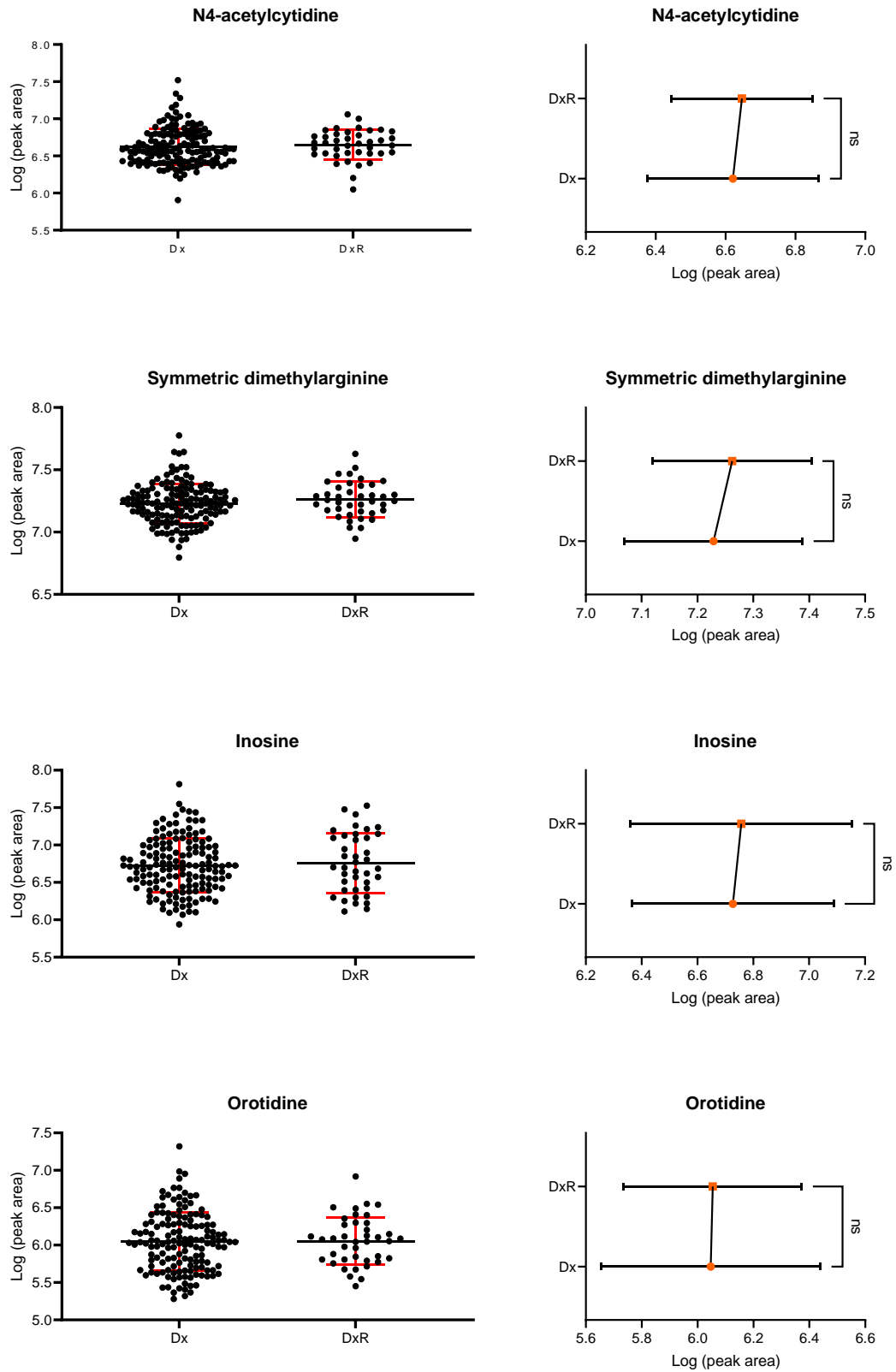


**Figure 3-40: Comparison between the means of CNS Dx vs CNS DxR patients.** Data was log transformed prior to statistical analysis. Two-tailed unpaired t-test;  $\alpha=0.05$ . Mean and Standard deviation shown on both plots. Scatter and line plots created on GraphPad Prism v9. CNS Dx (n=148) CNS DxR (n= 40)

Candidate biomarker	CNS Dx Mean	CNS DxR Mean	± SEM	95% confidence interval	R squared (eta squared)	P value
Xanthine	7.717	7.696	0.04524	-0.06835 to 0.1102	0.001146	0.644631
Creatine	9.547	9.552	0.01274	-0.03036 to 0.01992	0.0009021	0.682415
Phenylalanine	8.578	8.632	0.02159	-0.09697 to -0.01178	0.03298	0.012628
Pseudouridine	7.439	7.463	0.02828	-0.07969 to 0.03188	0.003828	0.398968
N4-acetylcytidine	6.621	6.647	0.04232	-0.1093 to 0.05767	0.001997	0.542553
Symmetric dimethylarginine	7.229	7.262	0.02778	-0.08800 to 0.02161	0.007618	0.233635
Inosine	6.727	6.757	0.06581	-0.1603 to 0.09932	0.001154	0.643489
Orotidine	6.047	6.054	0.06746	-0.1401 to 0.1260	5.851e-005	0.917026

**Table 3-20: Statistical analysis of the difference between candidate biomarker levels in the CNS Dx patient group against the Control CSF group.** Data was log transformed prior to statistical analysis. Two-tailed unpaired t-test;  $\alpha=0.05$ . Statistics performed on GraphPad Prism v9.

### 3.6 Summary and conclusions

The aim of this study was to extend the discovery pipeline for diagnostic biomarkers of CNS-ALL by identifying candidate biomarkers capable of measuring leukaemic burden within the CNS. This study first found two more metabolites to be added to the list of previously discovered metabolites which were taken forward for biomarker performance evaluation and validation experiments.

The eight candidate biomarkers were first analysed with a univariate approach in a small pilot study testing their behaviours in leukaemic patient samples against two types of CSF controls classed as either inflammatory or non-inflammatory. The majority of the biomarkers performed well, and the general behaviour of each candidate biomarker was concordant with the previous findings of the Halsey laboratory. Candidate biomarker levels were then tested (through the use of parametric univariate statistical tests and univariate ROC curve analysis) between the patient group and the combined control CSF groups to see if the findings held true, resulting in five of the eight candidate biomarkers showing discriminatory ability between the patient and control groups. Candidate biomarkers Phenylalanine, Pseudouridine and Orotidine, which did not show promise in this experiment were not excluded due to the low numbers of samples used and it was deemed that there was not enough evidence to dismiss any of the candidate biomarkers at this stage. Of note, Pseudouridine consistently performed the worst up to this point in the study.

Next, a multivariate approach was taken to test the discriminatory capability of the candidate biomarkers when combined as a panel of informative candidate biomarkers. The ultimate aim of creating a multivariate biomarker model is to develop a fixed algorithm combining the biomarker performance metrics of a panel

of candidate biomarkers into a single score which can be applied in a clinical setting to accurately predict the desired clinical outcome (positive or negative), in this case the presence of leukaemia in the CNS, through indirect measurement of biomarkers in the CSF. This analysis suggested that a six or seven candidate biomarker model was optimal for discriminating between the patient and control group. This analysis highlighted Pseudouridine as performing the worst, as expected, and concurred with the previous statistical analysis that Phenylalanine and Orotidine were trending towards redundant contributions to the model. Further manual model testing revealed that the exclusion of Pseudouridine and orotidine led to the highest discriminatory metrics between the patient and control group. The predicted class probabilities for this model demonstrated an overall predictive accuracy of 96.6% when classifying samples to their correct class (i.e., patient or control) with only one mis-classed control sample.

The creation of a biomarker model in this experiment is not without its limitations, sample size being the biggest to note however this small pilot study provided sufficient evidence to take the eight candidate biomarkers forward for secondary analysis with a larger and more comprehensive cohort of patient samples and for the re-implementation of this biomarker model for further performance evaluation in a large independent validation cohort.

The results of the secondary analysis of these candidate biomarkers demonstrated that with the exception of Pseudouridine, individually every marker held good-to-excellent ability to discriminate leukaemic CSF samples from control CSF samples. Pseudouridine was then excluded from further analysis because of its redundancy in discriminating between the patient and control group.

This cohort included a mixture of CNS1, CNS2 and CNS3 patients as classified by CSF cytology. These groups were searched for differences compared to the CSF control and every group behaved similarly to the CNS1 patient group with no discernible differences found. Only N4-acetylcytidine and Symmetric dimethylarginine showed elevated levels in the CNS3 patient group compared to the CNS1 patient group. The difference between the means of the CNS1 and CNS3 patient groups were statistically significant potentially suggesting a linear correlation with leukaemic burden in the CSF as classified by current CSF cytology, that is high leukaemic burden in CNS3 patients. However, the numbers of CNS1 patients heavily outweighed the CNS3 patients, thus further testing with higher numbers of CNS3 patients would be required to see if this trend holds true. CNS2 patients were not analysed statistically but were merely added for visualisation of the spread of the data for these patients as it is reported that CNS2 patients are often poorly diagnosed [30].

An important factor to note in the analysis of this study was the assumption that CNS1 patients are CNS-ALL positive as opposed to CNS-ALL negative, a more common approach in this field. CNS2 and CNS3 patients are classified as CNS-ALL positive as per CSF cytology due to the presence of blasts in the CSF and CNS1 as CNS-ALL negative due to the lack of blasts however, as discussed previously, there is strong evidence that leukaemia within the CNS is adherent to the walls of the leptomeninges and therefore may not be found freely floating in the CSF which possibly explains the lack of detectable blasts in CNS1 patients. The use of more sensitive methodologies for detection of CNS-ALL such as PCR or flow cytometry have been shown to increase the level of detectable leukaemia in CNS1 patients, corroborating this.

It could be argued that there should be a "dose-response" trend seen with the levels of these biomarkers to match current CSF cytology diagnoses and therefore CNS3 patients should potentially have the highest (or lowest) level of these biomarkers, followed by CNS2 patients and then CNS1 patients. However, as the soluble biomarkers being investigated in this study are secreted by leukaemic cells and are therefore an indirect form of measuring the presence of CNS-ALL, we cannot assume that there will be a clear CNS1 - CNS3 "dose-response" trend. Classification of CNS2 and CNS3 patients relies on the detection of free-floating cells which in the CSF show signs of cell-death. One could argue that these cells potentially under-express adhesion molecules and are therefore not as well suited to adapt to the leptomeningeal space and adhere to the walls of stroma as the evidence suggests. This would of course suggest that patients classified as CNS1 potentially over-express adhesion molecules resulting in fewer to undetectable levels of free-floating blasts. Future work in this regard would be interesting to test the expression of adhesion molecules of CNS1 vs CNS3 leukaemia to corroborate this hypothesis and potentially inform of fundamental CNS-ALL biology. However, it must be noted that high blast counts in the periphery and aggressive leukaemia's tend to be CNS3 patients thus suggesting that CNS3 patients most likely do have higher levels of leukaemic burden within the CNS. The rationale behind the approach of combining all CNS1, CNS2 and CNS3 patients together as one leukaemic patient group stems from the knowledge that these patients certainly have systemic leukaemia and most likely have CNS-leukaemia at diagnosis. There of course is also the chance that some patients simply do not have CNS-leukaemia at the time of diagnosis which cannot be ruled out.

An important limitation of this study is the lack of matched plasma samples for the patient CSF samples. Unfortunately, it was not possible to obtain matched plasma

samples for this study. It is possible that the levels of these metabolites reflect systemic levels found in the body instead of being CNS-leukaemia specific. This may explain why CNS1 CNS2 and CNS3 levels of all metabolites apart from N4-acetylcytidine and Symmetric dimethylarginine, stay relatively constant in comparison to each other. These two metabolites which show a "dose-response" trend with regards to leukaemic burden as classified by current CSF cytology, however, are more likely to be specific to the CNS and to the leukaemia. Considerations for future work should involve a study with matched CSF and plasma patient samples to confirm that these metabolites are differentially expressed in the CNS-compartment and are independent from systemic levels in the body. Animal models may also be a suitable alternative to perform this work to validate the behaviour of N4-acetylcytidine and Symmetric dimethylarginine.

The next step involved re-applying the multivariate biomarker modelling to this larger cohort of samples to see whether the model performed better or worse than the pilot study. The results from this analysis suggested that a seven-biomarker model performed best, encapsulating all the candidate biomarkers together to achieve the best discrimination with an overall predicted accuracy of 95.6%. This experiment was primarily run to validate the use of a multi-biomarker model for discriminating between the patient and control group and was subsequently tested on a small subset of different patient samples from the Halsey laboratory rather than the National Biobank and this model correctly classified all ten samples tested including one relapse sample taken from a CNS3 patient.

Finally, the true abundance of Creatine and Xanthine was calculated from a standard curve generated by pure external reference samples of each compound. This experiment was run to support the findings of this study and to begin the

process of validating these findings. Unfortunately, the true abundance of all candidate biomarkers could not be measured as they were not tested due to material and time limitations. Both Creatine and Xanthine however performed according to the previous analysis and when tested together as a multi-biomarker model, performed better in discriminating the patient group from the control group thus providing strong evidence of the use of a multi-biomarker model for the detection of CNS-ALL.

The candidate biomarkers were also tested for their prognostic capability by comparing samples from patients who did not go onto relapse with samples from patients who went onto relapse either in the CNS alone or in the CNS and bone marrow. Only Phenylalanine was found to have an elevated mean in the patients who went onto relapse potentially suggesting that higher levels of this biomarker could predict relapse, but this would have to be investigated further with a larger number of patient samples who went onto relapse as well as serial-samples from various time-points around the time and after relapses for tracking. This would involve several regular lumbar punctures which would need to be performed routinely to be able to quantify the level of a prognostic biomarker with the aim of predicting relapse. Currently this type of serial sampling has begun through the Altogether CSF-Flow study which provides an opportunity to analyse leftover CSF from these lumbar punctures for the presence of soluble biomarkers such as Phenylalanine in this setting [106].

The strengths of this study lie in the use of patient samples originating from two separate biobanks, one a local biobank in Glasgow and the other a national biobank. The majority of the biomarkers performed concordantly between the two datasets as well as with the previous analysis conducted in the Halsey Laboratory. Creatine,



Xanthine, N4-acetylcytidine, Symmetric dimethylarginine and Inosine in particular were concordant in all datasets. Phenylalanine, and Orotidine were proved to have strong discriminatory ability in the second experiment and contributions to the multivariate biomarker model's discriminatory ability. The use of adult CSF from patients who were cleared of any malignancy but underwent lumbar puncture for a range of either inflammatory or non-inflammatory conditions, was both a strength and a weakness of this study. The strength lies in that the wide range of CSF phenotypes included in this control capture the CSF phenotype of non-leukaemic children. The trends seen in this study mimicked the trends seen in the previous analysis by the Halsey lab thus giving us confidence that our statistically significant findings between the means of the leukaemic patient samples and the control CSF used in this study are comparable. The weakness lies in that the control CSF samples used in this study were obtained from adults and thus age-dependent metabolic phenotypes must be investigated alongside the phenotypes of the various conditions associated with the adult CSF samples. Of course, to truly measure the effect of this panel of candidate biomarkers, CSF samples from healthy volunteers matched for age and sex would be needed which may perhaps be an impossibility.

An important finding that must be addressed is the unavoidable phenomenon of drug-related metabolism. One possible explanation of the differences observed in between the leukaemic patient samples, and the control CSF samples in some of the metabolites tested may be due to the medication that the children were on at the time of diagnosis, specifically allopurinol a purine analogue which is metabolised by enzymes involved with purine and pyrimidine synthesis. Patients are known to be given allopurinol around the time of diagnosis. The effects of allopurinol metabolism can see seen in **Figure 3-41**.

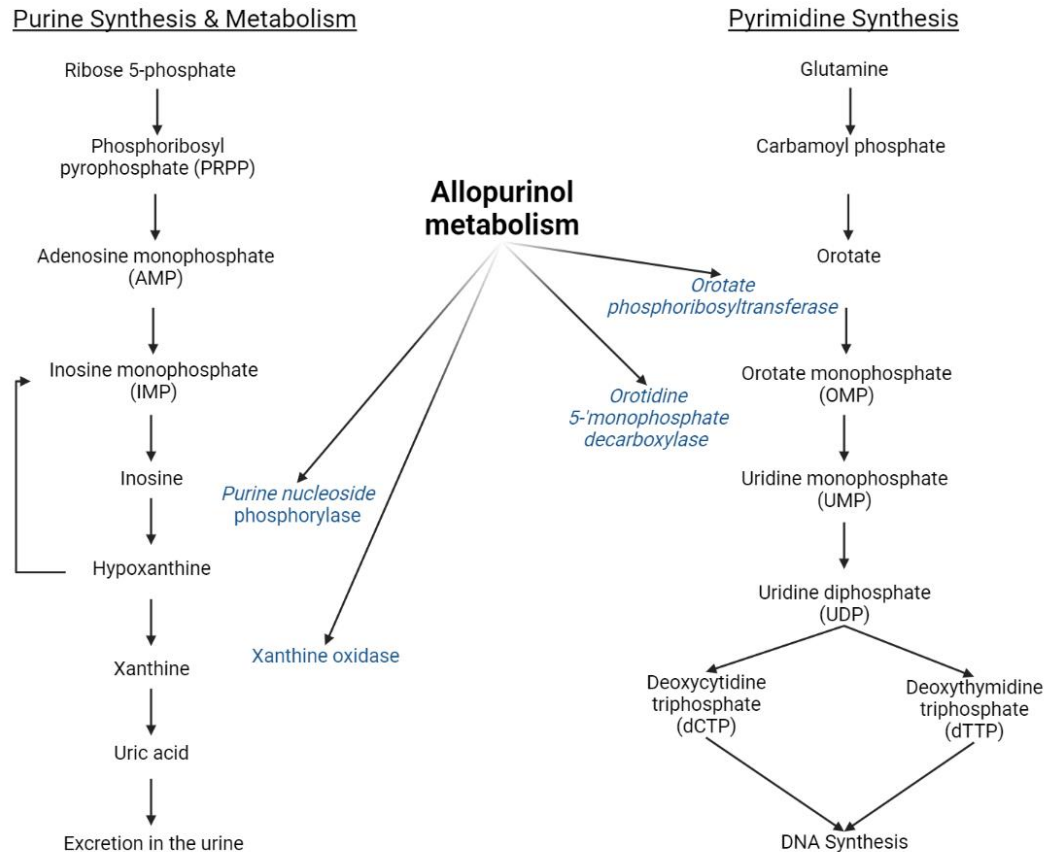


**Figure 3-41: Allopurinol metabolism.** Figure adapted from:

<https://www.ebmconsult.com/articles/allopurinol-febuxostat-zyloprim-uric-acid-gout-mechanism>

Allopurinol is known to inhibit enzymes such as Xanthine oxidase and other enzymes involved in DNA synthesis. This is a potential confounder for the results seen in metabolites Xanthine, Inosine, Orotidine and potentially Pseudouridine and calls into question whether these biomarkers are biologically plausible. Future work can potentially begin to address these questions through the use of *in vitro* studies investigating the consumption and secretion of these metabolites at various time-points in a CNS-like environment by using LC-MS or *in vivo* follow up studies using carefully constructed mouse-models.

Whether or not the other metabolites which are not potentially influenced by allopurinol or other medications (Creatine, N4-acetylcytidine, Symmetric Dimethylarginine, and phenylalanine) are biologically plausible remains to be investigated and validated. However, the data in this study suggests that even biomarker models with fewer numbers of biomarkers from this panel perform extremely well in discriminating between leukaemic CSF and control CSF.

This study has extended the metabolic biomarker discovery phase in this field and future directions should first and foremost involve investigating the metabolic pathways associated with these candidate biomarkers to shed light on the metabolic processes occurring within the CNS. Next, repeating these experiments independently on a larger scale with more sensitive technologies and age-appropriate CSF controls for validation will reveal the clinical utility of these candidate biomarkers as biomarkers for CNS-ALL.

Although there are some promising leads in this study, as demonstrated above, metabolomics is an extremely sensitive platform and can be very sensitive to individual patient differences and external factors potentially unrelated to CNS leukaemia. Therefore, this study progressed onto the discovery of candidate biomarkers which are more directly secreted by leukaemic cells in the form of soluble protein/cytokine molecules and cell-free DNA.

# **Chapter 4: Discovery of soluble biomarkers of Central-Nervous System Acute lymphoblastic leukaemia**

## **4 Introduction and aims**

Discovery of novel sensitive and specific soluble biomarkers with a method that is independent from the number of “free-floating” blasts in the CSF is essential to be able to detect, quantify and track levels of leukaemia in the CNS. A potential biomarker class in the CSF are secreted proteins, chemokines, and cytokines which can be detected using techniques such as immunoassays or ELISAs. Immunoassays are considered a gold standard for the detection and quantification of protein biomarkers and generally have higher sensitivity and specificity compared to conventional alternative methods. They are generally cost-effective, and the workflows are fast and simple to use. Luminex technology allows for the multiplexing of several analytes simultaneously and is thus an ideal technology for testing several potential biomarkers in the biomarker discovery phase, especially if sample volume is a limiting factor.

Luminex technology uses fluorescent beads which are assigned specific fluorophores capable of being detected and discerned from each other. These beads are then coated with capture antibodies specific to the target analyte. After incubation with the target sample, the beads are washed and then incubated with biotinylated detection antibodies and streptavidin-phycoerythrin (PE). The Luminex analyser subsequently excites the beads using a laser to detect the fluorophore and assigned analyte while another laser will determine the quantity of the PE signal which is proportional to the quantity of the analyte bound to the bead.

This part of the study used diagnostic CNS1 patient CSF samples from the Halsey laboratory biobank with matched control CSF taken a year into treatment as well as diagnostic CNS1, CNS2 or CNS3 from a national childhood leukaemia biobank. CSF from patients who were admitted to hospital for suspected non-inflammatory and inflammatory neurological conditions and had a lumbar puncture taken which returned a normal CSF profile, were also used as a control group.

Targets were chosen based on a literature search (Chapter 1.7.2.2) to attempt to discover new soluble biomarkers. In this study, the following analytes were tested CCL21, CXCL10, IL-2R $\alpha$ , Osteopontin, Thymidine Kinase-1 (TK-1), MMP-9, L-Selectin, VEGF-A, VEGF-C and CD27. The goal of this chapter was to test a variety of soluble protein analytes to discover potential diagnostic and prognostic biomarkers for CNS-ALL through the following aims:

- 1) To test a panel of analytes using diagnostic CNS1 samples and matched “late” control samples (take around one year into treatment) to identify potential diagnostic or prognostic biomarkers of interest – primary analysis
- 2) To test promising analytes with a cohort composed of non-inflammatory and inflammatory control CSF against patient samples currently classified by CSF cytology as CNS1, CNS2 or CNS3 – secondary analysis.
- 3) To analyse data from promising analytes as a combined group of patient diagnostic CSF samples (irrespective of their current classification of CNS1-3) against non-inflammatory and inflammatory control CSF to further assess biomarker performance – secondary analysis.

- 4) To test a select number of diagnostic patient CSF samples from patients who went onto relapse in the CNS against patients who did not relapse to elucidate whether the promising analytes have any prognostic biomarker utility – secondary analysis.

## 4.1 Primary analysis of potential soluble biomarker candidates

To test the chosen set of candidate analytes, an initial multiplex Luminex assay using 50  $\mu$ L of CSF was run using a small cohort of matched patient samples consisting of diagnostic CNS1 patients with matched “late” control samples taken around a year into treatment where leukaemic burden in the CNS would be expected to be low to non-existent due to the high intensity treatment given in that period (**Table 4-1**). The diagnostic patient samples were all taken from around 2010-2013 and have been stored at -80 °C until use with no freeze/thaw cycles. These samples were first thawed on ice, spun at 16,000  $\times$  g for 4 minutes at 4 °C and then diluted 1:2 with Calibrator Diluent RD6-52. Standards were prepared according to the manufacturer’s guide and the plate was run on a Bio-Plex 100 multiplex plate reader (Bio-rad).

This experiment detected 5 / 10 analytes tested (Osteopontin, CD27, L-selectin, VEGF-C & CXCL10) with values for both the diagnostic (dx) and late samples (**Table 4-2, Figure 4-1**). The remaining analytes (CCL21, IL-2R $\alpha$ , TK1, VEGF-A and MMP9) were below the range of the assay. Interestingly, CCL21 which was detected in previous experiments in the laboratory, was not detected in this experiment. Results from this experiment show low levels of CXCL10, VEGF-C and CD27 in the CSF of the patient sample cohort.

Osteopontin and L-selectin showed higher levels compared to the other analytes. Analysis of the differences between the patient sample groups (Dx vs late control) indicate very little change in the levels of CXCL10, VEGF-C, Osteopontin and

Patient ID	Immunophenotype	CNS Classification	Age at Dx (years)	Years Between Dx and Late Samples
P1	BCP-ALL	CNS1	1	1.05
P2	BCP-ALL	CNS1	7	1.10
P3	BCP-ALL	CNS1	5	1.22
P4	BCP-ALL	CNS1	3	1.04
P5	BCP-ALL	CNS1	2	0.94
P6	BCP-ALL	CNS1	2	0.96
P7	BCP-ALL	CNS1	2	0.99
P8	BCP-ALL	CNS1	1	0.96
P9	BCP-ALL	CNS1	4	0.75
P10	BCP-ALL	CNS1	15	1.12
P11	BCP-ALL	CNS1	6	0.99
P12	BCP-ALL	CNS1	4	1.19
P13	BCP-ALL	CNS1	4	0.92
P14	BCP-ALL	CNS1	2	0.94

**Table 4-1: Diagnostic patient sample information.** BCP-ALL = B-cell precursor ALL diagnosis.

L-selectin and statistical analysis showed no significant difference between these groups.

Levels of CD27 in the diagnostic patient sample group (368.6 pg/mL) were elevated compared to the matched late sample group (199.1 pg/mL) and statistical analysis indicated a significant difference between the two groups ( $p = 0.018$ ) (**Figure 4-1**).

To determine the diagnostic utility of CD27 to discriminate between the diagnostic CSF sample and the matched late sample (representing CSF with no blast presence), a receiver operator curve (ROC) analysis was run.



Analyte	Dx Av. (pg/mL)	SD	SEM	CV	CTL Av. (pg/mL)	SD	SEM	CV	P Value
<b>OPN</b>	111380.3	71160	17790	64%	81122.9	54074	13518	67%	0.112986
<b>CD27</b>	368.6	275	76	64%	199.1	124	35	53%	0.017599
<b>L-SLT</b>	5383.4	3590	960	64%	4000.9	3186	851	70%	0.177252
<b>VEGF-C</b>	444.1	93	23	21%	435.6	88	22	20%	0.511967
<b>CXCL10</b>	14.6	13	3.4	85%	18.5	24	6.1	122%	0.772527
<b>CCL21</b>	<OOR	-	-	-	<OOR	-	-	-	
<b>IL-2R<math>\alpha</math></b>	<OOR	-	-	-	<OOR	-	-	-	
<b>TK1</b>	<OOR	-	-	-	<OOR	-	-	-	
<b>VEGF-A</b>	<OOR	-	-	-	<OOR	-	-	-	
<b>MMP9</b>	<OOR	-	-	-	<OOR	-	-	-	

**Table 4-2: Analyte concentrations in range of standard curve and descriptive statistics calculated on GraphPad Prism v9.** <OOR = Out Of Range: below range of assay. SEM = Standard Error of the Mean. CV = coefficient of variation. Two-tailed paired t-test, statistical significance: \* =  $p < 0.05$ ; Statistics were calculated on GraphPad Prism v9.

ROC curve analysis plots the true positive rate (Sensitivity) against the False Positive rate (Specificity) at several different classification thresholds resulting in an area under the ROC curve (AUC) metric which measures the ability of the analyte to discriminate between individuals with disease (Dx sample) and those without the disease (late control sample).

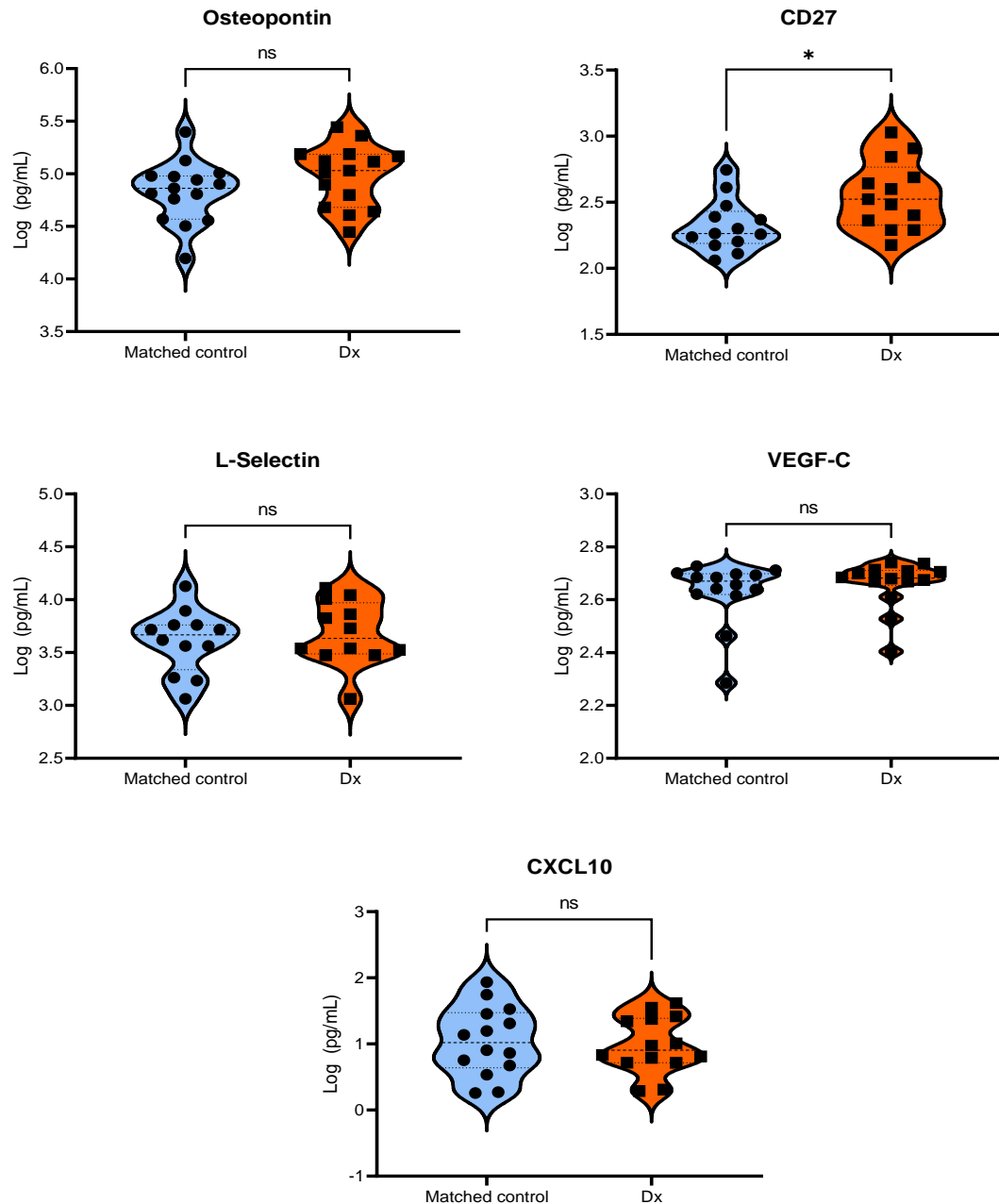
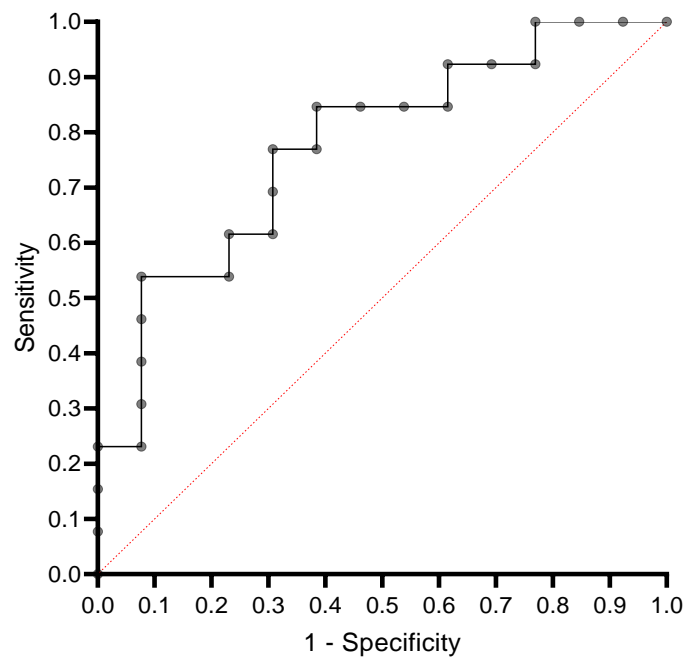


**Figure 4-1: Violin plots of several log<sub>10</sub> transformed analyte concentrations from dx vs matched late control sample data.** Dx samples n=14; matched late samples n=14. Two-tailed paired t-test, statistical significance: \* = p < 0.05; ns = not significant. Prior to statistical analysis, the data was log<sub>10</sub> transformed. Statistics were calculated on GraphPad Prism v9.

ROC curve: CD27 Dx vs Late



<b>Area under the ROC curve</b>	0.775
<b>Std. Error</b>	0.092
<b>95% confidence interval</b>	0.594 to 0.956
<b>p value</b>	0.017

**Figure 4-2: Receiver Operator Curve (ROC) analysis of diagnostic sample (Dx) vs matched late control sample (Late).** Alpha set at 0.05. Statistics were calculated on GraphPad Prism v9.

The result of the ROC analysis (AUC: 0.78, 95% CI: 0.6-0.96, p value= 0.017) demonstrate that initially CD27 has a moderate-high chance of 78% of discriminating between our CNS-ALL positive samples (diagnostic CSF samples) and CNS-ALL negative sample groups (matched late control CSF samples).

CD27 was thus chosen to take forward for further testing with a second cohort of patient and control samples as a potential biomarker for CNS-ALL. The average means of L-selectin and Osteopontin were higher in the Dx group (5383.4 & 111380.3 pg/mL) than in the late control group (4000.9 & 81122.9 pg/mL)

(**Table 4-2**). Even though statistical analysis did not report a significant difference between the means of the two groups, these two analytes were also investigated further in the secondary analysis.

## **4.2 Secondary analysis of soluble biomarker candidates**

### **4.2.1 CD27**

The next step was to measure levels of CD27 in CNS-ALL patients classified as CNS1, CNS2 or CNS3 against two groups of independent CSF controls made up of non-inflammatory CSF and inflammatory CSF with the aim of investigating the specificity of the analyte for ALL against a spectrum of control “normal” CSF (**Table 4-3**). The CSF controls available originate from adults ranging from 18-77 years of age who were admitted into hospital for a range of inflammatory or non-inflammatory neurological conditions but were cleared of any cancer.

For this experiment, it was chosen to compare the patient groups to the non-inflammatory control CSF to determine the capability of the analyte to discriminate between disease state and non-disease state. The CNS is considered to be an inflammatory leukaemic sanctuary at the time of diagnosis and relapse.

Results from this experiment indicate that CD27 levels in CNS2 and CNS3 patients were elevated compared to the non-inflammatory control CSF and statistical analysis indicated a significant difference between the compared groups ( $p = 0.002537$ ;  $p = 0.046783$  respectively) (**Figure 4-3A**).

Patient CSF sample types				
CNS1	CNS2	CNS3	CNS Dx	CNS DxR
n=10	n=10	n=10	n=22	n=8
Age at Dx ranges				Site of future relapse
1, 2, 6	1, 3, 4, 5, 8, 14	1, 2, 3, 4, 5, 7, 13, 15		relapse
Sex				CNS isolated: n=5
0F : 10M	4F : 6M	4F : 6M		CNS + BM: n=3
CSF control demographic				
Control type		Age	Sex	Diagnosis
NI control n=4		26	F	Migraine
		34	F	Headache
		37	M	Functional*
		57	M	Motor neuropathy
I control n=4		18	F	Post-infectious movement disorder
		27	M	Neurosarcoidosis
		30	F	GAD encephalitis**
		42	M	RRMS***

**Table 4-3: CSF sample types for secondary analysis of candidate biomarkers.** NI = non-inflammatory control CSF; I= inflammatory control CSF. Age at Dx = Age at diagnosis. All samples belonging to ALL groups CNS1-3 were diagnosed as B-cell ALL patients. CNS Dx = accumulated CNS1-3 patient samples; CNS DxR = Diagnostic patient samples of patients who went onto relapse in the future, CNS = central nervous system, BM = bone marrow. F= Female; M = Male. \* Functional = Body symptoms which appear to be caused by the CNS, but are not, medically unexplained. \*\* GAD encephalitis = Anti-glutamic acid decarboxylase encephalitis.\*\*\* RRMS = Relapsing-Remitting Multiple Sclerosis.

Levels of CD27 in the control and CNS1 patient group however had similar averages, and no statistically significant difference between the means ( $p = 0.736403$ ). This result shows a “dose-response” trend in line with CSF cytology potentially suggesting that CD27 is measuring increasing levels of leukaemia in the CNS

Interestingly, the inflammatory CSF control group had higher levels of CD27 than the non-inflammatory control CSF with a statistically significant difference between the means ( $p = 0.041082$ ), suggesting that inflammation within the CNS can also result in elevated levels of CD27 (**Table 4-3**) (**Figure 4-3C**).

When comparing CD27 levels in CNS1-3 patient groups against the inflammatory CSF controls, all patient groups had lower levels of CD27, and statistical analysis indicated significant differences between the means of the inflammatory control CSF and the CNS1 and CNS3 groups ( $p = 0.001576$ ;  $p = 0.044464$ , respectively). The level of CD27 in the CNS2 patient group showed similar levels to the inflammatory control CSF and no significant difference was found with statistical analysis between the groups (**Figure 4-3B**). This further supports the suggestion that inflammation within the CNS may be the cause of elevated CD27 in the CSF of leukaemic patients.

The next step was to re-analyse the CNS1, CNS2 and CNS3 CD27 data together as a cumulation of patients with CNS-ALL against the control CSF. The data shows, as expected, elevated CD27 levels in the CNS Dx group compared to the non-inflammatory control CSF and statistical analysis indicated a significant difference between the means of the two groups (**Figure 4-4**).

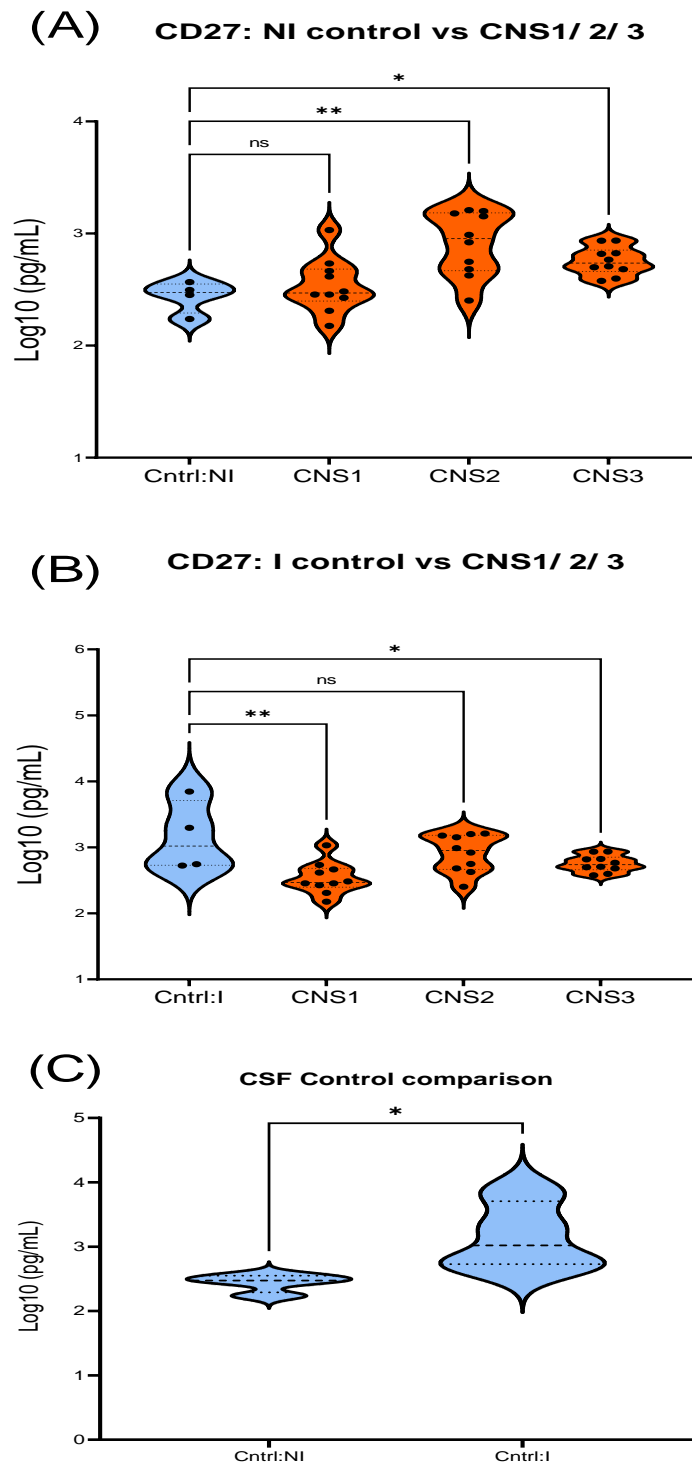


**Figure 4-3: CD27 - Violin plots of CD27 levels in control CSF vs CNS1, CNS2 & CNS3 patient sample groups. (A) Non-inflammatory control CSF vs patient samples (B) Inflammatory control CSF (I) vs patient samples. (C) Non-inflammatory control CSF (NI) vs inflammatory control CSF (I).** Statistics: (A-B) Unpaired Ordinary one-way ANOVA, multiple comparisons corrected using Dunnett's multiple comparison test, alpha threshold=0.05 and confidence level 95% confidence interval; ns = not significant; \* =  $p < 0.05$ ; \*\* =  $p < 0.01$ . (C) Two-tailed unpaired t-test, \* =  $p < 0.05$ . Statistics were calculated on GraphPad Prism v9.

The level of CD27 of the CNS Dx group was less than the level of the inflammatory control CSF but sat between the two control groups. Leukaemic cells are by nature inflammatory cells, so these results potentially suggest that elevated CD27 levels could potentially a phenotype of inflammatory CSF environment caused by the presence of CNS-ALL.

ROC curve analysis which was then performed on CNS Dx group against the non-inflammatory control CSF (**Figure 4-5**). The AUC for the NI vs CNS Dx (AUC: 0.842, 95% CI: 0.70-0.98,  $p = 0.028$ ) comparison suggest that CD27 shows excellent diagnostic capability, an 84% chance of discriminating between the non-inflammatory control CSF and the CNS Dx group. ROC curve analysis between the inflammatory control CSF and the CNS Dx group suggested that CD27 has no discriminatory utility between the two groups with a  $p$  value  $>0.05$  and had very wide 95% confidence intervals (AUC 0.775; 95% CI = 0.533 to 1.00) (**Figure 4-5**).

However, given the phenotype of elevated CD27 in the inflammatory control CSF and the similarity in elevated levels of CD27 in the leukaemic patient sample groups, these results cast doubt on the clinical utility of CD27 as a diagnostic biomarker for the presence of CNS-ALL. It's use alongside other tests that confirm the presence of CNS-leukaemia e.g., flow cytometry, may have some clinical utility however as elevated levels do correlate with our current classification of CNS leukaemia and its use in a panel of biomarkers similar to the panel mentioned in Chapter 1, may improve sensitivity and specificity within this biomarker class.



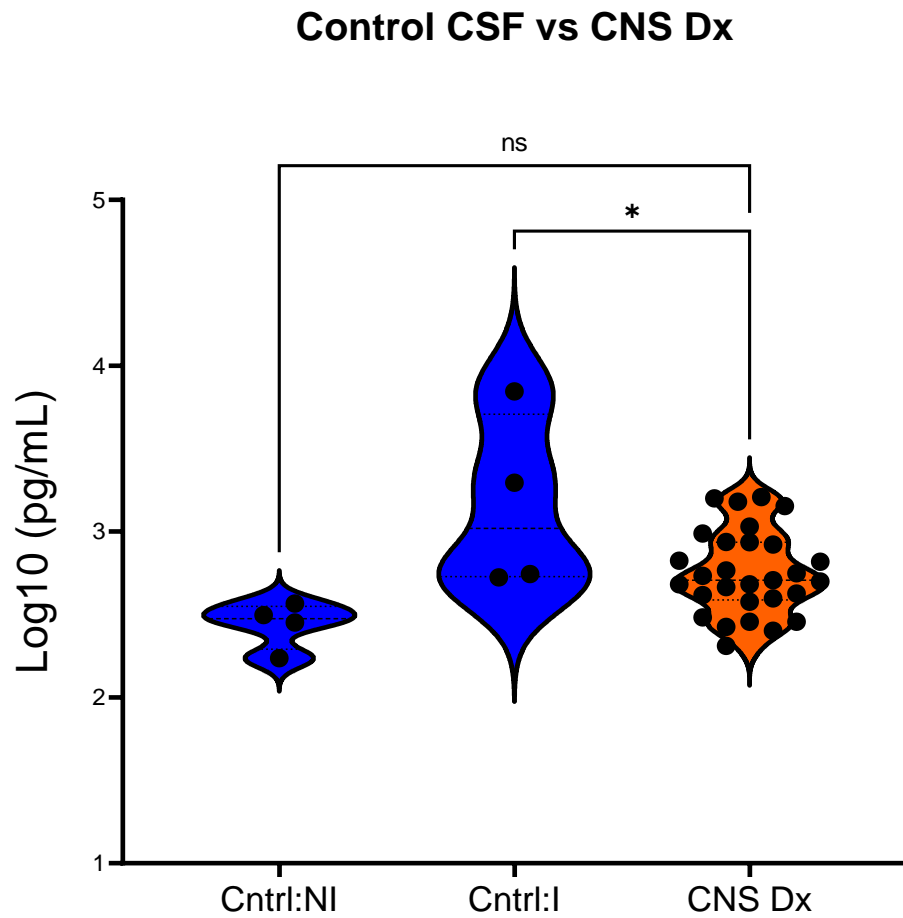
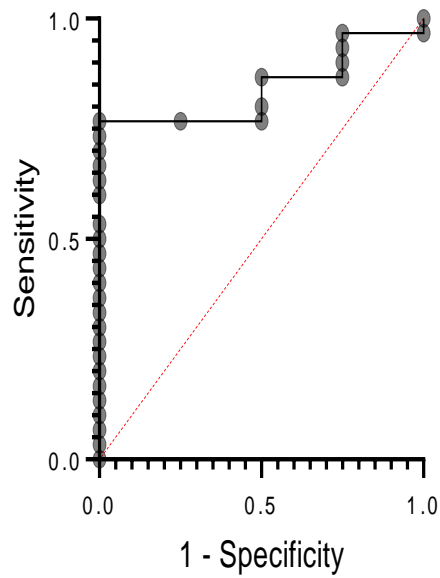


**Figure 4-4: CD27 – Violin plot of log10 transformed CD27 levels in control CSF vs CNS Dx patient sample group.** Non-inflammatory control CSF (NI) & inflammatory control CSF (I) vs CNS Dx combined patient samples. Statistics: Unpaired ordinary one-way ANOVA, multiple comparisons tested using Dunnett's multiple comparison test, alpha threshold=0.05 and confidence level 95% confidence interval; ns = not significant; \* =  $p < 0.05$ ; \*\* =  $p < 0.01$ . (Alpha set at 0.05. Statistics were calculated on GraphPad Prism v9.

ROC curve: NI Control CSF vs CNS Dx



ROC curve: I control CSF vs CNS Dx

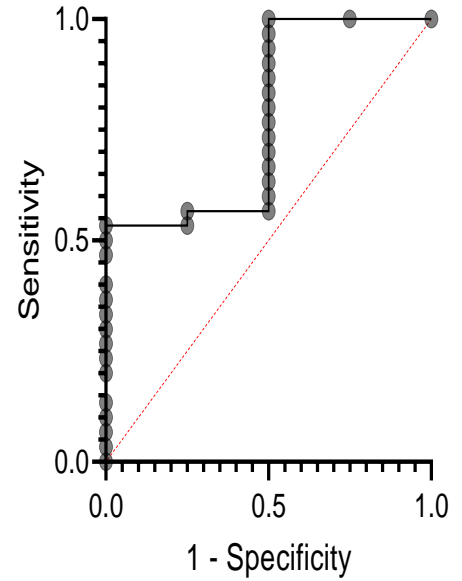


Figure 4B	NI vs CNS Dx	I vs CNS Dx
Area under the ROC curve	0.842	0.775
Std. Error	0.0708	0.123
95% confidence interval	0.703 to 0.980	0.533 to 1.000
p value – alpha <0.05	0.028	0.078

**Figure 4-5: ROC analysis CSF vs CNS Dx.** Receiver Operator Curve (ROC) analysis of non-inflammatory control CSF & inflammatory control CSF vs CNS1, CNS2 & CNS3 patient samples

Next, CD27 was tested for its ability as a prognostic biomarker for CNS-ALL. Within this cohort of patient samples, eight patients from all three CNS groups (1-3), were diagnostic samples from children who eventually had either an isolated relapse in the CNS or a relapse in both the CNS and the bone marrow. These samples are referred to as CNS DxR patient samples and were included for testing to see if there would be any difference in the levels of any promising analytes between the CNS Dx group and the CNS DxR group (**Table 4-3**).

Leukaemia's in children who went onto relapse tend to be more aggressive from diagnosis and it was hypothesized that with the right biomarker, these children would present with differing levels compared to diagnostic CSF, to predict CNS-relapse. The results show that CD27 cannot identify any difference between the levels of these diagnostic samples and statistical analysis indicates no significant difference between the means of these two groups of samples ( $p = 0.932592$ ) (**Figure 4-6**). Of note, sample numbers for these experiments are low and therefore may be too underpowered to see a difference between the CNS Dx and the CNS DxR groups.

## CNS Dx vs CNS DxR

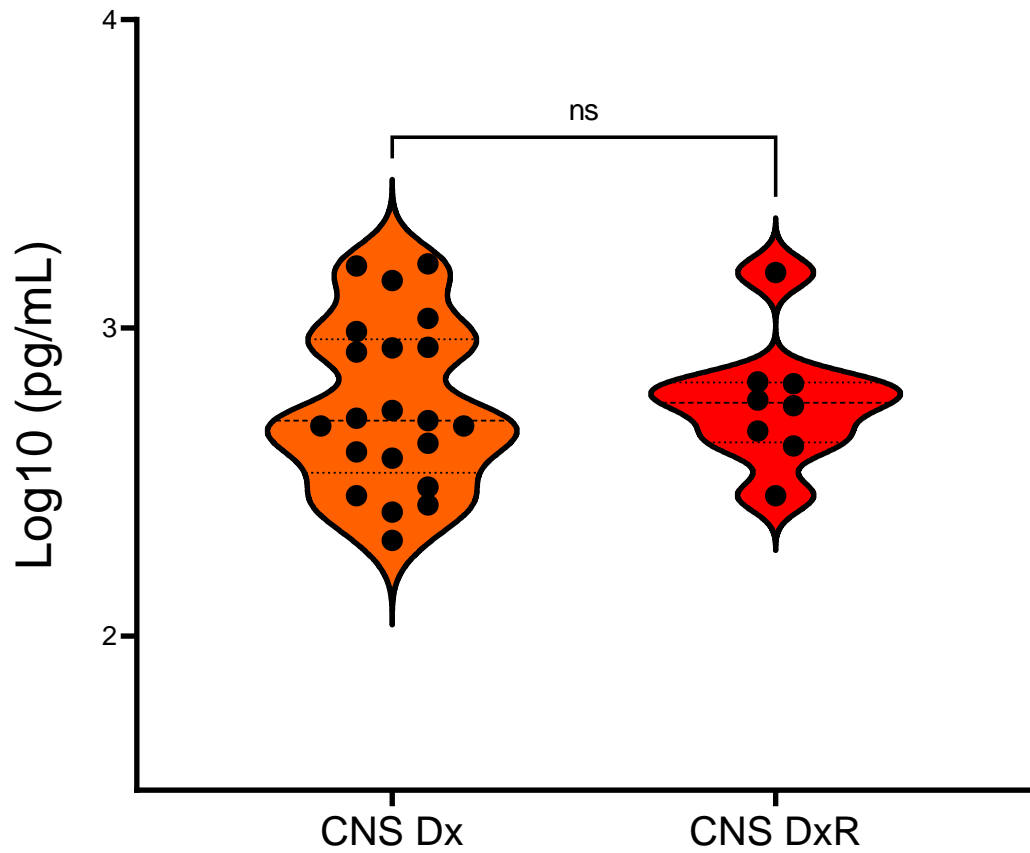


**Figure 4-6: Violin plot of log<sub>10</sub> transformed CD27 levels in CNS DX samples vs CNS DxR samples.** CNS DxR = Diagnostic patient samples of children who relapsed in the CNS in the future. Statistics: Two-tailed unpaired t-test, confidence level 95% statistical significance: \* =  $p < 0.05$ ; ns = not significant. Statistics were calculated on GraphPad Prism v9.

### 4.2.2 L-selectin & Osteopontin

L-selectin and Osteopontin were also examined further due to the high levels which were detected in (**Figure 4-2**) to investigate whether analysis with more patient sample groups could identify any role as diagnostic or prognostic biomarkers for CNS-ALL. As with CD27, various analyses were performed: First, the levels of both analytes were compared to both the non-inflammatory and inflammatory CSF controls, Then the samples were combined to test the CNS Dx group as a whole against the control CSF and finally the CNS Dx group were tested against a select number of diagnostic patient samples of which the patients went onto relapse in the future in the CNS and/or bone marrow (**Table 4-3**).

Initial results from the secondary analysis of L-selectin did appear to show an increasing trend in levels of the analyte with the intensifying CNS classifications CNS1-3, however statistical analysis did not report a significance different between the means of any of the CNS-ALL patient groups and both the non-inflammatory and inflammatory control CSF samples (NI CTL vs CNS Dx:  $p = 0.755930$ ;  $p = 0.0998161$ ;  $p = 0.099934$ , respectively) (I CTL vs CNS Dx:  $pp = 0.571275$ ;  $p = 0.993462$ ;  $p = 0.228448$ , respectively) (**Figure 4-7 A, B**).

Levels of L-selectin in both the non-inflammatory and inflammatory control CSF were very similar and when compared against the combined CNS Dx patient group and the data shows similar levels of L-selectin between all groups suggesting that this analyte is detectable in CSF irrespective of disease or non-disease state (**Figure 4-8**). This is further corroborated by the primary analysis result of L-selectin where levels between the Dx group and the late control group were very similar (**Figure 4-1**). This data does not indicate any utility as a diagnostic biomarker.

Analysis of L-selectin levels between the CNS Dx and CNS DxR groups also showed no significant indicating that it is not a prognostic biomarker in this sample set difference (**Figure 4-8**).

Results from the secondary analysis of Osteopontin follow suit with the trends seen for L-selectin. Levels of Osteopontin in the non-inflammatory control CSF vs CNS1, CNS2 and CNS3 patients were very similar and statistical analysis showed no significant difference between the means ( $p = 0.842095$ ;  $p = 0.940494$ ;  $p = 0.531488$ , respectively) (**Figure 4-9 A**). This trend was replicated in the results seen between the comparison of inflammatory control CSF and the CNS1-3 patient groups ( $p = 0.174992$ ,  $p = 0.775824$ ,  $0.066127$ , respectively) (**Figure 4-9 B**).

Comparison between the CNS Dx group and the non-inflammatory control and inflammatory control unsurprisingly revealed no significant difference between the means ( $p = 0.874376$ ;  $p = 0.219661$ , respectively) (**Figure 4-9 C**).

Analysis of Osteopontin levels between the CNS Dx and CNS DxR groups also showed no significant indicating that it is not a prognostic biomarker in this sample set difference ( $p = 0.883827$ ) (**Figure 4-9D**).

ROC analysis data shows that both analytes show very poor diagnostic capability to identify the CNS-ALL patient groups against the control CSF groups with p values for all comparisons being  $> 0.05$  , confirming that these two analytes are of no diagnostic utility (**Table 4-4**).

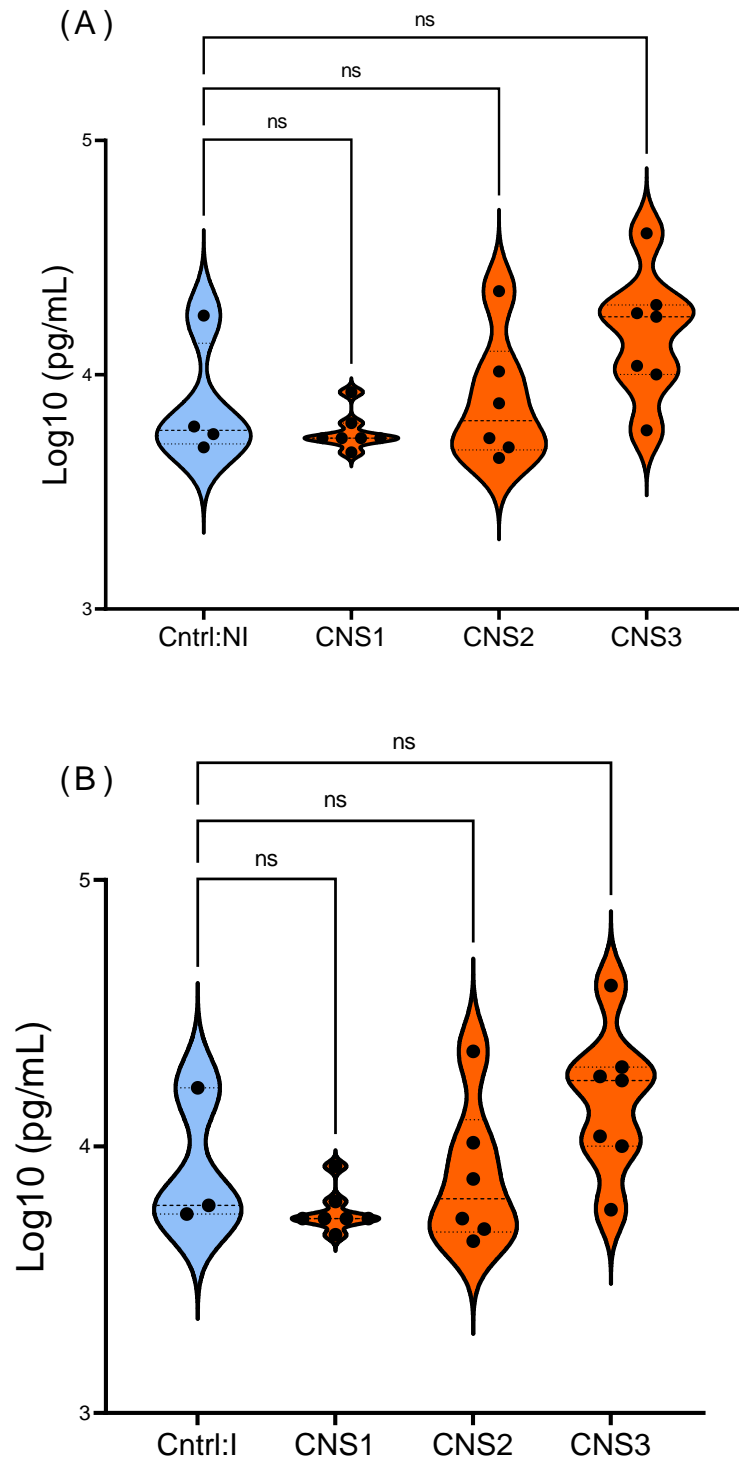


**Figure 4-7: L-selectin – Violin plots of log<sub>10</sub> transformed L-selectin levels of control CSF vs CNS1, CNS2 and CNS3 patient samples.** (A) Non-inflammatory control CSF vs patient samples. (B) Inflammatory control CSF (I) vs patient samples. Statistics: Unpaired ordinary one-way ANOVA, multiple comparisons tested using Dunnett's multiple comparison test, alpha threshold=0.05 ; ns = not significant. Graphs created on GraphPad Prism v9.

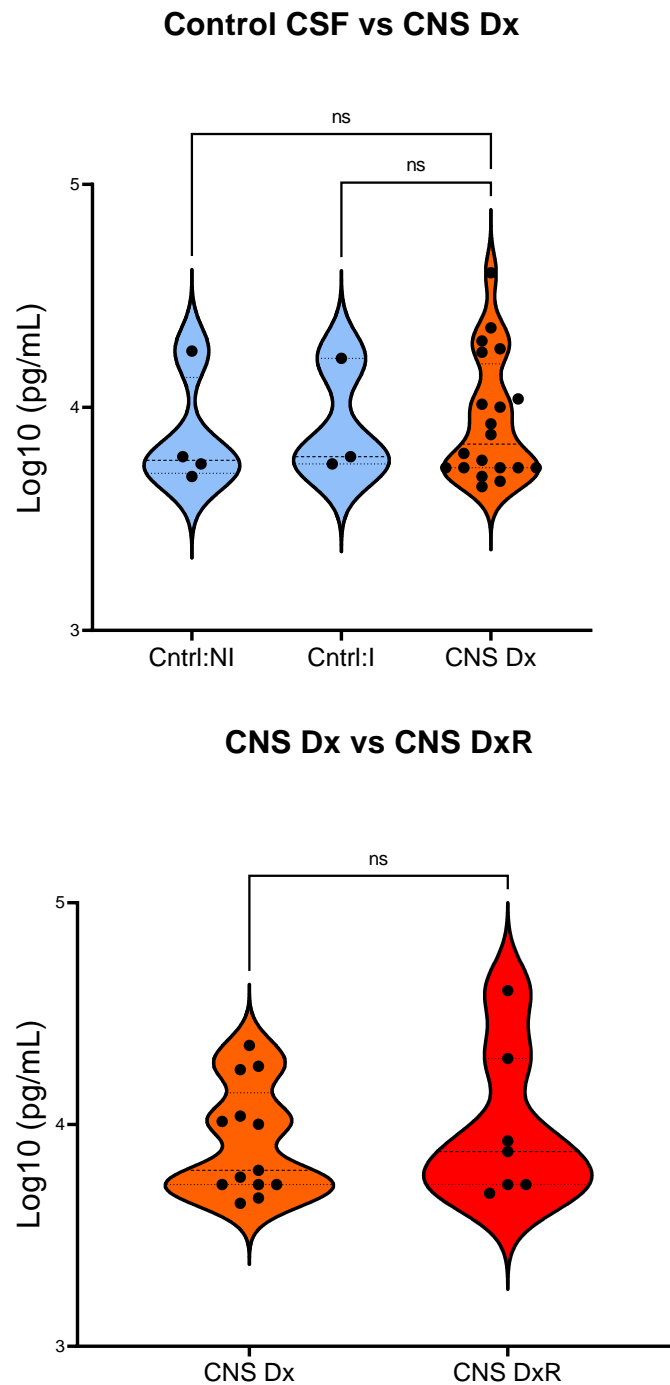


**Figure 4-8: L-selectin – Violin plots of log<sub>10</sub> transformed L-selectin levels of control CSF vs CNS Dx patient samples.** (A) Non-inflammatory control CSF (NI) & inflammatory control CSF (I) vs CNS Dx combined patient samples. Statistics: ordinary one-way ANOVA unpaired, multiple comparisons tested using Dunnett's multiple comparison test, alpha threshold=0.05 and confidence level 95% confidence interval \* ns = not significant. (B) CNS Dx vs CNS DxR group. CNS DxR = Diagnostic patient samples of children who relapsed in the CNS in the future. Statistics: unpaired t-test, ns = not significant. Graphs created on GraphPad Prism v9.



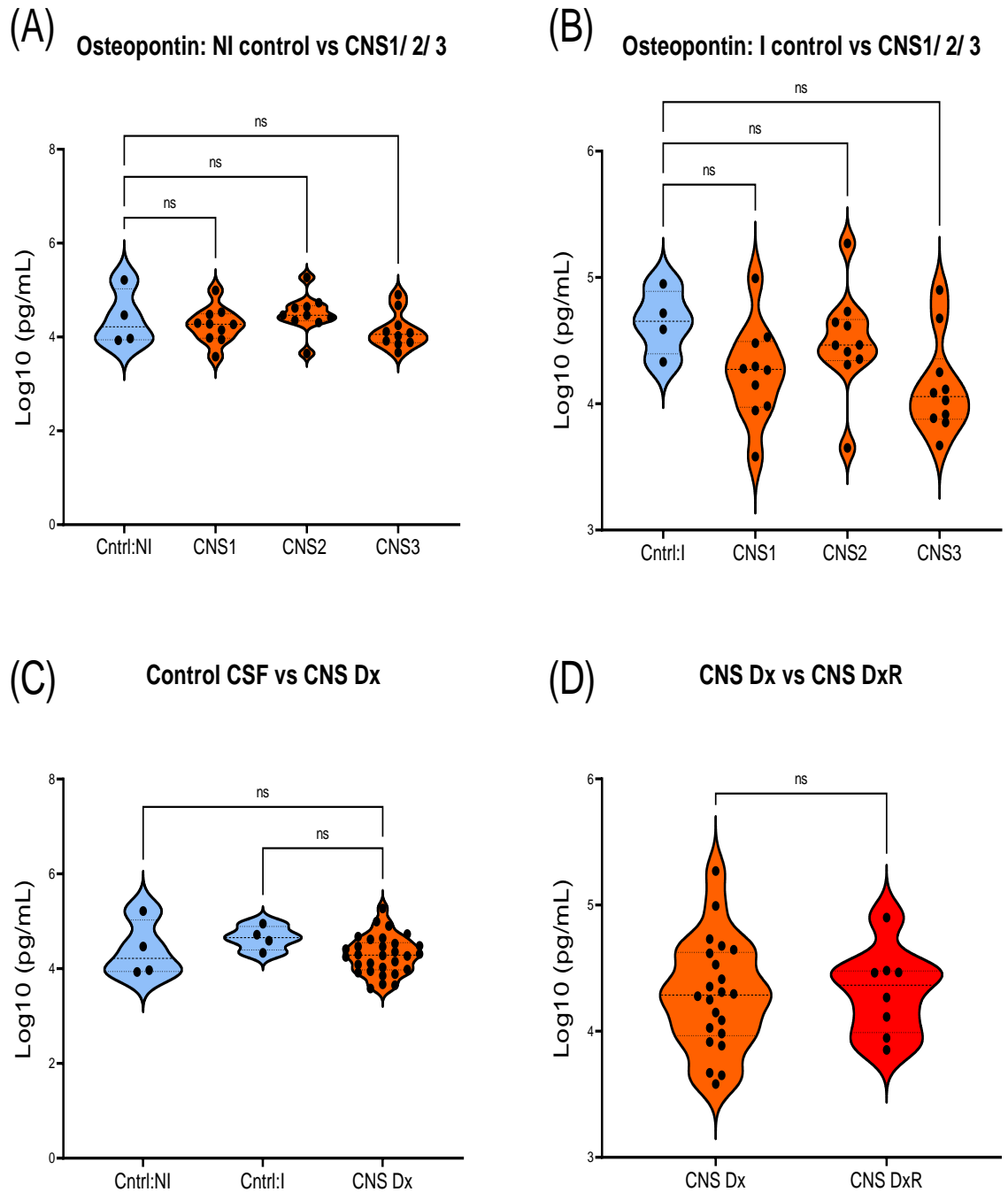


**Figure 4-9: Osteopontin – Violin plots of log<sub>10</sub> transformed Osteopontin levels of various analyses. (A)** Non-inflammatory control CSF vs patient samples. **(B)** Inflammatory control CSF (I) vs patient samples. **(C)** Non-inflammatory control CSF (NI) & inflammatory control CSF (I) vs CNS Dx combined patient samples. Statistic: Unpaired ordinary one-way ANOVA, multiple comparisons tested using Dunnett's multiple comparison test, alpha threshold=0.05 ; ns = not significant. **(D)** CNS Dx vs CNS DxR group. CNS DxR = Diagnostic patient samples of children who relapsed in the CNS in the future. Statistics: unpaired t-test, ns = not significant. Graphs created on GraphPad Prism v9.

ROC	Comparison	AUC	St. Err	95% CI	p value: alpha = 0.05
<b>L-selectin</b>	NI vs CNS Dx	0.629	0.109	0.416 – 0.842	0.407
	I vs CNS Dx	0.689	0.097	0.499 to 0.879	0.287
<b>Osteopontin</b>	NI vs CNS Dx	0.517	0.169	0.186 – 0.848	0.915
	I vs CNS Dx	0.783	0.092	0.604 to 0.963	0.069

**Table 4-4: Receiver Operator Curve (ROC) analysis of non-inflammatory control CSF & inflammatory control CSF vs CNS Dx patient sample groups for L-selectin & Osteopontin.**

Alpha set at 0.05. Statistics were calculated on GraphPad Prism v9.

Together, this data confirms that both analytes, although detectable and present in CSF, have no diagnostic clinical utility for detecting CNS-ALL in the CSF of children with acute lymphoblastic leukaemia, and do not appear to predict later risk of CNS relapse.

### 4.2.3 Summary and conclusions

The goal for this chapter was to discover novel sensitive and specific diagnostic or prognostic biomarkers for CNS-leukaemia. Current methods for classifying CNS-leukaemia are insensitive and unable to accurately predict CNS-relapse. Initial work involved a literature search for potential analytes of interest to use with Luminex multiplex immunoassay technology for the detection of multiple analytes simultaneously.

Primary analysis involved testing CNS1 diagnostic patient samples against matched late controls as a preliminary experiment to determine which analytes proved most interesting to take forward to a secondary analysis. This data revealed 5/10 analytes with detectable concentrations within range of the assay (Osteopontin, L-selectin, CD27, VEGF-C and CXCL10). Levels of these analytes were generally low and close to the lower limit of quantification apart from L-selectin and Osteopontin. Individual analyses indicated no real difference between the patient group and the control group in all but CD27. The strength of this experiment lies in the matched late controls from each patient. These controls are taken one year into treatment where the leukaemic burden is expected to be minimal to non-existent. Inflammation within the CNS is also expected to be minimal in these control samples and so this experiment is ideal for identifying potential biomarkers of interest. Although there was no real difference between the patient and control groups of L-selectin and Osteopontin, these two analytes alongside CD27 were chosen to take forward for a secondary analysis due to the high levels found in CSF.

Secondary analysis initially involved the testing of the chosen analytes with different groups of CNS-leukaemia current classification patient samples (CNS1, CNS2 &

CNS3) against both non-inflammatory and inflammatory control CSF. These two CSF control group samples were provided by the Glasgow Neuroimmunology Biobank and include CSF from patients who were admitted to the hospital for an exploratory lumbar puncture for a range of conditions but were cleared of any malignancies. The rationale behind using these CSF controls was to see if the non-inflammatory control would replicate the trend seen with matched late control CSF and to elucidate the behaviour of the analytes in an inflammatory CSF environment. A biomarker that presents with the same difference in both controls, is likely a specific biomarker for the presence of CNS-ALL.

Regarding CD27, the secondary analysis indicated that higher leukaemic burden, i.e. CNS2/3, as classified by the current gold standard method of CSF cytology, appear to have elevated CD27 when compared to the non-inflammatory control CSF. ROC curve analysis results support this finding, indicating that CD27 shows strong diagnostic capability to discriminate CNS-ALL burden in higher diagnostic classifications CNS2 and CNS3 against the non-inflammatory control CSF. CD27 did not show evidence of being clinically useful when differentiating between the control and the CNS1 patient sample group. However, given that CD27 was elevated in the inflammatory control CSF, the data strongly suggests that elevated CD27 is most likely a consequence of an inflammatory phenotype in the CNS space rather than it being indicative of the presence of CNS-leukaemia specifically. This experiment while showing promising signs of the right level of sensitivity needed for a good biomarker of CNS-ALL, greatly lacks the specificity needed to take this analyte further for testing by itself. It may have some clinical utility as a biomarker in combination with other parameters which may enhance the overall specificity of a multi-biomarker test.

This was further supported by moving away from the current classification systems (CNS1-3) by combining all patient samples regardless of their CSF cytology classification, uniting them as one CNS diagnosis population (CNS Dx) and comparing this group to both controls. This analysis put the levels of CD27 in-between the non-inflammatory and inflammatory control CSF, with CD27 levels of the CNS Dx group being closer to the inflammatory control than the former. Again, positioning CD27 as a sensitive but unspecific marker capable of detecting inflammation within the CNS rather than the presence of CD27.

ROC curve analysis requires the test (in this case the analyte in question) between the disease and non-disease groups to be as robust as possible to be able to provide an answer on the discriminatory utility of the test. While this test is commonly used in biomarker discovery, its use and interpretation must be performed with care. The use of two controls in this case revealed that while upon first sight, CD27 looked specific and sensitive for detecting CNS-ALL in the CNS2 and CNS3 patient sample groups when compared against our “normal” non-inflammatory control CSF. Analysis against the inflammatory control CSF however, revealed that CD27 is not clinically useful for identifying CNS-ALL.

Testing the CD27 levels for diagnostic samples from patients who went onto relapse in either the CNS or bone marrow against diagnostic samples from patients who did not relapse did not reveal any differences suggesting that it has no utility as prognostic biomarker.

Despite being implicated as potential biomarkers for CNS-ALL, L-selectin and Osteopontin were found to be universally detectable in all the CSF sample types analysed but no differences between the levels of the analytes in the groups were

found, suggesting little utility of these markers in this setting. The other potential biomarkers tested in the primary analysis were not even detectable in this study.

There are limitations in this study which must be addressed which could explain the behaviour of all the candidate biomarkers tested (apart from CD27). First, the pre-analytical variables i.e., sample stabilisation, storage and transport may have played an effect with the integrity of the proteins/ chemokines being investigated. Samples are often not collected, processed, and stored adequately from the bedside (post lumbar puncture) to the laboratory bench. These samples have also been in storage at -80 °C for several years. The data in these experiments are from a small cohort of patients so this study may be too underpowered to discern any real differences between the comparator groups. The CSF controls in the secondary analysis originate from adults and are thus not ideal for comparison against childhood ALL patients. Unfortunately, true control CSF from clinically well children is extremely rare-to-very difficult to obtain.

In summary, the results of this chapter, while they have not identified a protein biomarker suitable for detecting leukaemic burden in the CNS, have laid the foundation work by setting up the appropriate parameters in which a successful biomarker must behave in this setting i.e., must show clinically useful differences between non-inflammatory and inflammatory control CSF by the various different analyses used here to be considered sensitive and specific enough for further testing. Future studies should involve wider screening of more potential protein/ cytokine biomarkers through the use of large multiplex immunoassays.

# **Chapter 5: Circulating-tumour DNA as a biomarker of central-nervous system acute lymphoblastic leukaemia**

## **5 Introduction and aims**

The release of cell-free DNA into surrounding bodily fluids is ubiquitous around the body. cfDNA can be measured in various biological matrices such as plasma, serum, urine, and CSF and current research has a focus on the adoption of cfDNA analysis for routine application in areas such as prenatal screening, monitoring organ transplants, and detection of disease such as cancers [107]. Typically, cancer patients can present with higher levels of cfDNA than healthy persons of which, circulating tumour DNA (ctDNA) will make up a fraction, big or small, of the total cfDNA [108]. However, the level of ctDNA can be highly variable between patients depending on the type of cancer or disease stage [109]. ctDNA is an ideal target as a diagnostic and prognostic biomarker because in most cases, it is an “easy” molecule to extract by non-invasive procedures i.e., blood or urine samples and thus can be used effectively for tracking disease progression, response to treatment and for detecting potential relapses [110].

The use of cfDNA as a biomarker in cancer diagnostics, monitoring disease progression and predicting response is widely investigated but lacks an appropriate level of standardisation with regards to pre-analytical stages of the workflow. These needs must be met before widespread clinical implementation can be adopted. Of the preanalytical stages to consider, the following factors can have significant effects on the results: sample source, sample collection, sample transport and storage, sample volume, sample preparation, and sample extraction.

This part of the study focussed on the detection of ctDNA biomarkers in the CSF of children suffering from disseminated ALL in the CNS compartment. Patient samples used in this study were sourced from leftover CSF taken at diagnosis and various subsequent dates throughout the treatment period through lumbar puncture prior to intrathecal administration of chemotherapy in the CNS. Drops of CSF are taken into a “research” collection tube (plain universal container) and sent alongside the clinical diagnostic samples to the central laboratories at the Queen Elizabeth University Hospital, on receipt in the laboratory, the samples were stored at 4°C until retrieval by the research team. The majority of samples were processed within 6 hours of collection, but some were processed up to 48 hours later if taken at a weekend. This study currently had no influence and played no role in the origin and transport of samples until it reaches the research laboratory. Samples of CSF which were received by the Wolfson Wohl Cancer Research Centre were transported on dry ice, centrifuged at 4 °C and transferred into a -80°C freezer as per general sample storage guidelines to preserve the integrity of the samples. Freeze/thaw cycles were avoided where possible to again preserve the integrity of any DNA in the samples.

This study focussed on the remaining preanalytical considerations: sample volume, sample preparation and sample extraction to develop this part of the workflow in preparation for the use of highly sensitive platforms such as droplet-digital PCR and Next-generation sequencing (NGS) to detect ctDNA in samples of CSF.

The samples available for this part of the study were composed of diagnostic patient CSF samples as well as some matched CSF samples taken at day 8, day 29 and 1 year into of treatment. The samples taken 1 year into treatment serve as a matched control sample as there is expected to be little or no-leukaemia at this stage of



treatment. This study also included samples taken from three patients who relapsed in the CNS.

Part of the initial work in this chapter was performed on plasma as samples of CSF are extremely valuable as they require an invasive procedure, thus are difficult to obtain and are typically of low volume. A major challenge faced in this project was obtaining CSF of a high enough volume for all experiments. In lieu of this, a surrogate matrix composed of pooled plasma samples from six volunteer donors was used to complete part of the cfDNA extraction work below. When CSF was available, a pool of control CSF from six donors was used. This control CSF was obtained from childhood patients in hospital who were investigated for neurological conditions but were cleared of any cancer or significant neuropathology (i.e. CSF results were within normal limits). While plasma and CSF are fundamentally and constitutionally different matrices, their extraction methods are generally the same given the extraction kits and technologies currently available.

CSF is an ultrafiltrate of plasma mostly secreted into the subarachnoid space by the choroid plexus and is considered is a “content light” matrix compared to plasma. Plasma generally contains more background “noise” by means of having a high white cell number, a multitude of proteins and different electrolyte levels [12]. What may differ is the amount of cfDNA present in each matrix and the potential constituents which could alter its level such as the level of nucleases or protein-DNA complexes.

It was hypothesized that ctDNA is abundant in the CSF of patient samples and has the potential of being a sensitive and specific diagnostic, prognostic, and response biomarker for detecting and tracking CNS leukaemia. The goal for this part of the

project was to develop a robust and sensitive method for the detection of leukaemic circulating-tumour DNA (ctDNA) in CSF through the following aims:

1. To test and compare commercial cfDNA extraction kits using a surrogate cfDNA molecule (linearized plasmid fragment DNA) on samples of plasma to identify the best cfDNA extraction protocol.
2. To test the chosen cfDNA extraction protocol with a series of spike-in and recovery experiments to test the sensitivity and recovery yields, first with samples of plasma, followed by samples of CSF.
3. To analyse the quantity and quality of extracted CSF cfDNA from both control and patient samples.
4. To test and develop protocols for highly sensitive platforms such as ddPCR and NGS to target specific ctDNA targets and determine utility of these methods for ctDNA biomarker discovery.

## 5.1 Comparing commercial cfDNA extraction kits

### 5.1.1 Quantification by Qubit fluorometry

It was first decided to determine the most appropriate extraction method to isolate ctDNA from CSF by comparing several commercial extraction kits which are available on the market today. Six different commercial kits (QA, QB, NN, NM, COV & MX) were chosen which spanned a variety of different methodologies including one automated extraction kit (Described in **Table 2-4, pg. 86**). Most of these kits focus on extraction from blood (plasma and/or serum) and are primarily designed for liquid biopsy workflows. Of the kits chosen in this study, only one kit (NN), specifies CSF as a sample type for cfDNA extraction.

To test the performance of these kits, a cfDNA surrogate molecule (linearized DNA fragment from a pGL3 plasmid) 172 bp in length herein labelled as hTERT<sub>172</sub> (See materials & methods **2.5.3.1 pg. 86**) was used in a variety of spike-in and recovery experiments. The surrogate matrix for this experiment was composed of plasma samples pooled to 1 mL aliquots to create a stable matrix with a consistent background quantity of cfDNA for downstream extraction and analysis. Samples were divided into two groups, one control group (un-spiked) and one test group spiked with 5 ng of hTERT<sub>172</sub>. The aim of this experiment was to measure and compare extraction efficiency for each kit by comparing the spike-in recovery between the spike-in sample and the control sample. Each sample went through the manufacturer specified extraction process and was eluted in 50 µL of their respective elution buffer. The eluted cfDNA was then quantified using a Qubit 2 Fluorometer (Thermo Fisher) and the Qubit dsDNA HS Assay kit (Thermo Fisher) (**Figure 5-1**).

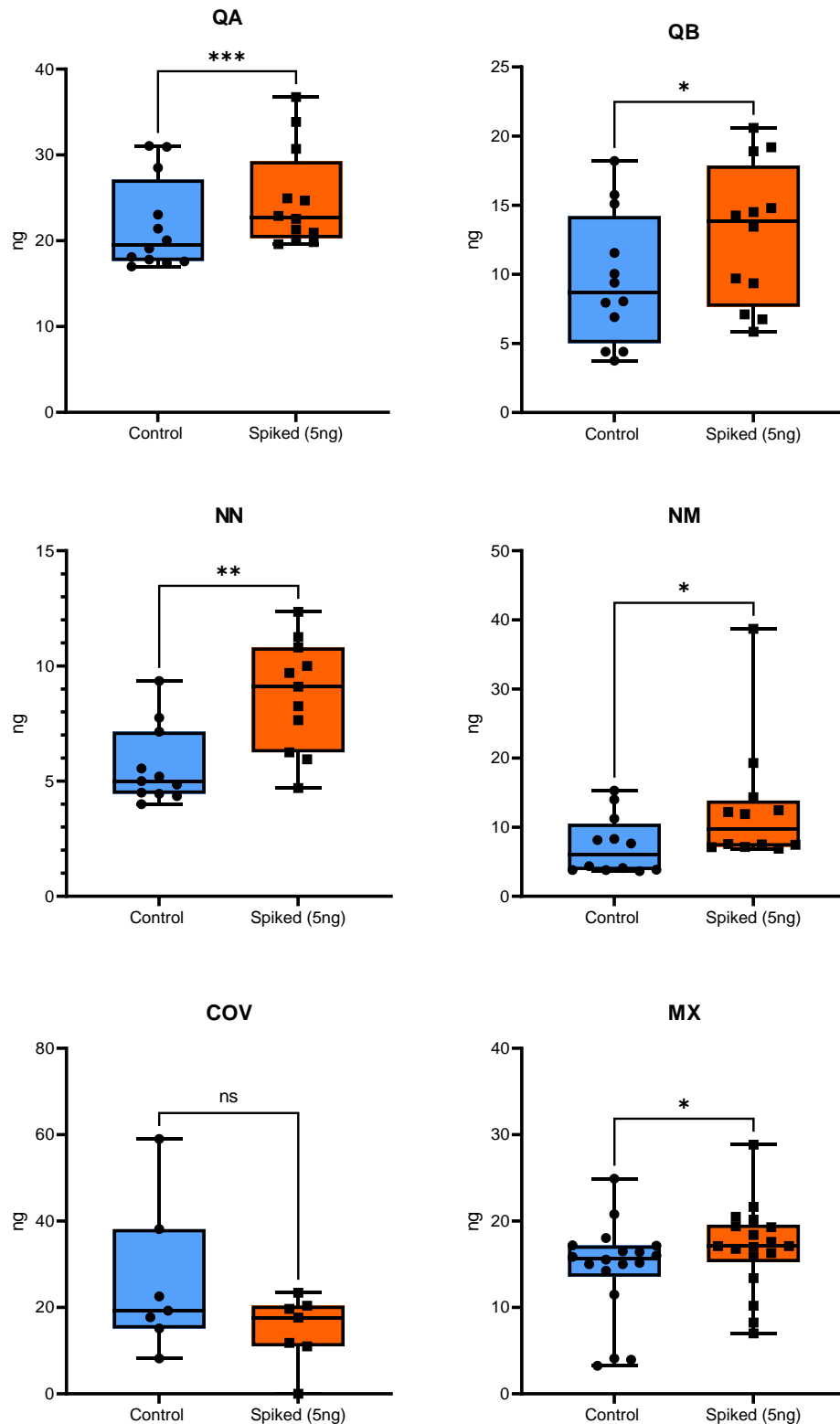


**Figure 5-1: Box plots of absolute cfDNA extracted quantified by Qubit (n=3-4).** CTL (Control-un-spiked = blue) vs Spiked (hTERT<sub>172</sub> spike-in = orange). cfDNA extracted from 1mL samples of surrogate pooled plasma matrix. Data expressed as absolute DNA calculated multiplying DNA concentration in ng/ $\mu$ L by the elution volume (50  $\mu$ L) Statistics: Two-tailed paired t-tests, alpha 0.05. \*p<0.05. Plots generated on GraphPad Prism v9.

Quantification by Qubit yields the total nucleic acid fraction present in the sample. Each kit in the experiment performed variably compared to each other but generally trended as expected, demonstrating a higher quantity of cfDNA in the hTERT<sub>172</sub> spiked sample compared to the control sample. Of note, extraction kit COV yielded the highest recovery of cfDNA in the control group but conversely a lower recovery in the spiked group (COV control = 25.7 ng. spiked = 17.33 ng). Extraction kit QA yielded the highest recovery of cfDNA in both control and spiked groups (QA control = 21.8 ng, spiked = 24.8 ng) (**Figure 5-1, Table 5-1**).

Statistical analysis between the means of the control and the spiked groups indicated significant differences in kits QA ( $p = 0.000604$ ), QB ( $p = 0.011034$ ), NN ( $p = 0.003069$ ), NM ( $p = 0.024219$ ) and MX ( $p = 0.042408$ ). The kit COV, did not have a statistically significant difference between the means of the control vs spiked groups ( $p = 0.118259$ ) (**Figure 5-1, Table 5-1**).

Next, given the high recovery of cfDNA by the QA kit in both groups (control & spiked), this kit was compared to all the other kits by combining both control and spiked values to measure general extraction efficiency. Kits QA and COV recovered higher levels of cfDNA than all other kits (23.3 ng & 20.3 ng respectively). Statistical analysis between the means of all the kits compared to QA indicated significant differences in all but the QA – COV comparator (**Figure 5-2, Table 5-2**).

Between the two highest performers in cfDNA recovery, kits QA and COV, COV showed higher variability in the measurements within the control and spiked groups compared to QA (**Figure 5-1, Table 5-1**).

Kit ID	Control				Spiked				p value
	Qubit [ng/uL]	Ab. DNA (ng) (i)	SD	SEM	Qubit value [ng/uL]	Ab. DNA (ng) (ii)	SD	SEM	
QA	0.44	21.83	5.36	1.547	0.497	24.85	5.791	1.672	0.000604
QB	0.19	9.63	4.737	1.367	0.26	12.87	5.11	1.475	0.011034
NN	0.11	5.65	1.697	0.5117	0.17	8.73	2.407	0.7258	0.003069
NM	0.15	7.35	4.21	1.215	0.25	12.71	9.046	2.611	0.024219
COV	0.51	25.72	17.3	6.54	0.35	17.33	7.957	3.008	0.118259
MX	0.29	14.48	5.655	1.333	0.34	16.94	5.059	1.192	0.042408

**Table 5-1: Descriptive statistics for each tested kit – Control vs Spiked.** (i-ii) Absolute DNA in ng was calculated by multiplying the concentration (ng/uL) by the elution volume (50uL)

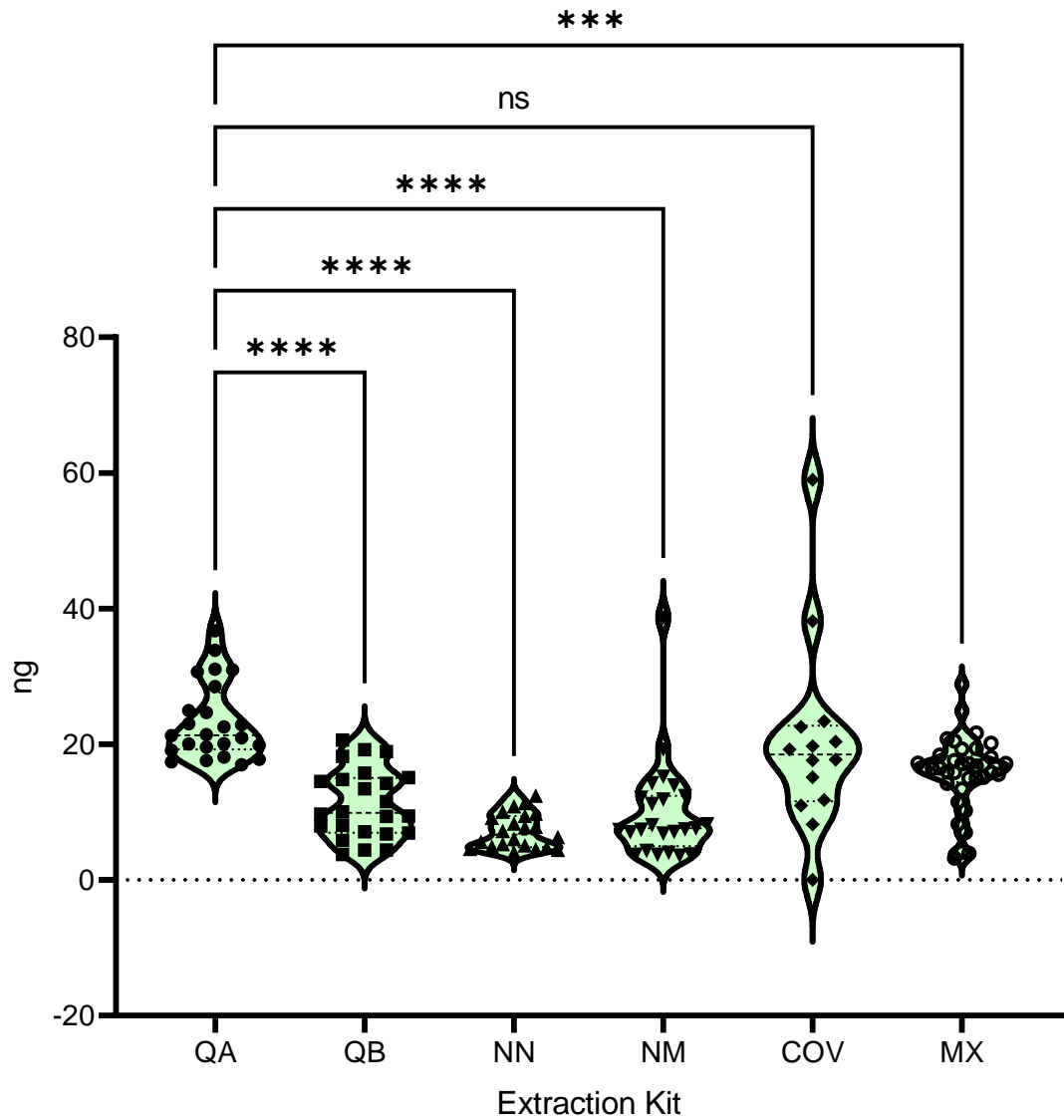


**Figure 5-2: Extraction efficiency of cfDNA kits compared to kit QA.** All kits were compared to kit QA which demonstrated the highest recovery of cfDNA. Statistics: Ordinary one-way ANOVA. Multiple comparisons corrected using Dunnett's multiple comparisons test with an alpha of 0.05.  $p < 0.05$ ,  $**p < 0.005$ ,  $***p < 0.001$ ,  $****p < 0.0001$  and ns=not significant. Graphs created on GraphPad Prism v9.

Dunnett's multiple comparisons test	P value summary <0.000001								
Comparison	QA Mean	SD	SEM	Comp. Mean	SD	SEM	Mean Diff.	95.00% CI of diff.	Adjusted P Value
QA vs. QB	23.3	5.67	1.16	11.2	5.1	1.04	12.1	7.10 to 17.1	<0.0001
QA vs. NN			1.16	7.19	2.57	0.548	16.2	11.1 to 21.3	<0.0001
QA vs. NM			1.16	10	7.42	1.52	13.3	8.32 to 18.3	<0.0001
QA vs. COV			1.16	20.3	14.1	3.77	3.06	-2.76 to 8.87	0.538078
QA vs. MX			1.16	15.7	5.43	0.905	7.63	3.08 to 12.2	0.000184

**Table 5-2: Statistical analysis of the differences between the means of kit QA vs all other kits.** Ordinary one-way ANOVA. Multiple comparisons corrected using Dunnett's multiple comparisons test with an alpha of 0.05.  $p < 0.05$ ,  $**p < 0.005$ ,  $***p < 0.001$ ,  $****p < 0.0001$  and ns=not significant Statistics calculated on GraphPad Prism v9.

### 5.1.2 Quantification by droplet-digital PCR

The next step was to confirm the presence and assess the quality of the hTERT<sub>172</sub> spike-in molecule. While DNA quantification by fluorometry (Qubit) gives us an accurate representation of the total quantity of double stranded DNA present in a sample, it is unspecific since it cannot discriminate specific nucleic acid sequences. With oligonucleotides for hTERT<sub>172</sub> DNA, we were able to confirm the presence of the spike-in molecule directly using droplet digital PCR (**Figure 5-3**). The purified cfDNA samples from both test groups were added to a droplet digital PCR reaction



using EvaGreen chemistry to get an absolute quantity in copies/ $\mu\text{L}$  of hTERT<sub>172</sub> (Figure 5-4). Interestingly, low quantities of endogenous hTERT<sub>172</sub> were detected in the un-spiked control samples as can be seen in the digital PCR rain plots (Figure 5-3).

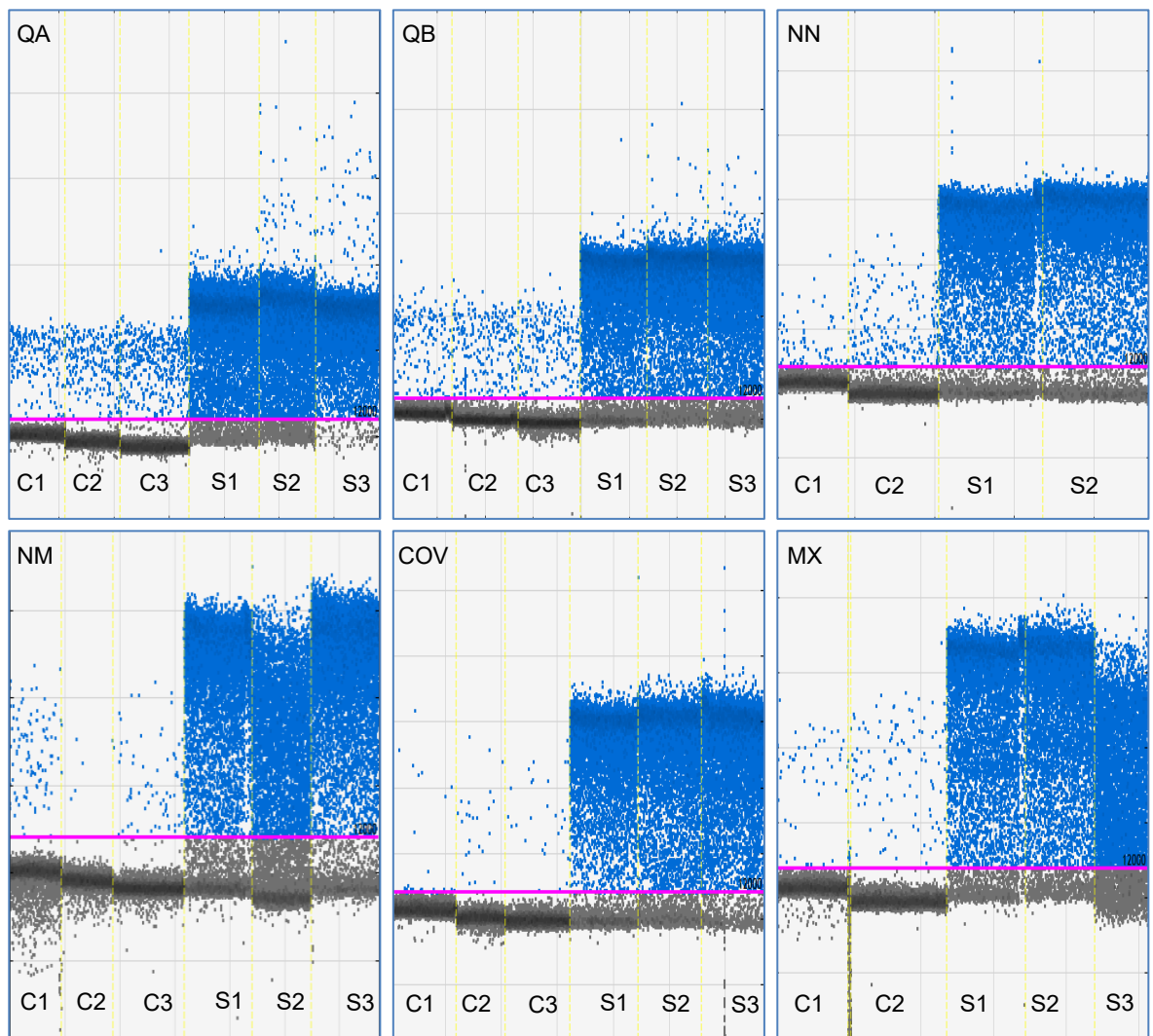


**Figure 5-3: Digital PCR Rain-plots : Confirmation of detection of hTERT<sub>172</sub>.** Data points indicate individual partitioned PCR reactions events per water-oil emulsion droplet. Purple line = common threshold set. Blue data points = positive droplets, grey data points = negative droplets . X Axis = sample replicate, Y axis = Fluorescence. Control samples designated as C. Spiked sample designated as S.

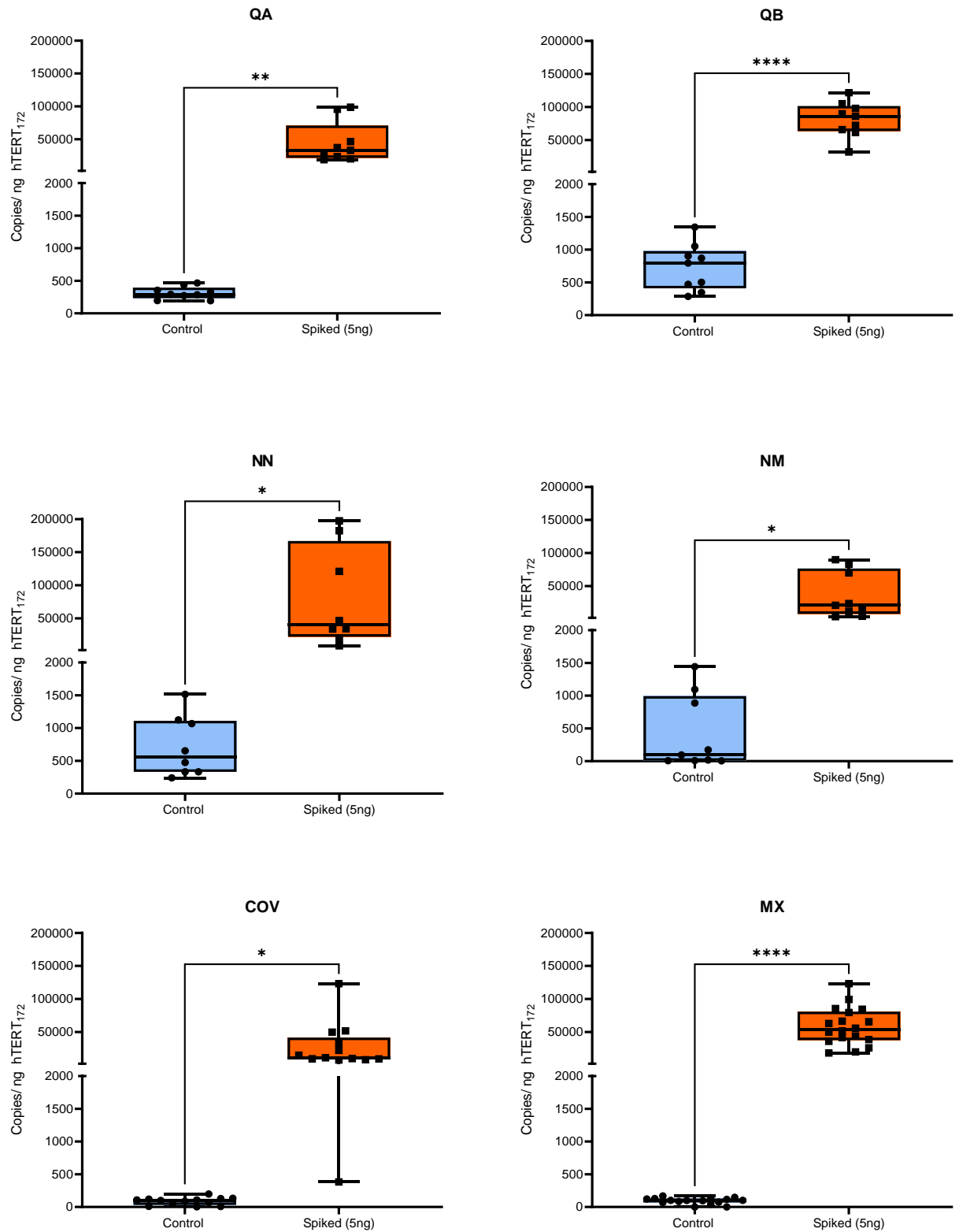


**Figure 5-4: Box plots of absolute quantity of hTERT<sub>172</sub> extracted quantified by ddPCR (n=3-4). CTL (Control-unspiked = blue) vs Spiked (hTERT<sub>172</sub> spike-in = orange). Data expressed as copies/ng of hTERT<sub>172</sub>. Statistics: Two-tailed paired t-tests, alpha 0.05. \*p<0.05. Plots generated on GraphPad Prism v9.**

These results show that the kits which detected the highest copies of hTERT<sub>172</sub> were kits QB (81351 ± 26704 copies/ng) and kit NN (80280 ± 75722 copies/ng).

Kits MX and QA performed similarly in terms of hTERT<sub>172</sub> quantity (59214 ± 29842; 44849 ± 30869, respectively). Of note, Kit MX demonstrated the highest precision between the sample replicates (SEM = 7460).

Kits COV and NM detected the least amount of hTERT<sub>172</sub> out of all the kits (27004 ± 33130; 36066 ± 34799, respectively) (**Figure 5-4, Table 5-3**).

Next, the efficiency of hTERT<sub>172</sub> recovery was assessed by comparing the means of hTERT<sub>172</sub> from each kit to the QA kit, as above. Statistical analysis demonstrated that there was no significant difference between the means of any of the comparisons (**Figure 5-5, Table 5-4**).

Kit ID	Control				Spiked				p value
	Ab. DNA (ng)	Copies/ng	SD	SEM	Ab. DNA (ng)	Copies/ng	SD	SEM	
QA	21.83	313.7	94.31	31.44	24.85	44849	30869	10290	0.002497
QB	9.63	730.1	353.4	117.8	12.87	81351	26704	8901	0.000017
NN	5.65	717.4	465.2	164.5	8.73	80280	75722	26772	0.020262
NM	7.35	415.4	566.1	188.7	12.71	36066	34799	11600	0.014173
COV	25.72	86.41	57.32	15.90	17.33	27004	33130	9189	0.012601
MX	14.48	93.51	48.52	12.13	16.94	59214	29842	7460	<0.000001

**Table 5-3: Descriptive statistics for each tested kit – Control vs Spiked.** (i-ii) Absolute DNA in ng was calculated by multiplying the concentration (ng/μL) by the elution volume (50 μL).

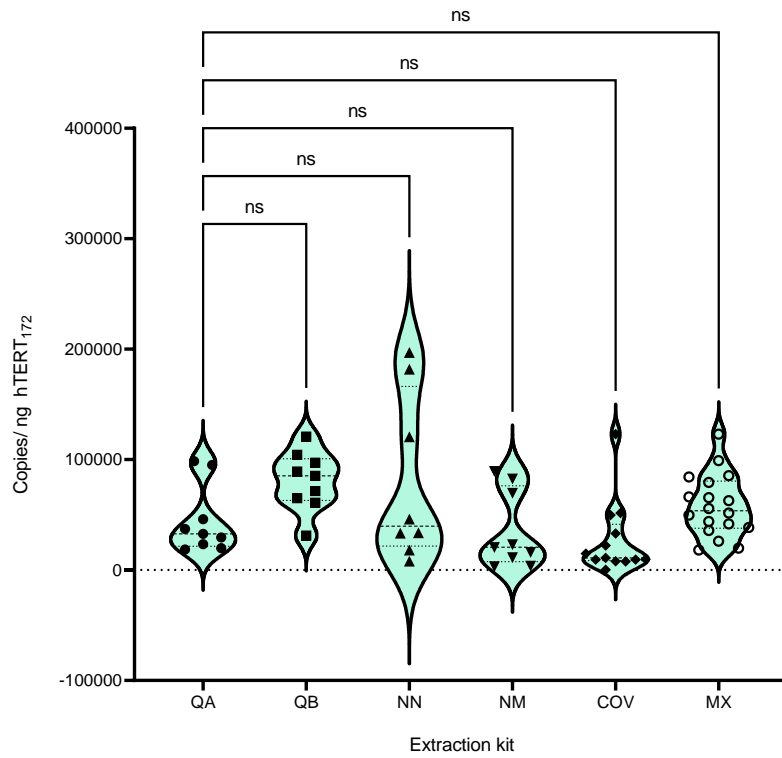


**Figure 5-5: Efficiency of hTERT<sub>172</sub> extraction in all kits compared to kit QA.** All kits were compared to kit QA. The spike-in values were baseline-subtracted (Spike-in minus average control value for each kit respectively). Statistics: Ordinary one-way ANOVA. Multiple comparisons corrected using Dunnett's multiple comparisons test with an alpha of 0.05.  $p < 0.05$ ,  $**p < 0.005$ ,  $***p < 0.001$ ,  $****p < 0.0001$  and ns=not significant. Graphs created on GraphPad Prism v9.

Dunnett's multiple comparisons test	P value summary <0.009575								
Comparison	QA Mean	SD	SEM	Comp. Mean	SD	SEM	Mean Diff.	95.00% CI of diff.	Adjusted P Value
QA vs. QB	44535	30869	10290	80621	26704	8901	-36086	-82920 to 10748	0.180972
QA vs. NN				79562	75722	26772	-35027	-83303 to 13248	0.225031
QA vs. NM				35651	34799	11600	8884	-37950 to 55718	0.982203
QA vs. COV				26917	33130	9189	17618	-25464 to 60699	0.723344
QA vs. MX				58169	28166	6639	-13634	-54194 to 26925	0.843803

**Table 5-4: Statistical analysis of the differences between the means of kit QA vs all other kits.**

Ordinary one-way ANOVA with multiple comparisons corrected using Dunnett's multiple comparisons test with an alpha of 0.05. p<0.05, \*\*p<0.005, \*\*\*p<0.001, \*\*\*\*p<0.0001 and ns=not significant Statistics calculated on GraphPad Prism v9.

The results show variability in terms of total cfDNA recovered and of the levels of hTERT<sub>172</sub> recovered. Kit QA recovered most total cfDNA compared to all other kits and recovered higher amounts of hTERT<sub>172</sub> compared to kits COV and NM. It behaved similarly to kit MX but its recovery of the hTERT<sub>172</sub> plasmid fragment was outperformed by kits QB and NN.

Despite higher levels of recovered hTERT<sub>172</sub> in kits QB and NN, Statistical analysis demonstrated however that there was no significant differences between the means of kit QA and all other kits tested suggesting that these kits all perform similarly with regards to recovery of a cfDNA surrogate spike-in molecule. Given the performance of kit QA, extracting the highest quantity of total cfDNA of all the kits, this kit was chosen to be our desired cfDNA extraction kit for the remainder of the project. The samples of CSF available are also typically of low volume, so choosing a kit which maximises the capture of cfDNA from the CSF samples is imperative.

### 5.1.3 Testing of kit QA sensitivity: Spike-in & recovery

Having chosen our cfDNA extraction kit (QIAamp circulating nucleic acids kit, QA), we now moved onto further spike-in and recovery experiments to investigate further key factors in the extraction process. The research samples of CSF available to the lab are typically of low volume ranging between ~0.08 mL to 0.2 mL and on rare occasion between 0.5mL – 2 mL. Therefore, the influence of sample volume on recovery was investigated first.

To begin, a range of volumes (2 mL, 1 mL, and 0.5 mL) of the surrogate pooled plasma matrix were tested using two test groups, a control group and a spike-in group which was spiked in with a known concentration of hTERT<sub>172</sub> (**Figure 5-4**). The data shows that cfDNA was extracted from all three volumes tested in both test groups despite decreasing starting volume. Interestingly, levels of extracted cfDNA increased with decreasing volume in both the control and spike-in groups demonstrating that at 0.5 mL of plasma, cfDNA could be extracted and quantified.

Next, with the lowest tested volume (0.5mL), further spike-in and recovery experiments were carried out using known concentrations of hTERT<sub>172</sub>. Two test groups were again used, an un-spiked control of the surrogate matrix and spiked samples of the surrogate matrix which were spiked with hTERT<sub>172</sub> to the following concentrations: 25 ng/mL, 10 ng/mL, 5 ng/mL, and 2 ng/mL (**Figure 5-5 A**). Post-extraction, the samples were quantified using both Qubit fluorometry and the presence of the hTERT<sub>172</sub> molecule was confirmed by microchip electrophoresis using a 2100 Bioanalyzer instrument (Agilent) and the High Sensitivity DNA Assay Kit (Agilent).

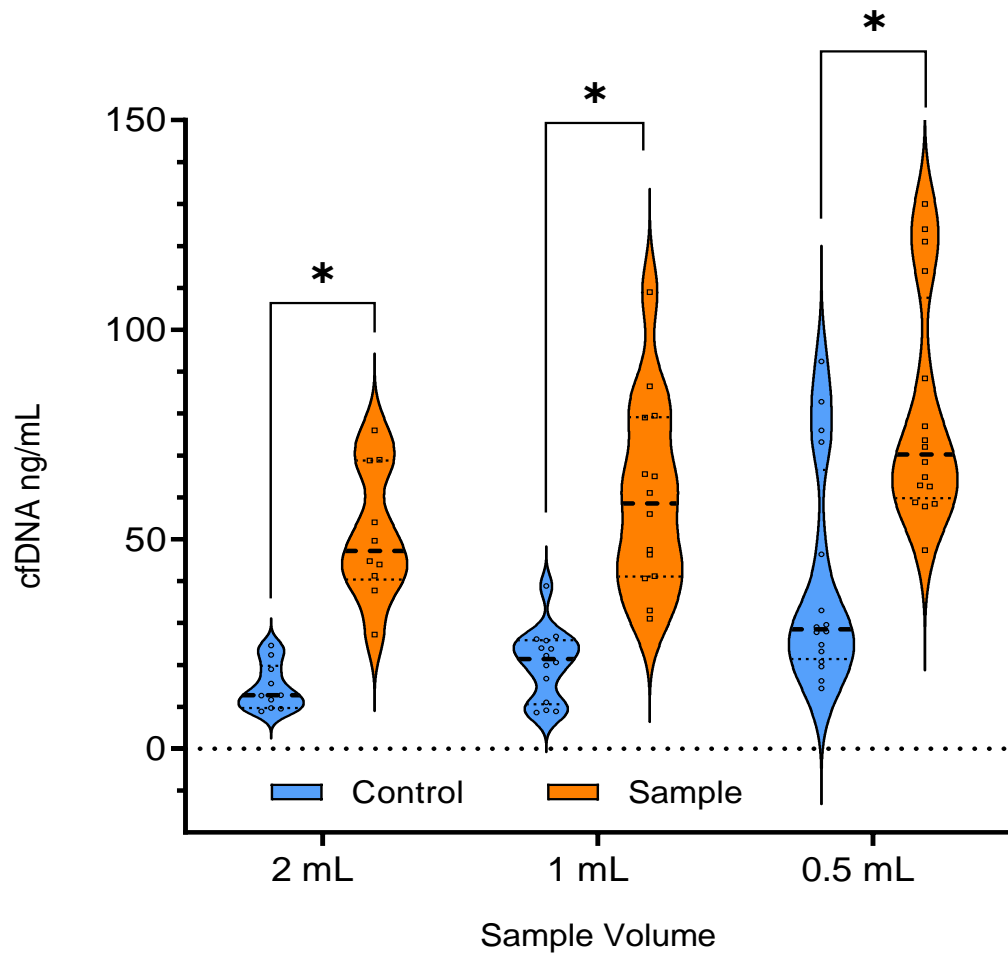


**Figure 5-6: Violin plots of cfDNA extraction volume testing in 2 mL, 1mL and 0.5 mL of plasma surrogate matrix.** All samples were performed in triplicate (n = 3). (Blue) Control samples were un-spiked; (Orange) Samples were spiked with a known concentration of hTERT<sub>172</sub>. Multiple paired t-tests with multiple comparison correction using Holm-Sidak methodology with an alpha of 0.05. \* = P<0.05. All graphs were created on GraphPad Prism v7. Statistics were calculated on GraphPad Prism v9.

The concentrations of the spike-in molecule were then compared with the un-spiked control (**Figure 5-7 A**). The baseline level of cfDNA (control) was subtracted from the mean of the hTERT<sub>172</sub> spike-in samples to give an estimate of the recovered spike-in (**Figure 5-7 B**).



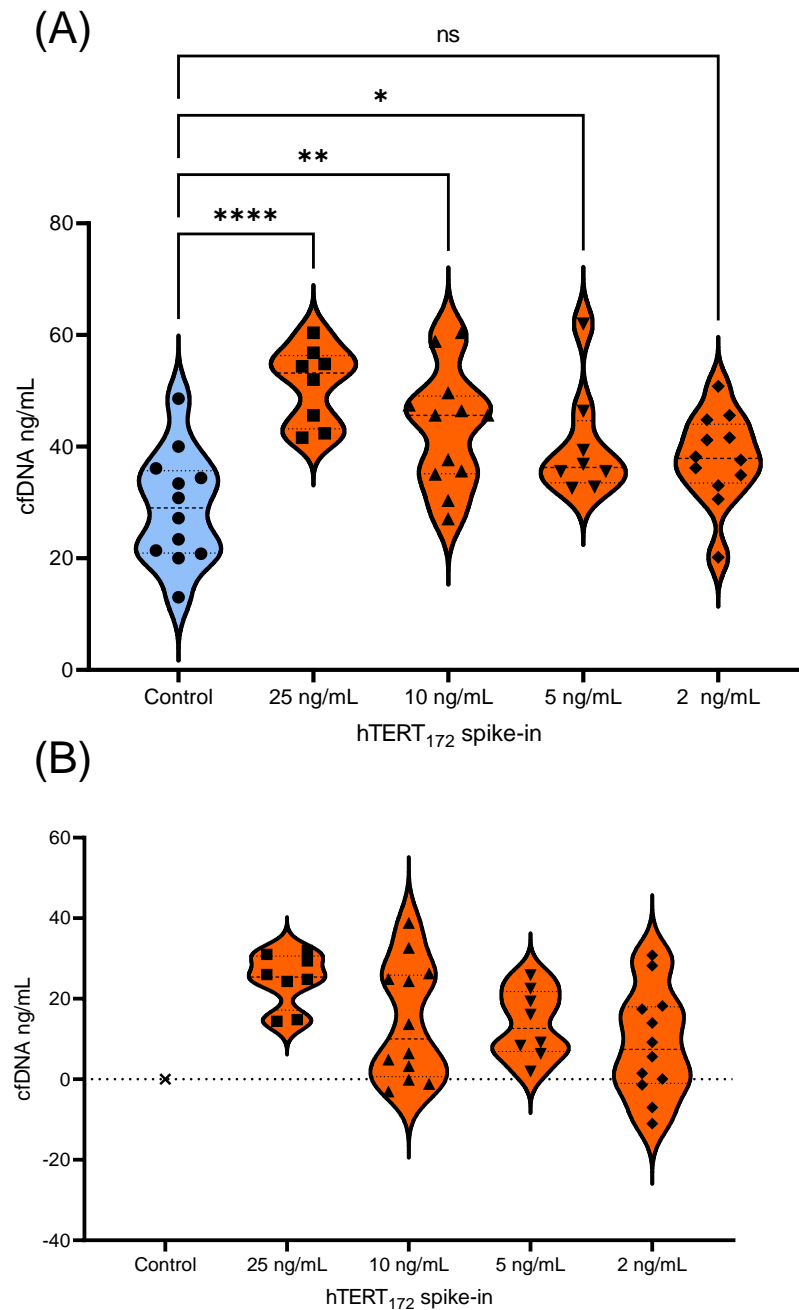


**Figure 5-7: cfDNA Spike-in & recovery experiment from 0.5 mL pooled plasma surrogate matrix.** (A) Qubit data of control surrogate matrix cfDNA vs spike-in hTERT<sub>172</sub> at various concentrations: 25 ng/mL, 10 ng/mL, 5 ng/mL & 2 ng/mL. n=3. (B) Baseline-subtracted graph of (A) on GraphPad Prism v9. This function zeros the value for extracted cfDNA from control pooled plasma sample (blue dot) and subtracts its value from the values of extracted cfDNA containing plasmid fragment spike-in (orange shapes).

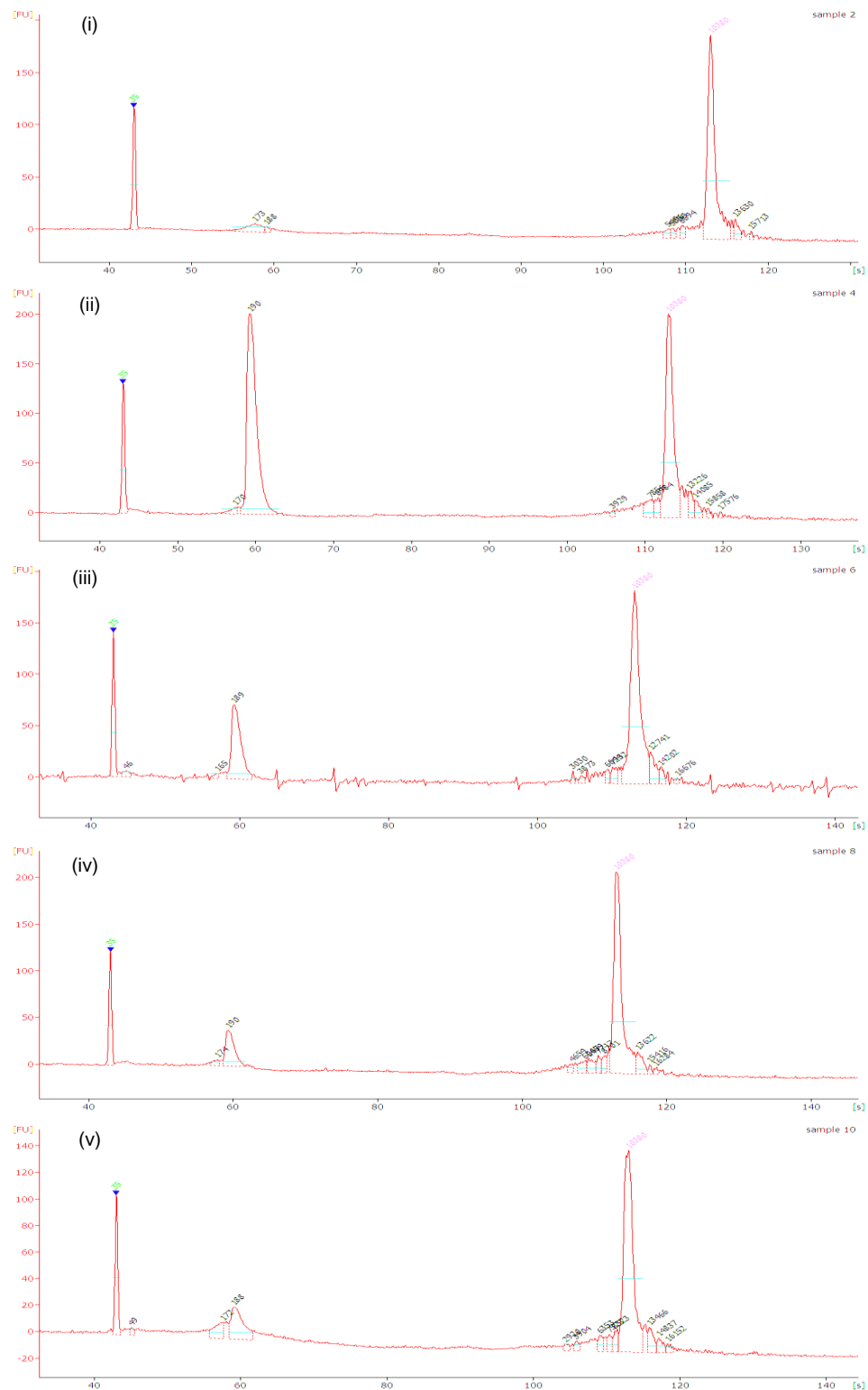


**Figure 5-8: Bioanalyzer electropherograms** (i) Control – un-spiked (ii) 25 ng/mL hTERT<sub>172</sub> (iii) 10 ng/mL hTERT<sub>172</sub> (iv) 5 ng/mL hTERT<sub>172</sub> (v) 2 ng/mL hTERT<sub>172</sub>. Peak at 35 bp (left hand of electropherogram) corresponds to the lower marker. Peak at ~10380 bp (right hand of electropherogram) corresponds to the upper marker. X-axis is measured in Fluorescence Units [FU], Y-axis measured in time. All samples were baseline corrected and peaks were detected automatically by Expert 2100, software version 1.03

The hTERT<sub>172</sub> spike-in molecule can be identified by its size (172 bp). The Bioanalyzer 2100 Expert software uses measured peak densities to calculate the size and the quantity of dsDNA relative to a ladder of reference molecules included within the kit and depicts this data through electropherograms (**Figure 5-8**).

The data indicates that upon first inspection using the baseline-subtraction method with the qubit values, recovery of the hTERT<sub>172</sub> plasmid fragment follows a downwards trend from the highest to the lowest spike-in with relatively concordant recovery between the theoretical recovery and the actual recovery down to 10 ng/mL (**Table 5-5**). The data suggests that hTERT<sub>172</sub> can be recovered down to the 2 ng/mL spike-in and analysis with the Bioanalyzer confirms the presence of the plasmid fragment, indicating a peak at ~172 bp. However, the quantification values given by the Qubit indicates a significantly higher yield than expected \*.8 ng/mL for the 2 ng/mL spike-in. The Bioanalyzer data indicated that the actual recovery of the hTERT<sub>172</sub> plasmid fragment, was 4.4 ng/mL (**Figure 5-8, Table 5-5**) .

This data suggests even at the low concentrations of spike-in hTERT<sub>172</sub>, the extraction kit can recover this molecule from 0.5 mL of our pooled plasma surrogate matrix, however the discordance of the quantification values must be noted.

Next, the experiment was repeated with samples of control CSF obtained from childhood patients in hospital who were investigated for neurological conditions but were cleared of any cancer or significant neuropathology (i.e., CSF results were within normal limits). To establish a stable baseline quantity of CSF cfDNA and repeat the process as above, equal volumes of control CSF were pooled to create a pooled control CSF matrix and cfDNA was extracted from both 0.5 mL and 0.2 mL aliquots of the pool.

Qubit values	Control	25 ng/mL	10 ng/mL	5 ng/mL	2 ng/mL
Means (Figure 7A)	29.1	51	43.3	40.2	37.9
Std. Deviation	10	6.97	10.5	9.86	7.98
Std. Error of Mean	2.89	2.47	3.02	3.48	2.3
Theoretical recovery	0	25	10	5	2
Baseline subtracted means (Figure 7B)	0	24.6	14.2	13.8	8.8
Std. Deviation	0	6.77	14.5	8.49	13.3
Std. Error of Mean	0	2.39	4.19	3	3.83
Bioanalyzer confirmation	0	31.6	9.7	7.5	4.3

**Table 5-5: hTERT<sub>172</sub> Spike-in recovery using Qubit and confirmation by Bioanalyzer.**

Using the same methodology from the experiment in **Figures 5-7, 5-8** with the pooled plasma surrogate matrix, the spike-in and recovery process was repeated and comparing 0.5 mL and 0.2 mL of pooled control CSF matrix data.

The data indicates that the hTERT<sub>172</sub> plasmid fragment was recoverable in all spike-in concentrations through confirmation using the Bioanalyzer (**Table 5-6, Figures 5-9, 5-10**). The spike-in recovery followed a general downwards trend from the 25 ng/mL spike-in down to the 5 ng/mL spike-in with both 0.5 mL and 0.2 mL volumes however there was significant variability by Qubit quantification down at the 2 ng/mL spike-in compared to the theoretical spike-in. Bioanalyzer analysis however reported concordant data to the theoretical yield (**Table 5-6**).

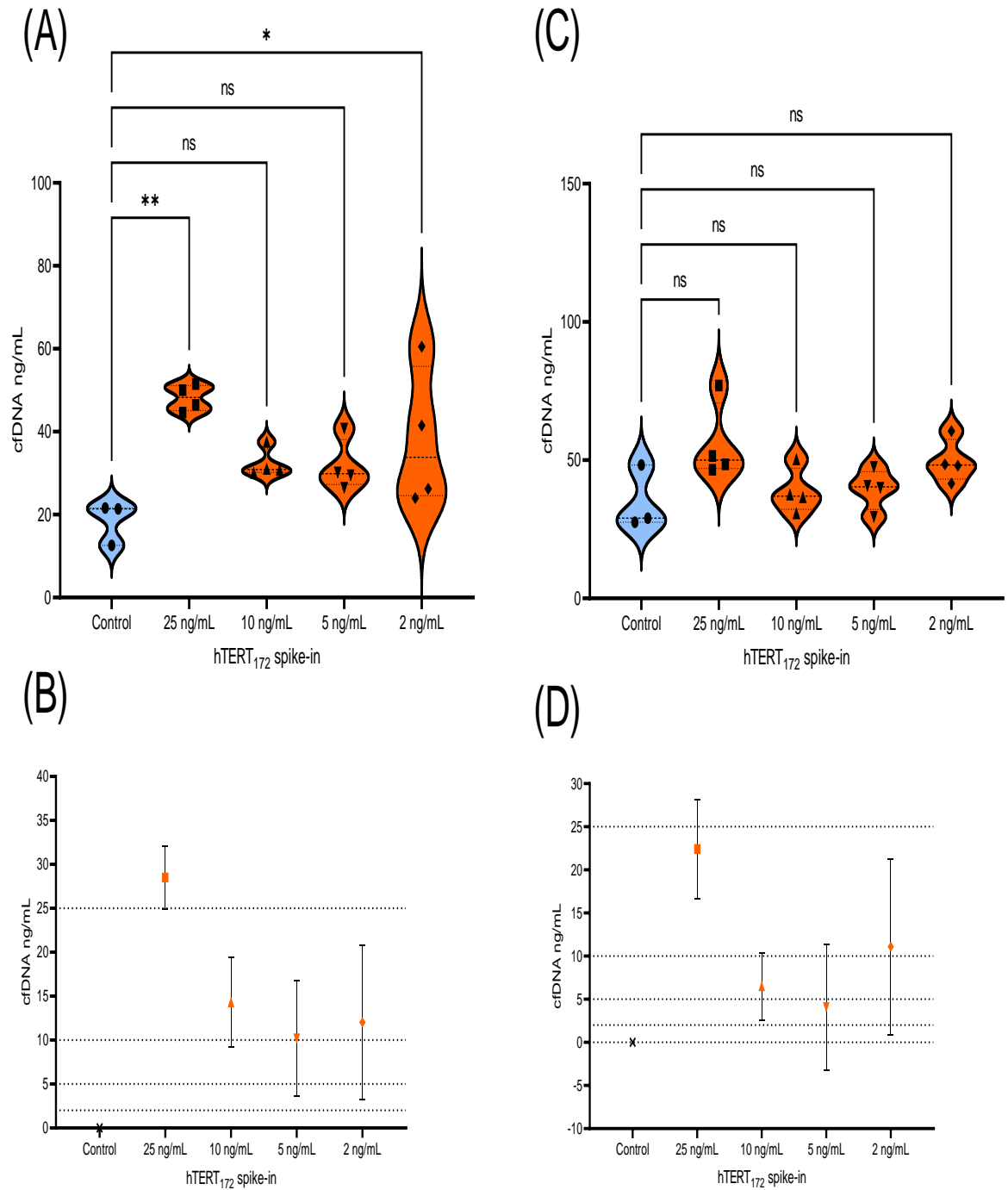


**Figure 5-9: cfDNA Spike-in & recovery experiment from 0.5 mL and 0.2 mL CSF pooled matrix.**

(A,C) Qubit data of control CSF cfDNA vs spike-in hTERT<sub>172</sub> at various concentrations: 25 ng/mL, 10 ng/mL, 5 ng/mL & 2 ng/mL. n=3. (B,D) Baseline-subtracted graph of (A,C). Dotted line indicate theoretical yield. Graphs created on GraphPad Prism v9

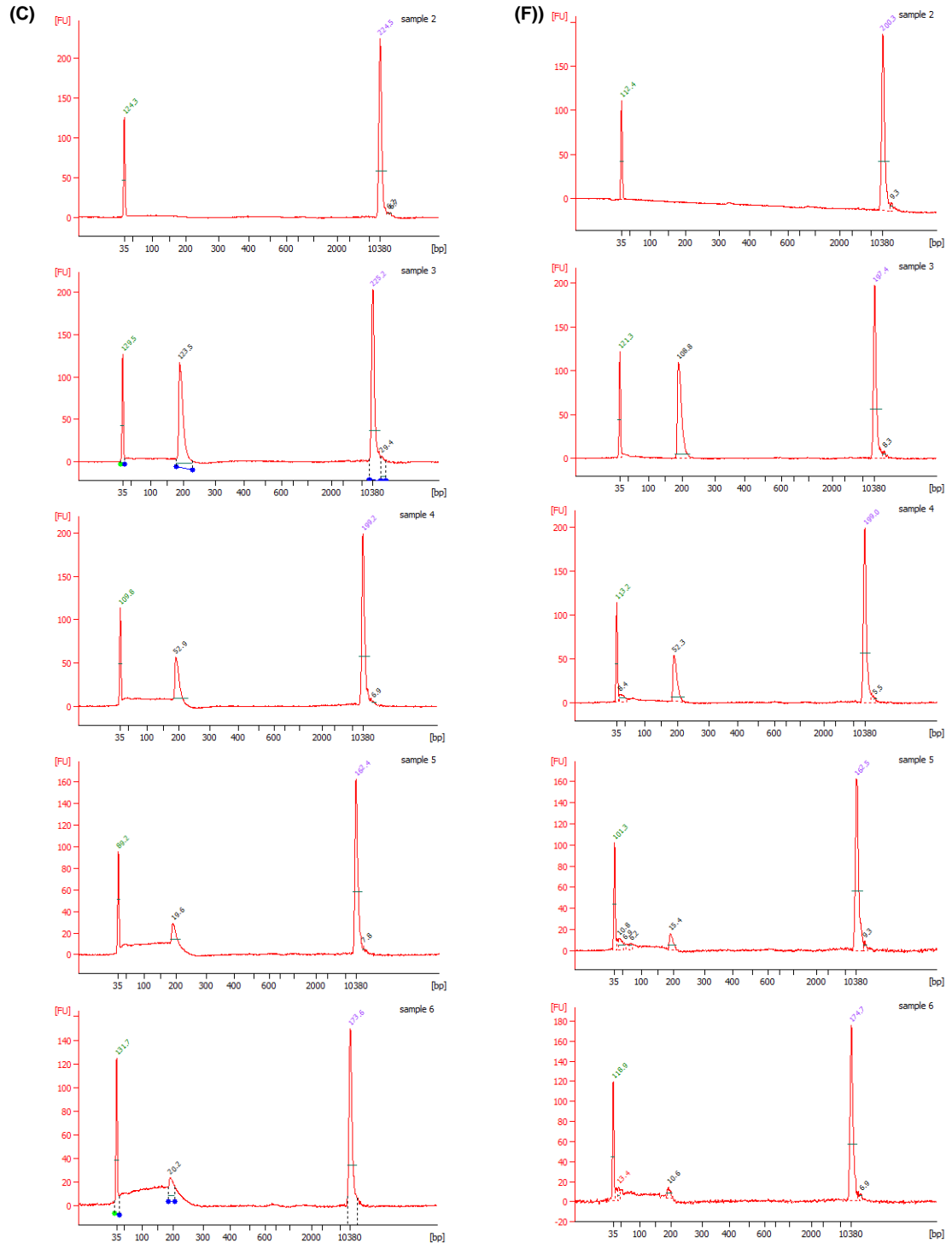


**Figure 5-10: Bioanalyzer electropherograms** (i) Control (ii) 25 ng/mL hTERT<sub>172</sub> (iii) 10 ng/mL hTERT<sub>172</sub> (iv) 5 ng/mL hTERT<sub>172</sub> (v) 2 ng/mL hTERT<sub>172</sub>. Peak at 35 bp (left hand of electropherogram) corresponds to the lower marker. Peak at ~10380 bp (right hand of electropherogram) corresponds to the upper marker. X-axis is measured in Fluorescence Units [FU], Y-axis measured in time. All samples were baseline corrected and peaks were detected automatically by Expert 2100, software version 1.03.

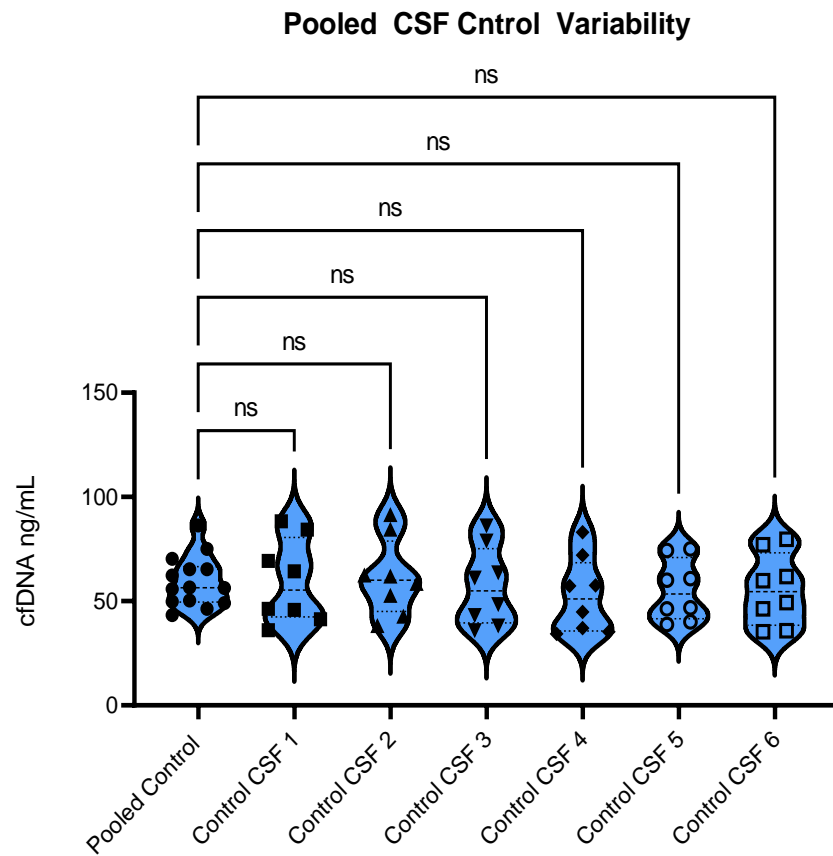
0.5 mL CSF					
Qubit Values	Control	25 ng/mL	10 ng/mL	5 ng/mL	2 ng/mL
Mean (Figure 9A)	18.5	48.2	32.3	31.7	38.1
Std. Deviation	5.14	3.16	3.48	6.22	16.9
Std. Error of Mean	2.97	1.58	1.74	3.11	8.43
Theoretical recovery	0	25	10	5	2
Baseline subtracted means (Figure 9B)	0	28.5	14.3	10.2	12
Std. Deviation	0	3.55	5.09	6.56	8.76
Std. Error of Mean	0	2.05	2.94	3.79	5.06
Bioanalyzer confirmation (Figure 10A)	0	19.6	10.7	4.2	2.5
0.2 mL CSF					
Qubit Values	Control	25 ng/mL	10 ng/mL	5 ng/mL	2 ng/mL
Mean (Figure 9C)	34.9	55.9	38.8	39.4	49.6
Std. Deviation	11.6	14.2	8.22	7.43	7.92
Std. Error of Mean	6.68	7.12	4.11	3.72	3.96
Theoretical recovery	0	25	10	5	2
Baseline subtracted means (Figure 9D)	0	22.4	6.5	4.08	11.1
Std. Deviation	0	5.76	3.91	7.32	10.2
Std. Error of Mean	0	3.32	2.25	4.22	5.89
Bioanalyzer confirmation (Figure 10B)	0	23.8	6.1	3.5	0.9

Table 5-6: 0.5 and 0.2 mL CSF spike-in and recovery experiments.

Collectively, these results suggest that at low volumes of CSF, recovery of hTERT<sub>172</sub> surrogate cfDNA spiked-in at various concentrations is possible and the molecule can even be detected down to the 2 ng/mL concentration.

We also examined the potential for any variability in our pooled control CSF samples by comparing extracted cfDNA quantities from individual control CSFs to the pooled CSF matrix. All of the six individual control CSFs which were pooled had very similar levels of cfDNA recovered compared to the pooled CSF control matrix and statistical analysis indicated no significant differences between the means of the individual samples compared to the pool, indicating a stable background level of cfDNA (**Figure 5-7**).





**Figure 5-11 : Pooled control CSF variability.** cfDNA was extracted from 0.2 mL CSF from six individuals. Quantification by Qubit dsDNA HS Assay. Two 3  $\mu$ L readings were taken for each individual. Data is presented as a mean of two readings and  $\pm$  SD error bars. Blue dot represents pooled control CSF sample. Two-tailed One-way ANOVA with multiple comparisons corrected by Dunnett's multiple comparisons tests; alpha 0.05 All graphs were created on GraphPad Prism v9.

#### 5.1.4 Patient sample CSF cfDNA

Having carried out several spike-in and recovery experiments investigating the performance of the cfDNA extraction kit, the next step was to extract cfDNA from patient CSF samples. The Halsey biobank contains several CSF samples taken at various time-points spanning from diagnosis to end of treatment. During a patient's treatment, CSF is removed during intrathecal administration of chemotherapy, typically at diagnosis, day 8, day 29 of induction therapy and then between 10 and 26 more times during 2-3 years of continuing therapy.

This project used samples taken during induction (early) and included a late CSF sample taken after 1 year of treatment, henceforth known as "late sample". At this point in treatment, the leukaemic burden within the CNS is expected to be low to non-existent due to the intensive chemotherapy treatment. This biobank also included samples from patients who went onto relapse in the CNS and patients who were classified as CNS3, i.e., high leukaemic burden in the CNS at diagnosis.

The first question to be addressed was what levels of cfDNA are expected at these different CSF sample time-points. cfDNA kinetics inside the CNS space may be affected by different factors, for example ongoing treatment. It is hypothesized that the majority of cfDNA comes from cell death processes such as apoptosis and necrosis, but it is also reported that cfDNA can be actively secreted by living and healthy cells. One can hypothesize that as treatment continues past diagnosis date (Dx) more and more cells will die within the CNS, thus releasing more cfDNA assuming that the majority of cfDNA is released by cell death. One could also hypothesize that the levels of cfDNA at diagnosis could be higher compared to a year into treatment due to leukaemic cells in the CNS which could be potentially

actively secreting cfDNA compared to a year into the intensive treatment where the leukaemic burden is very low or non-existent.

The majority of samples in this cohort had ~100  $\mu$ L of CSF and cfDNA was extracted from 100  $\mu$ L of CSF and eluted in 50  $\mu$ L elution buffer. As demonstrated in **Figure 5-12**, all the diagnostic samples averaged around 10.86 ng (SD: 1.873; SEM: 0.2418; Lower 95% confidence interval 10.38; Upper 95% confidence interval 11.35) of cfDNA recovered, a relatively small amount of DNA.

First, total levels of cfDNA in diagnostic samples and late control samples were compared and no significant difference between the groups (**Figure 5-13 A**). Comparison between diagnostic samples and matched day 8 and day 29 samples saw no significant difference between the groups with all groups again averaging around 10 ng of extracted cfDNA (**Figure 5-13 B**).

When examined individually, the quantity of cfDNA recovered for the matched diagnostic, day 8 and day 29 samples followed no consistent trend to support the hypothesis above of a treatment induced increase in cfDNA release through cell-death mechanisms (**Figure 5-13C**).

Next, the extracted levels of cfDNA from the CSF of three patients taken at the time of relapse were analysed. The hypothesis being that these samples would likely have abundant cells in the CNS and thus potentially secrete cfDNA. These patient samples had very similar levels of cfDNA present compared to the other test groups averaging around 10 ng (**Figure 5-14**) .

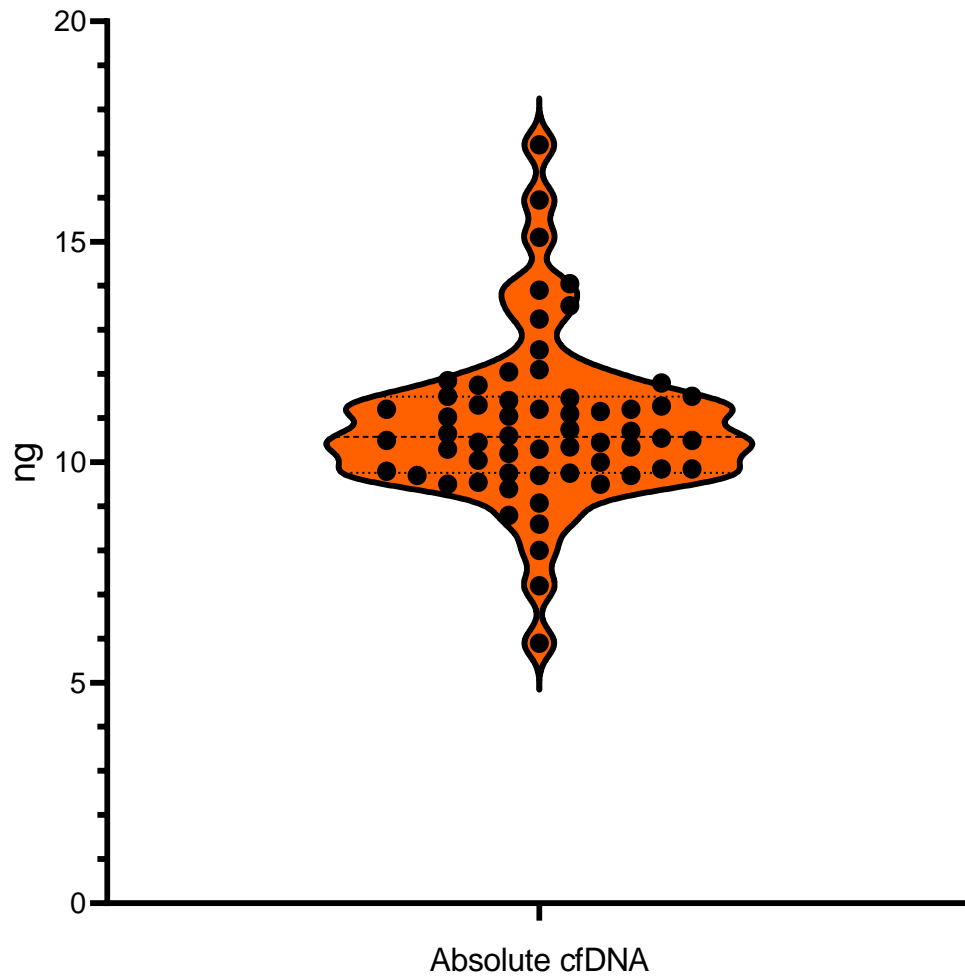


**Figure 5-12: Absolute cfDNA quantity from ~100  $\mu$ L diagnostic CSF samples.** cfDNA recovered from CSF of diagnostic patient samples using QIAamp circulating nucleic acids kit (n=60). Data obtained by Qubit quantification. Data is represented as absolute cfDNA by multiplying the Qubit value in ng/ $\mu$ L by elution volume (50  $\mu$ L). Graphs created on GraphPad Prism v9.

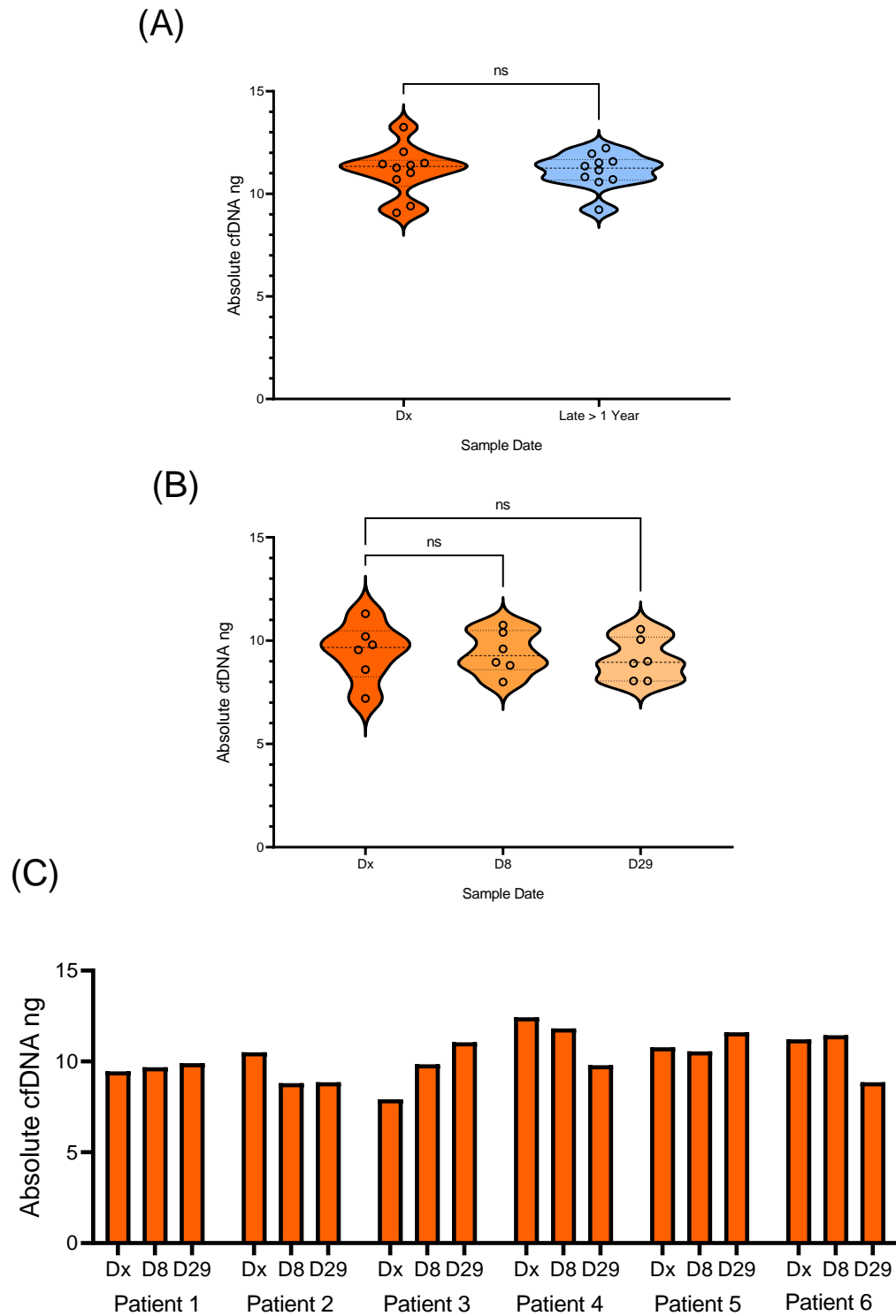


**Figure 5-13: Total levels of extracted cfDNA from patient samples.** Investigation into various patient cfDNA samples. All CSF samples were ~100  $\mu$ L and cfDNA was extracted using QIAamp circulating nucleic acids kit. All data generated from Qubit quantification. (A) cfDNA levels in Dx vs late control samples. (B) cfDNA levels in Dx, day 8 and day 29 matched samples. (C) Individual matched patient sample levels of cfDNA from Dx, day 8 and day 29. Graphs created on GraphPad Prism v9.

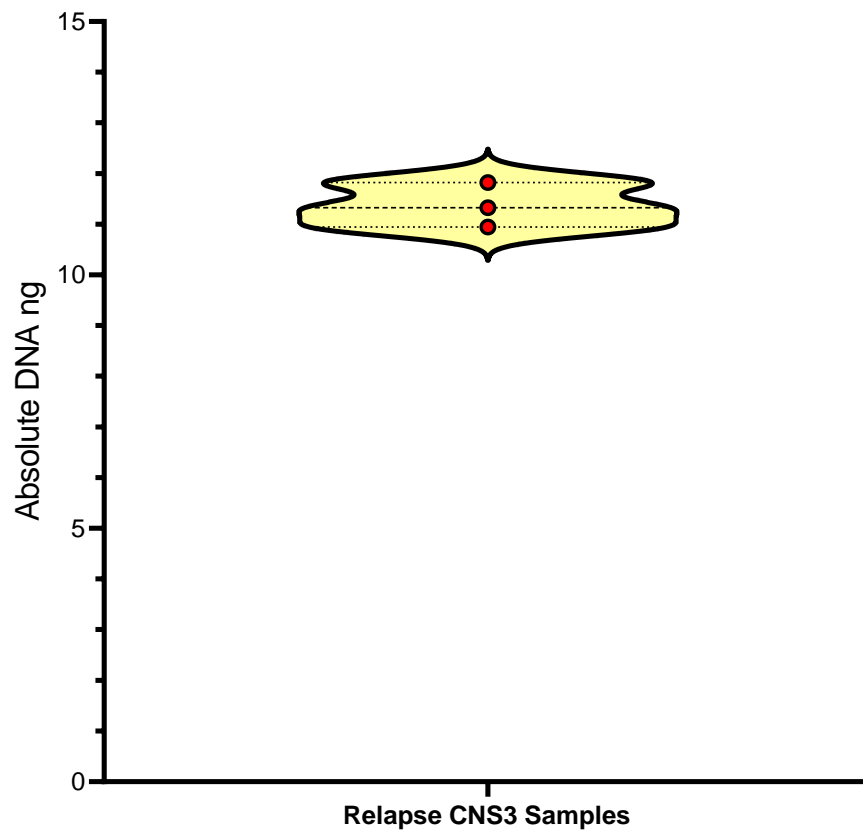


**Figure 5-14: Total cfDNA levels of Relapse patient samples**

Given the uniformity in the quantity of cfDNA and the lack of any true variability even between the different sample types, there may be external factors leading to this consistent quantity recovered. Whether this be factors out of our control such as the way the samples are handled post lumbar puncture or how they are handled and transported is unfortunately unknown.

Next, using the 2100 Bioanalyzer instrument (Agilent) and the High Sensitivity DNA Assay kit (Agilent), matching diagnostic and late samples as well as control CSF cfDNA samples were analysed to investigate the type of size distribution of cfDNA fragments from patient CSF samples. Purified cfDNA (1  $\mu$ L) was loaded onto a pressurized microchip along with a reference ladder for size determination. Using

2100 Expert software (Agilent), a smear analysis was run between the 100-300 bp range to determine the concentration of cfDNA fragments between this range.

The data in **Figure 5-15 B, Table 5-7** shows an increased distribution of small fragments between 100-300bp in all six individual control CSF groups, consistent with the size distribution of cfDNA reported in the literature. When these samples were pooled, the distribution of these cfDNA fragments appears diluted but still consistent between this size range, as expected given the pooling effects of six samples into one (**Figure 5-15 B, Table 5-7**).

Next, six diagnostic patient CSF samples and matched late control samples were compared. In the diagnostic patient CSF samples, again a distribution of fragments within this range was observed in patients P1, P4 and P5. The other three do not appear to have any cfDNA in that size range or in any range within the range limit of the Bioanalyzer assay (**Figure 5-16 A, Table 5-8**) .

Interestingly in the late samples, there appears to be a shift in the cfDNA distribution to slightly larger fragments in patient samples P1 and P5 (**Figure 5-16B, Table 5-8**). Patient P4 did not exhibit this shift and appeared to have the majority of its cfDNA fragments at a similar size to its matched diagnostic sample. The remaining three appear to have very little amounts of cfDNA in the tested range and within the range limit of the Bioanalyzer assay (**Figure 5-11**). This data suggests that cfDNA from patient diagnostic CSF samples likely lie in the 100-300 bp range thus supporting the hypothesis that this cfDNA is of apoptotic origin.

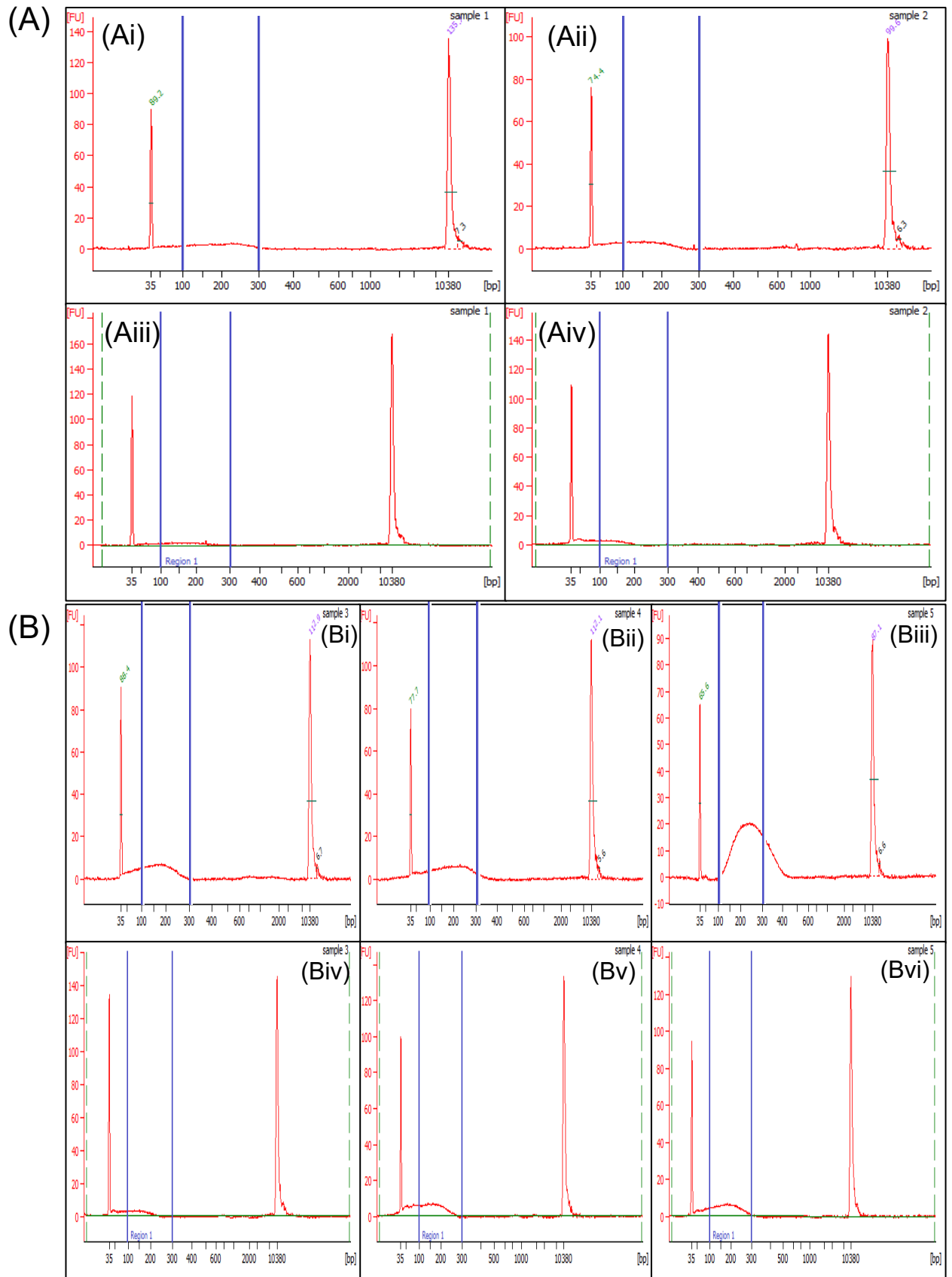
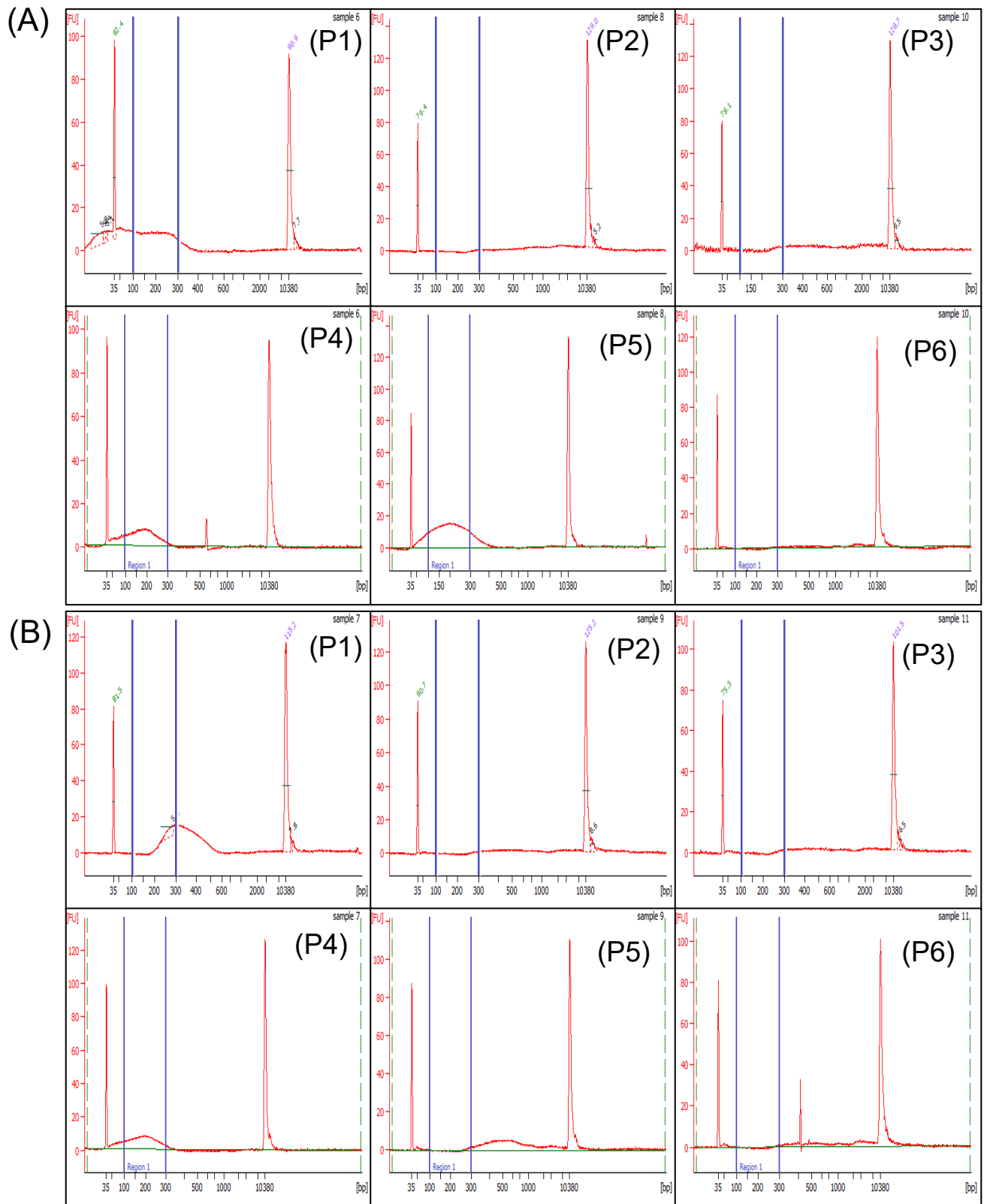


Figure 5-15: Electropherograms of control CSF: cfDNA fragment size analysis



Sample ID	From [bp]	To [bp]	Corr. Area	% of Total	Average Size [bp]	Conc. [pg/μl]	Molarity [pmol/l]	Size distribution in CV [%]
<b>Pooled 1 (Ai)</b>	100	300	32.4	29	138	38.16	432.1	18.6
<b>Pooled 2 (Aii)</b>	100	300	60.9	52	164	90.98	909.5	24.9
<b>Pooled 3 (Aiii)</b>	100	300	43.4	49	174	44.82	427	26.1
<b>Pooled 4 (Aiv)</b>	100	300	66.8	68	196	78.45	676.5	26.7
<b>Control 1 (Bi)</b>	100	300	131.4	55	168	150.27	1,468.90	24.8
<b>Control 2 (Bii)</b>	100	300	137.6	69	185	147.8	1,334.10	26.6
<b>Control 3 (Biii)</b>	100	300	387	79	223	539.08	3,878.30	20.2
<b>Control 4 (Biv)</b>	100	300	39.4	21	177	46.69	300	56.4
<b>Control 5 (Bv)</b>	100	300	39.5	44	149	42.71	455.9	20.5
<b>Control 6 (Bvi)</b>	100	300	160.6	59	199	193.92	1,651.80	27.2

**Table 5-7: cfDNA size fragment analysis from control CSF.** Electropherograms of six individual control CSF samples. The table depicts the exported data extrapolated from the electropherograms.



**Figure 5-16: Electropherograms of patient and matched control CSF: cfDNA fragment size analysis.** (A) Electropherograms of six different diagnostic CSF cfDNA patient samples. (B) Electropherograms of six matched late CSF cfDNA patient samples.

Sample ID	From [bp]	To [bp]	Corr. Area	% of Total	Average Size [bp]	Conc. [pg/ $\mu$ l]	Molarity [pmol/l]	Size distribution in CV [%]
Patient 1 - Day 1	100	300	156.8	71	185	190.9	1,720.40	26.5
Patient 2 - Day 1	100	300	388.3	70	198	428.7	3,670	27.6
Patient 3 - Day 1	100	300	1.5	3	283	1.6	8.3	4.4
Patient 4 - Day 1	100	300	185.1	42	196	269	2,355.90	29
Patient 5 - Day 1	100	300	1.2	1	283	1.2	6.7	11.1
Patient 6 - Day 1	100	300	6.1	5	275	5.8	32.3	10.1
Patient 1 - Late	100	300	164.4	73	192	202.7	1,766.60	26.4
Patient 2 - Late	100	300	4.5	2	275	5.1	30.3	14.5
Patient 3 - Late	100	300	2.4	2	260	3.8	26.9	24.6
Patient 4 - Late	100	300	124.4	33	263	123.2	709.6	9.3
Patient 5 - Late	100	300	1.9	2	284	2	10.7	9.7
Patient 6 - Late	100	300	5.8	6	264	7.2	46.7	19.8

**Table 5-8: cfDNA size fragment analysis from diagnostic (DX) and late (>1 year) samples.** The table depicts the exported data extrapolated from the electropherograms.

## **5.2 Detecting ctDNA from Samples of CSF**

The next step in this project was to attempt to detect ctDNA from samples of CSF to identify potential ALL-specific genetic biomarkers using two different highly sensitive platforms. The extraction experiments indicate that cfDNA can be extracted from low volumes of patient sample CSF and the data indicates a uniformity in the extraction quantification values with a potential expected range of cfDNA fragments around the 100 – 300 bp range. Given the low quantity of cfDNA recovered from our low-volume samples, using highly sensitive next-generation platforms such as droplet digital PCR (ddPCR) and next generation sequencing (NGS) for detection of leukaemia specific targets is essential.

### **5.2.1 Detection of KRAS G12D using ddPCR**

Droplet digital PCR is a third generation PCR technology and a highly favourable alternative to RQ-PCR which is considered the gold-standard. It does not require a standard curve as DNA samples are partitioned into several thousand oil-in-water droplets allowing absolute quantification of the DNA sample through fluorescent probes. The amplification reaction that occurs within each individual droplet is enhanced due to the high ratio of DNA molecules to PCR reagent and the fact that PCR inhibitors no longer influence the reaction, creating a pro-amplification environment. The droplets are then independently analysed and quantified using Poisson statistics to determine absolute copy number of target molecules in positive droplets [111, 112].

Detection of tumour-specific mutations in ctDNA from CSF samples is reported in the literature for various CNS tumours, typically from oncogenes such as TP53, BRAF, NRAS & KRAS [113]. NRAS and KRAS frequently undergo mutations

associated with CNS-ALL and can typically present in around 10-25% of newly diagnosed childhood ALL patients and 35% of all childhood ALL relapse cases [114, 115]. In this study a QX200 Droplet Digital PCR system (Bio-Rad) was used to attempt to detect low frequency mutant KRAS G12D in our patient samples of CSF ctDNA. KRAS G12D has been reported to be present in 20-25% of newly diagnosed ALL patients and recent research has reported variant allelic frequencies of KRAS G12D at ~0.4% [114, 116].

First, to test the performance of a ddPCR KRAS G12D assay, a multiplex reference standard DNA set (RSS) containing different allelic frequencies of  $\frac{Mut}{WT}$  genes for EGFR, KRAS, NRAS, PI3KCA at 100% WT, 5%, 1% and 0.1%. The expected allelic frequencies however for KRAS specifically are set at 100%WT, 6.3%, 1.3% and 0.13% (**Table 5-9**). For this experiment, samples of the QA elution buffer were spiked with the different allelic frequencies at various concentrations of the RSS DNA: 50 ng, 10ng, 5ng and 1 ng to determine the limit of input DNA needed to replicate these allelic frequencies.

The results show that expected and observed allelic frequencies are matched closely at 50 ng, 10 ng and 5ng of input RSS cfDNA (**Figure 5-17**). At 1 ng of input RSS cfDNA, WT KRAS is detected however no mutant KRAS G12D is detected at any of the allelic frequencies tested.

This data suggests an ideal input DNA of 5ng is needed to be able to detect KRAS G12D at the various allelic frequencies tested down to 0.13%. Of note, a false positive was detected 5 ng RSS DNA in the negative control wildtype resulting in an observed allelic frequency of 99.67% instead of 100% WT.

	Acceptance criteria	Reference Standard Set DNA Expected Frequency ( EGFR, KRAS, NRAS, PI3KCA)	Expected frequency $\frac{Mut}{WT}$
Allelic frequency (AF)	0% expected frequency for WT up to 0.01%	100% WT	100% WT
	AF $\geq 5\%$ <10% $\pm 30\%$	5%	6.30%
	AF $\geq 1\%$ <5% $\pm 40\%$	1%	1.30%
	AF < 1% $\pm 50\%$	0.10%	0.13%

**Table 5-9:Expected frequencies and Acceptance criteria for KRASG12D Multiplex I cfDNA RSS – Horizon**

Next, using cfDNA extracted from 0.2 mL of pooled control CSF (Mean ~0.26 ng/uL; 13 ng absolute cfDNA), the assay performance was tested to attempt to see if WT KRAS would be detectable in such low volumes of CSF. Mutant KRAS G12D was not expected to be detected in these samples as these samples were from “healthy” volunteers.

The low concentration of cfDNA extracted and the maximum volume of DNA input into the ddPCR reactions allows a total cfDNA input of ~1.5 ng per total PCR reaction, only around 30% of the ideal amount (5 ng) to confidently detect KRAS mut/WT at our lowest allelic frequency of 0.1%. The results show that WT KRAS was detected in all pooled CSF samples at these low volumes, suggesting that even with this low amount of CSF and extracted cfDNA, the assay can detect cfDNA targets in cfDNA (**Table 5-10**).

The last experiment run before testing patient CSF samples, was designed to test the performance of the extraction and assay workflow end-to end. For this experiment, 5 ng of RSS cfDNA (spike-in quantity based off data from **Figure 5-17**) was spiked-in to 0.2 mL of control pooled CSF and extracted using the QIAamp Circulating nucleic acids kit (QA). Due to material limitations, this experiment was only run once to inform of the end-to-end performance. The data showed that at 5 ng of spike-in input RSS cfDNA, KRAS G12D was able to be detected down to an allelic frequency of 1% Mut/WT. At 0.1% allelic frequency, only WT KRAS was detected (**Figure 5-18**).

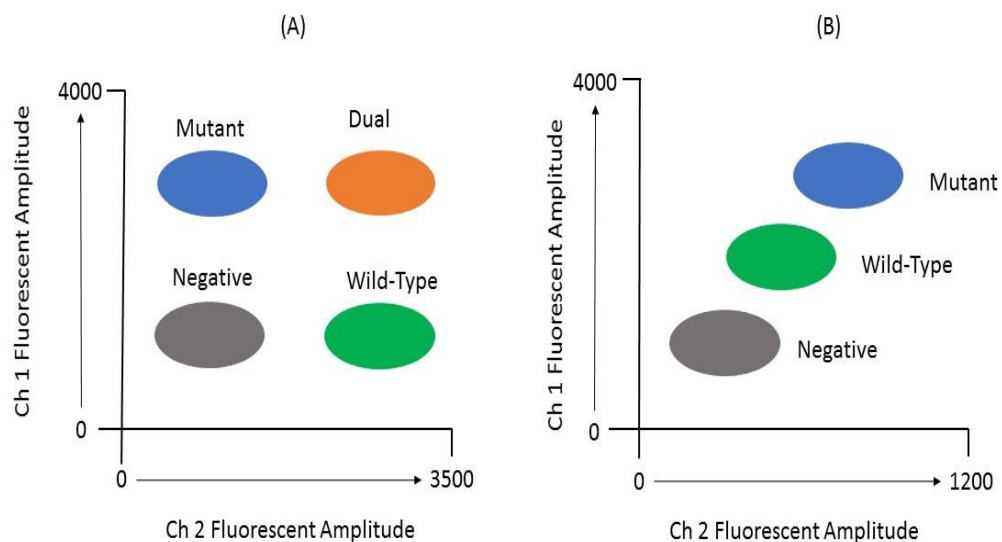
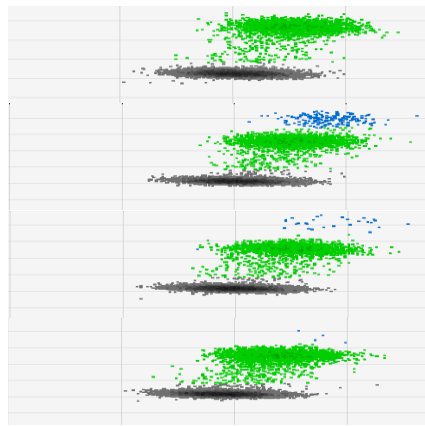
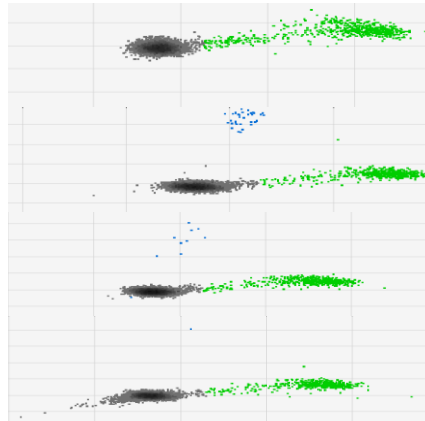


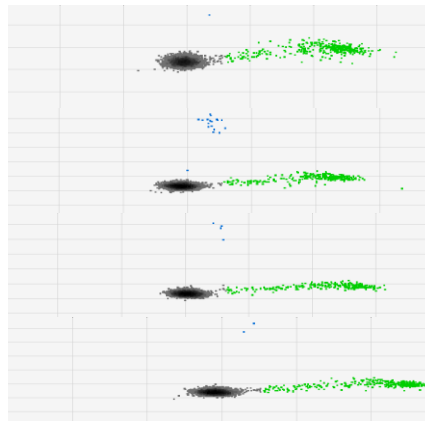
**Figure 5-17-1:** ddPCR rain plot interpretation. (A) Probe method 1: FAM + HEX probes. Dual labelled FAM probes cause mutant only positive droplets to cluster in the blue mutant bubble. Dual labelled HEX probes cause WT only positive droplets to cluster in the green WT bubble. Positive droplets containing both FAM and HEX probes cause dual positive droplets to cluster in the orange bubble. Negative droplets containing neither FAM nor HEX cluster in the grey bubble. (B) Probe method 2: FAM only probe. The dual labelled FAM probe causes mutant only positive droplets to cluster in the blue mutant bubble. In the absence of HEX probes, WT KRAS will bind to single-labelled WT probes contained within the FAM probe solution. The single-labelled probe causes WT KRAS positive droplets to cluster below FAM positive and above negative grey droplets. The WT KRAS cluster had to be manually recognised as HEX cluster to obtain a value in copies/ $\mu$ L for allelic frequency calculations. This was achieved by setting thresholds above the negative droplet cluster and below the FAM cluster. Ch1 Fluorescent Amplitude refers to the fluorescence corresponding to FAM probes. Ch2 Fluorescent Amplitude refers to the fluorescence corresponding to HEX probes. Note the x-axis scale difference between (A) and (B) due to the absence of HEX probes and the single-labelled WT probes.



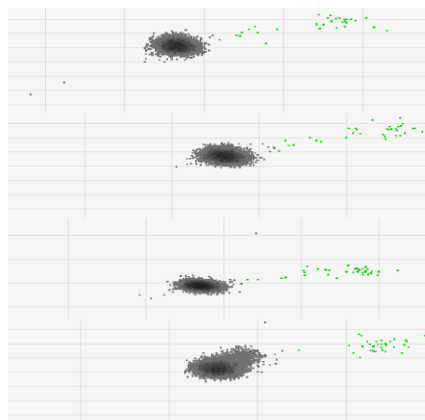
50 ng FAM probe only	Target	Copies per 1 $\mu$ L Well	Copies per 20 $\mu$ L Well	Expected Allelic Frequency	Observed Allelic Frequency	Accepted Droplets
WT 100%	FAM	0	0	100% WT	100% WT	15652
	HEX	281	5620			15652
5% AF	FAM	13.8	276	5%	5%	14692
	HEX	267	5340			14692
1% AF	FAM	2.4	48	1%	1%	14761
	HEX	232	4640			14761
0.1% AF	FAM	0.3	6	0.10%	0.10%	15886
	HEX	290	5800			15886



10 ng FAM + HEX probes	Target	Copies per 1 $\mu$ L Well	Copies per 20 $\mu$ L Well	Expected Allelic Frequency	Observed Allelic Frequency	Accepted Droplets
WT 100%	FAM	0	0	100% WT	100% WT	16830
	HEX	52	1040			16830
5% AF	FAM	2.8	56.0	5%	6%	17351.3
	HEX	46.4	928.7			17351.3
1% AF	FAM	0.8	16.3	1%	2%	15652.7
	HEX	43.6	872.7			15652.7
0.1% AF	FAM	0.1	2.1	0.1%	0.20%	15111.0
	HEX	50.3	1006.7			15111.0



5 ng FAM + HEX probes	Target	Copies per 1 $\mu$ L Well	Copies per 20 $\mu$ L Well	Expected Allelic Frequency	Observed Allelic Frequency	Accepted Droplets
WT 100%	FAM	0.09	1.8	100% WT	99.67%WT	12349
	HEX	27.6	552.7			12349
5% AF	FAM	1.3	26.0	5%	5.7%	14189
	HEX	22.7	453.3			14189
1% AF	FAM	0.3	6.0	1%	1.6%	15642
	HEX	18.9	378.0			15642
0.1% AF	FAM	0.1	2.8	0.1%	0.4%	17206
	HEX	24.3	486.0			17206



1 ng FAM + HEX probes	Target	Copies per 1 $\mu$ L Well	Copies per 20 $\mu$ L Well	Expected Allelic Frequency	Observed Allelic Frequency	Accepted Droplets
WT 100%	FAM	0	0	100% WT	100%WT	14330
	HEX	2.5	50			14330
5% AF	FAM	0	0	5%	ND	16241
	HEX	2.3	46			16241
1% AF	FAM	0	0	1%	ND	14994
	HEX	2.8	56			14994
0.1% AF	FAM	0	0	0.10%	ND	14031
	HEX	2.8	56			14031

**Figure 5-17: Fluorescence Amplitude plots of allelic frequencies.** These amounts of RSS DNA were obtained by diluting stock solutions [40 ng/ $\mu$ L] of RSS DNA in Buffer AVE. Values given in copies/ $\mu$ L for both FAM (Mut) and HEX (WT). Allelic Frequencies calculates as follows:  $\frac{Mut}{WT} \times 100$ . Data interpretation given in Figure 5-17-1.



Sample	Target	Copies Per 1 $\mu$ L Well	Copies Per 20 $\mu$ L
Pooled control CSF 1	FAM	0	0
FAM + HEX probes	HEX	1	20
Pooled control CSF 1	FAM	0	0
FAM + HEX probes	HEX	1.2	24
Pooled control CSF 1	FAM	0	0
FAM + HEX probes	HEX	1	20
Pooled control CSF 1	FAM	0	0
FAM only probes	HEX	1	20
Pooled control CSF 2	FAM	0	0
FAM + HEX probes	HEX	0.21	4.2
Pooled control CSF 2	FAM	0	0
FAM + HEX probes	HEX	0.5	10
Pooled control CSF 2	FAM	0	0
FAM only probes	HEX	0.5	10

**Table 5-10: ddPCR results from 0.2 mL CSF extracted cfDNA.** Values given in copies for FAM (mutant) and HEX (WT)



**Figure 5-18: Frequency Amplitude plots 5 ng spiked into control CSF.** Extracted 5 ng RSS DNA – 5 ng of RSS DNA was spiked into 0.2 mL pooled control CSF samples. Following extraction by QIAamp CNA kit, the sample of cfDNA was analysed by ddPCR.

Finally, 13 patient samples, each with a diagnostic and a matched late sample, were tested for the presence of WT KRAS and mutant KRAS G12D. The cfDNA extracted from all samples again averaged around 0.23 ng/ $\mu$ L thus giving us around 1.5 ng of total input DNA per ddPCR reaction. Only patients 3, 6 and 12 presented with positive KRAS G12D droplets out of all sets of 13 patient samples. Patients 3 and 6 both presented with detectable WT KRAS in both diagnostic and late samples. Patient 12 presented with Mutant KRAS and WT KRAS in the late sample suggesting the extremely low presence of ctDNA in the late sample (**Figure 5-19**).

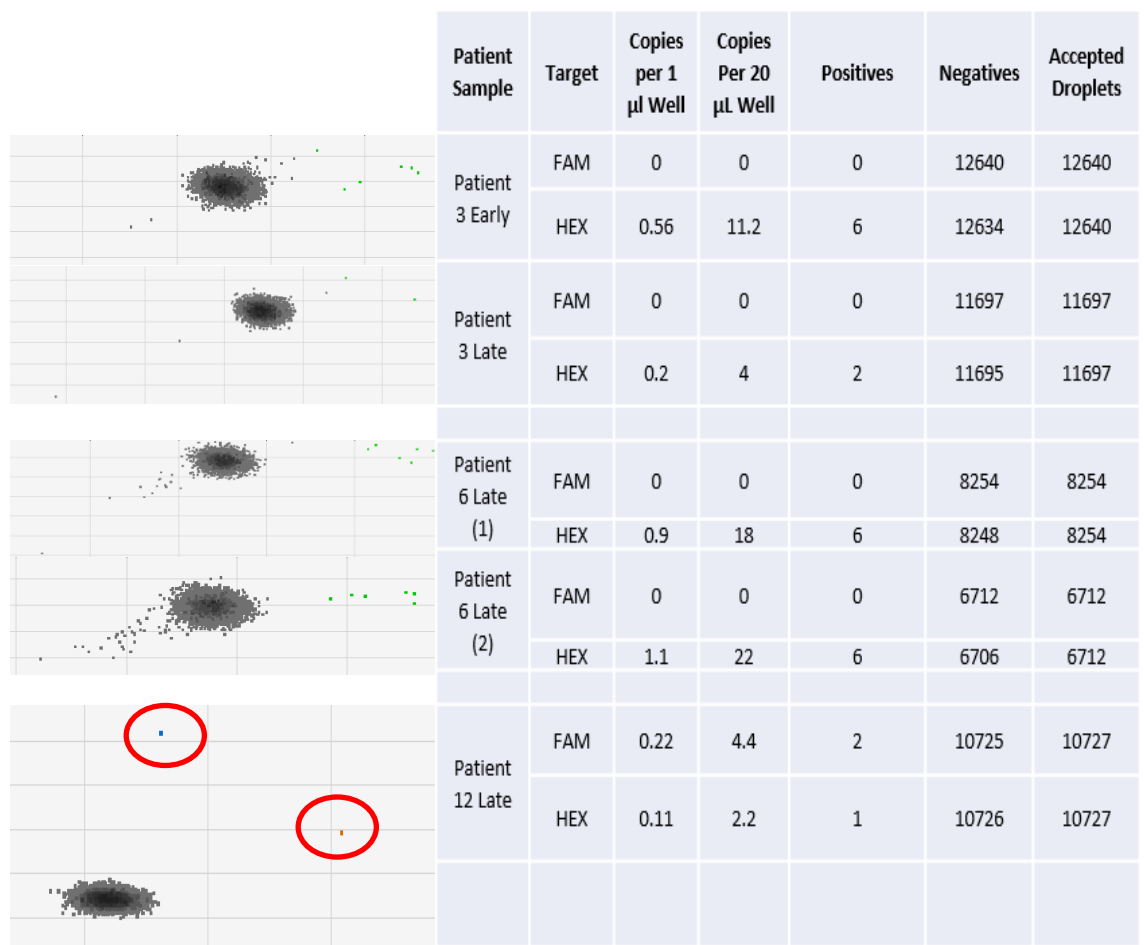


**Figure 5-19: KRAS G12D/ WT KRAS assay results from 13 patient samples cfDNA extracted with QIAamp circulating nucleic acids kit. Patients 3,6 and 12 present with positive droplets.**

However, given the extremely low number of positive droplets in patient 12 and factoring in the potential for false positives as seen in **Figure 5-17**, this result does not give us full confidence of the presence of ctDNA in these samples. What these results do show is that cfDNA can be extracted and detected using sensitive platforms such as ddPCR given the low volume and concentration of our starting DNA sample. There may be several factors at play in this situation which could lead to the poor recovery of ctDNA tested in these experiments. These patient samples have been in storage at -80 for ~4 years and the manner of their processing and handling from the point of lumbar puncture CSF sampling to storage is known to be poor.

Of course, the low quantity of CSF which underwent the cfDNA extraction process in conjunction with the low quantity of cfDNA present in those samples also may contribute to the quality of the results. Also, the low prevalence of KRAS G12D mutations in diagnostic ALL samples could mean that these patient samples simply do not have this mutation at diagnosis. Nevertheless, the detection of WT KRAS in patient samples indicates that cfDNA can be detected from the samples of CSF using droplet digital PCR.

### 5.2.2 Detection of IGH rearrangements using NGS

An ideal target to measure leukaemic burden in the CNS would be one which is ubiquitous and highly specific for acute lymphoblastic leukaemia. Immunoglobulin gene rearrangements are such targets as they are composed of variable (V), diversity (D) and joining (J) gene segments which recombine partially or fully resulting in a unique complementary determining region 3 (CDR3), highly specific to leukaemia cells. This target is currently used in MRD monitoring for bone marrow samples in initial diagnoses and follow ups for children with ALL.

The final stage of this project was to test another highly sensitive platform (NGS) to detect ctDNA from the CSF of leukaemic ALL patients. NGS is a promising tool for monitoring MRD in childhood ALL. All Ig/TCR gene rearrangements can be fully sequenced and importantly, clonal evolutions of ALL blasts can be sequenced and tracked both in the bone marrow as well as in extramedullary sites such as the CNS throughout treatment. Bartram and colleagues (2016) developed a thorough HTS-MRD workflow for monitoring MRD in ALL using NGS to identify rearrangements and by using known quantities of spiked in IGH sequence DNA from 3 different ALL cell lines to patient sample DNA and pooled donor lymphocyte DNA to measure the sensitivity of using ddPCR. They reported a sensitivity of  $10^{-6}$ , a 10-fold increase in sensitivity by using both ddPCR and NGS, compared to conventional RQ-PCR MRD monitoring [117].

The EuroClonality-NGS group has been involved in the standardisation of novel techniques and technologies for use in MRD analysis, building upon the fundamental work of EuroClonality-BIOMED-2 2003 study. The group recently developed and validated the use of an *in vitro/in silico* NGS protocol for MRD marker identification and analysis using five EuroMRD laboratories. The group

demonstrated higher reproducibility, a more comprehensive range of coverage of Ig/TCR loci, successful identification of bi-allelic rearrangements and a more streamlined workflow when using NGS compared to traditional Sanger sequencing methods [118]. They also provided supporting data for the use of these NGS protocols on frozen and formalin-fixed paraffin embedded tissue specimens highlighting the wide applicability of the technique and strengthening the need to implement these methodologies into the clinic.

The translation of these HTS workflows from the laboratory bench to the clinic however is a long process with many considerations. It would have to be cost-effective, quick and show increased sensitivity and specificity compared to traditional techniques of monitoring ALL MRD with RT-PCR. These may be addressed by multiplexing patient samples, a complex process which requires stringent measures to avoid inaccurate treatment stratification. The workflow would also have to be robust and consistent for it to be adapted into routine clinical practise.

In this study, a targeted NGS approach was used to target V-D-J recombination's of the IGH gene. NGS is a highly sensitive and specific platform capable of detection of leukaemia-specific nucleic acid sequences and given the complexity of the gene rearrangements, should allow for correct discrimination of leukemic cfDNA molecules. The strategy used for these experiments was based off Bartram et al., [117] with alterations to increase the amount of DNA input into the nested PCR reactions before sequencing to account for the very low quantity of cfDNA recovered from our samples of CSF.

### 5.2.2.1 *in vitro* testing of NGS protocol

First, to test the protocol, genomic DNA from four ALL cell lines was extracted and purified. The purified DNA then underwent two PCR stages for the dual adapter ligation (as described in **2.5.6.1 pg. 101**). Two sets of consensus primers were tested, one for complete IGH gene rearrangements (V-D-J) and one for incomplete IGH gene rearrangements (D-J).

VDJ sequences were detected in all cell lines, three of which were complete IGH gene rearrangements (REH and SUPB15) and two which were incomplete IGH gene rearrangements (**Figure 5-20, Table 5-11**). CDR3 sequences for the complete gene rearrangements were confirmed by comparison to Bartram et al., [117].

Next, cell culture supernatant from REH, SD1 and SEM cell lines was collected, centrifuged, and carefully filtered through a 0.2 µm filter to remove any cells and cfDNA was extracted using the QIAamp Circulating nucleic acids kit (QA). The cfDNA was then quantified and used in the 2 stage PCR reaction as above before being sequenced resulting VDJ sequences matched the genomic DNA sequences (**Figure 5-20, Table 5-11**). These experiments were performed to test the workflow end-to-end and ensure that we can detect VDJ rearrangements *in vitro* before moving onto patient samples.

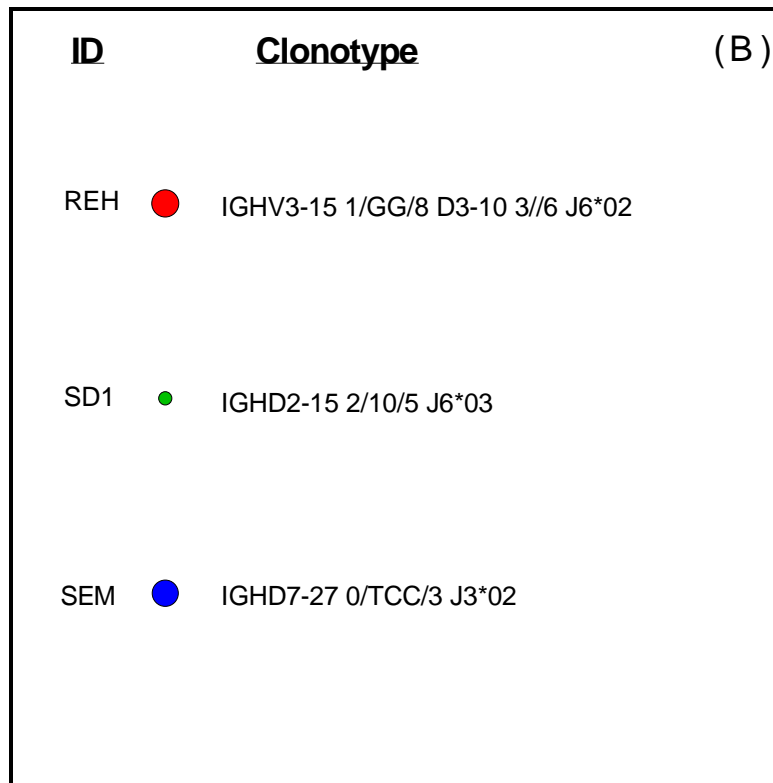
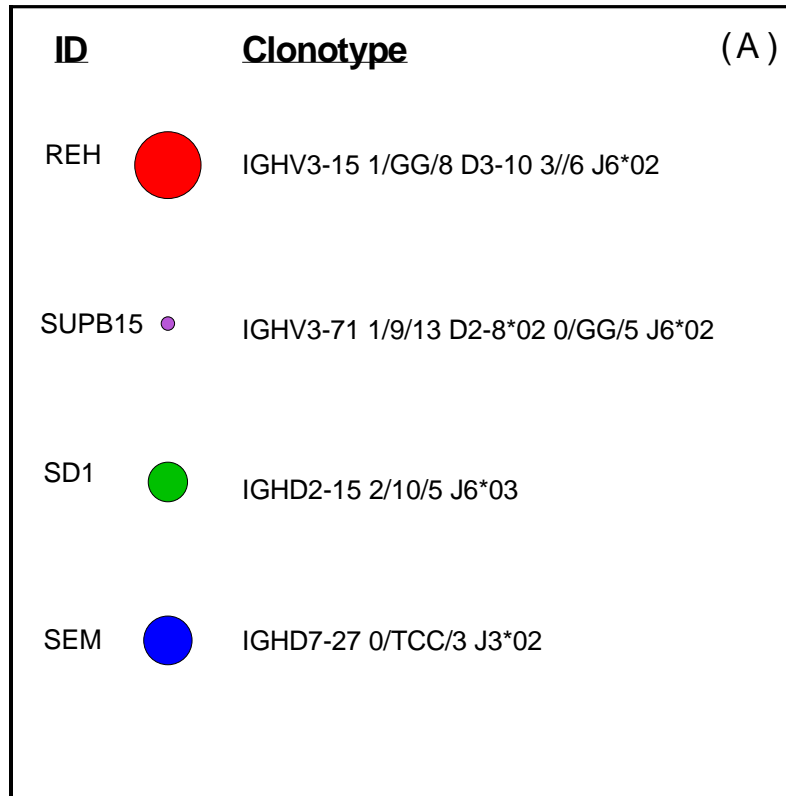


**Figure 5-20: Bubble plots: VDJ clonotypes from ALL cell-line gDNA and cfDNA detected by NGS.** (A) Sequences detected from genomic DNA. (B) Sequences detected from cfDNA. Bubbles are sized according to their read number in **Table 11**. Graphs created in GraphPad Prism v9.

Cell line ID	Clonotype	Type	V	D	J	Read #	L	% tot. reads
<b>gDNA</b>								
REH	IGHV3-15 1/GG/8 D3-10 3//6 J6*02	IGH	IGHV3-15*01	IGHD3-10*01	IGHJ6*02	208285	220	96.8
SD1	IGHD2-15 2/10/5 J6*03	IGH+		IGHD2-15*01	IGHJ6*03	26097	150	98.6
SEM	IGHD7-27 0/TCC/3 J3*02	IGH+		IGHD7-27*01	IGHJ3*02	59008	150	98.6
SUPB15	IGHV3-71 1/9/13 D2-8*02 0/GG/5 J6*02	IGH	IGHV3-71*01	IGHD2-8*02	IGHJ6*02	251	227	0.12
<b>cfDNA</b>								
REH	IGHV3-15 1/GG/8 D3-10 3//6 J6*02	IGH	IGHV3-15*01	IGHD3-10*01	IGHJ6*02	120194	140	95.5
SD1	IGHD2-15 2/10/5 J6*03	IGH+		IGHD2-15*01	IGHJ6*03	57250	150	98.6
SEM	IGHD7-27 0/TCC/3 J3*02	IGH+		IGHD7-27*01	IGHJ3*02	112446	117	98.8

**Table 5-11: NGS metrics. Type = complete or incomplete IGH rearrangements.**



### 5.2.3 Patient cfDNA

#### 5.2.3.1 Diagnostic, Day 8 and Day 29 CSF samples

It was first hypothesized that leukaemia cells release ctDNA into CSF by active secretion or by cell-death mechanisms and that levels of ctDNA may correlate to leukaemic burden within the CNS at diagnosis. cfDNA was first extracted from the diagnostic CSF of three CNS3 patients, two CNS2 patients and six CNS1 patients using the QIAamp circulating nucleic acids kit. The average concentration of cfDNA extracted was 0.253 ng/ $\mu$ L allowing an average of 3.8 ng of starting DNA sample per 1<sup>st</sup> stage PCR reaction (15  $\mu$ L) (**Table 5-12**). The cfDNA from these diagnostic CSF samples was then sequenced to attempt to detect VDJ gene rearrangements in cfDNA.

Following the 1<sup>st</sup> stage PCR reaction and subsequent sample purification, a QC check was performed to identify amplified template molecules indicating the presence of any potential IGH sequences in the CSF cfDNA samples. Unfortunately, no VDJ sequences were detected as there was no amplification in any of the samples tested (**Table 5-12**).

Next, matched diagnostic, day 8 and day 29 CSF cfDNA samples from four CNS1 patients were then tested to test the hypothesis that CNS-directed therapy causes increased cell-death within the CNS, thus releasing ctDNA in abundance. The average concentration of cfDNA extracted was 0.185 ng/ $\mu$ L allowing an average of 2.78 ng of cfDNA per 1<sup>st</sup> stage PCR reaction (**Table 5-13**). The cfDNA from these CSF samples was then sequenced to attempt to detect VDJ gene rearrangements in cfDNA.

CSF cytology classification	Original sample conc. (ng/μL)	Av. cfDNA PCR rx. Input (ng)	Post 1st PCR QC quantification
CNS3	0.271	4.065	Out of range<
CNS3	0.281	4.215	Out of range<
CNS3	0.302	4.53	Out of range<
CNS2	0.197	2.955	Out of range<
CNS2	0.344	5.16	Out of range<
CNS1	0.319	4.785	Out of range<
CNS1	0.213	3.195	Out of range<
CNS1	0.235	3.525	Out of range<
CNS1	0.237	3.555	Out of range<
CNS1	0.201	3.015	Out of range<
CNS1	0.19	2.85	Out of range
<b>Average</b>	0.253	3.8	

**Table 5-12: Cohort of CNS3, CNS2 and CNS2 patient samples tested for IGH gene rearrangements**

Patient ID	Original sample conc. (ng/μL)	Av. cfDNA PCR rx. input
P1 Dx	0.172	2.58
P1 D8	0.176	2.64
P1 D29	0.18	2.7
P2 Dx	0.191	2.865
P2 D8	0.16	2.4
P2 D29	0.161	2.415
P3 Dx	0.144	2.16
P3 D8	0.179	2.685
P3 D29	0.201	3.015
P4 Dx	0.196	2.94
P4 D8	0.192	2.88
P4 D29	0.211	3.165
P5 Dx	0.226	3.39
P5 D8	0.215	3.225
P5 D29	0.178	2.67
<b>Average</b>	0.185	2.78

**Table 5-13: Quantified cfDNA from diagnostic CSF samples. cfDNA quantified by Qubit**

Interestingly, only a diagnostic patient sample (P2) presented with a unique clonotype and identifiable CDR3 sequence at a very low abundance suggesting the presence of a lymphoblast in the CNS (**Figure 5-21, Table 5-14**). This clone disappeared in the following matched day 8 and day 29 samples (**Figure 5-22**). No clones were detected in any of the day 8 or day 29 CSF cfDNA samples.

These results while not abiding to the hypotheses put forward, at the minimum confirm that IGH gene rearrangements can be detected in the cfDNA extracted from CSF. There may be several explanations to the low sensitivity seen in these results. The presence of contaminating genomic DNA from the REH cell-line in some of the patient samples tested, including all samples from Figure 21 may be a factor (**Figure 5-28**). The samples tested in Table 12 however did not contain any genomic DNA contamination as this would have been detected in the 1<sup>st</sup> PCR stage QC check analysis. This suggests that either any ctDNA present in the samples of CSF is either at a level below the limit of detection of this method (discussed below), or that it is simply not present.

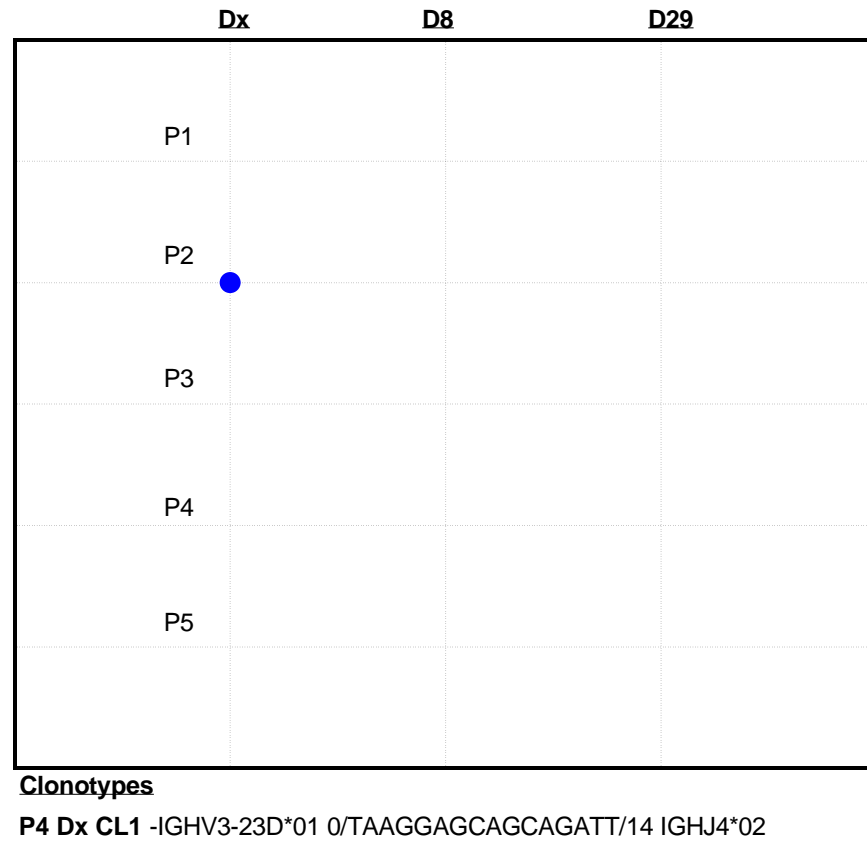


**Figure 5-21: Bubble plot representing diagnostic patient cfDNA sequencing results from 7 DX samples. CL1 = clone. Bubbles are sized according to the read number in Table 14. Graphs created in GraphPad Prism v9.**

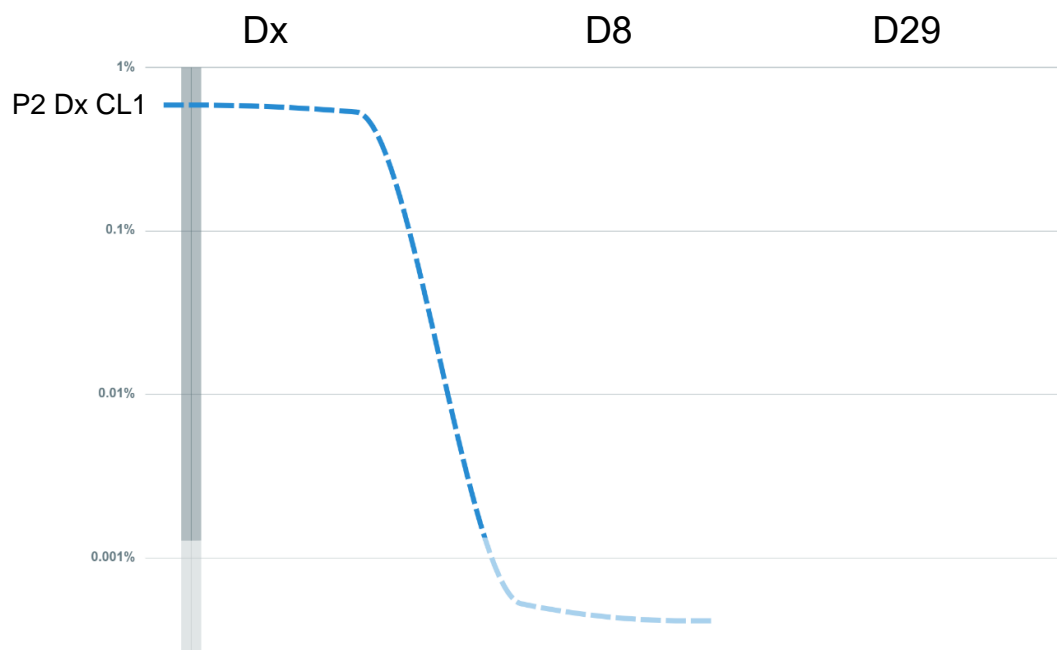


**Figure 5-22: P2 clone prevalence in Dx, D8 and D29 CSF samples**

Putative Clonotype	Size (bp)	Read #	% of total reads
IGHV3-23D*01 0/TAAGGAGCAGCAGATT/14 IGHJ4*02	112	2297 reads	0.591
<b>V-D-J sequence</b>			
TCTGCAAATGAACAGCCTGAGAGCCGAGGACACGGCCGTATATTACTGTGCGAAAGATAAGGAGCAG CAGATTTGGGGCCAGGGAACCCTGGTCACCGTCTCCTCAGGTAAG			
<b>CDR3</b>			
GCGAAAGATAAGGAGCAGCAGATT			
<b>V region end</b>			
AAAGA			
<b>V-D Junction</b>			
TAAGG			
<b>D region</b>			
AGCAGCAG			
<b>D-J Junction</b>			
ATT			
<b>J region start</b>			
TGGGG			
<b>Top V gene matches</b>	<b>Top D gene match</b>	<b>Top J gene matches</b>	
IGHV3-23*01	IGHD6-13*01	IGHJ4*02	
IGHV3-23*02		IGHJ5*02	
IGHV3-23*03			

**Table 5-14: VDJ sequence data of detected clone in diagnostic CSF sample from P2.**

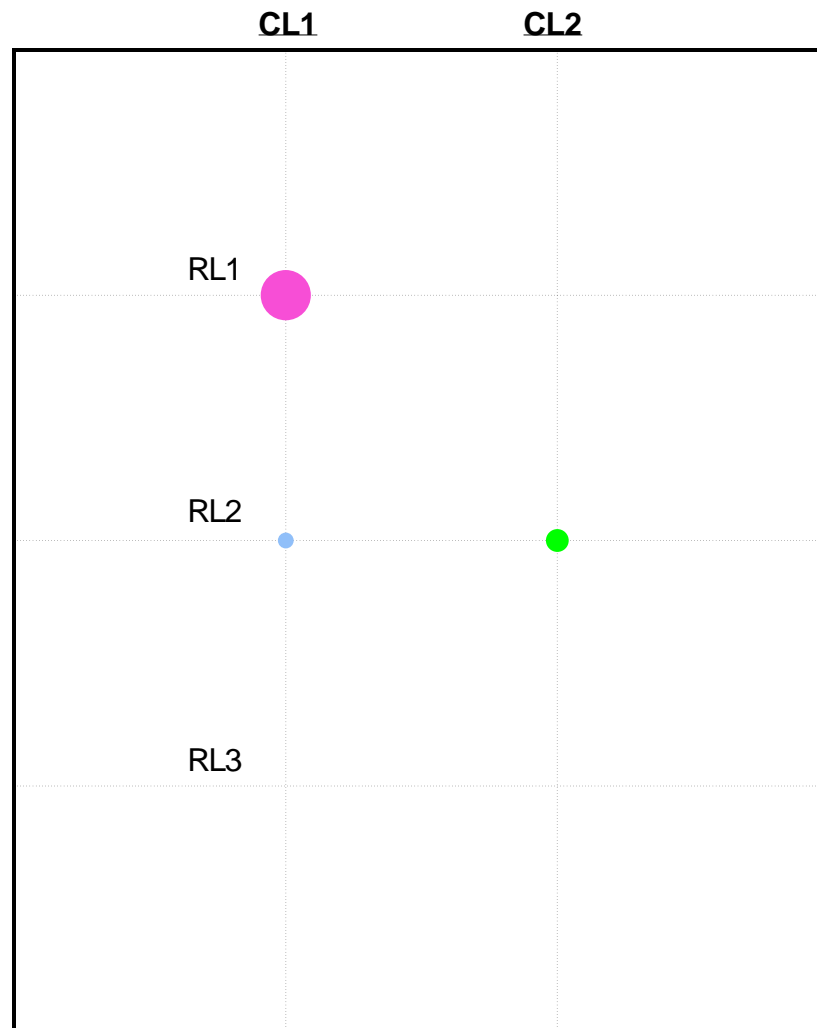
### 5.2.3.2 Relapse Samples

Next, three CNS3 relapse samples from patients who had isolated CNS relapses were tested. Leukaemic burden at time of relapse is expected to be high providing an opportunity to test whether VDJ rearrangements can be detected in the cfDNA extracted from these samples. cfDNA was extracted and quantified and values did not show any higher or lower levels of total cfDNA than any of the samples tested before (**Figure 5-23, Table 5-15**).

Patient ID	Original sample conc. ng/ $\mu$ L	Av. cfDNA PCR rx input
RL1	0.215	3.23
RL2	0.199	2.99
RL3	0.206	3.09

**Table 5-15: Relapse sample cfDNA quantification post- extraction**

The cfDNA from these CSF samples was then sequenced to attempt to detect VDJ gene rearrangements and 2/3 patients (RL1 and RL3) presented with unique clonotypes and identifiable CDR3 sequences (Figure 23). RL1 presented with one unique clonotype potentially suggesting the presence of only one clonal population of leukaemic cells in the CNS (**Table 5-18**) and RL2 presented with two unique clonotypes suggesting the presence of 2 clonal leukaemic populations in the CNS (**Tables 5-19, 5-20**).



#### Clonotypes

**RL1 CL1** - IGHV3/OR16-9\*01 16/CCTACAGGTCCGCAT/0  
IGHJ6\*02

**RL2 CL1** - IGHV4/OR15-8\*01  
1/GGGGAGAGATCCGATCGAGGGGGAACCTTTCT/1  
IGHD3-10\*01 0//5 IGHJ4\*02

**RL2 CL2** - IGHV3-13\*03 1/TCTGGGGGAACCTTTCT/1  
IGHD3-10\*01 0//5 IGHJ4\*02

**Figure 5-23: Bubble plot representing relapse patient cfDNA sequencing results from 4 RL samples.** CL = clone. Bubbles are sized according to their read number in Tables 16-18 . Graphs created in GraphPad Prism v9.

To confirm that the presence of these clones was really of leukaemic origin, the diagnostic bone marrow VDJ sequences were obtained from the Queen Elizabeth University Hospital, Glasgow, UK for cross-referencing. Only patient sequences from RL1 and RL2 were able to be obtained.

At diagnosis patient RL1 presented with a bone marrow leukaemic population composed of several different clonal sub-populations (**Table 5-16**), including an IGH complete rearrangement which had an identical CDR3 sequence to the sequence detected in the cfDNA from the patient relapse sample (**Table 5-17**). The only difference between the BM sequence and the CSF ctDNA sequence was a base mismatch (T->C) in the V gene segment, upstream of the CDR3 sequence. This suggests that this leukaemic clone was potentially the cause of the CNS relapse. However, this study only tested for IGH complete (Vh-Jh) and IGH incomplete (Dh-Jh) gene rearrangements thus there remains the possibility of another clonal leukaemic population with other gene locus rearrangements.

At diagnosis, patient RL2 presented with a bone marrow leukaemic population composed of an incomplete IGH rearrangement which was determined as non-specific (very unlikely to be leukaemic origin) and a TCR $\beta$  gene rearrangement (**Table 5-16**). The presence of two IGH clones in the cfDNA of the relapse CSF samples of this patient potentially suggests the presence of 2 subsets of leukaemic populations in the CNS at the time of relapse. RL CL1 presented with a higher number of reads compared to RL CL2, potentially acting as the major clonal population (**Table 5-19, 5-20**). Again, there remains the possibility of another clonal leukaemic population with other gene locus rearrangements as only IGH gene rearrangements were tested.



	Rearrangement chain type	VDJ rearrangement	Type
RL1	V $\delta$ 2 D $\delta$ 3	V2*02(-19)/n=5/(-4)D $\delta$ 2(0)/n=3/(-19)D $\delta$ 3	Incomplete TCR $\delta$
	V $\gamma$ 1 J $\gamma$ 1.1	V2*02(0)/n=6/(-11)JP2*01	TCR $\gamma$
	V $\gamma$ 1 J $\gamma$ 1.3	V $\gamma$ 5*01(-5)/n=2/JP2*01(-1)	TCR $\gamma$
	VH3	VH3-74*01(-18)/n=15/(0)J6*02	IGH - complete
RL2	DH2	Non-specific	IGH - incomplete
	Mix 26 J $\beta$ 2.3- V $\beta$ 19 J $\beta$ 2.2	V $\beta$ 19*01(-7)/n=12/(-6)J $\beta$ 2.2P	TCR $\beta$

**Table 5-16: Diagnostic bone marrow VDJ clonotypes detected for patients RL1 and RL2.**

Patient RL1 CDR3:	
CGCATATTACTACTACTACTACGGTATGGACGTC	
BM gDNA	
TCTGCAAATGAACAG <b>T</b> CTGAGAGCCGAGGACACGGCTGT <b>CTACAG</b> GTC <b>CGCAT</b> <b>ATTACTACTACTA</b> <b>CTACGGTATGGACGTC</b> TGGGGCCAAGGGACCACGGTCACCGTNTNCNCANGTA	
CSF ctDNA	
TCTGCAAATGAACAG <b>C</b> CTGAGAGCCGAGGACACGGCTGT <b>CTACAG</b> GTC <b>CGCAT</b> <b>ATTACTACTACTA</b> <b>CTACGGTATGGACGTC</b> TGGGGCCAAGGGACCACGGTCACCGTCTCCTCAGGTAAG	

**Table 5-17: IGH complete rearrangement (VH3) VDJ sequence comparison between bone marrow clone and CSF ctDNA clone.** Yellow highlight = V gene segment; Red highlight = D gene segment; Green highlight = J gene segment. CDR3 spans part of the D-J junction and J gene segment. Enlarged base – mismatch between BM and CSF sequences.

RL1 - Putative Clonotype	Size (bp)	Read #	% of total reads
IGHV3/OR16-9*01 16/CCTACAGGTCCGCAT/0 IGHJ6*02	122	7732	8.913
RL1 – Confirmed Clonotype			
VH3-74*01(-18)/n=15/(0)J6*02			
V-D-J sequence			
TCTGCAAATGAACAGCCTGAGAGCCGAGGACACGGCTGTCCTACAGGTC <b>CGCATATTACTACTACTAC</b> <b>TACGGTATGGACGTC</b> TGGGGCCAAGGGACCACGGTCACCGTCTCCTCAGGTAAG			
CDR3			
<b>CGCATATTACTACTACTACTACGGTATGGACGTC</b>			
V region end			
GCTGT			
V-D Junction			
C			
D region			
CTACAG			
D-J Junction			
GTCCGCAT			
J region start			
ATTAC			
Top V gene matches	Top D gene match	Top J gene match	
IGHV3-21*01	IGHD4-11*01	IGHJ6*02	
IGHV3-21*02	IGHD4-4*01		
IGHV3-21*05			

**Table 5-18: VDJ sequence data of detected cline in diagnostic CSF sample from RL1.**

RL2 CL1 -Putative Clonotype	Size (bp)	Read #	% of total reads
IGHV3-13*03 1/TCTGGGGGAACCTTTCT/1 IGHD3-10*01 0//5 IGHJ4*02	149	329	0.323
<b>V-D-J sequence</b>			
TCTGCAAATGAACAGCCTGAGAGCCGGGGACACGGCTGTGTATTACTGTGCAAGTCTGGGGGAACCT TTCTTATTACTATGGTTCGGGGAGTTATTATAACTTTGACTACTGGGGCCAGGGAACCCTGGTCACCGT CTCCTCAGGTAAG			
<b>CDR3</b>			
GCAAGTCTGGGGGAACCTTTCTTATTACTATGGTTCGGGGAGTTATTATAACTTTGACTAC			
<b>V region end</b>			
GCAAG			
<b>V-D Junction</b>			
TCTGGGGGAACCTTTCT			
<b>D region</b>			
TATTACTATGGTTCGGGGAGTTATTATA			
<b>D-J Junction</b>			
N/A			
<b>J region start</b>			
ACTTT			
<b>Top V gene matches</b>	<b>Top D gene match</b>	<b>Top J gene match</b>	
IGHV3-13*01	IGHD3-10*01	IGHJ4*02	
IGHV3-13*02			
IGHV3-13*03			

**Table 5-19: VDJ sequence data of detected cline in diagnostic CSF sample from RL CL1**

RL2 CL2 -Putative Clonotype	Size (bp)	Read #	% of total reads
IGHV4/OR15-8*01 1/GGGGAGAGATCCGATCGAGGGGAAC CTTTCT/1 IGHD3-10*01 0//5 IGHJ4*02	157	76	0.074
<b>V-D-J sequence</b>			
GAGCTCTGTGACCGCCGCGGACACGGCCGTGTATTACTGTGCGAGAGGGGGAGAGATCCGATCGAG GGGGAACCTTTCTTATTACTATGGTTCGGGGAGTTATTATAACTTTGACTACTGGGGCCAGGGAACCC TGGTCACCGTCTCCTCAGGTAAG			
<b>CDR3</b>			
GCGAGAGGGGGAGAGATCCGATCGAGGGGGAACCTTTCTTATTACTATGGTTCGGGGAGTTATTATAA CTTTGACTAC			
<b>V region end</b>			
GAGAG			
<b>V-D Junction</b>			
GGGGAGAGATCCGATCGAGGGGGAACCTTTCT			
<b>D region</b>			
TATTACTATGGTTCGGGGAGTTATTATA			
<b>D-J Junction</b>			
N/A			
<b>J region start</b>			
ACTTT			
<b>Top V gene matches</b>	<b>Top D gene match</b>	<b>Top J gene match</b>	
IGHV4-39*06	IGHD3-10*01	IGHJ4*02	
IGHV4-39*07			
IGHV4-4*02			

**Table 5-20: VDJ sequence data of detected cline in diagnostic CSF sample from RL CL2**

In summary, these results show that IGH gene rearrangements can be detected in ctDNA extracted from very low samples of CSF (100 µL). Only one diagnostic patient and 2/3 relapse samples presented with unique clonotypes and identifiable CDR3 sequences identifying the presence of leukaemic clones in the CNS.

### 5.2.4 TruePrime amplification

One major limitation of this study was the low amount of starting cfDNA extracted from patient CSF samples. This is most likely due to the low CSF volumes available for cfDNA extraction (100  $\mu$ L). To attempt to overcome this challenge without obtaining more CSF, a novel method of multiple displacement amplification was applied to 4 patient samples including RL1 and the three CNS3 patients tested in the experiment described by **Table 5-12**. This method globally amplifies any DNA material from a purified DNA solution. The kit used, specifically targets small cfDNA fragments which are believed to arise from apoptosis using a *TthPrimPol* DNA primase and Phi29 DNA polymerase to amplify cfDNA.

The reaction amplified the starting patient cfDNA samples significantly, from an average of 0.283 ng/ $\mu$ L to 90.8 ng/ $\mu$ L. cfDNA from the REH cell-line was used as a positive control for this experiment and the starting cfDNA was also significantly amplified (3.19 ng/ $\mu$ L to 155 ng/ $\mu$ L) (**Figure 5-24, Table 5-21**).

The amplified cfDNA was then subjected to the NGS workflow starting with the 1st and 2nd stage adapter ligation. The quality control checks after the 1st stage indicated amplification of a template which was confirmed at the second quality control check after the second PCR reaction.

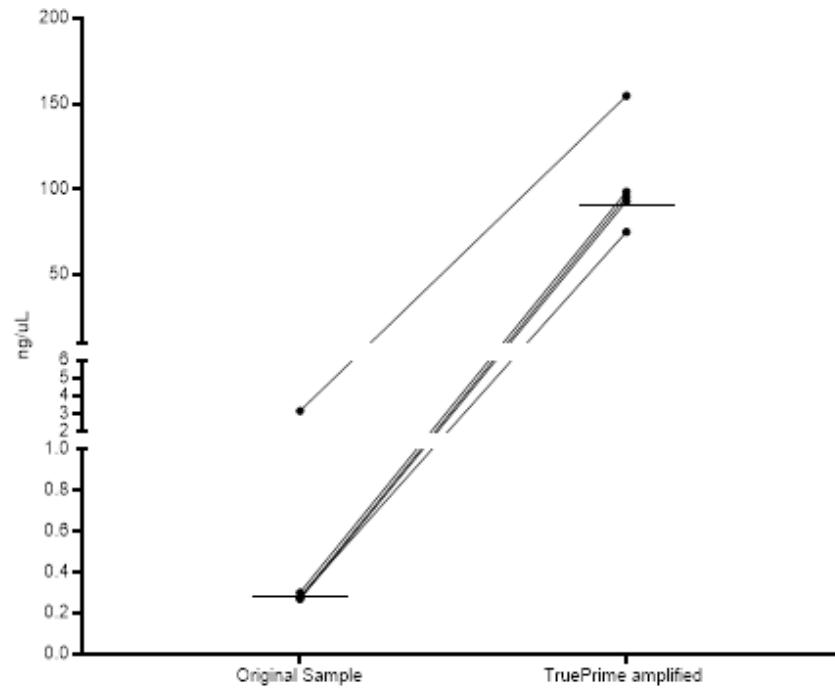


**Figure 5-24: Line graph: TruePrime cfDNA amplification of RL1, and three CNS3 patient cfDNA samples.** Positive control:: REH cfDNA isolated & extarcted from cell culutre supernant. Black line represents the mean of the samples. Graph created on GraphPad prism v9.

Sample	Starting conc (ng/μL)	Post - TP amp ( ng/μL)
RL1	0.277	96
CNS3	0.271	93.2
CNS3	0.281	75.2
CNS3	0.302	98.8
Average	0.283	90.8
+ REH cfDNA	3.19	155

**Table 5-21: TruePrime cfDNA amplification of RL1, and three CNS3 patient cfDNA samples.**

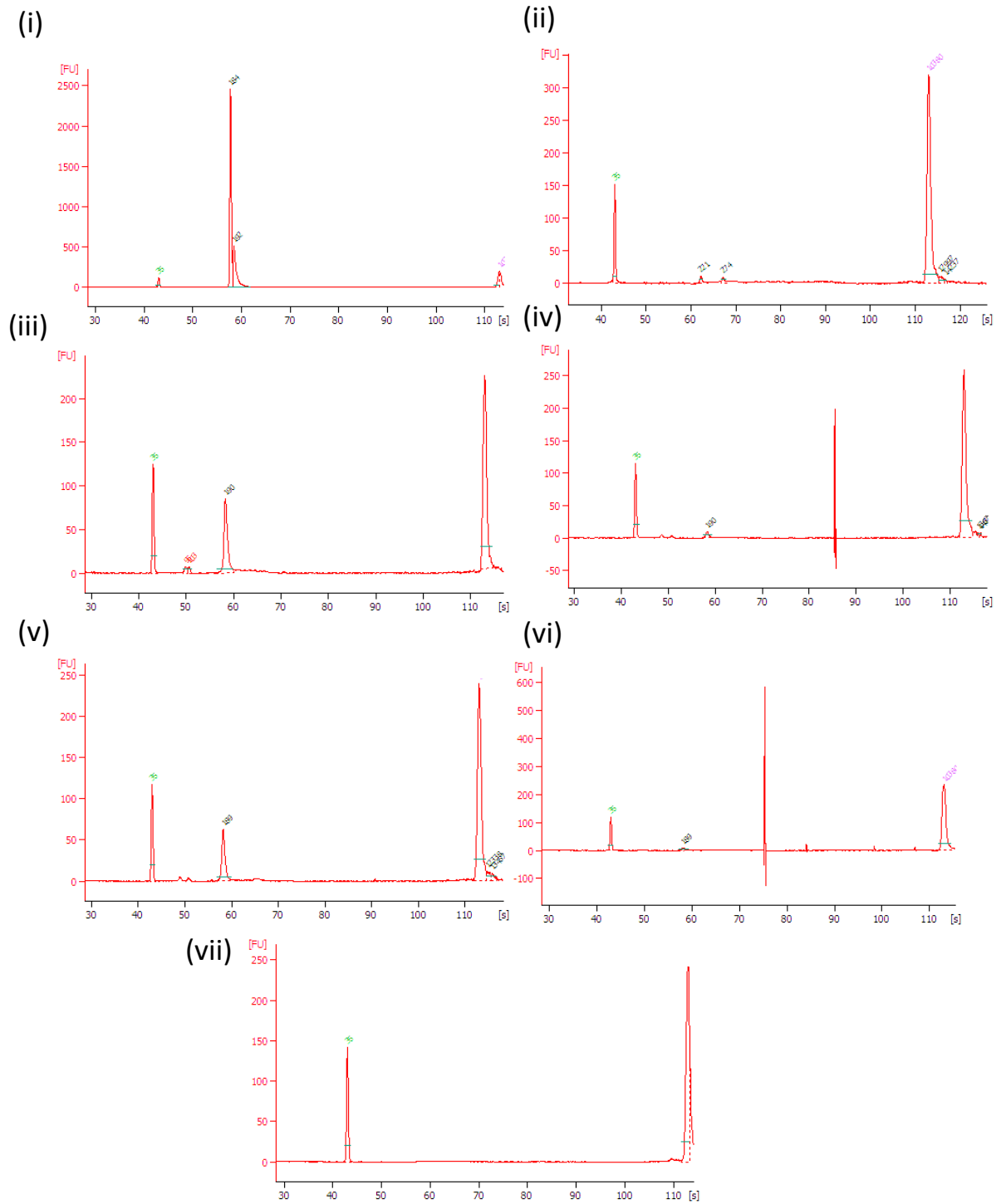


**Figure 5-25: Electropherograms of 1st stage PCR QC check. X-axis= time [s]; Y axis = Fluorescence Units.** (i) hTERT positive control; (ii) REH cfDNA control; (iii-v) CNS3 patients; (vi) RL1; (vii) Negative control.

Bioanalyzer analysis revealed expected peaks around 180-190bp for the four patient samples and a peak of ~220bp for the REH cfDNA positive control. The samples were then pooled and sequenced (**Figure 5-25**).

Analysis of the VDJ rearrangements detected revealed a large number of sequences for each sample which were analysed using IgBlast and IMGT/VQUEST online web tools (**Table 5-22**). Only the REH cfDNA positive control sample returned a matching clonotype with an identical sequence to the REH genomic DNA sequence (**Figure 5-26 E, Table 5-22**). Interestingly, this clone only made up 14.3% of the total reads compared to the original result where the cfDNA REH clone made up 95.5% of total reads (**Table 5-11**). The starting amount of cfDNA in the original experiment was similar to the starting amount used in the TruePrime experiment (original = 2.87 ng/μL TruePrime = 3.19 ng/μL) (**Tables 5-15, 5-23**).

All other sequences detected did not have identifiable CDR3 sequences or unique clonotypes (**Figure 5-26 A-D, Table 5-22**). The nature of these sequences is currently unknown, but one could speculate that they may stem from the various amplification processes in the workflow starting from the TruePrime amplification reaction to the subsequent PCR reactions and sequencing resulting in a cumulative creation of artefactual sequences.

The use of TruePrime amplification showed some promise in overcoming a major limiting variable of this study. Sequencing of TruePrime-amplified cfDNA of the leukaemic REH cell-line was able to detect the REH clonotype however the RL1 patient sample with the known leukaemic gene rearrangement was not detected for reasons currently unknown.



Sample	Sequences detected	Identifiable CDR3 sequence	Unique Clonotype	% of total reads
REH cfDNA (+ control)	67	1	1	14.29
RL1	60	0	0	N/A
CNS3	39	0	0	N/A
CNS3	59	0	0	N/A
CNS3	94	0	0	N/A

**Table 5-22: IgBlast analysis of TruePrime amplified cfDNA sequences.**

Sample cfDNA	Starting conc. (ng/μL)
REH cfDNA	3.19
REH cfDNA TP	2.87

**Table 5-23: Starting concentrations of REH cfDNA in original workflow experiment and TruePrime amplification experiment**

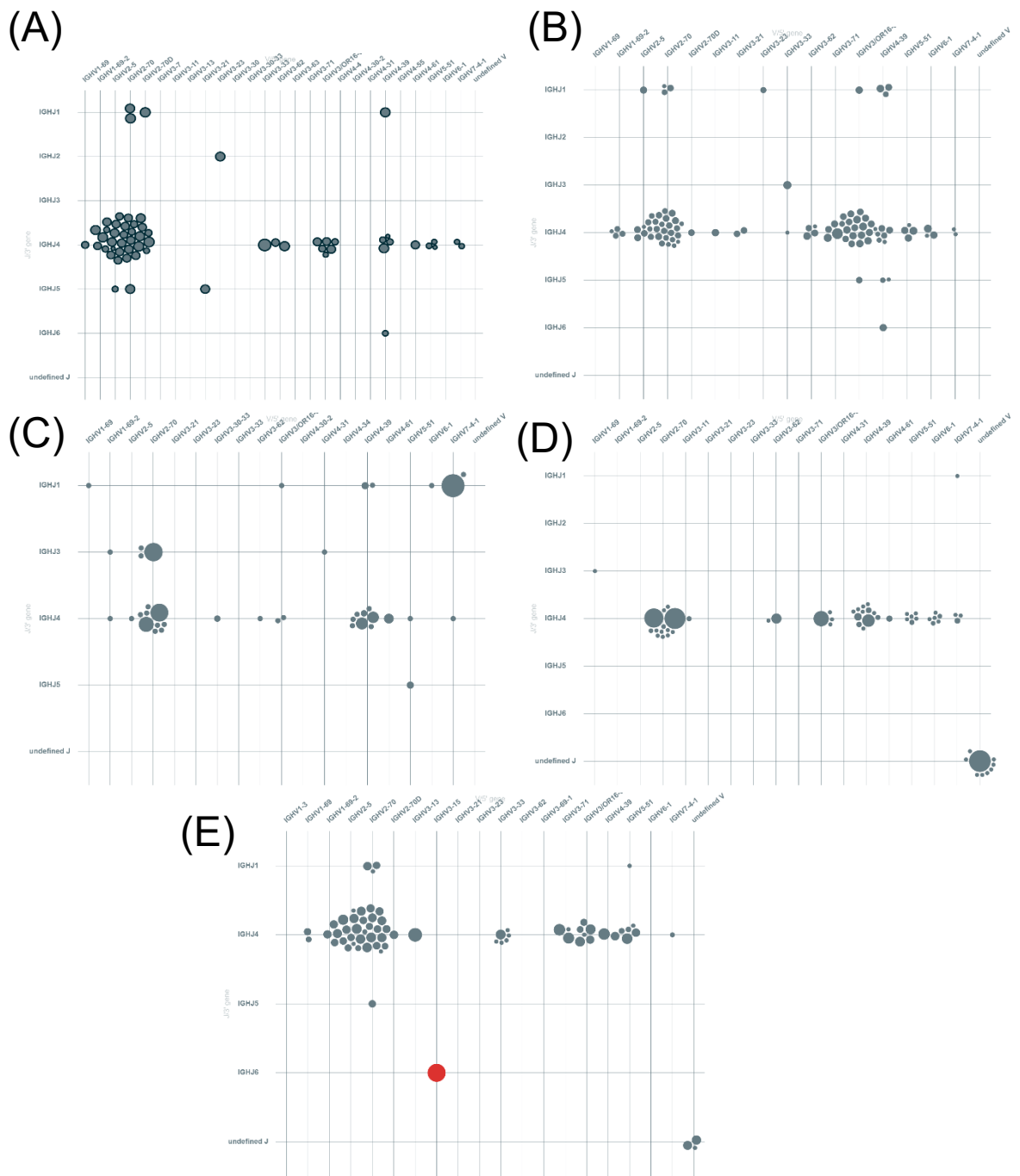


**Figure 5-26: Bubble plots of TruePrime amplified cfDNA.** (A) RL1 patient (B) CNS3 patient 1; (C) CNS3 patient 2; (D) CNS3 patient 3; (E) REH cfDNA positive control. Graphs exported from Vidjil.

### 5.3 Summary and discussion

This study set out to discover soluble biomarkers in the CSF capable of detecting and tracking CNS leukaemia in children with ALL. Cell-free DNA is an attractive biomarker as with the appropriate genetic target, can be highly specific. The advent of highly sensitive next-generation platforms such as ddPCR and NGS has significantly advanced research into the future application of liquid biopsies to the clinic.

One of the major challenges in the implementation of cfDNA analysis in clinical practise is the lack of standardisation with regards to controlling for pre-analytical variables. Factors such as sample volume, transportation, processing, preparation, and extraction methodology can significantly influence the sensitivity of cfDNA analysis.

The first step in this project was to test six commercial cfDNA extraction kits to test the efficiencies of different extraction methodologies including silica-based membrane extraction, magnetic bead-based extraction, ultrasonication-based extraction, as well as an automated workflow for cfDNA extraction. This experiment demonstrated the variability in total cfDNA extraction between the different kits with kit QA extracting the most total cfDNA of all the kits. Quantification of the spike-in hTERT<sub>172</sub> molecule by droplet digital PCR demonstrated that each kit was able to recover the cfDNA surrogate spike-in molecule with a similar efficiency. Based on these results the QA kit was chosen to take forward given it recovered the highest quantity of total cfDNA. It is important to note that these experiments were performed on samples of plasma and not CSF due to the lack of control CSF that is available for experimentation. Whether these kits would perform in a similar manner

is unknown however, the composition of CSF is much less dense and less complex than that of plasma, which may in theory suggest that the extraction process may be less hindered by any inhibitory constituents present in the sample. cfDNA is typically of low abundance in plasma and CSF however, in CNS-cancers, CSF has the advantage of having less quantity of native cfDNA in this space [119, 120]

Next, recovery of the spike-in cfDNA surrogate molecule at different concentrations was tested. hTERT<sub>172</sub> was spiked into samples 0.5 and 0.2 mL of pooled control CSF which was subsequently extracted and quantified by Qubit. The variability seen with the qubit measurements are perhaps to be expected as subtracting the baseline is a crude method to calculate spike-in recovery. Confirmation of the recovery of spike-in molecules down to 2 ng/mL in low volumes of CSF (0.5 and 0.2 mL) by Bioanalyzer demonstrated that it is possible to capture DNA molecules of a similar size to cfDNA from CSF using the chosen extraction kit at a low concentration.

CSF cfDNA yields of diagnostic patient samples, day 8 CSF, day 29 CSF, the matched controls take a year into treatment and the three relapse CNS CSF samples and demonstrated little variability, all averaging around 10 ng. This consistency may be explained perhaps by the fact that these samples have been in storage at – 80 °C for several years. It is also known that the handling of the samples post-lumbar puncture may be inadequate, and the samples may not be handled appropriately enough to preserve the integrity of the samples. Size fragment demonstrated that 3/6 patients had a clear sign of a size distribution signature around the 170-200bp area, consistent with an apoptotic release mechanism of cfDNA. There is the potential that larger (>1000 bp) fragments represent the remaining fraction of cfDNA present in the sample. The literature reports that apoptotic cfDNA tends to appear in fragments of ~200 bp or multiples thereof

whereas, necrotic cfDNA tend to be much larger cfDNA fragments. Elucidating the nature of larger cfDNA fragments is interesting work which should be investigated but was beyond the scope of this project.

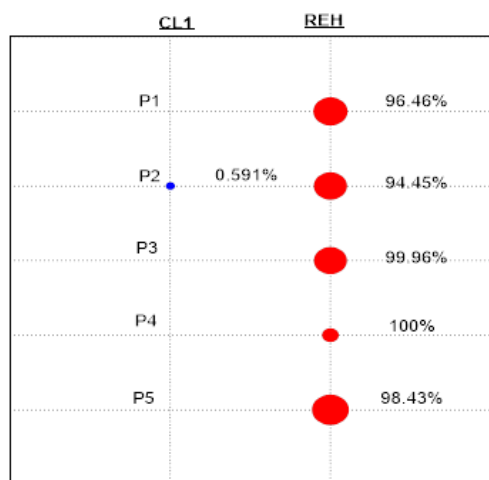
Highly sensitive platforms such as digital PCR and next-generation sequencing can be powerful tools in the search for diagnostic and prognostic biomarkers. In this study, both tools were used to detect leukaemia-specific targets capable of providing insight into leukaemic burden within the CNS. The first target tested was the KRAS G12D mutation, a very common cancer mutation which is present in 20-25% of newly diagnosed childhood ALL patients. By testing the performance of the assay, it was determined that 5 ng of input DNA would be needed to detect KRAS down to a variant allelic frequency of 0.13%. Given the low volume and concentration of our starting samples, only 1.5 ng of starting cfDNA was able to be analysed per patient sample. One CNS1 patient did present with very low levels of KRAS G12D mutation indicating the presence of CNS-leukaemia suggesting that digital PCR can detect leukaemia in CNS1 patients. Negative controls composed of 100% WT KRAS were used with only 1 false positive being recorded however more negative controls (~60 minimum suggested by the Clinical and Laboratory Standard Institute) would have to be analysed to determine the false-positive rate for ddPCR assays [121]. A necessary investigation to be performed in future work when adapting digital PCR assays to a clinical setting. A limitation of the KRAS G12D target was that it is a low-prevalence mutation in newly diagnosed ALL. A further limitation of this experiment was the low number of patient samples that were able to be tested. At the time of experimentation, only a small amount of CNS1 patients with matched controls were available.

The final stage of the project was to attempt to sequence cell-free DNA with an ubiquitous target; Ig gene rearrangements. A workflow was tested on cell-line genomic DNA and cell-free DNA providing unique clonotypes and CDR3 sequences which matched previously reported IG rearrangement sequences [117].

A small cohort composed of CNS3, CNS2 and CNS1 patients were then tested to test the hypothesis that increased leukaemic burden as classified by CSF cytology (i.e., CNS /CNS3) would have abundant cfDNA capable of being detected compared to CNS1 patients acting as a diagnostic biomarker for CNS-ALL. Initial results indicated no amplification with regards to an IGH complete or incomplete gene rearrangement present in any of the samples tested. cfDNA sample inputs into the 1<sup>st</sup> stage PCFR reaction were higher than that of digital PCR with an average input of 3.8 ng per reaction. This result suggested that either IGH gene rearrangements are not present in the ctDNA or that the starting amount of cfDNA was still too low to be able to detect the target. It was then decided to test the hypothesis that post administration of CNS-directed therapy at diagnosis, the result of treatment would cause an increase in the abundance of cfDNA released by cell-death mechanisms such as apoptosis or necrosis which would give an indication of the utility of ctDNA as a response biomarker. Matched diagnostic, day 8 and day 29 CSF samples from 5 patients were sequenced and interestingly, only one patient diagnostic sample presented with a unique clonotype and CDR3 sequence. This contradicts the hypothesis put forward about the effects of treatment on cfDNA release in the CNS but suggested that it is possible to detect IGH gene rearrangements in the cfDNA extracted from diagnostic patient CSF.

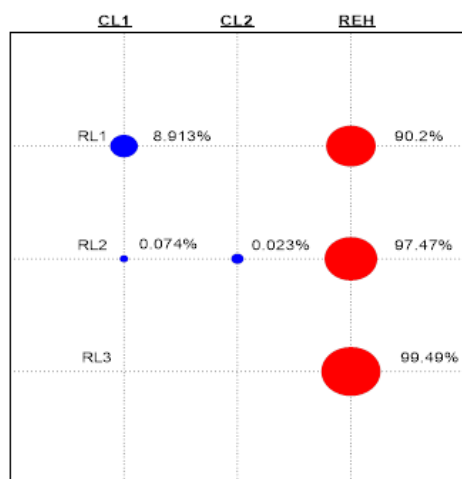
Of note, some samples unfortunately had some level of genomic DNA contamination from the REH cell-line. Significant efforts went into reducing this

contamination including intense decontamination procedures in the workspace and the replacement of new reagents in the entire workflow, and the use of several sample preparation areas which mostly worked. This may have had an effect on the detection of any leukaemic clones in the CSF however the primers used are designed for multiplex detection of various IGH gene rearrangements. The extent of the REH cell line contaminations can be seen in **Figure 5-27** where it can be observed that the majority of sequencing reads were dominated by the REH clone.



**Clonotypes**

P2 Dx CL1 -IGHV3-23D\*01 0/TAAGGAGCAGCAGATT/14 IGHJ4\*02  
 REH - IGHV3-15 1/GG/8 D3-10 3//6 J6\*02



**Clonotypes**

REH - IGHV3-15 1/GG/8 D3-10 3//6 J6\*02  
 RL1 CL1 - IGHV3/OR16-9\*01 16/CCTACAGGTCCGCAT/0 IGHJ6\*02  
 RL2 CL1 - IGHV4/OR15-8\*01 1/GGGGAGAGATCCGATCGAGGGGAACCTTTCT/1 IGHD3-10\*01 0//5 IGHJ4\*02  
 RL2 CL2 - IGHV3-13\*03 1/TCTGGGGGAACCTTTCT/1 IGHD3-10\*01 0//5 IGHJ4\*02

**Figure 5-27: REH cell line contamination**

Three relapse samples from patients who had isolate relapses in the CNS were then tested to see if IGH gene rearrangements were able to be detected in these truly positive CNS-ALL samples. Two of three of the patients presented with unique clonotypes and CDR3 sequences with one patient presenting with two clones. The VDJ sequences were then compared to the diagnostic bone marrow profile of these respective patients and one patient was confirmed to have an identical clone both at the time of diagnosis and at relapse in the CNS. The other patient presented with an incomplete IGH gene rearrangement at diagnosis which was not present at relapse and two IGH complete rearrangements at relapse which were not present at diagnosis potentially identifying the leukaemic subpopulations that were the cause of the CNS-relapse. This result suggests that ctDNA can potentially be used as a biomarker capable of detecting CNS leukaemia at relapse, however, further evidence from the testing of a higher number of relapse samples would be necessary to support this and time-point CSF samples taken around the time of relapse would also be needed to test whether or not the ctDNA biomarker can track the disappearance of leukaemia after treatment. These samples were not available to this study unfortunately although this type of serial sampling has begun in the Altogether CSF-Flow study providing an opportunity to analyse leftover CSF for ctDNA analysis [106].

Finally, in an attempt to overcome a limitation of this study, the low starting concentration of cfDNA, a method of global cfDNA amplification was tested (TruePrime). The relapse patient RL1 was tested alongside three CNS3 patients and cfDNA from the REH cell line as a positive control. Interestingly only the positive control was able to be detected in the TruePrime amplified cfDNA. An explanation for this may be that as TruePrime multiple displacement amplification amplifies the global repertoire of DNA molecules present in purified sample of DNA



indiscriminately, this process seemingly might turn a “needle in a haystack” scenario (the needle being the target of interest i.e., IGH gene rearrangements, and the haystack being background cfDNA composition) into a scenario with a higher quantity of “needles” but also many more “haystacks”. This is potentially an ideal solution for this setting as this global amplification could increase low levels of a desired target to levels above the limit of detection. However, the TruePrime amplified RL1 patient cfDNA did not present with a matched clonotype, as discovered in **Figure 23**, whereas the original NGS workflow did, contradicting this notion. Why the TruePrime amplification reaction did not amplify the RL1 clone present in the CSF cfDNA sample is unknown. The amplification of the REH cfDNA clone indicates that the TruePrime amplification is capable of amplifying these complex gene rearrangements and perhaps repeated experiments may reveal the frequencies at which certain areas of the genome are amplified or not. As this experiment was only conducted once it is not possible to speak to variability in the depth of coverage in this regard.

The data in this part of the study has provided that IGH gene rearrangements, highly specific to leukaemia are able to be detected in the ctDNA of patients with CNS-ALL, particularly in patients who had isolated CNS relapses. This study only targeted complete and incomplete IGH gene rearrangements which means that there may exist the possibility of the presence of more detectable clones in all of the samples tested here. This study proved the concept that leukaemic IGH gene rearrangements are able to be detected in the ctDNA extracted from the CSF of children with leukaemia and future work can expand on this discovery by testing for the full clonal repertoire of IG and TCR gene rearrangements.

## **Chapter 6: Final Conclusions, discussion and future Directions**

This study set out to discover and develop sensitive biomarkers for CNS-leukaemia capable of detecting, tracking response to therapy and predicting relapse with the following aims:

- 1 – To validate novel metabolic biomarkers in CSF capable of detecting and tracking CNS leukaemia and test the hypothesis that this biomarker is able to track the response of CNS leukaemia to treatment;
- 2 - To discover novel soluble biomarkers in CSF, as alternatives to metabolomic-based methods, using the same criteria as aim 1;
- 3 – To develop a robust and sensitive method for detection of leukaemic cell-free DNA in CSF, using the same criteria as aim 1;
- 4 – To use data gathered from aims 1-3 to identify the optimal biomarker(s) to take forward for further validation and clinical testing.

The main findings of this study are summarised below.

## 5.4 Summary and discussion of the main findings

### 5.4.1 Metabolic biomarkers

The relationship between leukaemia (and cancers in general) and cellular metabolism is convoluted but it is known that leukaemia's rely heavily on the deregulation of a wide range of metabolic pathways to survive. In order to proliferate and survive, blasts require high amounts of energy obtained by the hijacking of core metabolic processes such as glucose uptake, aerobic glycolysis as well as other non-glycolytic mechanisms such as the oxidation of glutamine, amino acids and fatty acids [122, 123]. Metabolomics is a powerful tool which can be used to profile the metabolic signature of leukaemic blasts through the identification of small metabolites.

Metabolic profiling of leukemic cells has previously identified that replicating ALL cells are dependent on asparagine. This dependence was consequently manipulated by the introduction of L-asparaginase as a standard chemotherapeutic treatment regimen. L-asparaginase functions by starving blast cells of asparagine by catalysing the degradation of asparagine into aspartate and ammonia[124]. Research on the leukaemic metabolome has widely shifted to the identification of biomarkers which can aid in the improvement of personalised treatment.

Leukaemic cells have a vastly different metabolic signatures to that of normal healthy cells. Given that leukaemic blasts are known to migrate and adhere to the walls of the leptomeninges in the CNS, their presence in the CSF will ultimately alter the metabolic composition of the CSF. Localised metabolic analysis of CSF samples from patients with ALL may provide a means to screen for clinically relevant biomarkers capable of revealing metabolic signatures of disease in the CNS.

This study has validated a panel of metabolites that show promise as diagnostic biomarkers for the presence of leukaemia in the CNS of patients with ALL in a large comprehensive cohort of CSF samples composed of patients classified as CNS1, CNS2 and CNS3. The data generated provides clear evidence that these metabolites have the ability to discriminate between patient CSF and control CSF, each demonstrating high levels of sensitivity and specificity when tested individually. The panel of metabolites which show the most promise as biomarkers for CNS-ALL are Creatine, N4-acetylcytidine, Symmetric dimethylarginine, Phenylalanine Xanthine, Inosine and Orotidine.

The levels of creatine in CSF in the context of paediatric ALL biomarkers is poorly reported. Creatine is primarily synthesized in the liver, kidneys and pancreas but it is also known to be synthesized in the brain. The brain requires significant amounts of energy to function and relies on creatine, phosphocreatine and the creatine kinase metabolic pathway as a reserve source of energy due to it being an organ with a high demand for ATP [125]. Studies have also shown that the BBB contains active membrane-bound creatine transporters (CrT) that continually transport creatine from the blood, through the BBB and into the CNS against a creatine concentration gradient [126]. This provides an explanation for the source of creatine present in the CSF.

In this study, the levels of creatine in the CSF of ALL patients were decreased compared to controls. Creatine levels have been shown to be decreased in the serum of patients with ALL and AML compared to age and gender matched healthy controls [127]. In the patients with ALL, Creatine was only slightly downregulated compared to healthy controls in concordance with the findings of this study and in AML, its down regulation was considerably larger. Another study compared the

levels of creatine in peripheral blood samples from patients with ALL at the time of diagnosis and at day 29 and interestingly, levels of creatine were lower at diagnosis than at day 29 (at which patients were considered to be in remission through clearance of peripheral leukaemic burden) further supporting the findings of this study [74].

This trend can also be seen in both serum and tissue samples of colorectal cancer patients compared to healthy controls [128]. In pancreatic cancer, Creatine and Inosine formed part of a panel of metabolites detected in samples of plasma which show great promise for use as diagnostic biomarkers [129]. Again, the trend observed here was of decreased levels of Creatine in the patient group compared to healthy volunteers.

A possible explanation for the difference in the levels of creatine in patient CSF samples compared to control CSF samples seen in this study, may be due to the use of creatine metabolism by leukaemic blasts in the CNS to provide energy for proliferation and survival in this nutrient-poor microenvironment. It is known that leukaemic cells, in particular ecotropic virus integration site 1 (EVI1) over-expressing AML cells, are highly dependent on arginine-creatine metabolism in the mitochondria [130]. Amongst causing other metabolic changes, aberrant EVI1 expression in AML results in high expression of mitochondrial creatine kinase which catalyses the phosphorylation of creatine to phosphocreatine for energy storage [131]. There is evidence that over-expression of EVI1 is also present in paediatric ALL patients, particularly in patients between late childhood and adolescence [132].

Another potential mechanism which could explain decreased Creatine in the CSF of ALL patients compared to controls can perhaps be explained by a mechanism

exhibited in colorectal cancer in the liver microenvironment. Colorectal cancer cells are known to secrete creatine kinase into the extracellular space to allow phosphorylation of exogenous creatine into phosphocreatine in the extracellular space. Uptake of phosphocreatine into the cancer cell then occurs through the membrane-bound CrT and the phosphocreatine is then used for as an energy buffer by its conversion back into Creatine mediated by intracellular creatine kinase to produce ATP to promote survival in the liver microenvironment [133]. A similar mechanism in the CNS could potentially provide an explanation for the phenotype we observed here, however this mechanism is currently poorly understood and future studies will be required to address whether this mechanism occurs in the CNS-ALL context.

N4-acetylcytidine is modified cytidine pyrimidine nucleoside that has important functions in mRNA regulation and promotes translation efficiency [134]. It is widely reported as a urinary metabolite which can function as a potential biomarker for several different types of solid tumours. N4-acetylcytidine has been reported as a potential biomarker of epithelial ovarian cancer in the urine of patients where levels of the metabolite returned to normal following surgical treatment [135]. This metabolite has also been implicated as a potential biomarker for breast cancer, colorectal cancer, urogenital cancer from patient samples of urine where levels of N4-acetylcytidine were higher in-patient samples than controls [136-139].

It's use as a biomarker for detection of leukaemia is poorly reported. There is, however, some research into N-acetyltransferase 10 (NAT10) which catalyses RNA modifications on mRNA, 18S rRNA and tRNA, specifically the acetylation of cytidine to N4-acetylcytidine. High expression of NAT10 in cancer cells has been reported to upregulate expression of oncogenes. In AML, NAT10 has been reported as a

potential prognostic biomarker as it is upregulated in patients compared to normal controls and patients with high NAT10 expression had poorer progression-free survival and overall survival [140]. Whether high expression of NAT10 results in detectable levels of N4-acetylcytidine may perhaps provide an explanation for the increased levels of this metabolite in CNS-ALL.

N4-acetylcytidine is also known to be reported in instances of inflammatory disease. Elevated levels of the metabolite in the urine of patients with inflammatory conditions such as interstitial cystitis have been observed [141]. In contrast however, Patients with pulmonary fibrosis exhibit a decreased level of N4-acetylcytidine in plasma compared to normal levels [142]. In microglia in the brain, a NLRP3 neurogenic inflammatory response is reported to be induced by N4-acetylcytidine [143]. As the CNS-ALL is considered to be an inflammatory environment, it may be possible that the detection of this metabolite is a result of inflammation caused by CNS-ALL however further extensive research is required.

Symmetric dimethylarginine is an alpha amino acid derivative of L-arginine which is formed through the methylation of protein arginine by protein arginine methyltransferases (PRMTs) . It is typically present in human blood as a result of the degradation of methylated proteins. Again, the literature does not reveal much research into this metabolite in the context of CNS-ALL, however, increased levels of Symmetric dimethylarginine appears to be associated with both solid and haematological malignancies.

One study detected elevated levels of Symmetric dimethylarginine in the plasma of patients with AML, non-Hodgkin's lymphoma and chronic lymphocytic leukaemia compared to controls which were matched for age, sex, co-morbidities and smoking

habits [144]. In patients with myelodysplastic syndrome, increased levels of this metabolite were also found in the sera compared to healthy donors [145].

Increased expression of PRMTs can be observed in a wide range of cancers including AML and has been reported to play a role in tumorigenicity [146, 147]. Whether this increased expression can explain the elevated level of Symmetric dimethylarginine observed in this study remains to be investigated.

Xanthine and Inosine form part of the purine synthesis and metabolism metabolic pathway and Orotidine is part of the pyrimidine synthesis metabolic pathway. Nucleotide synthesis is a vital part of cellular metabolism in both healthy and malignancy cells and actively proliferating ALL cells have a high demand for the building blocks of DNA and RNA. L-phenylalanine is an essential amino acid which is metabolized into acetoacetic acid and fumaric acid and is also a precursor to Tyrosine which is essential in protein synthesis.

Previous studies have reported increased levels of Xanthine, Inosine and L-phenylalanine in the plasma of ALL patients compared to controls (with no history of leukaemia). In this study, patients with high plasma inosine levels had poorer prognoses than patients who had Inosine levels close to the normal range [148].

In a recent study similar to this, levels of Xanthine, Phenylalanine were reported to be elevated in the CSF of patients with CNS leukaemia compared to control leukaemic patients who were negative for CNS leukaemia via flow cytometric analysis (FCA) and cytomorphological examination of the CSF. Interestingly, in one study levels of phenylalanine were reported to be elevated in the serum of patients with ALL compared to age and gender matched healthy controls in concordance



with the findings of this study, but the levels of phenylalanine in patients with AML were conversely greatly decreased [127].

As many of the chemotherapies given to patients with ALL target metabolic pathways, the elevation of these metabolites observed in leukaemic patients could potentially be explained by drug-related metabolism. For example, methotrexate is known to inhibit enzyme dihydrobiopterin reductase and interrupt the formation of tetrahydrobiopterin which is integral to the hydroxylation of L-phenylalanine and other nucleotides. This results in accumulation of intracellular L-phenylalanine which is known to diffuse to the extracellular space and as these treatments cause cell-death, this could further increase the extracellular concentrations of this metabolite. This phenomenon may perhaps explain the increased levels of L-phenylalanine in the CSF of patients with CNS-ALL but requires further investigation.

6-mercaptopurine can cause the accumulation of Inosine as it causes the inhibition of AMP, XMP synthesis however, this drug is typically given orally and is not part of the intrathecal treatment of ALL. The BBB does not allow transport of this treatment into the CNS thus the metabolic signature observed for Inosine here, may perhaps reflect leukaemic burden. Nevertheless, as discussed in the results section, allopurinol is known to be administered to ALL patients and is known to inhibit key enzymes involved in purine and pyrimidine synthesis which may explain the increased levels of Xanthine, Inosine and Orotidine.

When combined in a multivariate biomarker model these candidate biomarkers performed excellently in detecting a leukaemic signature in the CSF of patients with ALL compared to control CSF, outperforming the performance of each individual biomarker on its own. Application of the seven -biomarker model to small, previously

untested cohort of diagnostic CNS1 patients and one CNS3 relapse patient resulted in the correct classification of all samples as leukaemic samples. Measuring true abundance of two of the best performing metabolites provided data strongly supporting the application of the multi-biomarker model.

Phenylalanine showed promise as a potential prognostic biomarker for CNS leukaemia with elevated levels in patients who went on to have isolated relapses in the CNS or combine CNS and bone marrow relapses compared to patients who did not relapse. The patient samples were matched for age, sex, CNS status and risk. This result suggests an increased risk of CNS-relapse in patients with increased levels of Phenylalanine.

N4-acetylcytidine and Symmetric dimethylarginine showed a concordant trend with current CSF cytology. Patients classified as CNS3 showed elevated levels of both metabolites compared to the control group CNS1 patients.

A key strength of this validation was the large number of patient samples which were tested comprised of CNS1, CNS2 and CNS3 patients from a wide range of ages (childhood to young adult), giving a true representation of a leukaemic population. The use of two CSF controls with this large cohort of samples allowed thorough testing of the behaviour of each metabolite by comparison against normal CSF (from patients who were admitted to hospital for suspected non-inflammatory neurological conditions and had a lumbar puncture taken which returned normal results with clinical profiles parallel to normal CSF) and inflammatory CSF, allowing the ability to rule out potential false positives caused by CNS inflammation rather than leukaemia.

The major limitation of this study was the lack of matched plasma samples which would indicate whether these metabolites were differentially expressed in the CNS. As discussed above, there also exists the possibility of the effects of drug-related metabolism on the differences between the leukaemia samples and control CSF samples.

#### **5.4.2 Soluble protein, cytokine biomarkers**

Several protein-based biomarkers were tested for their ability as diagnostic and prognostic biomarkers. Only CD27, a proapoptotic protein belonging to the TNF superfamily, showed some promise in discriminating between leukaemic patient samples and control CSF.

CD27 is known to regulate the functions of lymphocytes and with its ligand CD70 is known to promote survival and proliferation in lymphocytes. It is known to be expressed in B-cell lymphoma, adult T-cell leukaemia/ lymphoma, as well as in high-risk paediatric and adult BCP-ALL [149, 150]. It has been shown to correlate with disease progression in B-cell chronic lymphocytic leukaemia (CLL) as well as being a prognostic biomarker in AML where one study reported significantly elevated CD27 in the serum of diagnostic AML patients compared to controls [151-153].

In concordance with the findings of this study, a previous study examined the CSF of 102 patients with a range of diseases with and without suspected leptomeningeal involvement including: B and T-non-Hodgkin's lymphoma, B-lymphocytic leukaemia, multiple myeloma, Waldenströms disease, B and T-cell ALL, CML, myelodysplastic syndrome, AML and various solid tumours. Elevated levels of CD27 were not specific to disease with leptomeningeal involvement and were elevated in

cases which presented with other forms of infection which would prompt T-lymphocyte activation and inflammation [154].

The soluble form of CD27 is typically secreted following lymphocyte activation and thus one can postulate that in context of CNS-ALL, where the immune system of patients is typically compromised, response to infection and inflammation may potentially cause the phenotype of elevated CD27 in the CSF of patients with ALL [155].

In this study, the levels of CD27 were elevated in the inflammatory control to levels similar to the leukaemia patient samples, suggesting that elevated CD27 is most likely a phenotype for inflammation in the CNS rather than being specific for leukaemia. The levels of CD27 did show concordance with CSF cytology, with CNS3 patients having higher levels than CNS1 patients. Nevertheless, the CNS is known to be a site of inflammation in leukaemia which may provide an explanation for this elevation.

#### **5.4.3 Cell-free DNA**

Cell-free DNA can be detected in various bodily fluids and the targeting of tumour-derived cfDNA is an area that shows great promise with respect to measuring residual tumour burden. cfDNA is periodically released from cells (malignant and healthy alike) by cell death mechanisms such as apoptotic, necrotic and it is also known to be actively secreted [156]. Its use as a diagnostic and prognostic biomarker is well reported for solid tumours in blood plasma/ serum and for brain/ spinal cord tumours in CSF [157-160]

In haematological disease, extraction of cfDNA from blood simply requires a blood sample whereas unfortunately, in CNS disease, repeated invasive procedures i.e., lumbar punctures are required for CSF extraction. There are already several studies investigating brain tumour ctDNA from CSF. One study compared samples of CSF and plasma from several cancers including glioblastoma, medulloblastoma, or brain metastases (from lung/breast cancer) and found that ctDNA was consistently detected in higher levels in CSF than in plasma suggesting that the CSF provides the most suitable medium for liquid biopsy of brain malignancies compared to plasma [161].

Leukaemic cfDNA can be identified by targeting rearrangements of the immunoglobulin heavy (IgH) and T-cell receptor (TCR) rearrangements. The Ig loci constitutes germline rearrangements of several variable (V), diversity (D), and joining (J) segments. These segments undergo various rearrangements during early lymphoid differentiation and effectively act as 'fingerprints', specific to the original transformed lymphoid cell [162]

Analysis of IGH gene rearrangements in cfDNA from different body fluids is reported in the literature for patients with haematological malignancies such as the plasma of Non-Hodgkin's lymphoma patients and CSF in CNS lymphoma [163, 164]. Studies have tried to address whether the detection of these rearrangements in cfDNA from plasma samples can be used in minimal disease detection by assessing diagnostic samples against samples taken following treatment and the data provides evidence that detection of clearance of the haematological malignancies is possible in both AML and multiple myeloma [165].

Several commercial cfDNA extraction kits were tested and compared for their extraction efficiencies of total native cfDNA and of a surrogate cfDNA spike-in molecule (a linearized hTERT plasmid fragment) from samples of plasma and CSF. One kit (QA) performed best in recovery of total cfDNA. It is a popular and effective kit used in several studies for the extraction of cfDNA from various biological fluids of patients with different cancers. [119, 166, 167]. One study compared four different cfDNA extraction methods from samples of pooled plasma and demonstrated that QIAGEN's QIAamp circulating nucleic acids kit surpassed the cfDNA recovery yield compared to other methods in concordance with the findings of this study [119].

There are currently no universal standardized methods for extraction and quantification of cfDNA and study designs differ greatly. The majority of studies focus on the extraction of cfDNA from blood plasma and serum and little details are given for cfDNA extraction methods from CSF. As cfDNA is typically detected in low concentrations and because of the difference in composition of CSF compared to blood plasma/ serum, there is a need for optimising the extraction process for maximal cfDNA yield from CSF. Sample handling, processing, storage and analysis methods also vary between institutions; therefore, it is difficult to draw comparisons between studies. This relates to both samples of CSF post-lumbar puncture to samples of extracted cfDNA. cfDNA yield is known to be significantly affected by poor handling of these samples and the lack of standardized methods must be acknowledged.

Detection of leukaemic cfDNA from low volumes of CSF (~100  $\mu$ L) was achieved using highly sensitive platforms like ddPCR and NGS. The KRAS G12D mutation was detected by ddPCR in a CNS1 patient, providing evidence of the presence of leukaemia in the CNS of a patient currently classified as CNS-negative by current

CSF cytology. Highly specific IGH gene rearrangements were sequenced by NGS in the cfDNA of patients who relapsed in the CNS revealing the clonal architecture of the leukaemia that caused the CNS relapse. leukaemic cfDNA was also sequenced in a diagnostic CNS1 patient which disappeared in day 8 and day 29 CSF samples correlating with clearance of CNS leukaemia.

The low starting volume of CSF and total cfDNA concentration was a major challenge in this study, which may explain the low sensitivity observed using both of these platforms. Amplification of global cfDNA levels from patient samples using multiple displacement amplification (TruePrime) showed promise in increasing the amount of target cfDNA molecules as seen by successful amplification and detection of REH cell-line cfDNA. However, this amplification resulted in a high level of artefactual sequences, potentially confounding the detection of any starting leukaemic cfDNA.

## **5.5 Final conclusions and future directions**

The path towards personalised CNS-directed therapy lies in replicating the excellent track record for delivering risk-adapted therapy for systemic leukaemia. A biomarker(s) that can measure how well a patient responds to initial therapy will allow highly accurate prediction of a patient's risk of relapse, as occurs with bone marrow MRD. It not only reveals the behaviour of the biology of the leukaemia but also of the patient's individual biology i.e., how well the therapy is metabolised and the response of the microenvironment i.e., bone marrow or CNS.

The major challenge in adopting current MRD methods to the CNS is that leukaemic cells are adherent to the walls of the leptomeninges. Therefore, in order to achieve

CSF MRD, an extracellular based approach is required. In summary, this project aimed to develop and validate the necessary tools to enable sensitive detection of CNS leukaemia and tracking of its response to treatment akin to bone marrow MRD.

The greatest need for future biomarker discovery and development in CNS leukaemia is the standardisation of all the procedures involved in the journey of a CSF sample from the bedside to the laboratory bench. This work should involve the optimisation and standardisation of all of the preanalytical variables including CSF sample source, sample collection, sample transport and storage, sample volume, sample preparation and sample extraction to maximise the integrity of a CSF liquid biopsy for downstream analysis.

Several candidate metabolic biomarkers described in this thesis show excellent promise as diagnostic biomarkers capable of detecting the presence of a leukaemic metabolic signature in the CSF of patients with leukaemia. In order to validate these findings further, a large cohort of patient samples composed of paired CSF and plasma samples is imperative to investigate the differential expression of these metabolites in the CNS.

Next, an investigation into the effects of drug-related metabolism on the levels of these metabolites in the CNS using *in vitro* and *in vivo* models of metabolite consumption and secretion are essential to determine the biological plausibility of these biomarkers. Further work is needed into broadening the understanding of the metabolic pathways associated with these candidate metabolic biomarkers again to confirm biological plausibility. With a final panel of candidate metabolic biomarkers repeating these experiments with a more sensitive technology and a fully targeted metabolomic approach measuring true abundance of all the candidate biomarkers,



with the aim to apply a multivariate biomarker model to a large independent cohort of patient samples and age-matched CSF controls will reveal the clinical utility of these candidate biomarkers as biomarkers for CNS-ALL and utility in the development of CSF MRD.

Targeting IGH gene rearrangements in leukaemic cell-free DNA showed promise in being a highly specific biomarker for CNS-ALL. Although, the lack of sensitivity observed in this study may be explained by the effects of long-term storage and pre-extraction preanalytical variables. This study adapted the workflows from the BIOMED-2 multiplex PCR study which is currently in practise with sanger sequencing. Work involving the standardisation and validation of NGS workflows (in lieu of current practise with Sanger sequencing workflows) for the targeting of Ig and TCR gene rearrangements in ALL has begun through the Euroclonality-NGS validation study [118]. Future work involving the development and application of these workflows for the detection of the complete clonal repertoire of Ig and TCR gene rearrangements in cell-free DNA and testing in independent patient cohorts will elucidate the clinical utility of this biomarker for CSF MRD.

In future, achieving CSF MRD akin to current bone marrow MRD, is likely to be driven by the use of a multifaceted risk-score for CNS-ALL composed of various biomarkers in combination. The finale milestone would be to show that intervention on the basis of CSF MRD permits safe reduction of CNS directed therapy for low-risk children and that escalation of CNS therapy reduces CNS relapse in high-risk children. This would free many children from the burden of intensive, unnecessary and toxic CNS-directed therapy, whilst potentially improving the outlook for patients with resistant disease by targeting them for more intensive up-front treatment to prevent relapse.

## Chapter 7: References

1. Cancer Research UK.
2. Steinherz, P.G., et al., *Treatment of patients with acute lymphoblastic leukemia with bulky extramedullary disease and T-cell phenotype or other poor prognostic features: randomized controlled trial from the Children's Cancer Group*. *Cancer*, 1998. **82**(3): p. 600-12.
3. Pui, C.H., K.E. Nichols, and J.J. Yang, *Somatic and germline genomics in paediatric acute lymphoblastic leukaemia*. *Nat Rev Clin Oncol*, 2019. **16**(4): p. 227-240.
4. Greaves, M., *The 'delayed infection' (aka 'hygiene') hypothesis for childhood leukaemia*. *The Hygiene Hypothesis and Darwinian Medicine* 2009: p. pp 239-255.
5. Smith, M., et al., *Uniform approach to risk classification and treatment assignment for children with acute lymphoblastic leukemia*. *J Clin Oncol*, 1996. **14**(1): p. 18-24.
6. Reaman, G.H., et al., *Treatment outcome and prognostic factors for infants with acute lymphoblastic leukemia treated on two consecutive trials of the Children's Cancer Group*. *J Clin Oncol*, 1999. **17**(2): p. 445-55.
7. Frankel, L.S., et al., *Therapeutic trial for infant acute lymphoblastic leukemia: the Pediatric Oncology Group experience (POG 8493)*. *J Pediatr Hematol Oncol*, 1997. **19**(1): p. 35-42.
8. Griesinger, F., et al., *Leukaemia-associated immunophenotypes (LAIP) are observed in 90% of adult and childhood acute lymphoblastic leukaemia: detection in remission marrow predicts outcome*. *Br J Haematol*, 1999. **105**(1): p. 241-55.
9. Kadan-Lottick, N.S., et al., *Survival variability by race and ethnicity in childhood acute lymphoblastic leukemia*. *JAMA*, 2003. **290**(15): p. 2008-14.
10. Lim, J.Y., et al., *Genomics of racial and ethnic disparities in childhood acute lymphoblastic leukemia*. *Cancer*, 2014. **120**(7): p. 955-62.
11. Ransohoff, R.M. and B. Engelhardt, *The anatomical and cellular basis of immune surveillance in the central nervous system*. *Nat Rev Immunol*, 2012. **12**(9): p. 623-35.
12. Spector, R., S. Robert Snodgrass, and C.E. Johanson, *A balanced view of the cerebrospinal fluid composition and functions: Focus on adult humans*. *Exp Neurol*, 2015. **273**: p. 57-68.
13. Rahimi, J. and A. Woehrer, *Overview of cerebrospinal fluid cytology*. *Handb Clin Neurol*, 2017. **145**: p. 563-571.
14. Telano, L.N. and S. Baker, *Physiology, Cerebral Spinal Fluid*, in *StatPearls*. 2022: Treasure Island (FL).
15. Brinker, T., et al., *A new look at cerebrospinal fluid circulation*. *Fluids Barriers CNS*, 2014. **11**: p. 10.
16. Basso, D.M., et al., *Neurologic Rehabilitation: Neuroscience and Neuroplasticity in Physical Therapy Practice*. 2016: McGraw-Hill Education.
17. Williams, M.T., et al., *The ability to cross the blood-cerebrospinal fluid barrier is a generic property of acute lymphoblastic leukemia blasts*. *Blood*, 2016. **127**(16): p. 1998-2006.

18. Yao, H., et al., *Leukaemia hijacks a neural mechanism to invade the central nervous system*. Nature, 2018. **560**(7716): p. 55-60.
19. Price, R.A., *Histopathology of CNS leukemia and complications of therapy*. Am J Pediatr Hematol Oncol, 1979. **1**(1): p. 21-30.
20. Price, R.A. and W.W. Johnson, *The central nervous system in childhood leukemia. I. The arachnoid*. Cancer, 1973. **31**(3): p. 520-33.
21. Aspelund, A., et al., *A dural lymphatic vascular system that drains brain interstitial fluid and macromolecules*. J Exp Med, 2015. **212**(7): p. 991-9.
22. Pui, C.H. and S.C. Howard, *Current management and challenges of malignant disease in the CNS in paediatric leukaemia*. Lancet Oncology, 2008. **9**(3): p. 257-268.
23. Akers, S.M., et al., *Cellular elements of the subarachnoid space promote ALL survival during chemotherapy*. Leuk Res, 2011. **35**(6): p. 705-11.
24. Munch, V., et al., *Central nervous system involvement in acute lymphoblastic leukemia is mediated by vascular endothelial growth factor*. Blood, 2017. **130**(5): p. 643-654.
25. Lenk, L., A. Alsadeq, and D.M. Schewe, *Involvement of the central nervous system in acute lymphoblastic leukemia: opinions on molecular mechanisms and clinical implications based on recent data*. Cancer Metastasis Rev, 2020. **39**(1): p. 173-187.
26. Buonamici, S., et al., *CCR7 signalling as an essential regulator of CNS infiltration in T-cell leukaemia*. Nature, 2009. **459**(7249): p. 1000-4.
27. Bartram, J., et al., *High throughput sequencing in acute lymphoblastic leukemia reveals clonal architecture of central nervous system and bone marrow compartments*. Haematologica, 2018. **103**(3): p. e110-e114.
28. Frishman-Levy, L. and S. Izraeli, *Advances in understanding the pathogenesis of CNS acute lymphoblastic leukaemia and potential for therapy*. Br J Haematol, 2017. **176**(2): p. 157-167.
29. Bonadio, W., *Pediatric lumbar puncture and cerebrospinal fluid analysis*. J Emerg Med, 2014. **46**(1): p. 141-50.
30. de Haas, V., et al., *Flowcytometric evaluation of cerebrospinal fluid in childhood ALL identifies CNS involvement better than conventional cytomorphology*. Leukemia, 2021. **35**(6): p. 1773-1776.
31. Burger, B., et al., *Diagnostic cerebrospinal fluid examination in children with acute lymphoblastic leukemia: significance of low leukocyte counts with blasts or traumatic lumbar puncture*. J Clin Oncol, 2003. **21**(2): p. 184-8.
32. Abbott, B.L., et al., *Clinical significance of central nervous system involvement at diagnosis of pediatric acute myeloid leukemia: a single institution's experience*. Leukemia, 2003. **17**(11): p. 2090-6.
33. Gajjar, A., et al., *Traumatic lumbar puncture at diagnosis adversely affects outcome in childhood acute lymphoblastic leukemia*. Blood, 2000. **96**(10): p. 3381-4.
34. Ranta, S., et al., *Detection of central nervous system involvement in childhood acute lymphoblastic leukemia by cytomorphology and flow cytometry of the cerebrospinal fluid*. Pediatr Blood Cancer, 2015. **62**(6): p. 951-6.
35. Martinez-Laperche, C., et al., *Detection of occult cerebrospinal fluid involvement during maintenance therapy identifies a group of children with acute lymphoblastic leukemia at high risk for relapse*. Am J Hematol, 2013. **88**(5): p. 359-64.

36. Levinsen, M., et al., *Leukemic blasts are present at low levels in spinal fluid in one-third of childhood acute lymphoblastic leukemia cases*. *Pediatr Blood Cancer*, 2016. **63**(11): p. 1935-42.
37. Thastrup, M., et al., *Correction: Flow cytometric detection of leukemic blasts in cerebrospinal fluid predicts risk of relapse in childhood acute lymphoblastic leukemia: a Nordic Society of Pediatric Hematology and Oncology study*. *Leukemia*, 2020.
38. Pine, S.R., et al., *Detection of central nervous system leukemia in children with acute lymphoblastic leukemia by real-time polymerase chain reaction*. *J Mol Diagn*, 2005. **7**(1): p. 127-32.
39. Krishnan, S., et al., *Temporal changes in the incidence and pattern of central nervous system relapses in children with acute lymphoblastic leukaemia treated on four consecutive Medical Research Council trials, 1985-2001*. *Leukemia*, 2010. **24**(2): p. 450-9.
40. G, N., *United Kingdom National Randomised Trial For Children and Young Adults with Acute Lymphoblastic Leukaemia and Lymphoma 2011*. Reference Number: ISRCTN64515327, 2013.
41. Pui, C.H. and W.E. Evans, *A 50-year journey to cure childhood acute lymphoblastic leukemia*. *Semin Hematol*, 2013. **50**(3): p. 185-96.
42. Bruggemann, M., et al., *Standardized MRD quantification in European ALL trials: proceedings of the Second International Symposium on MRD assessment in Kiel, Germany, 18-20 September 2008*. *Leukemia*, 2010. **24**(3): p. 521-35.
43. Goulden, N.J., et al., *UKALL 2011: Randomised Trial Investigating a Short Induction Dexamethasone Schedule for Children and Young Adults with Acute Lymphoblastic Leukaemia*. *Blood*, 2017. **130**(Supplement 1): p. 141-141.
44. Jackson, R.K., et al., *Impact of dose and duration of therapy on dexamethasone pharmacokinetics in childhood acute lymphoblastic leukaemia-a report from the UKALL 2011 trial*. *Eur J Cancer*, 2019. **120**: p. 75-85.
45. Nair, A., *Implications of Intrathecal Chemotherapy for Anaesthesiologists: A Brief Review*. *Scientifica (Cairo)*, 2016. **2016**: p. 3759845.
46. Jacola, L.M., et al., *Longitudinal Assessment of Neurocognitive Outcomes in Survivors of Childhood Acute Lymphoblastic Leukemia Treated on a Contemporary Chemotherapy Protocol*. *J Clin Oncol*, 2016. **34**(11): p. 1239-47.
47. Schmiegelow, K., et al., *Consensus definitions of 14 severe acute toxic effects for childhood lymphoblastic leukaemia treatment: a Delphi consensus*. *Lancet Oncol*, 2016. **17**(6): p. e231-e239.
48. Halsey, C., et al., *The impact of therapy for childhood acute lymphoblastic leukaemia on intelligence quotients; results of the risk-stratified randomized central nervous system treatment trial MRC UKALL XI*. *J Hematol Oncol*, 2011. **4**: p. 42.
49. Kumar, S., *Second malignant neoplasms following radiotherapy*. *Int J Environ Res Public Health*, 2012. **9**(12): p. 4744-59.
50. Biojone, E., et al., *Minimal residual disease in cerebrospinal fluid at diagnosis: a more intensive treatment protocol was able to eliminate the adverse prognosis in children with acute lymphoblastic leukemia*. *Leukemia & Lymphoma*, 2012. **53**(1): p. 89-95.

51. Denys, B., et al., *Improved flow cytometric detection of minimal residual disease in childhood acute lymphoblastic leukemia*. *Leukemia*, 2013. **27**(3): p. 635-41.
52. Campana, D., *Determination of minimal residual disease in leukaemia patients*. *Br J Haematol*, 2003. **121**(6): p. 823-38.
53. van Dongen, J.J., et al., *Design and standardization of PCR primers and protocols for detection of clonal immunoglobulin and T-cell receptor gene recombinations in suspect lymphoproliferations: report of the BIOMED-2 Concerted Action BMH4-CT98-3936*. *Leukemia*, 2003. **17**(12): p. 2257-317.
54. Jung, D., et al., *Mechanism and control of V(D)J recombination at the immunoglobulin heavy chain locus*. *Annu Rev Immunol*, 2006. **24**: p. 541-70.
55. Hesse, J.E., et al., *V(D)J recombination: a functional definition of the joining signals*. *Genes Dev*, 1989. **3**(7): p. 1053-61.
56. Shlyakhtenko, L.S., et al., *Molecular mechanism underlying RAG1/RAG2 synaptic complex formation*. *J Biol Chem*, 2009. **284**(31): p. 20956-65.
57. Helmink, B.A. and B.P. Sleckman, *The response to and repair of RAG-mediated DNA double-strand breaks*. *Annu Rev Immunol*, 2012. **30**: p. 175-202.
58. Hesse, J.E., et al., *Extrachromosomal DNA substrates in pre-B cells undergo inversion or deletion at immunoglobulin V-(D)-J joining signals*. *Cell*, 1987. **49**(6): p. 775-83.
59. Lewis, S.M., et al., *Novel strand exchanges in V(D)J recombination*. *Cell*, 1988. **55**(6): p. 1099-107.
60. Cazzaniga, G., et al., *Defining the correct role of minimal residual disease tests in the management of acute lymphoblastic leukaemia*. *Br J Haematol*, 2011. **155**(1): p. 45-52.
61. van Dongen, J.J., et al., *Minimal residual disease diagnostics in acute lymphoblastic leukemia: need for sensitive, fast, and standardized technologies*. *Blood*, 2015. **125**(26): p. 3996-4009.
62. van der Velden, V.H., et al., *Analysis of minimal residual disease by Ig/TCR gene rearrangements: guidelines for interpretation of real-time quantitative PCR data*. *Leukemia*, 2007. **21**(4): p. 604-11.
63. C., H., *Towards personalized medicine in childhood acute lymphoblastic leukemia*. *Controversies in Paediatric and Adolescent Haematology*, 2013. **17**: p. 98-115.
64. van der Velden, V.H., et al., *New cellular markers at diagnosis are associated with isolated central nervous system relapse in paediatric B-cell precursor acute lymphoblastic leukaemia*. *Br J Haematol*, 2016. **172**(5): p. 769-81.
65. Vora, A., et al., *Treatment reduction for children and young adults with low-risk acute lymphoblastic leukaemia defined by minimal residual disease (UKALL 2003): a randomised controlled trial*. *Lancet Oncol*, 2013. **14**(3): p. 199-209.
66. Vora, A., et al., *Augmented post-remission therapy for a minimal residual disease-defined high-risk subgroup of children and young people with clinical standard-risk and intermediate-risk acute lymphoblastic leukaemia (UKALL 2003): a randomised controlled trial*. *Lancet Oncol*, 2014. **15**(8): p. 809-18.

67. Bowman, W.P., et al., *Augmented therapy improves outcome for pediatric high risk acute lymphocytic leukemia: results of Children's Oncology Group trial P9906*. *Pediatr Blood Cancer*, 2011. **57**(4): p. 569-77.
68. Strimbu, K. and J.A. Tavel, *What are biomarkers?* *Curr Opin HIV AIDS*, 2010. **5**(6): p. 463-6.
69. Masucci, G.V., et al., *Validation of biomarkers to predict response to immunotherapy in cancer: Volume I - pre-analytical and analytical validation*. *J Immunother Cancer*, 2016. **4**: p. 76.
70. Ray, P., et al., *Statistical evaluation of a biomarker*. *Anesthesiology*, 2010. **112**(4): p. 1023-40.
71. Califf, R.M., *Biomarker definitions and their applications*. *Exp Biol Med* (Maywood), 2018. **243**(3): p. 213-221.
72. Tennant, D.A., R.V. Duran, and E. Gottlieb, *Targeting metabolic transformation for cancer therapy*. *Nat Rev Cancer*, 2010. **10**(4): p. 267-77.
73. Avramis, V.I. and P.N. Tiwari, *Asparaginase (native ASNase or pegylated ASNase) in the treatment of acute lymphoblastic leukemia*. *Int J Nanomedicine*, 2006. **1**(3): p. 241-54.
74. Tiziani, S., et al., *Metabolomics of the tumor microenvironment in pediatric acute lymphoblastic leukemia*. *PLoS One*, 2013. **8**(12): p. e82859.
75. Liesenfeld, D.B., et al., *Review of mass spectrometry-based metabolomics in cancer research*. *Cancer Epidemiol Biomarkers Prev*, 2013. **22**(12): p. 2182-201.
76. Yu, L., et al., *Metabolomic phenotype of gastric cancer and precancerous stages based on gas chromatography time-of-flight mass spectrometry*. *J Gastroenterol Hepatol*, 2011. **26**(8): p. 1290-7.
77. Vinayavekhin, N. and A. Saghatelian, *Untargeted metabolomics*. *Curr Protoc Mol Biol*, 2010. **Chapter 30**: p. Unit 30 1 1-24.
78. Ncesoy-Özdemir, S.S., G.; Bozkurt, C.; Ören, A.C.; Balkaya, E.; Ertem, U, *The relationship between cerebrospinal fluid osteopontin level and central nervous system involvement in childhood acute leukemia*. *Turk. J. Pediatr*, 2013. **55**: p. 42-49.
79. Kersten, M.J., et al., *Elevation of cerebrospinal fluid soluble CD27 levels in patients with meningeal localization of lymphoid malignancies*. *Blood*, 1996. **87**(5): p. 1985-9.
80. Stucki, A., et al., *Cleaved L-selectin concentrations in meningeal leukaemia*. *Lancet*, 1995. **345**(8945): p. 286-9.
81. Ferrara, N., H.P. Gerber, and J. LeCouter, *The biology of VEGF and its receptors*. *Nat Med*, 2003. **9**(6): p. 669-76.
82. Markovic, A., K.L. MacKenzie, and R.B. Lock, *Induction of vascular endothelial growth factor secretion by childhood acute lymphoblastic leukemia cells via the FLT-3 signaling pathway*. *Mol Cancer Ther*, 2012. **11**(1): p. 183-93.
83. Kato, I., et al., *Hypoxic adaptation of leukemic cells infiltrating the CNS affords a therapeutic strategy targeting VEGFA*. *Blood*, 2017. **129**(23): p. 3126-3129.
84. Tang, Y.T., et al., *Expression and significance of vascular endothelial growth factor A and C in leukemia central nervous system metastasis*. *Leuk Res*, 2013. **37**(4): p. 359-66.
85. Moon, Y., et al., *Plasma soluble interleukin-2 receptor (sIL-2R) levels in patients with acute leukemia*. *Ann Clin Lab Sci*, 2004. **34**(4): p. 410-5.

86. Lee, W., et al., *Significance of cerebrospinal fluid sIL-2R level as a marker of CNS involvement in acute lymphoblastic leukemia*. Ann Clin Lab Sci, 2005. **35**(4): p. 407-12.
87. Jagarlamudi, K.K. and M. Shaw, *Thymidine kinase 1 as a tumor biomarker: technical advances offer new potential to an old biomarker*. Biomark Med, 2018. **12**(9): p. 1035-1048.
88. Topolcan, O. and L. Holubec, Jr., *The role of thymidine kinase in cancer diseases*. Expert Opin Med Diagn, 2008. **2**(2): p. 129-41.
89. O'Neill, K.L., et al., *Thymidine kinase 1--a prognostic and diagnostic indicator in ALL and AML patients*. Leukemia, 2007. **21**(3): p. 560-3.
90. Musto, P., et al., *[Determination of thymidine kinase in the cerebrospinal fluid as a marker of leukemic meningitis]*. Medicina (Firenze), 1989. **9**(1): p. 49-51.
91. Huang, H., *Matrix Metalloproteinase-9 (MMP-9) as a Cancer Biomarker and MMP-9 Biosensors: Recent Advances*. Sensors (Basel), 2018. **18**(10).
92. Feng, S., et al., *Matrix metalloproteinase-2 and -9 secreted by leukemic cells increase the permeability of blood-brain barrier by disrupting tight junction proteins*. PLoS One, 2011. **6**(8): p. e20599.
93. Mandel, P. and P. Metais, *Nuclear Acids In Human Blood Plasma*. C R Seances Soc Biol Fil, 1948. **142**(3-4): p. 241-3.
94. Jahr, S., et al., *DNA fragments in the blood plasma of cancer patients: quantitations and evidence for their origin from apoptotic and necrotic cells*. Cancer Res, 2001. **61**(4): p. 1659-65.
95. Luger, K., et al., *Crystal structure of the nucleosome core particle at 2.8 Å resolution*. Nature, 1997. **389**(6648): p. 251-60.
96. Diehl, F., et al., *Detection and quantification of mutations in the plasma of patients with colorectal tumors*. Proc Natl Acad Sci U S A, 2005. **102**(45): p. 16368-73.
97. Underhill, H.R., et al., *Fragment Length of Circulating Tumor DNA*. PLoS Genet, 2016. **12**(7): p. e1006162.
98. Cheng, F., L. Su, and C. Qian, *Circulating tumor DNA: a promising biomarker in the liquid biopsy of cancer*. Oncotarget, 2016. **7**(30): p. 48832-48841.
99. Ma, X., et al., *Cell-Free DNA Provides a Good Representation of the Tumor Genome Despite Its Biased Fragmentation Patterns*. PLoS One, 2017. **12**(1): p. e0169231.
100. Egyed, B., et al., *MicroRNA-181a as novel liquid biopsy marker of central nervous system involvement in pediatric acute lymphoblastic leukemia*. J Transl Med, 2020. **18**(1): p. 250.
101. Iyer, N.S., et al., *Chemotherapy-only treatment effects on long-term neurocognitive functioning in childhood ALL survivors: a review and meta-analysis*. Blood, 2015. **126**(3): p. 346-53.
102. Wishart, D.S., et al., *HMDB: the Human Metabolome Database*. Nucleic Acids Res, 2007. **35**(Database issue): p. D521-6.
103. Xia, J., et al., *Translational biomarker discovery in clinical metabolomics: an introductory tutorial*. Metabolomics, 2013. **9**(2): p. 280-299.
104. Duez, M., et al., *Correction: Vidjil: A Web Platform for Analysis of High-Throughput Repertoire Sequencing*. PLoS One, 2017. **12**(2): p. e0172249.
105. Mandrekar, J.N., *Receiver operating characteristic curve in diagnostic test assessment*. J Thorac Oncol, 2010. **5**(9): p. 1315-6.
106. *ALLTogether CSF-FLOW*.

107. Ranucci, R., *Cell-Free DNA: Applications in Different Diseases*. Methods Mol Biol, 2019. **1909**: p. 3-12.
108. Bredno, J., et al., *Clinical correlates of circulating cell-free DNA tumor fraction*. PLoS One, 2021. **16**(8): p. e0256436.
109. Markus, H., et al., *Evaluation of pre-analytical factors affecting plasma DNA analysis*. Sci Rep, 2018. **8**(1): p. 7375.
110. Fici, P., *Cell-Free DNA in the Liquid Biopsy Context: Role and Differences Between ctDNA and CTC Marker in Cancer Management*. Methods Mol Biol, 2019. **1909**: p. 47-73.
111. Whale, A.S., et al., *Comparison of microfluidic digital PCR and conventional quantitative PCR for measuring copy number variation*. Nucleic Acids Res, 2012. **40**(11): p. e82.
112. Hindson, C.M., et al., *Absolute quantification by droplet digital PCR versus analog real-time PCR*. Nat Methods, 2013. **10**(10): p. 1003-5.
113. McEwen, A.E., S.E.S. Leary, and C.M. Lockwood, *Beyond the Blood: CSF-Derived cfDNA for Diagnosis and Characterization of CNS Tumors*. Front Cell Dev Biol, 2020. **8**: p. 45.
114. Irving, J., et al., *Ras pathway mutations are prevalent in relapsed childhood acute lymphoblastic leukemia and confer sensitivity to MEK inhibition*. Blood, 2014. **124**(23): p. 3420-30.
115. Qian, J., et al., *Effects of NRAS Mutations on Leukemogenesis and Targeting of Children With Acute Lymphoblastic Leukemia*. Front Cell Dev Biol, 2022. **10**: p. 712484.
116. Amanda C. Lorentzian, M.G., Enes K. Ergin, Neha M. Akella, Nina Rolf, C. James Lim, Gregor S.D. Reid, Christopher A. Maxwell, View ORCID ProfilePhilipp F. Lange, *Proteogenomic analysis identifies the persistence of targetable lesions and proteomes through disease evolution in pediatric acute lymphoblastic leukemia*. 2022.
117. Bartram, J., et al., *Accurate Sample Assignment in a Multiplexed, Ultrasensitive, High-Throughput Sequencing Assay for Minimal Residual Disease*. J Mol Diagn, 2016. **18**(4): p. 494-506.
118. Bruggemann, M., et al., *Standardized next-generation sequencing of immunoglobulin and T-cell receptor gene recombinations for MRD marker identification in acute lymphoblastic leukaemia; a EuroClonality-NGS validation study*. Leukemia, 2019. **33**(9): p. 2241-2253.
119. Devonshire, A.S., et al., *Towards standardisation of cell-free DNA measurement in plasma: controls for extraction efficiency, fragment size bias and quantification*. Anal Bioanal Chem, 2014. **406**(26): p. 6499-512.
120. Gibson, D.A., P.T.K. Saunders, and I.J. McEwan, *Androgens and androgen receptor: Above and beyond*. Mol Cell Endocrinol, 2018. **465**: p. 1-3.
121. Milbury, C.A., et al., *Determining lower limits of detection of digital PCR assays for cancer-related gene mutations*. Biomol Detect Quantif, 2014. **1**(1): p. 8-22.
122. Suganuma, K., et al., *Energy metabolism of leukemia cells: glycolysis versus oxidative phosphorylation*. Leuk Lymphoma, 2010. **51**(11): p. 2112-9.
123. Tabe, Y., M. Konopleva, and M. Andreeff, *Fatty Acid Metabolism, Bone Marrow Adipocytes, and AML*. Front Oncol, 2020. **10**: p. 155.
124. Jiang, J., S. Batra, and J. Zhang, *Asparagine: A Metabolite to Be Targeted in Cancers*. Metabolites, 2021. **11**(6).
125. McLeish, M.J. and G.L. Kenyon, *Relating structure to mechanism in creatine kinase*. Crit Rev Biochem Mol Biol, 2005. **40**(1): p. 1-20.



126. Ohtsuki, S., et al., *The blood-brain barrier creatine transporter is a major pathway for supplying creatine to the brain*. J Cereb Blood Flow Metab, 2002. **22**(11): p. 1327-35.
127. Musharraf, S.G., et al., *Serum metabonomics of acute leukemia using nuclear magnetic resonance spectroscopy*. Sci Rep, 2016. **6**: p. 30693.
128. Ni, Y., G. Xie, and W. Jia, *Metabonomics of human colorectal cancer: new approaches for early diagnosis and biomarker discovery*. J Proteome Res, 2014. **13**(9): p. 3857-70.
129. Luo, X., et al., *Metabolomics identified new biomarkers for the precise diagnosis of pancreatic cancer and associated tissue metastasis*. Pharmacol Res, 2020. **156**: p. 104805.
130. Fenouille, N., et al., *The creatine kinase pathway is a metabolic vulnerability in EVI1-positive acute myeloid leukemia*. Nat Med, 2017. **23**(3): p. 301-313.
131. Hettling, H. and J.H. van Beek, *Analyzing the functional properties of the creatine kinase system with multiscale 'sloppy' modeling*. PLoS Comput Biol, 2011. **7**(8): p. e1002130.
132. Stevens, A., et al., *EVI1 expression in childhood acute lymphoblastic leukaemia is not restricted to MLL and BCR/ABL rearrangements and is influenced by age*. Blood Cancer J, 2014. **4**: p. e179.
133. Kazak, L. and P. Cohen, *Creatine metabolism: energy homeostasis, immunity and cancer biology*. Nat Rev Endocrinol, 2020. **16**(8): p. 421-436.
134. Arango, D., et al., *Acetylation of Cytidine in mRNA Promotes Translation Efficiency*. Cell, 2018. **175**(7): p. 1872-1886 e24.
135. Zhang, T., et al., *Identification of potential biomarkers for ovarian cancer by urinary metabolomic profiling*. J Proteome Res, 2013. **12**(1): p. 505-12.
136. Li, H., et al., *Modified metabolites mapping by liquid chromatography-high resolution mass spectrometry using full scan/all ion fragmentation/neutral loss acquisition*. J Chromatogr A, 2019. **1583**: p. 80-87.
137. Zi, J., et al., *Targeting NAT10 Induces Apoptosis Associated With Enhancing Endoplasmic Reticulum Stress in Acute Myeloid Leukemia Cells*. Front Oncol, 2020. **10**: p. 598107.
138. Feng, B., et al., *[Application of urinary nucleosides in the diagnosis and surgical monitoring of colorectal cancer]*. Zhonghua Wai Ke Za Zhi, 2005. **43**(9): p. 564-8.
139. Szymanska, E., et al., *Altered levels of nucleoside metabolite profiles in urogenital tract cancer measured by capillary electrophoresis*. J Pharm Biomed Anal, 2010. **53**(5): p. 1305-12.
140. Liang, P., et al., *NAT10 upregulation indicates a poor prognosis in acute myeloid leukemia*. Curr Probl Cancer, 2020. **44**(2): p. 100491.
141. Parsons, C.L., et al., *Role of urinary cations in the aetiology of bladder symptoms and interstitial cystitis*. BJU Int, 2014. **114**(2): p. 286-93.
142. Laguna, T.A., et al., *Metabolomics analysis identifies novel plasma biomarkers of cystic fibrosis pulmonary exacerbation*. Pediatr Pulmonol, 2015. **50**(9): p. 869-77.
143. Duan, J., et al., *N(4)-acetylcytidine is required for sustained NLRP3 inflammasome activation via HMGB1 pathway in microglia*. Cell Signal, 2019. **58**: p. 44-52.

144. Chachaj, A., et al., *Asymmetric and symmetric dimethylarginines and mortality in patients with hematological malignancies-A prospective study*. PLoS One, 2018. **13**(5): p. e0197148.
145. Stikarova, J., et al., *Enhanced levels of asymmetric dimethylarginine in a serum of middle age patients with myelodysplastic syndrome*. J Hematol Oncol, 2013. **6**: p. 58.
146. Stopa, N., J.E. Krebs, and D. Shechter, *The PRMT5 arginine methyltransferase: many roles in development, cancer and beyond*. Cell Mol Life Sci, 2015. **72**(11): p. 2041-59.
147. Serio, J., et al., *The PAF complex regulation of Prmt5 facilitates the progression and maintenance of MLL fusion leukemia*. Oncogene, 2018. **37**(4): p. 450-460.
148. Zakaria, M., et al., *HPLC analysis of aromatic amino acids, nucleosides, and bases in plasma of acute lymphocytic leukemia on chemotherapy*. Clin Chim Acta, 1982. **126**(1): p. 69-80.
149. Dong, H.Y., A. Shahsafari, and D.M. Dorfman, *CD148 and CD27 are expressed in B cell lymphomas derived from both memory and naive B cells*. Leuk Lymphoma, 2002. **43**(9): p. 1855-8.
150. Shao, H., et al., *Minimal residual disease detection by flow cytometry in adult T-cell leukemia/lymphoma*. Am J Clin Pathol, 2010. **133**(4): p. 592-601.
151. Kara, I.O., B. Sahin, and R. Gunesacar, *Levels of serum and cerebrospinal fluid soluble CD27 in the diagnosis of leptomeningeal involvement of hematolymphoid malignancies*. Adv Ther, 2007. **24**(4): p. 741-7.
152. Riether, C., et al., *CD70/CD27 signaling promotes blast stemness and is a viable therapeutic target in acute myeloid leukemia*. J Exp Med, 2017. **214**(2): p. 359-380.
153. Chen, D., et al., *CD27 expression and its association with clinical outcome in children and adults with pro-B acute lymphoblastic leukemia*. Blood Cancer J, 2017. **7**(6): p. e575.
154. van den Bent, M.J., et al., *Increased levels of soluble CD27 in the cerebrospinal fluid are not diagnostic for leptomeningeal involvement by lymphoid malignancies*. Ann Hematol, 2002. **81**(4): p. 187-91.
155. Huang, J., et al., *Soluble CD27-pool in humans may contribute to T cell activation and tumor immunity*. J Immunol, 2013. **190**(12): p. 6250-8.
156. Kustanovich, A., et al., *Life and death of circulating cell-free DNA*. Cancer Biol Ther, 2019. **20**(8): p. 1057-1067.
157. Yoon, K.A., et al., *Comparison of circulating plasma DNA levels between lung cancer patients and healthy controls*. J Mol Diagn, 2009. **11**(3): p. 182-5.
158. Pantel, K., *Blood-Based Analysis of Circulating Cell-Free DNA and Tumor Cells for Early Cancer Detection*. PLoS Med, 2016. **13**(12): p. e1002205.
159. Wang, Y., et al., *Detection of tumor-derived DNA in cerebrospinal fluid of patients with primary tumors of the brain and spinal cord*. Proc Natl Acad Sci U S A, 2015. **112**(31): p. 9704-9.
160. Shi, W., et al., *Prognostic value of free DNA quantification in serum and cerebrospinal fluid in glioma patients*. J Mol Neurosci, 2012. **46**(3): p. 470-5.
161. De Mattos-Arruda, L., et al., *Cerebrospinal fluid-derived circulating tumour DNA better represents the genomic alterations of brain tumours than plasma*. Nat Commun, 2015. **6**: p. 8839.

162. Pongers-Willemsse, M.J., et al., *Primers and protocols for standardized detection of minimal residual disease in acute lymphoblastic leukemia using immunoglobulin and T cell receptor gene rearrangements and TAL1 deletions as PCR targets: report of the BIOMED-1 CONCERTED ACTION: investigation of minimal residual disease in acute leukemia*. Leukemia, 1999. 13(1): p. 110-8.
163. Ekstein, D., et al., *CSF analysis of IgH gene rearrangement in CNS lymphoma: relationship to the disease course*. J Neurol Sci, 2006. 247(1): p. 39-46.
164. He, J., et al., *IgH gene rearrangements as plasma biomarkers in Non-Hodgkin's lymphoma patients*. Oncotarget, 2011. 2(3): p. 178-85.
165. Zhong, L., et al., *Monitoring immunoglobulin heavy chain and T-cell receptor gene rearrangement in cfDNA as minimal residual disease detection for patients with acute myeloid leukemia*. Oncol Lett, 2018. 16(2): p. 2279-2288.
166. Pan, W., et al., *Brain tumor mutations detected in cerebral spinal fluid*. Clin Chem, 2015. 61(3): p. 514-22.
167. van Ginkel, J.H., et al., *Droplet digital PCR for detection and quantification of circulating tumor DNA in plasma of head and neck cancer patients*. BMC Cancer, 2017. 17(1): p. 428.